

Transport and Biodegradation of Petroleum Hydrocarbon Vapors in the Subsurface.

A Laboratory Soil Column Study

by

Elsy Escobar Melendez

A Dissertation Presented in Partial Fulfillment
of the Requirements for the Degree
Doctor of Philosophy

Approved May 2012 by the
Graduate Supervisory Committee:

Paul Johnson, Chair
Jean Andino
Edward Kavazanjian
Rosa Krajmalnik-Brown
Erica Forzani

ARIZONA STATE UNIVERSITY

May 2012

ABSTRACT

In this work, the vapor transport and aerobic bio-attenuation of compounds from a multi-component petroleum vapor mixture were studied for six idealized lithologies in 1.8-m tall laboratory soil columns. Columns representing different geological settings were prepared using 20-40 mesh sand (medium-grained) and 16-minus mesh crushed granite (fine-grained). The contaminant vapor source was a liquid composed of twelve petroleum hydrocarbons common in weathered gasoline. It was placed in a chamber at the bottom of each column and the vapors diffused upward through the soil to the top where they were swept away with humidified gas. The experiment was conducted in three phases: i) nitrogen sweep gas; ii) air sweep gas; iii) vapor source concentrations decreased by ten times from the original concentrations and under air sweep gas. Oxygen, carbon dioxide and hydrocarbon concentrations were monitored over time. The data allowed determination of times to reach steady conditions, effluent mass emissions and concentration profiles. Times to reach near-steady conditions were consistent with theory and chemical-specific properties. First-order degradation rates were highest for straight-chain alkanes and aromatic hydrocarbons. Normalized effluent mass emissions were lower for lower source concentration and aerobic conditions. At the end of the study, soil core samples were taken every 6 in. Soil moisture content analyses showed that water had redistributed in the soil during the experiment. The soil at the bottom of the columns generally had higher moisture contents than initial values, and soil at the top had lower moisture contents. Profiles of the number of colony forming units of hydrocarbon-utilizing bacteria/g-soil indicated that the highest concentrations of degraders were located at the vertical intervals where maximum degradation activity was suggested by CO₂ profiles. Finally, the near-steady conditions of each phase of the study were simulated using a three-dimensional transient numerical model. The model was fit to the Phase I data by adjusting soil properties, and then fit to Phase III data to obtain

compound-specific first-order biodegradation rate constants ranging from 0.0 to 5.7×10^3 d^{-1} .

To my parents, who were always there to cheer, push, pull and pick me up when I needed it. And to my accomplice of many dawns, who help me remain myself in this crazy path by reminding me to look into the mirror once in a while and see the dialectic within myself which certainly was the one that did not allow me to give up.

ACKNOWLEDGEMENTS

I wish to thank my advisor, Dr. Paul Johnson for opening the door to the vapor intrusion and bioremediation world for me and teaching me to think outside limitations, as well as for his constant motivation, challenge, and guidance throughout my PhD student life.

I would like to thank the members of my committee: Dr. Rosa Krajmalnik-Brown, Dr. Erica Forzani, Dr. Edward Kavazanjian and Dr. Jean Andino, who encourage me and help me improve and finish this project by providing good suggestion and observations.

This project could not have been possible without Paul Dahlen who helped me set up and take down the very much heavy and “needy” soil columns. I am sure we both were a bit stronger after taking down the last column.

Many good ideas used in this project were suggested and inspired by my lab accomplices: Ryan Ekre, Bridget Cavanagh, Chase Holton, Sean Wilson, Emma Luo and Lisa Clifton. Thank you guys, I would not have made it without your constant help, support and suggestions.

Special thanks to Michal Ziv-El who took time from her busy schedule to teach me to do DNA extractions and to run lots of samples for qPCR analysis.

I want to thank my friends who filled my student life with great memories and adventures: Bella de la Garza, Ayla Kiser, Michal Ziv-El, Michelle Barry and my lab mates above mentioned.

Finally I want to thank the people who believed in me from the beginning (when I was a clueless undergrad): Ing. Carlos Canas, Dr. Daniel Zitomer, Dr. Switzembaum, my friends back home (marmotos) and of course my family.

Thank you, thank you, thank you!!

TABLE OF CONTENTS

	Page
LIST OF TABLES.....	x
LIST OF FIGURES.....	xiii
CHAPTER	
1 LITERATURE REVIEW AND OBJECTIVE.....	1
1.1 Vapor Intrusion.....	1
1.1.1 Vapor Intrusion Assessment.....	4
1.2 Fate and Transport of VOCs through the Subsurface.....	9
1.3 Natural Attenuation of Petroleum Hydrocarbon Vapors.....	13
1.3.1 Biodegradation Kinetics.....	19
1.3.2 Oxygen Transport to the Subsurface.....	20
1.4 Previous Studies on the Fate and Transport of Petroleum Hydrocarbon Vapors.....	20
1.4.1 Experimental Studies.....	20
1.4.2 Mathematical Models.....	22
1.5 Objective of the Soil Column Experiment.....	24
2 EXPERIMENTAL DESIGN.....	26
2.1 Experimental Apparatus.....	27
2.2 Stratigraphic Layout.....	30
2.3 Soil Characterization.....	31
2.4 Oxygen Leak Test.....	32
2.5 Packing the Columns.....	37
2.6 Vapor Hydrocarbon Source.....	38
2.6.1. Source Composition.....	38
2.6.2. Source Concentration changes.....	40

CHAPTER	Page
2.6.3. Hydrocarbon Vapor Source Preparation and Replacement in the Columns.....	41
2.7 Temperature and Pressure Differential in the Columns.....	43
2.8 Sweep Gas Flow.....	43
2.9 Shutting Down the Soil Columns.....	44
2.9.1 Tests performed before opening the soil columns.....	45
i) Effective Diffusion coefficient Test.....	45
ii) Permeability profile.....	45
2.9.2 Tests performed after opening the soil columns.....	46
i) Moisture Content and Fraction of Organic Carbon.....	47
ii) Microbial Analyses.....	47
2.10 Quality Assurance and Quality Control.....	48
2.10.1 Apparatus.....	49
i) GC-FID-TCD and TD-GC-MS.....	49
ii) Pressure Transducer and Data Logger.....	49
3 RESULTS AND DISCUSSION. PHASE I: OXYGEN DEPLETED CONDITIONS.....	50
3.1 Soil Characterization.....	50
3.2 Times to Reach Near-Steady State Conditions.....	51
3.3 Normalized Flux vs. Time.....	56
3.3.1. Mass Emissions.....	58
3.4 Concentration and Diffusion Coefficient Profiles.....	61
3.5 Carbon Dioxide, Oxygen and Methane Concentration.....	67
3.6 Summary.....	67
4 RESULTS AND DISCUSSION. PHASE II: SURFACE AEROBIC CONDITIONS.....	69

CHAPTER	Page
4.1. Normalized Flux vs. Time.....	69
4.2. Soil Vapor Profiles.....	72
4.2.1. Concentration Profiles Over Time.....	72
4.2.2. Oxygen and Carbon Dioxide Concentrations.....	75
4.3 Aerobic Degradation Rates and Diffusive Flux Ratios.....	83
4.4 Summary.....	88
5 RESULTS AND DISCUSSION. PHASE III: DECREASE OF VAPOR HYDROCARBON SOURCE UNDER AEROBIC SURFACE CONDITIONS.....	90
5.1 Normalized Flux vs. Time.....	90
5.2 Soil Vapor Profiles.....	92
5.2.1 Concentration Profiles Over Time.....	92
5.2.2 Oxygen and Carbon Dioxide Profiles.....	95
5.3 Aerobic Degradation Rates and Mass Emission Reduction.....	102
5.3.1. Zero-Order Degradation Rates.....	102
5.3.2. Diffusive Flux Ratio.....	103
5.4 Summary.....	105
6 POST-EXPERIMENT CHARACTERIZATION.....	110
6.1 Soil Parameters.....	110
6.2 Microbial Analyses.....	117
6.3 Summary.....	122
7 MATHEMATICAL MODEL SIMULATION OF THE SOIL COLUMNS EXPERIMENT.....	125
7.1 Step I: Model Domain and Effective Diffusion Coefficients. Simulation of Experimental Phase I.....	126

CHAPTER	Page
7.1.1 Input Parameters.....	126
i) Soil Characteristics.....	126
ii) Chemical characteristics.....	128
7.1.2 Simulation Results.....	132
7.2 Step II: First-Order Degradation Rate Constants. Simulating Experimental Phase III.....	138
7.2.1 Model Inputs.....	138
i) Reaction rates.....	141
7.2.2 Simulation results.....	141
7.3 Simulation of Experimental Phase II: Aerobic Conditions.....	154
7.3.1 Model Inputs.....	154
7.3.2 Model Results.....	154
7.4 Summary.....	160
8 CONCLUSIONS AND RECOMMENDATIONS.....	162
8.1 Conclusions.....	162
8.2 Recommendations.....	167
REFERENCES.....	170
APPENDIX	
I PROCEDURES TO DETERMINE SOIL CHARACTERISTICS.....	179
II EFFLUENT NORMALIZED FLUX VS. TIME.....	186
III VAPOR CONCENTRATION PROFILES. ANAEROBIC PHASE.....	199
IV VAPOR CONCENTRATION PROFILES. AEROBIC PHASE.....	212
V VAPOR CONCENTRATION PROFILES. PHASE III: 10X LOWER VAPOR SOURCE CONCENTRATION – AEROBIC.....	225

APPENDIX	Page
VI NEAR STEADY CONDITIONS SIMULATION RESULTS. VAPOR CONCENTRATION PROFILES.....	238

LIST OF TABLES

Table		Page
1.1	Minimal Risk Levels (MRLs) for the inhalation of a select group of VOCs.....	3
1.2	Target indoor air concentrations for some hydrocarbon compounds for cancer risk level = 1×10^{-5} and hazard quotient = 1.0.....	5
2.1	Experimental variables.....	26
2.2	Parameters utilized for tube desorption.....	30
2.3	Summary of the soil characteristics and analytical methods employed..	32
2.4	Oxygen flow into the empty soil columns.....	36
2.5	Oxygen flow rate necessary to completely oxidize the hydrocarbons in the soil columns.....	36
2.6	Experimental mass fractions and their comparison to mass fractions in weather gasoline.....	39
2.7	Vapor source composition compared to weathered gasoline.....	40
2.8	Carbon No. comparison to weather gasoline.....	40
2.9	Hydrocarbon volumes added to the vapor source liquid used in Phase III.....	41
2.10	Concentrations of hydrocarbon compounds above source liquid.....	42
2.11	Microbial analyses.....	47
3.1	Soil characteristics measured prior packing the soil columns.....	51
3.2	Time to reach near-steady state conditions.....	53
3.3	Comparison of the theoretical expected times to reach near steady state conditions vs. times obtained experimentally (Columns A, B, C)...	55
3.3	(Continued) Comparison of the theoretical expected times to reach near steady state conditions vs. times obtained experimentally (Columns D, E, F).....	56

Table	Page
3.4 Effluent mass emissions of each soil column.....	59
3.5 Benzene effective diffusion coefficient in each soil layer for each of the soil columns.....	60
4.1 Comparison of CO ₂ calculated by stoichiometry vs. the CO ₂ measured from the soil columns.....	80
4.2 Location of the “degradation zone” in each soil column.....	82
4.3 Flux ratio results.....	83
4.4 Zero-order degradation rates, mg/Kg-h.....	85
4.5 Diffusive flux ratio.....	86
5.1 Comparison of CO ₂ calculated mass emissions by stoichiometry vs. CO ₂ mass emissions measured from the soil columns (experimental)..	99
5.2 Comparison of the location of the “degradation zone” in each soil column during Phases II and III.....	101
5.3 Flux ratio results.....	102
5.4 Zero-order degradation rates, mg/Kg-h.....	103
5.5 Diffusive flux ratio.....	104
6.1 Initial vs. final water content in the soil (mass).....	112
6.2 Water filled porosity [cm ³ -water/cm ³ -soil] based on the water mass in the soil columns.....	116
6.3 Comparison of the location of the degradation zone vs. location of the maximum number of CFU/g of hexane and benzene degraders in the soil column.....	122
7.1 Calculated total and water filled porosities for the simulation of each soil column.....	129
7.2 Chemical characteristics inputs for simulating experimental phase I.....	131

Table	Page
7.3 Comparison of mass emissions: experimental vs. simulation during phase I (anaerobic phase).....	136
7.4 Chemical characteristics inputs for simulating experimental phase III...	140
7.5 First-order degradation rates along the length of the columns for each compound.....	142
7.6 Comparison of mass emissions: experimental vs. simulation for experimental phase III.....	152
7.7 Comparison of mass emission: experimental vs. simulation for experimental phase II.....	158

LIST OF FIGURES

Figure	Page
1.1 Vapor intrusion schematic.....	11
2.1 Soil column schematic.....	28
2.2 Lithologic layout schematic.....	31
2.3 O ₂ Concentration vs. Time (O ₂ leak test).....	35
2.4 Moisturizing and mixing the soil.....	37
2.5 Column packing (compressing down the soil layer).....	37
2.6 Sweep gas flow schematic.....	44
2.7 Column shut down sampling intervals.....	46
2.8 Sampling device and soil cores.....	47
3.1 Normalized flux vs. time. Anaerobic conditions.....	57
3.2 Benzene concentration vapor profiles change with time. Anaerobic conditions.....	62
3.3 Concentration and diffusion coefficient profiles.....	65
4.1 Normalized flux vs. time.....	71
4.2 Benzene concentration vapor profiles change with time – Phase II.....	73
4.3 Total petroleum hydrocarbon, CO ₂ , O ₂ concentration profiles.....	76
4.4 Columns flux emissions schematic.....	79
4.5 Benzene flux profiles.....	81
5.1 Normalized flux vs.time.....	91
5.2 Benzene concentration vapor profiles over time-Phase III.....	93
5.3 Total petroleum hydrocarbon, CO ₂ , O ₂ concentration profiles.....	96
5.4 Benzene flux profiles.....	100
5.5 Comparison of the normalized flux of each chemical during the three conditions studied in the soil columns.....	106
6.1 Helium effective diffusion coefficient profiles.....	111

Figure	Page
6.2 Moisture content, permeability and foc profiles.....	113
6.3 Microbial populations in the soil columns.....	118
7.1 Model domain schematic.....	127
7.2 Step I: model domain and effective diffusion coefficients calculation. Simulation fitted to near-steady conditions of experimental Phase I.....	132
7.3 Phase I simulation profile results at near-steady conditions and their comparison to the experimental results.....	133
7.4 Step II: First-order degradation rate constants calculation. Simulation outputs fitted to near-steady conditions results from experimental Phase III.....	139
7.5 Simulated vs. experimental profiles. Experimental Phase III.....	145
7.6 Experimental vs. simulated vapor concentration profiles.....	155
8.1 Roggemans et al. (2001) conceptual models vs. soil column experiment conceptual model.....	166

CHAPTER 1

LITERATURE REVIEW AND OBJECTIVE

This chapter provides a brief overview of the vapor intrusion pathway, vapor intrusion assessments and guidance documents, as well as a review of previous studies on fate and transport and biodegradation of petroleum hydrocarbons. Finally, the objective of the soil column experiment is discussed.

1.1 Vapor Intrusion

Soil and groundwater contamination due to accidental spills of solvents, petroleum liquids, or other volatile organic chemicals (VOCs) pose a potential for vapor migration from the subsurface to indoor air. Accumulation of these chemicals in enclosed spaces can lead to risks such as, immediate flammability, acute health risks when concentration levels are high, health risks through long term inhalation of low concentrations (chronic risks) or even aesthetic risks (odor related) (Johnson, 1999; API, 1998). This exposure pathway is referred as “vapor intrusion”, and is defined by the EPA as “the migration of volatile chemicals from the subsurface into overlying buildings” (EPA, 2002). It occurs when VOCs accumulate beneath or adjacent to the foundation of a building or there is a pressure differential between the subsurface and the building. The VOCs migrate into buildings through cracks and openings for pipes and utilities when the building’s pressure is less than the outside pressure (Allard, 2007).

Vapor intrusion concerns generally involve two kinds of vapors: (i) vapors originating from dissolved chlorinated compounds or dense non-aqueous phase liquids (DNAPL); and, (ii) vapors from mixtures of volatile petroleum hydrocarbon compounds. Examples of the former include tetrachloroethylene (PCE) and trichloroethylene (TCE), which are commonly found at sites near landfills, dry-cleaning facilities, or places where chlorinated solvents are produced or have been used. Chlorinated compounds are persistent in the environment as they are not easily degraded, they tend to be mobile in

the subsurface as volatilized vapor or dissolved chemicals, and they have high odor thresholds so they may not be noticed by indoor occupants (Little et al., 1992). The latter originate from leaking underground storage tanks, leaking transport lines, refineries, gas stations or fuel spills. They are comprised mostly of volatile aliphatic and aromatic hydrocarbons. Unlike chlorinated compounds, many petroleum hydrocarbons are readily biodegradable in the presence of oxygen and a few have a noticeable odor and taste when present in air or drinking water. Significant differences between the fate and transport of chlorinated and petroleum hydrocarbon VOCs have been observed (Little et al., 1992; Barbee, 1994; Fritzpatrick et al., 2002; Allard, 2007; EPA, 2011). The petroleum hydrocarbon vapor source composition will change with time as the components volatilize; therefore, the vapor composition of a gasoline spill is more difficult to predict with time than the vapor composition at a chlorinated solvent site.

The exposure pathways for individuals living close to an impacted site include long-term inhalation of volatile contaminants, ingestion of contaminated water and dermal sorption while showering (Little et al., 1992). Constant exposure to VOCs can increase the risk of cancer, affect the nervous system causing symptoms such as dizziness, headaches, confusion, weakness, fatigue; it also can affect the liver, immunological system and increase the risk of spontaneous miscarriages. Table 1.1 shows minimal risk levels published by ASTDR in 2008 for some chlorinated and petroleum compounds.

Table 1.1

Minimal Risk Levels (MRLs) for the inhalation a select group of VOCs (ASTDR, 2008).

Compound	Duration	MRL
Benzene	Acute	0.009 ppm
	Chronic	0.03 ppm
Hexane	Chronic	0.6 ppm
MTBE	Acute	2 ppm
	Chronic	0.7 ppm
Tetrachloroethylene	Acute	0.2 ppm
	Chronic	0.04 ppm
Toluene	Acute	1 ppm
	Chronic	0.08 ppm
Trichloroethylene	Acute	2 ppm
Vinyl chloride	Acute	0.5 ppm
Xylenes	Acute	2 ppm
	Chronic	0.05 ppm
1,1-Dichloroethene	Intermediate	0.02 ppm

Radon intrusion has been intensively studied beginning in the 1980's (Nazaroff et al., 1987; Loureiro et al., 1990); that work established a base for vapor intrusion research. Vapor intrusion was recognized as a significant contamination pathway in the early 1990's by Johnson and Ettinger (1991) and this was validated in the 1990's when research on the vapor transport of soil gas into buildings performed by the Massachusetts Department of Environmental Protection (MassDEP) showed its significance. Prior to this, regulators and environmental scientists viewed contaminated groundwater as a potential threat to the drinking water supply. So, as long as individuals were not in contact or drinking contaminated water, there was thought to be no risk of exposure (radon is an exception) (ITRC, 2007, Folkes et al., 2003).

The finding of vapor intrusion in a residential community raises apprehension and anxiety among the building occupants, and questions and concerns are addressed to the regulators such as "is the air safe, not only in our houses, but outside at schools or day cares?", "what are the effects on property values?". These concerns may become issues that can affect the strategy for addressing the vapor intrusion pathway (ITRC, 2007).

There are some well-known cases of concerns about vapor intrusion involving spills in residential areas, such as the petroleum hydrocarbon plume in Greenpoint, Brooklyn, where up to 30 million gallons of petroleum from dozens of refineries migrated into Newtown Creek and surrounding neighborhoods affecting about 100 acres of land. Also, recent testing has found the presence of tetrachloroethene (PCE) and trichloroethylene (TCE). Residents have expressed concerns about their health and value of their properties, and even fear of having their properties condemned. This creates resistance from the public to open their homes for testing which can slow down the mitigation process. Another example is the spill that occurred at the 52nd Street in Phoenix, AZ where chlorinated chemicals were spilled from the nearby Motorola Plant. 1,1,1-trichloroethane (1,1,1-TCA), TCE and PCE and their degradation products have been detected at this site. Even though the United States Environmental Protection Agency (EPA) has not found evidence to suggest that vapor intrusion is taking place, the residents have expressed concerns over health issues and they want the EPA to do more to protect them such as the installation of depressurization systems in each home in the area (EPA, 2012; USA Today, 2012).

1.1.1 Vapor intrusion pathway assessment.

In 2002 the EPA issued draft guidance on how to determine the existence of a “complete exposure pathway”. The guidance is an approach to help users to determine if there is vapor intrusion from subsurface vapors into indoor air spaces. The draft is based on an empirical analysis of an EPA database, the use of the Johnson and Ettinger Model (1991), and professional judgement (Abreu, 2005). The EPA draft includes tables with target breathing indoor air concentrations for carcinogenic and non-carcinogenic compounds. The carcinogenic compound targets are based on the target cancer risk exposure frequency (1×10^{-4} , 1×10^{-5} , 1×10^{-6}) and duration, and the non-carcinogens, are calculated using the target hazard quotient (i.e. 1.0). Table 1.2 shows the target indoor air concentration for some hydrocarbon compounds (EPA, 2002). The EPA plans to issue a

Final Subsurface Vapor Intrusion Guidance by November, 2012. The guidance is a revision of the 2002 draft that accounts for variability in the data due to differences in subsurface conditions, building structural conditions and weather conditions (EPA, 2010).

Table 2.1

Target indoor air concentrations for some hydrocarbon compounds for cancer risk level = 1×10^{-5} and hazard quotient = 1.0 (EPA, 2002)

Compound	Basis for Target Concentration	Target indoor concentration (ug/m³)	Target shallow soil gas concentration corresponding to target indoor air concentration where the air attenuation factor = 0.01	Target deep soil gas concentration corresponding to target indoor air concentration where the air attenuation factor = 0.01
Benzene	Cancer risk	3.1	31	310
1,1-Dichloroethylene	Noncarcinogen	200	2,000	20,000
Hexane	Noncarcinogen	200	2,000	20,000
MTBE	Noncarcinogen	3,000	30,000	300,000
PCE	Carcinogen	8.1	81	810
Toluene	Noncarcinogen	400	4,000	40,000
Trichloroethylene	Carcinogen	0.22	2.2	22
Xylenes	Noncarcinogen	7,000	70,000	700,000
1,3,5-Trimethylbenzene	Noncarcinogen	6	60	600
Vinyl Chloride	Carcinogen	2.8	28	280

Besides the EPA guidance (2002) there are other documents such as Health Canada (2004), American Petroleum Institute (API) (1998) and the IRTC guideline (2007). The Health Canada Document was written with the objective to unify and assist with consistent assessment of risks since provincial regulatory agencies across Canada. Similarly to the EPA guidance (2002), this document suggests the performance of a preliminary quantitative risk assessment (PQRA) in which the risk is determined depending on two categories: (i) non-carcinogens and (ii) carcinogens, in which the incremental lifetime cancer risk (ILCR) is calculated related to the exposure. If the PQRA

determines that the exposure is unacceptable for human health, a more complex site-specific assessment (SSA) is performed prior defining remedial actions.

The API document (Assessing the significance of Subsurface Contaminant Vapor Migration to Enclosed Spaces) (1998) includes a discussion of data requirements, data presentation and interpretation for vapor intrusion assessments. It suggests the incorporation of some key technical considerations during an assessment such as, the collection of soil gas samples near the surface or foundation, direct measurements of enclosed-space vapor concentrations, the use of site-specific diffusion coefficients and the potential for increased vapor attenuation due to soil stratigraphy, moisture content, biodegradation, source depletion, as well as times required for vapors to reach near-steady conditions (which is also affected by the chemical properties of the compound of interest).

The ITRC guidance document (2007) states that a complete vapor intrusion pathway includes the identification of three components: a source of VOCs in the subsurface (groundwater and/or soil), inhabited building or the potential for future inhabited buildings and a migration route that connects the subsurface with the building. This guidance provides steps to build-up a site specific assessment starting with the development of a conceptual site model in which the type of volatile chemicals and concentrations, sources, location and identification of receptors are identified. Then, steps of a site investigation are given in which the majority of field data is collected and vapor intrusion scenarios are discussed and finally remediation strategies of vapor intrusion impacts are studied. The guidance suggests the use of multiple lines of evidence to reach decisions based on professional judgment. This document also includes steps for implementing a community outreach program which can help during the initial screening step.

Even though the specific recommended investigation procedures vary across guidance documents, most of them utilize step-wise evaluation processes that include preliminary screening and field investigations (GSI, 2007). Each guidance document provides strategies and steps to perform a vapor intrusion assessment; however, each group of researchers and consulting firms, may have their own preferred methods and toxicological references values (TRVs) for risk characterization. Therefore, variability is unavoidable, and as a consequence, the topic is subject of continuous debate in order to determine the best approach for screening a site. A way of enlightening this debate is to create a better understanding of the vapor concentrations and flux profiles from the source zone to the subsurface, ground surface or buildings, and in that way better predict the risks on each site.

Even though these guidance documents provide suggestions on how to assess the vapor intrusion pathway, many challenging issues arise, making the assessment particularly difficult, such as

- (i) The existence of background concentrations which increases the difficulty in identifying the vapor intrusion pathway via indoor air sampling . Thus, prior to indoor air sampling efforts should be made to address sources of background contamination. The EPA (2011) issued a technical report with a compilation of information on expected ranges and variability of typical background indoor air concentration of VOCs measured in North American residents. McHugh et al. (2011) proposed a method using compound-specific stable isotope analysis to distinguish between indoor and vapor intrusion sources.
- (ii) Temporal factors which affect the subsurface measurement such as seasonal changes in building depressurization due to the use of fireplaces, open window, HVAC systems or wind. Also, variations in barometric pressures due to weather patterns could induce air intrusion into the subsurface affecting monitoring activities during vapor intrusion assessments. Massmann et al. (1992) observed that

fluctuations in barometric pressure causes vertical transport in soil columns with open ground surface; fresh air may migrate several meters into the subsurface depending on the permeability; the air migration may affect the results of soil gas analysis since the VOCs concentrations may be lowered during high barometric pressure events. Fluctuations in the barometric pressure could cause horizontal transport of fresh air into the subsurface which may significantly impact the results of gas monitoring activities. Moisture content also changes with time affecting the effective diffusion coefficient of the soil or may cause the water table to rise and with it the contaminant source or the source may become trapped beneath the infiltrating recharge, reducing their ability to volatilize into the soil gas. These conditions can impact field data results.

- (iii) Biodegradation can reduce soil gas concentrations and vapor intrusion by several orders of magnitude (IRTC, 2007).
- (iv) The presence of preferential pathways can also affect the pathway significance. The permeability of subsurface materials can be highly variable, especially in fractured geological media and gravel. If this migration routes connects a source to a building or allows higher levels of groundwater contamination to migrate under a building, vapor intrusion may be exacerbated.
- (v) Community concerns and fears, leading to a lack of cooperation between parties making the assessment more difficult. Communication and education are essential components of any community outreach program.

The significance of the vapor intrusion pathway involves sampling and interpretation of soil vapor concentrations, so it is necessary to understand the subsurface migration of individual chemicals in complex mixtures of vapors and how it is affected by biodegradation in order to be more confident in our ability to identify the settings where vapor transport leads to safety and human health risks (Roggemans, et al. 2001).

When developing a vapor intrusion study strategy on a site, it is important to take into account the spatial and temporal variability of the data. Various studies have determined that there is a wide range of variability in the results when sampling within the same site and at different times of year. Folkes, et al. (2009), determined that summer concentrations were on average 50% higher and 20% lower during winter. Luo et al. (2009) observed significant spatial variability of petroleum hydrocarbon concentrations (from 0.01 to 200 mg/L) on a site with a building on top of approximately 15 m by 14 m (50 x 45 ft); it was determined that the factor controlling the soil-gas distribution was the oxygen concentrations in the soil.

Knowledge of the different physical processes and reactions occurring in the soil during a spill event will provide a better understanding of how the VOCs are transported and therefore, complete assessments of the pathways can be performed.

1.2 Fate and Transport of VOCs in the Subsurface

After a soil spill occurs, the petroleum hydrocarbon or chlorinated components redistribute in the soil into the gas phase, sorb onto the soil, and dissolve in the soil water or groundwater. The degree of chemical sorption and volatilization is controlled by the physical and chemical properties of the soil such as moisture content, porosity and organic matter content, as well as the physical and chemical characteristics of the contaminant such as vapor pressure, solubility, and polarity. Other factors that affect vapor transport are: environmental variables such as airflow rates over the surface, barometric pressure, soil temperature and physical variables such as the lithology of the soil (Batterman et al., 1995; Fine et al., 1997; Pasteris et al., 2001).

Patterson et al. (2009) stated that to better quantify vapor intrusion, it is necessary to understand all vapor pathways into buildings. Some of the pathways include the discharge of vapors from the uncovered open ground soil adjacent to the building and subsequent advection into the building, diffusion of the vapors through the concrete slab

and, pressure-driven advection through cracks or gaps in the building's substructure. These pathways are consequences of short-term barometric pressure changes due to winds, rainfall, thermal differences between indoors or outdoors, and imbalanced building ventilation. The flow of vapors into a buildings induced by a pressure differential between the indoors and outdoors. It has been observed that the slightest underpressurization causes the organic vapor to move through the cracks or openings in the building substructure or even through building materials (See Figure 1.1) (Little et al., 1992; Patterson et al., 2009). Nazaroff et al. (1987) demonstrated in his study on intrusion of radon (^{222}Rn) that depressurized basements (due to wind or temperature variations) have an effect on the pressure field and air movement in the soil. In addition, Garbesi et al (1989) observed variations in the soil gas flow depending on the permeability of the soil and noted that it is important to take into account the pressure-driven flow through permeable building foundation material. If this pathway is ignored, it is possible underestimate the soil gas intrusion related concentrations in buildings.

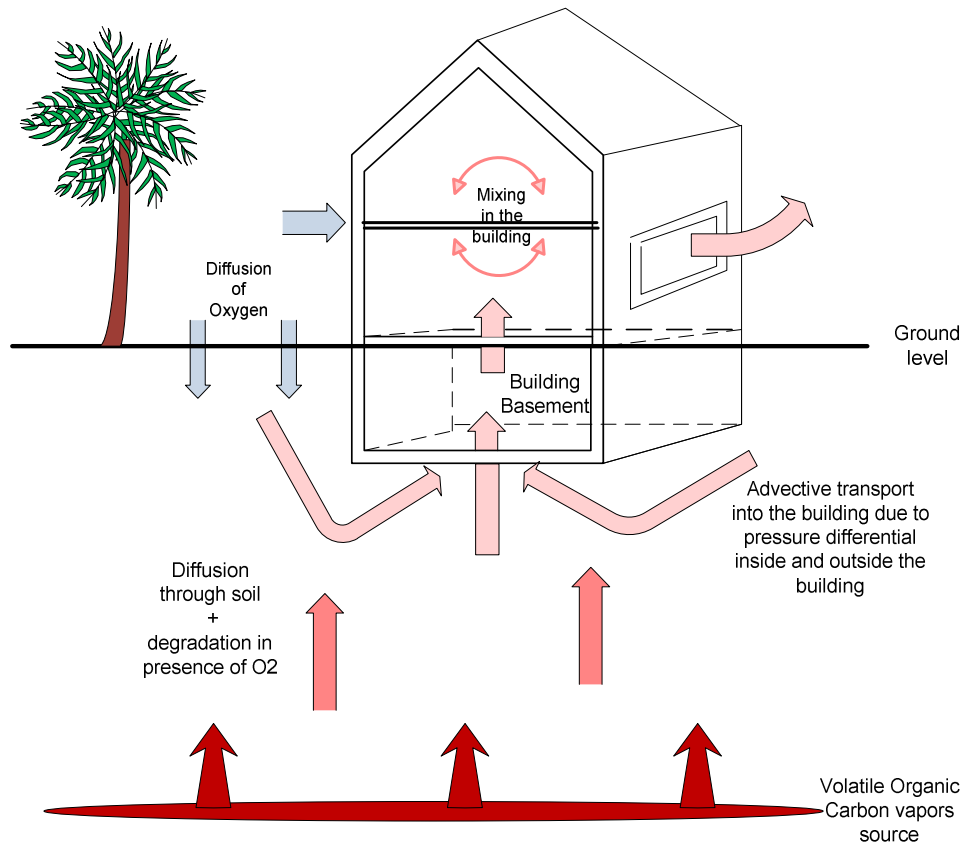


Figure 1.1. Vapor intrusion schematic

The fate of spilled products varies depending on the soil and chemical characteristics; so the released chemicals will have different distribution in the air, soil, and water. For example, gasoline is a mixture of different chemicals with different characteristics, so each one will behave according to its properties.

The partitioning of the chemicals in soil, water and gas plays a very important role in the gas mobility and transport (Fine et al., 1997). Thus, in a spill event, the liquid migrates downward through the unsaturated zone; some of it is trapped in the pore spaces at residual saturation. In the case of gasoline, it migrates downward until the water table is reached; while for solvents, the liquid travels past the water table forming pools of contaminants in the subsurface. The residual petroleum hydrocarbons or solvents trapped in the soil might volatilize forming a vapor phase contaminant plume

within the soil gas. The vapor plume spreads by diffusion (and potentially by density-induced advection); as it spreads, it will cause contamination of the soil moisture and soil matrix due to phase-partitioning. Contamination of groundwater may happen by vapor migration to the capillary fringe, a rise of the water table into the contaminated zone, or liquid infiltration into the groundwater, becoming then, a source of contamination (Conant et al., 1996).

As explained above, the vapor moves from the source through the soil by diffusion (See Figure 1.1). If there is an open space (with no building on top) diffusion is the dominant transport of the vapor until it reaches the surface. At the same time, oxygen from the surface diffuses down into the soil. If aerobic organisms are present, a biodegradation reaction may occur affecting the diffusive flux of the compounds to the surface. If there is a building on the surface, the vapor might reach a point during its migration in the vadose zone where there is a pressure differential; at this point, the vapor is transported by advection into the buildings through cracks in the foundation, pipes or diffusion through building materials. This pressure gradient is the result of factors such as indoor-outdoor temperature differences, wind loading on the building structure, operation of air conditioning systems, exhaust fans or furnaces which causes imbalances in the building ventilation (Johnson et al., 1991; Little et al., 1992; Patterson et al., 2009)

Vapor diffusion is affected by moisture content and temperature. When the moisture content increases (i.e. close to the capillary fringe or in fine-grained layers) the pore cross-sectional area available for vapor diffusion is reduced. Batterman et al (1995) studied the effect of soil moisture on vapor transport of hydrocarbon vapors in different media by determining the retardation factor the soil at different moisture contents. They determined that the retardation factors increased at higher soil moisture contents. Soil temperature affects the diffusivity of the chemicals, Conant et al. (1996) performed an experiment in which diffusion of TCE was observed during the winter and summer; they observed that vapor concentrations in the source area were significantly higher during the

summer than during winter, this was the result of an increase in the diffusion coefficients of the chemicals during the summer, and a decrease in retardation due to vapor dissolution and sorption.

Volatilization of the chemicals in the vadose zone depends on the depth, and the soil and chemical characteristics. Ong et al., (1992) observed that when the source is 10 m below ground level, the contaminant volatilization is less under dry conditions than under wet conditions which is an indication that “enhanced vapor-phase partitioning” in a deep, dry, soil profile can play an important role in the retardation of organic pollutants in the subsurface. The experiment was repeated for a 4 m below ground surface conditions and in this case, volatilization under dry conditions was greater than under wet conditions. They concluded that under dry conditions, vapor-phase sorption of organic pollutants may significantly retard the transport of volatile pollutants; however, for contaminated soils close to ground level, the volatilization of organic vapor is controlled by vapor diffusion, even in dry soils where vapor-phase sorption is expected to be high. Since physical-chemical properties of a contaminant act to influence vapor behavior, it was observed that volatilization was favorable for contaminants with high Henry’s law constant and low aqueous partition coefficients.

In summary, partitioning of vapor to the soil matrix and soil moisture affects the vapor transport and it will determine the contaminant distribution in the unsaturated zone. Partitioning of the contaminant between the soil gas and soil moisture is influenced mostly by the Henry’s Law constant (Conant et al., 1996).

1.3 Natural Attenuation of Petroleum Hydrocarbon Vapors

Natural attenuation is one of the primary mechanisms by which petroleum hydrocarbon and other pollutants are eliminated from the environment. It has been observed that the unsaturated zone of the soil can work as a “porous filter layer” which naturally attenuates the vapor pollutants through microbiological degradation; and that

petroleum hydrocarbon vapors are rapidly and completely biodegraded in the unsaturated zone. Natural attenuation of chemicals in soils is due to different processes: physical, such as volatilization, diffusion in pores, dispersion or adsorption; chemical, such as oxidation or reduction; and biological: aerobic or anaerobic biodegradation (Andre et al., 2009).

The principal limiting factor for biodegradation in most of the petroleum hydrocarbon contaminated sites is the amount of oxygen (O_2) present in the soil. Bacteria are naturally present in most soils. The degradation reactions occur in the presence of an electron-acceptor substrate (O_2), an electron-donor substrate (sugar or natural gas) and inorganic nutrients (i.e. nitrogen, phosphorus, sulfur and iron). Mostly the bacteria utilize only dissolved solutes; thus, the vapor must enter into a soluble phase with enough O_2 to be degraded by the bacteria. Degradation of environmentally significant quantities of hydrocarbon usually requires the addition of O_2 to begin the degradation process by forming an alcohol from the hydrocarbon, which is later used as a terminal electron-acceptor for energy generation (Borden, 1986). In order to have a good biodegradation rate, the oxygen concentration should be above 1 to 2 mg/L, although it has been proved that biodegradation can be supported at levels of 0.2 mg/L (Neale et al., 2000).

Although most hydrocarbon vapors are readily biodegradable when O_2 concentration and microorganisms are available, in some cases the amount of contaminant is large and the microorganisms consume the O_2 supply and the vapors pass through regions of the subsurface without being degraded (Jin et al., 1994). In cases where there is no advective transport and diffusion is the driving transport, it can be observed that biodegradation causes vertical gradients of O_2 in the presence of biodegradable compounds. In cases where there is no O_2 , anaerobic degradation may occur at slower rates (Pasteris et al., 2002).

An important key to the understanding of biodegradation is in the prediction of the O_2 subsurface redistribution and transport into contaminated areas (Neale et al.,

2000). Oxygen moves down from the atmosphere to the subsurface layers, where it can be completely or partially depleted through biodegradation and carbon dioxide (CO₂) is produced as a byproduct; as a result, the upward hydrocarbon vapor flux is reduced and oxygen depleted zones may be created (Wilson et al., 2005). It has been observed that the O₂ concentrations decrease with depth in impacted soils and that the CO₂ concentrations increase. Both processes should be consistent with each other since the latter is produced due to the utilization of the former (Roggemans et al. 2001, Wilson et al., 2005, Davis et al., 2009).

Re-aeration of the soil is very important to maintain the biodegradation rate. Neale et al (2000) observed that soil water content has a great influence on decreasing the biodegradation rates; and that, factors such as soil type, soil oxygen demand and thickness imparted little resistance to the transport of oxygen through the unsaturated zone. Laubacher et al. (1997) determined that the presence of buildings on the top of impacted zones can influence the vapor profiles and their degradation; the basements can serve as barriers (if there are very small or no cracks) preventing hydrocarbon vapors from dissipating or atmospheric oxygen from the surface from replenishing the soil.

Petroleum hydrocarbons have different susceptibility to microbial degradation; it has been ranked as follows (Leahy et al., 1990):

n – alkanes > branched alkanes > low – molecular – weight aromatics > cyclic alkanes > high – molecular weight aromatics > polar compounds

This is not universally agreed upon, but it has been reported by Pasteris et al. (2000) that the higher biodegradation rates they observed in their lysimeter study were the long chain alkanes such as octane, decane and dodecane follow by the cyclic alkanes (i.e. cyclohexane). The most volatile alkanes and high-molecular-weight aromatics presented very low to zero degradation rate constants. Broholm et al. (2005) performed a study in which synthetic hydrocarbon jet-fuel mixed with sand was placed in

the vadose zone of a site, they looked at the biodegradation of individual hydrocarbons and found that the aromatic compounds depleted faster than the aliphatic compounds.

Aerobic degradation can be affected by different factors such as the availability of nutrients, soil pH and temperature. The amount of nitrogen and phosphorus in the soil might limit the microbial degradation. It has been studied that the addition of N-P-K fertilizers, urea-phosphate and ammonium salts accelerates the degradation of the chemicals (Leahy et al., 1990). The pH is important because the microbial population activity is better at a pH range of 5.0 to 7.4. Leahy et al. (1990) note that the rates of microbial degradation are faster at this range than in acidic environments; however, the bacteria are always present. The soil temperature affects biodegradation due to its effect on the physical and chemical composition of the chemicals; at low temperature, the volatilization of the vapors decreases and the water solubility increases leading to a decrease in the biodegradation activity.

Aerobic biodegradation is also affected by the contaminant concentration. There is a threshold concentration at which biodegradation may occur. Scopa et al. (2006) studied the number of heterotrophic bacteria in a soil spiked with different amounts of petroleum hydrocarbons; with a concentration of 5000 mg/kg-soil of fuel in the soil, the number of heterotrophic bacteria increased and the number of fungi and actinomyces decreased. When the concentration was increased to 10000 mg/kg-soil the number of heterotrophic bacteria increase more rapidly but the soil diversity decreased intensely and so did the soil degradation activity.

Another factor that affects the biodegradation activity is the exposure of the microbial communities to the hydrocarbon compounds. Once a microbial community is adapted to the hydrocarbons presence, the rates of hydrocarbon transformation increase (Leahy et al., 1990). There is a high diversity of microbial communities known that are able to degrade hydrocarbons, a single bacteria usually has a relatively small degradation range, and not all the fraction of the gasoline or fuel components can be

degraded by a single species (Popp et al., 2006); then, degradation is often the result of community-interacting microbial populations ('consortium') (Boopathy, 2004) and so, the studies focus on different microbial communities. The ability to degrade and/or utilize hydrocarbon substrate is present in a wide variety of bacterial and fungal communities. Petroleum hydrocarbon degraders have been classified in: Bacteria (*Proteobacteria*, *Actinobacteria*, *Fimicutes*, *Bacteroidetes*, *Chlamydiae* and *Thermus*), Archaea (Halobacteriales), Fungi and algae (Milliton et al., 2010). Leahy et al. (1990) list *Achromobacter*, *Acinetobacter*, *Alaligenes*, *Arthrobacter*, *Bacillus*, *Flavobacteriu*, *Nocardia*, and *Pseudomonas* spp; Greene et al. (2000) identified by 16 srRNA *Pseudomonas* spp, *Alcaligenes* spp, *Rhodococcus*, *Microbacter* sp and *Arthrobacter*. Since the microbial population changes with the ecosystem (i.e. hydrocarbons and oxygen concentrations present) and local environmental conditions, it is difficult to determine all the communities that degrade the hydrocarbons and the extent at which each organism participate in the degradation of the petroleum hydrocarbons. For example, Popp et al. (2006) observed that *Gammaproteobacteria* are dominant in soils that just have been contaminated; in cold climate soils, Margesin et al. (2003) found genotypes containing genes from gram-negative bacteria *P. putida* and *Acinetobacter* sp. among others.

Anaerobic biodegradation also can occur, it depends on the soil moisture content, nutrients, microorganisms presence, thickness of the anaerobic layer and rate of the reactions (Wilson et al., 2005). Boopathy (2004) observed that anaerobic biodegradation was very effective at removing 88% of diesel No. 2 in soil in the presence of various electron acceptors such as nitrate, sulfate, carbonate and a nitrogen source.

It is necessary to consider that biodegradation of hydrocarbon compounds has been proven to be highly variable (EPA, 2002); also, it has been understood that it can be very important in the reduction of hydrocarbon vapors (Abreu et al., 2006). However, it is believed that aerobic biodegradation will not have great effects in sites where oxygen is

limited and therefore, EPA (2002) suggests that biodegradation significance be determined through vertical vapor profiles and its effects estimated by analysis methods. When screening a site it is necessary to choose a conceptual migration model. The knowledge of the vapor profiles will provide confidence in the modeled and measured data if they are consistent with each other. Wilson et al. (2005) notes that “a soil-gas vertical profile consists of two or more samples collected from a single location between the top of the source and the ground surface of building foundation”. The objective is to learn and demonstrate the depletion of chemicals concentrations vertically from the source to the buildings foundations of ground surface or to determine the significance of vapor transport in to the building (when sources are beneath the building). The knowledge gained from the vertical profiles of a soil column on a site will give more confidence in the data which will provide a more accurate prediction with the conceptual migration model chosen. Also, for the better understanding of vapor migration it is necessary to have a “photo log” of the soil geological profile and the physical properties of the soil layers of the vadose zone: soil moisture, bulk density, air-filled porosity, water-filled porosity, total organic carbon, hydraulic conductivity and air permeability.

With the objective of gaining a better understanding of the effect of aerobic degradation in the vapor migration, Roggemans et al. (2001) performed a study at petroleum hydrocarbon contaminated sites in which, soil gas profiles were divided into four aerobic degradation behaviors:

- Behavior A: aerobic biodegradation occurs over a narrow interval of soil; above that interval no hydrocarbons are detected, and the soil has high concentrations of O₂ and CO₂. Below the bio-attenuation interval no CO₂ or O₂ are detected.
- Behavior B: aerobic biodegradation occurs along the whole length of the soil column and it is limited by the degradation rates.

- Behavior C: aerobic degradation consumed the usable oxygen in the soil gas and the oxygen re-supply is lower than the oxygen consumption rate, so little to no oxygen concentrations are detected in the subsurface
- Behavior D: biodegradation occurs close to the vapor source. This occurs when the soil has a higher diffusion resistant zone immediately above the vapor source.

The study concluded that the significance of biodegradation varied across categories and no correlation was observed of gas profile behavior with depth to vapor source, lithology or surface cover.

1.3.1 Biodegradation kinetics.

Many studies estimate or assume in model applications that biodegradation is zero-order and/or first-order kinetics (Hohener et al., 2003; DeVaul, 2007). In the zero-order kinetics, the rate of mass consumption is constant and independent of the concentration of the chemicals being degraded. In the first-order approach, the rate of mass consumption is directly proportional to the concentration of the compound being consumed. First-order degradation rate constants are commonly used to define the kinetics of the petroleum hydrocarbon biodegradation reactions not only for simplicity but also it had been found to match adequately experimental and field results.

Davis et al. (2009) consider that the biodegradation rate is instantaneous, or rapid compared to soil vapor diffusion in the subsurface. So, whenever oxygen and petroleum hydrocarbons are collocated in the subsurface, they react and the location at which this occurs is controlled only by the transport to that location and the stoichiometry of the reactions.

The biodegradation of petroleum hydrocarbons is a complex process that depends quantitatively and qualitatively on the nature and amount of the spill, environment and soil ecosystem; microbial community and its adaptive response to the

presence of petroleum hydrocarbons. There are a wide number of studies on this topic (Leagy et al., 1990; Greene et al., 2000; Scopa et al., 2006; Li et al., 2007; Militon et al., 2010), however the factors are numerous and it is difficult to cover them all. Summary tables on the different parameters affecting biodegradation and its behavior under different conditions are necessary to identify gaps and unify observations.

1.3.2 Oxygen transport to the subsurface.

The magnitude of petroleum vapor intrusion depends on the source concentration, relative position of the building, building characteristics, soil matrix characteristics, chemical properties and the oxygen diffusive flux from the atmosphere to the subsurface (Lundegard et al., 2008).

Petroleum hydrocarbons degrade at relatively short distances (<1m) when the soil contains approximately 5 to 21% v/v of O₂ (Luo, 2009). Therefore oxygen flux to the subsurface is critical to decrease petroleum hydrocarbon vapor intrusion and determine the significance of bio-attenuation (Lundegard, et al. 2008).

Oxygen diffusion to the vadose zone might change in case of rain or snow. This study is not taking into account weather seasonal changes in the oxygen capacity of replenishment of the soil.

1.4 Previous Studies on the Fate and Transport of Petroleum Hydrocarbon Vapors

1.4.1 Experimental studies.

In order to develop an appropriate risk assessment for a site, a good understanding of the vapor transport behavior, the effect of physical soil characteristics, biodegradation kinetics and oxygen demands, as well as, the chemicals involved is necessary. Hence, a number of laboratory soil column experiments (Andre et al., 2009; Höhener et al., 2006; Höhener et al, 2003; Jin et al., 1994); bioreactors and microcosms (Baker et al., 2000; Höhener et al., 2003; Pasteris et al., 2002; Solano-Serena et al., 2000) and field studies (Davis et al., 2005; Lundegard et al., 2008; Luo et al., 2009;

Patterson et al., 2009; Roggemans et al., 2001) have been performed. Also, There is a number of studies observing the transport behavior and aerobic degradation of individual compounds (i.e. benzene, toluene) (Jin et al., 1994; Adams et al., 2003), however, Carroll, et al. (2009) observed that the migration behavior varies accordingly to the composition of the source, affecting the partitioning of the mixture and distribution in the soil. Thus, in order to understand the contaminant distribution, partitioning and aerobic degradation, multi-component mixtures should be studied. Only a few studies have observed the soil gas behavior of multi-component contaminants (Lahvis et al., 1999; Solano-Serena et al., 2000; Pasteris et al., 2001; Hohener et al., 2003; Broholm et al., 2005; DeVauil et al., 2007) and even fewer studies have observed the multi-components flux and biodegradation profiles under near steady-state conditions and their changes in different types of soils and/or lithological layouts (Batterman et al., 1995; Davis et al., 2005; DeVauil et al., 2004). Most of these studied vapor transport at near-steady conditions and they focused on the determination of degradation rate constants, with the first-order kinetics being the most commonly utilized (Andre et a., 2009; DeVauil et al., 2004; Lahvis et al., 1999; Pasteris et al., 2002). However, none of these studies focus on the gas behavior of individual chemicals in complex mixtures during transient state, near-steady state when there is no aerobic degradation occurring and only a few have studied the effect of the stratigraphic layers on the vapor concentration profiles and effluent flux with and without aerobic degradation reactions (Bozkourt et al, 2009). This can be of great importance since the stratigraphy of most spill sites is not homogeneous. Bozkourt et al. (2009) performed a simulation using a 3-dimensional finite element model to study howf soil layers with different physical characteristics affect the concentration profiles and vapor intrusion rates into buildings. Results suggested that soil gas profiles and flow patterns reflect the characteristics of the subsurface.

1.4.2 Mathematical models.

The use of screening mathematical models to predict vapor intrusion risks has been of great importance to date. They are used to estimate potential indoor impacts at sites, determine whether it is necessary to perform a site-specific assessment, develop cleanup target concentrations, and predict variations in the “site-specific” indoor air concentration or soil and groundwater concentrations due to site or chemical characteristics changes. The use of mathematical models is limited mainly due to the impracticability in many sites to do a physical assessment from the cost-effective point of view; which can go in excess of one million US dollars (Johnson, 2005).

One of the most widely-used models is the Johnson-Ettinger model (J&E model), which is recommended by the U.S. EPA vapor intrusion guidance (2002). The model is used as a “risk assessment screening-level tool” (Johnson et al., 1991) to assess potential indoor contamination levels that can result in vapor intrusion. The model extends some of the assumptions employed originally in radon vapor intrusion models to represent diffusive and advective transport of VOCs from a source. It is based on the assumptions that chemical or biological transformations are not significant, so biodegradation is not taking place. There are two contaminant transport mechanisms that contribute to the migration into the building: diffusion and advection. The diffusion mechanism is the dominant mechanism to transport vapors from the contamination source to the soil region near the foundation of the building. Advection is the mechanism that takes the vapor from the foundation through the cracks into the building due to pressure gradients. The model also assumes that the advective flow is uniform in the area close to the foundation (Johnson et al., 1991).

An evaluation of the Johnson and Ettinger model (J&E model) done by Johnson et al. (2002) determined that the model is capable of predicting reasonable values for the sites; however, there are uncertainties in the estimation of site-specific effective diffusion coefficients (Hers et al., 2003). It has also been noted that this model has been

reasonably successful in predicting chlorinated compound vapor intrusion (which are difficult to degrade) but it might overestimate the indoor air concentrations for petroleum hydrocarbon vapors since it does not take into account biodegradation (Devauill, 2002; Hers et al., 2003). Even if the J&E model was found conservative, the evaluations confirm that the model is reliable when recognizing its limitation and appropriate inputs are utilized such as cases where degradation is insignificant (Johnson et al., 2002; Hers et al., 2003).

With the intention of having less conservative results and address some of the restrictions of the J&E model, as well as determine degradation rate constants, other mathematical models have been proposed, among them are Lahvis et al. (1999) in which first-order degradation constants are calculated by calibrating the model to O₂ and CO₂ concentration data; Hers et al., (2000) in which the diffusion, sorption and biodecay as well as different kinetics can be simulated for the vadose zone; DeVauill (2007) which simulates steady-state conditions with constant chemical source concentration, homogeneous soils properties and diffusion dominated vapor transport. It also includes the estimation of first-order degradation rate constants. However, it neglects the attenuating effect of the buildings and foundations on the chemical vapor transport yielding higher estimations of indoor air concentration than scenarios where chemical attenuation due to the building is included. Davis et al. (2009) model is similar to that proposed in Roggemans et al. (2001) and it is based on the ratio of diffusion coefficients of oxygen and hydrocarbon vapors, the ratio of maximum concentrations of oxygen and hydrocarbon vapor, the depth to the maximum hydrocarbon source concentration and stoichiometric coefficients; Yu et al. (2009) developed a three-dimensional multi-phase compositional model (*CompFlow Bio*) that includes variable lateral offset between the source and foundation slab, variable footprint dimensions of the source zone and dual-monod aerobic degradation; Pennell et al. (2009) model is capable of simulating advective and diffusion transport, three-dimensional pressure, velocity and chemical

concentration profiles. Abreu et al. (2005) proposed a more complex numerical simulation. This is a transient, three-dimensional mathematical model including multi-component transient transport by advection and diffusion variable, lateral offset between the source zone and foundation slab, variable dimensions of the source zone, transient indoor and atmospheric pressure variations, a range of biodegradation kinetic expressions (zero-order, first-order and dual-Monod kinetics), heterogeneous soil lithology in which the air permeability and moisture content can be varied and flexibility for distributing the cracks anywhere across the foundation of the building in study. One of the objectives of the model is “to anticipate the relationships between vapor source-lateral separation, building construction, and indoor air impacts” (Abreu et al., 2005). This model was further extended by Luo (2009) to allow non-uniform pressure distribution and transient changes in indoor air quality. Also, new features were added in order to be able to study multi-source scenarios, the effects of wind and transient pressure and concentration changes on a heterogeneous geology site (Luo, 2009). This model was heavily tested with satisfactory results given its complexity (Luo, 2009).

1.5 Objective of the Soil Column Experiment

As explained above, there are a number of factors that influence the vapor intrusion pathway assessment such as, background concentrations, the use of non-site-specific attenuation factors to estimate indoor air concentration which can lead to errors due to spatial and temporal variability of the data, the existence of not identified preferential pathways, and biodegradation (ITRC, 2007; Tillman, 2005). Thus, in order to develop an appropriate vapor intrusion assessment, a good understanding of the compound-specific vapor transport behavior in the subsurface on a site is key, as well as the knowledge of factors affecting the vapor migration (source concentration, moisture content, biodegradation).

What is particularly of importance in vapor intrusion pathway assessment is the ability to interpret soil gas profile data, which requires understanding of how the soil gas profiles reflect subsurface conditions and processes. Hence, in this research the diffusive vapor transport and bio-attenuation of individual compounds from a multi-component petroleum vapor mixture were studied in 1.8 m experimental soil columns, with each column represented an idealized geological setting. The objective was to provide insight of the diffusive vapor migration of individual petroleum hydrocarbon vapors and their attenuation behavior for different stratigraphic scenarios in the vadose zone. Knowledge of compound-specific vapor transport and biodegradation can help in the interpretation of soil gas data, especially as it is used for the identification of risks during vapor intrusion assessments and decisions regarding mitigation.

CHAPTER 2

EXPERIMENTAL DESIGN

In this work, the diffusive vapor transport and aerobic bio-attenuation of individual compounds in complex petroleum vapor mixtures are being studied for idealized lithologies in 1.8-m tall laboratory soil columns. Six columns, representing different geological settings were prepared using 20-40 mesh sand (medium grained soil) and 16-minus mesh decomposed granite (fine-grained soil). Vertical vapor concentration profiles as well as, oxygen, carbon dioxide and hydrocarbon vapor concentration of each chemical are monitored over time.

The data allow determination of compound-specific times for steady profiles to be achieved and specific extents of bio-attenuation under aerobic surface conditions.

The experiment is conducted for three conditions: i) anaerobic condition, in which a 100% nitrogen (N₂) surface atmosphere condition is maintained; ii) aerobic condition, in which a 21% of O₂, 79% of N₂ surface condition is maintained; and iii) reduced vapor source concentration with the aerobic condition discussed above, in which the vapor source concentration is lowered ten times from original concentrations.

The experimental variables in this study are presented in Table 2.1.

Table 2.1

Experimental variables

Controlled	Measured
<ul style="list-style-type: none">- Vapor Source Concentration (typical weather gasoline)- Geological stratigraphy- Soil moisture content- Sweep gas oxygen concentration (surface atmospheric condition)	<ul style="list-style-type: none">- Pressure differential- Soil vapor diffusion coefficients- Soil temperature- Sweep gas humidity- Carbon dioxide and oxygen concentration profiles- Component concentrations profiles and emission rates

2.1 Experimental Apparatus

A schematic of the basic apparatus is shown in Figure 3.1. The columns are constructed from stainless steel pipe that is 1.8 m (6 ft) long by 10.2 cm (4 in) in diameter. They are sealed on both ends with 15.2-cm (6-in) cylindrical aluminum covers having a square base that are sealed to the column using four 12.7-cm (5-in) compression bolts with a rubber seal in between the cover and the ring to avoid any vapor leaks. A coarse stainless steel screen support with a fine stainless steel mesh screen sits within the base of the aluminum covers providing for a cavity between the soil and the bottom and the top of the covers. Along the length of the column, there are 17 stainless steel needle sampling ports (Pipetting needles blunt end standard hub 0.16"x4", Popper) coupled with three-way nylon Luer-type plastic valves (Kentos, Glass Company, Vineland, New Jersey). One sampling port is also installed at each cap (top and bottom) to monitor outlet and source concentrations. The needles are placed every 10.2 cm (4 in) along the column. Pressure and temperature are monitored every 20 min through pressure transducers (Omega) placed 8.9 cm (3.5 in) from the top and bottom and thermocouples installed at 8.9 cm (3.5 in) from the top, 90 cm (3 ft) from the bottom and 8.9 cm (3.5 in) from the bottom inside the soil columns. A humidified sweep gas is passed through the top cap of the column (N_2 or air) to maintain the soil moisture content constant through the experimental period. The humidity of the sweep gas is monitored every 20 min using an Omega data-logger.

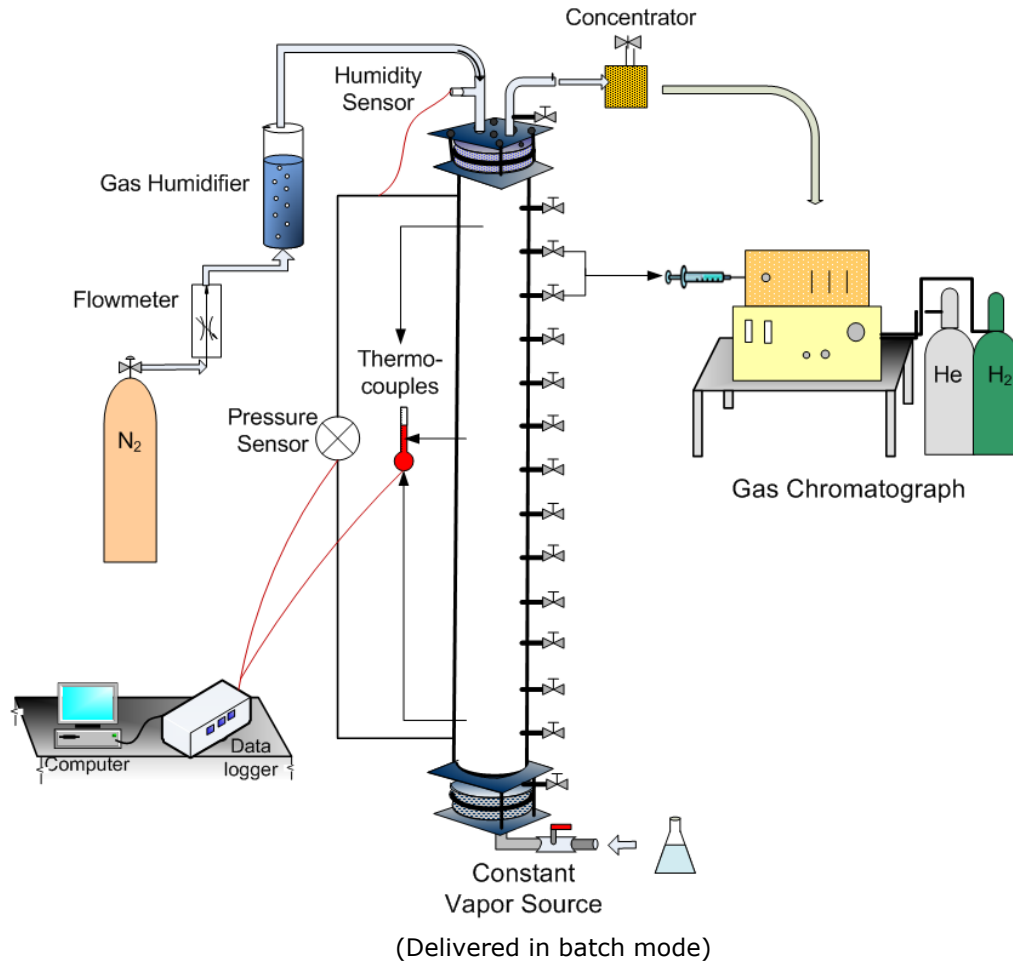


Figure 2.1. Soil column schematic

Gas samples were taken to measure the concentrations of the hydrocarbon compounds, as well as carbon dioxide (CO_2), O_2 and methane (CH_4); the latter was measured only during Phase I. During the start-up of the columns, the transient period was monitored by taking samples from the effluent of the columns every 2 to 4 h. Once near-steady conditions were reached, the effluent was monitored once a day for approximately 80 days; after which, the effluent was sampled every three days. Vertical soil gas profile snapshots were performed every three to four weeks. The samples were analyzed using a gas chromatograph (SRI 8610C, SRI instruments) equipped with a flame ionization detector (FID), a 60 m RTX-I stainless steel column (Alltech Associates,

Inc., Deerfield, IL, USA), and a thermal conductivity detector (TCD) with a CTR I stainless steel column 6'x1/4"x120" (Alltech Associates, Inc., Deerfield, IL, USA) (GC-TCD-FID) to determine hydrocarbon, and carbon dioxide, oxygen and nitrogen concentrations respectively. Samples are injected into a sampling loop that carries the gas into the GC columns (0.5 ml loop for the FID and 1.0 ml loop for the TCD). The carrier gas is helium (He) at a flow of 20 cm³/min. The minimum detection limit for the FID and TCD detectors are 0.001 mg/L for the hydrocarbon compounds and 1% and 0.2% v/v for O₂ and CO₂, respectively. The GC temperature program is set at 40°C for 2 minutes and then is ramped up at 15 °C/min until it reaches 200°C, where it is maintained for 2.5 minutes.

During the aerobic phases of the experiment (Phases II and III), some of the effluent hydrocarbon concentrations dropped below the GC detection limit; therefore, a Thermal Desorber (TD) sample concentration unit was utilized. Effluent gas samples were collected into a 1-L tedlar bag, and then the gas was pulled from the bag into sorption tenax tubes (Marks International) with a peristaltic pump (Cole-Parmer) operated at a flow of 50 mls/min. The tubes are desorbed in a Unity Thermal Desorber (Markes International). The apparatus is equipped with a cold trap U-T8CUS (Markes Internations) that contains 10 mmQuarz wool, 15 mm Carbopack C, 15 mm Carbopack B, and 20 mm Carbosieve SIII. The thermal desorption unity is in line with a gas chromatograph – mass spectrometry (GC-MS) (5890 HP GC and 5972 HP MS) to analyze the gas desorbed from the cold trap. The tubes are desorbed utilizing the program shown in Table 3.2. The GC-MS is equipped with a Rtx-VGC 60 m column with 0.25 in of internal diameter. The carrier gas is He at 1 ml/min flow rate. The GC oven temperature is held at 40°C for 2 minutes and ramped up at 15 °C/min until it reaches 240°C where is held for 2 minutes.

Table 2.2

Parameters utilized for tube desorption

Unity Function		Setting
Prepurge time		1.0 min.
Tube purge time		1.0 min.
Tube desorption	Temperature	290 °C
	Time	20.0 min.
	Split flow	20 ml/min
Cold Trap	Sorption Temperature	0.0 °C
	Sorption hold	5.0 min
	Desorption Temperature	300 °C
	Desorption time	20 min
	Split flow	20 ml/min
	Transfer line temperature	180 °C

2.2 Stratigraphic Layout

Six soil columns representing different geological settings were prepared using two types of soils: 20-40 mesh sand (medium-grained soil) and 16 minus-mesh crushed granite (fine-grained soil). The soils were chosen based on their helium effective diffusion coefficients when containing 2.5% v/v of moisture content in the case of the sand and 11% v/v for the granite; allowing in this manner, the study of vapor gas profiles through soils with different physical characteristics. In this case, the sand has the highest helium diffusion coefficient ($0.1 \text{ cm}^2/\text{s}$) and the granite has the lowest one ($0.06 \text{ cm}^2/\text{s}$).

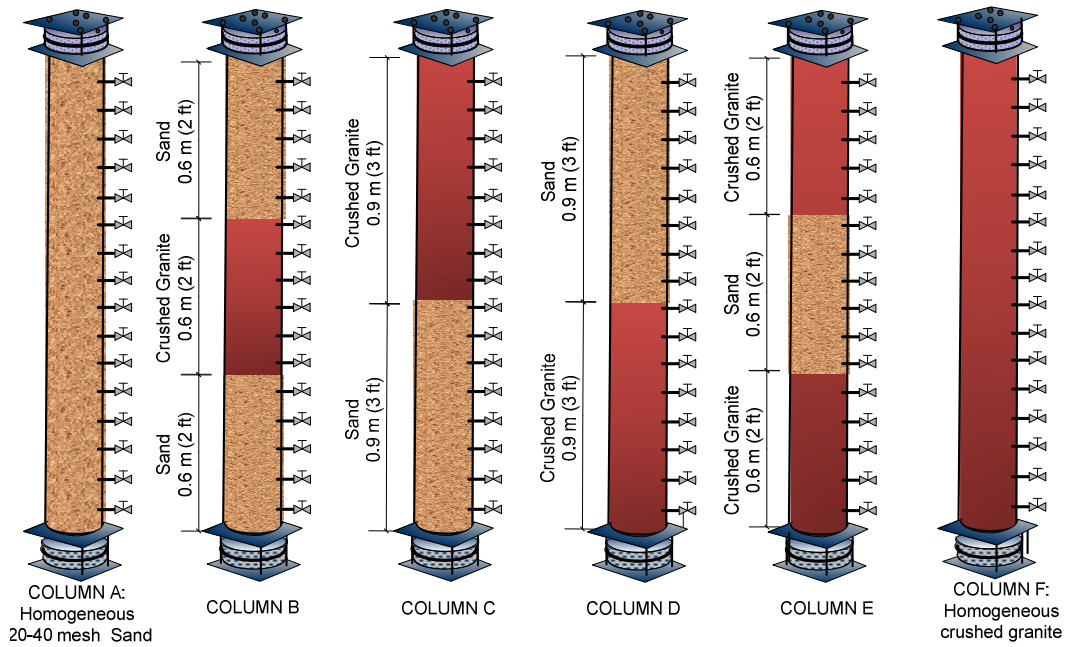


Figure 2.2. Lithologic layout schematic

2.3 Soil Characterization

As mentioned above, two types of soils were used to pack the columns: 20-40 mesh sand and 16-minus mesh crushed granite. As stated by Johnson et al (2005), in order to have a good characterization of a site, it is necessary to determine the soil characteristics that affect the vapor profile. Thus, soil bulk density, moisture content, organic carbon content, permeability and helium effective diffusion coefficients were determined prior to packing the columns. A description of the methodology used are summarized in Table 2.3. A detailed description of each method can be found in Appendix I.

Table 2.3.

Summary of the soil characteristics and analytical methods employed

Parameter	Units	Instruments	Method	Citation
Moisture Content	g-H ₂ O/ g-soil	- Analytical balance - Oven at 110 °C	Standard test methods for laboratory determination of water (moisture) content of soil and rock by mass	ASTM D2216-05
Bulk Density, ρ_b	g-soil /cm ³ -total	- Scale - Volumetric container	Weight of a known volume of soil	-
Fraction of Organic Carbon (FOC)	100 x g-oc/ g-soil	- Analytical balance - Furnace at 350 °C	Loss of ignition method (LOI)	Schumacher, 2002 (EPA)
Permeability	cm ²	- ASU permeater	An air flow is passed through a cylinder containing the compacted soil sample with a controlled flow and the pressure differential is measured $K = \frac{(Q/A) \times \mu \times L}{\Delta P}$	Luo, 2009
Total Porosity (ϕ_T)	cm ³ voids/ cm ³ -soil	- Burette - 4 in. PVC pipe with sampling port at the bottom (soil column, Figure 1.3 in Appendix I)	- Water saturation method: water is introduced from at the bottom of a soil column by gravity until soil is saturated. $\phi_t = V_{\text{water}}/V_{\text{soil}}$ - Calculation from the specific gravity (G_s): $\phi_t = 1 - (\rho_b/G_s)$	Clifton, 2008; ASTM D-854
Effective Diffusion Coefficient (D^{eff})	cm ² /s	- Soil column with sampling port in the middle - Gas Chromatograph with TCD (N ₂ as carrier)	Johnson et al. (1998) protocol. Tracer gas = Helium Volume injected = 0.4 ml Volume withdrawn = 5 ml Diffusion time = 15 s	Johnson et al., 1998

2.4. Oxygen leak tests.

Oxygen leak tests were performed prior to packing the columns. As explained above, anaerobic conditions are maintained in the columns during the first phase of the experiment, any gas exchange between the column and the atmosphere would introduce

significant errors to the experiments. Thus, two tests were performed to determine if leaks were occurring:

i. Column pressurization.

Nitrogen was injected into the columns until a pressure of 3 – 4 psi was reached. The columns were then leak checked using snoop (Swagelok) at every union and sample port. Any leaks detected were addressed by tightening the unions or replacing the pieces involved. The columns were then re-pressurized to 4 psi and left pressurized for 24 hours to check if the columns maintained the pressure. Once the columns were able to maintain a constant pressure, the second leak test was performed.

ii. O₂ flow rate into the columns.

The objective of this test is to determine the flux of O₂ that the columns might have during the experimental period. The test consisted of flushing the empty columns with N₂ for 10 minutes, after which, they were sealed and the pressure was released in order to have atmospheric pressure conditions inside the columns. Three ports, two at the ends and one in the middle of the columns were sampled daily for a week and analyzed for O₂. The gas sample analyses were performed using a SRI 8610C GC-TCD with a CTR I stainless steel column 6'x1/4"x120" (Alltech Associates, Inc., Deerfield, IL., USA). The O₂ concentrations were plotted against time (Figure 2.5) and from them, the O₂ leak rates into the columns in mg/s were obtained using equation 2.1 (Table 2.4). The resultant flow rates were then compared against the O₂ flow rates necessary to completely oxidize the hydrocarbons that the columns were going to contain (Table 2.5). These were calculated using Fick's First Law and a stoichiometry expression as shown in equations 2.2, 2.3 and 2.4.

$$F_{O_2} \left[\frac{mg}{s} \right] = \frac{F_{O_2} \left[\frac{\%v/v}{d} \right] \times V_{column}}{\rho_{O_2} \times x} \cdot \left(1000 \frac{mg}{g} \right) \cdot \phi_T \quad (2.1)$$

Where,

F_{O_2} = Oxygen flow into the column

V_{column} = Volume of the empty soil column

ρ_{O_2} = Oxygen density = 1.429 g/L

ϕ_T = Total porosity [cm^3 -voids/ cm^3 -soil]

$$F_i = D_i^{eff} \left(\frac{\Delta C}{L} \right) \cdot A_c \quad (3.2)$$

$$D_i^{eff} = D_{He} \cdot \frac{D_i^{air}}{D_{He}^{air}} \quad (3.3)$$

$$F_{O_2} = \frac{F_i \cdot \left(\text{stoichiometric relation} \frac{\text{mol } O_2}{\text{mol } i} \right) \cdot MW_{O_2}}{MW_i} \quad (3.4)$$

Where,

F_i = Flow of compound i [mg/s]

D_i^{eff} = Effective diffusion coefficient of component i [cm^2/s]

ΔC = Concentration gradient along the length of the column [mg/L] -

Concentration at the source minus the concentration at the top which is very small = ~ 0)

D_{He} = Diffusion coefficient of helium [cm^2/s] (determined by the diffusion coefficient test)

D_i^{air} = Diffusion of compound i in air [cm^2/s]

D_{He}^{air} = Diffusion coefficient of helium in air [cm^2/s]

MW_{O_2} = Molecular weight of oxygen [g/mol]

MW_i = Molecular weight of compound i [g/mol]

Tables 2.4 and 2.5 showed that the flow of oxygen that entered the columns was lower than the flow necessary to oxidize each one of the hydrocarbons in study; therefore, it was concluded that the soil columns were sealed.

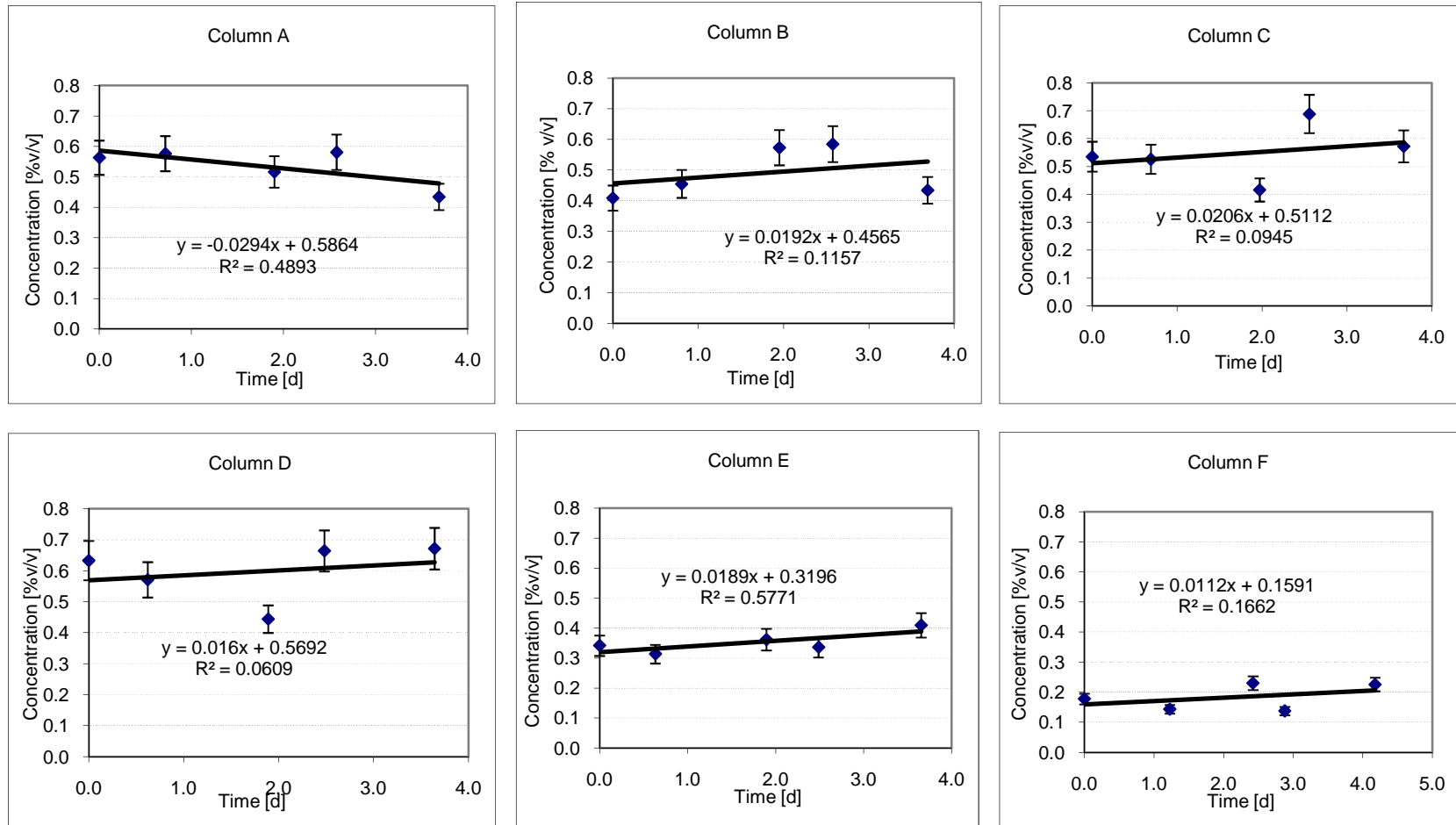


Figure 2.3. O₂ Concentration vs. Time (O₂ leak test)

Table 2.4

Oxygen flow into the empty soil columns (calculated using equation 2.1)

Column	Slope O ₂ conc. vs time %/v/d	Assuming sand total porosity, mg/s	Assuming crushed granite total porosity, mg/s
A	-0.0294	0.00	0.00
B	0.0192	1.69E-05	1.93E-05
C	0.0206	1.81E-05	2.07E-05
D	0.016	1.41E-05	1.60E-05
E	0.0189	1.66E-05	1.90E-05
F	0.0112	9.86E-06	1.12E-05

Table 2.5

Oxygen flow rate necessary to completely oxidize the hydrocarbons in the soil columns

Chemical	O ₂ flow, mg/s	
	Sand	Crushed Granite
Pentane	2.40E-03	1.30E-03
2-methyl-2-butene	8.52E-04	4.61E-04
MTBE	8.55E-05	4.63E-05
Hexane	6.92E-04	3.75E-04
Benzene	1.17E-04	6.36E-05
Cyclohexane	5.37E-04	2.91E-04
Iso	4.75E-04	2.57E-04
Heptane	2.10E-04	1.14E-04
Toluene	1.60E-04	8.67E-05
p-xylene	8.34E-05	4.52E-05
Octane	5.76E-05	3.12E-05
1,3,5-trimethylbenzene	1.46E-04	7.92E-05
Total	5.82E-03	3.15E-3

2.5 Packing the Columns

As discussed above, the desired soil moisture condition was created before placing the soils into the columns. To do this, distilled (DI) water was added to the soils until the desired moisture content was reached (2.5% for the sand and 11% for the crushed granite). The soils and DI water were mixed using a cement mixer (see Figure 2.4). The columns were then packed by pouring the soil into the stainless steel pipe using small buckets. After a bucket was poured down the soil was tightly packed inside of the column by compressing it down by dropping a weight attached to a rope repeatedly (Figure 2.5).

To create the different soil layers, the soil level (sand or crushed granite) was measured after a bucket of soil was poured and compressed. Once the soil was at the desired level, the other type of soil was poured down the pipe following the same procedure. Once the column was tightly packed, the column was closed and the sampling needles were inserted into the column.



Figure 2.4. Moisturizing and mixing the soil



Figure 2.5. Column packing (compressing down the soil)

2.6 Vapor Hydrocarbon Source

2.6.1 Source composition.

The hydrocarbon vapor source is liquid composed of 12 petroleum hydrocarbons. The source was designed so it generates vapor concentrations representative of weathered gasoline. Table 2.6, 2.7 and 2.8 show the mass fraction and composition of the solution utilized as a vapor source and its comparison to the weathered gasoline mass fraction and composition published by Johnson et al (1990).

Table 2.6

Experimental mass fractions and their comparison to weathered gasoline mass fraction reported by Johnson et al. (1990)

Chemical	Formula	Density [g/ml]	Molecular Weight [g/mol]	Mass Fraction in Weather Gasoline (Johnson et al. 1990)	Experimental Mass Fraction	Mass in 50 g of liquid [g]	Volume per 50 g of liquid [mL]
Pentane	C ₅ H ₁₂	0.626	72.2	0.022	0.018	0.88	1.46
2-methyl-2-butene	C ₅ H ₁₀	0.662	70.1	0.012	0.010	0.48	0.86
MTBE	C ₅ H ₁₂ O	0.742	88.2	0.012	0.010	0.48	0.11
Hexane	C ₆ H ₁₄	0.659	86.2	0.03	0.024	1.20	3.86
Benzene	C ₆ H ₆	0.879	78.1	0.008	0.006	0.32	0.29
Cyclohexane	C ₆ H ₁₂	0.779	84.2	0.05	0.040	2.00	3.79
Heptane	C ₇ H ₁₆	0.683	100.2	0.12	0.096	4.79	4.88
Toluene	C ₇ H ₈	0.865	92.1	0.028	0.022	1.12	2.17
p-xylene	C ₈ H ₁₀	0.87	106.2	0.025	0.020	1.00	2.49
Octane	C ₈ H ₁₈	0.703	114.2	0.025	0.020	1.00	3.97
1,3,5-trimethylbenzene	C ₉ H ₁₂	0.864	120.2	0.22	0.176	8.79	7.27
Mineral Oil	-	0.84		0.7	0.559	27.96	33.2801
TOTAL			100.0 (AVG)	1.252	1.000	50.00	61.8442

Table 2.7

Vapor source composition compared to weathered gasoline

Compound	Alkanes	Cycloalkanes	Alkenes	Aromatics	Total
Mass fraction in weathered gasoline vapor (Johnson et al.,1990)	63.87	14.60	16.57	4.96	100.00
Mass fraction measured in headspace above hydrocarbon mixture in experimental batch	63.90	14.33	16.85	4.92	100.00

Table 2.8

Carbon No. comparison to weathered gasoline

Compound	<C3	C3-C6	C6-C9	≥C9	Total
Mass fraction in gasoline (Johnson et al.,1990), %	0.00	3.14	61.77	35.09	100.00
Mass fraction in experimental liquid, %	0.00	3.67	22.84	73.48	100.00

2.6.2 Source concentration changes.

After the aerobic conditions phase of the experiment was run for approximately 110 days, the source vapor concentration was decreased by 10X. Table 3.9 shows the volumes added to the batch mixture in order to create the vapor source for experimental phase III.

Table 2.9

Hydrocarbon volumes added to the vapor source liquid used in Phase III

Chemical	Volume per 50 g of source NAPL, ml
N-Pentane	0.1
2-methyl-2-butene	0.08
MTBE	0.01
N-Hexane	0.4
Benzene	0.03
Cyclohexane	0.4
N-Heptane	0.5
Toluene	0.2
p-xylene	0.2
N-Octane	0.4
1,3,5-trimethylbenzene	0.7
<i>Mineral Oil</i>	60
TOTAL	61.8442

2.6.3 Hydrocarbon vapor source preparation and replacement in the columns.

The hydrocarbon vapor source liquid was prepared in a 125 ml container with a septum cap at room temperature. Hydrocarbon chemicals in the liquid phase were added to 33.28 mL of mineral oil as presented in Table 3.6. Mineral oil was used as a base since the liquid hydrocarbons mix well in it and easily volatilize from it. Once the solution is made, the pressure inside the bottle is released to equalize it to atmospheric pressure and it is mixed with a stir bar on a stir plate for 10 minutes before a quality check analysis is performed. Since the vapor source in the columns should be constant, the concentration of the mixture is checked by injecting a sample of the source headspace into the GC-FID. The concentration of each chemical was verified to be in the ranges shown in Table 3.10 before it was placed at the bottom of the columns.

The vapor source mixture is placed at the bottom of each column after first removing the previous solution by pulling the oil out with a glass syringe through a ball valve on the bottom cap. Once the previous mixture has been removed, the new batch is injected through the same ball valve into the bottom cap cavity using a 60-ml glass syringe at ambient temperature and pressure conditions. The solution was replaced approximately every two and half weeks with monitoring in between, to ensure that the vapor source was constant during the experiment. It was determined from preliminary column studies that the vapor source is reduced by about 13% for the most volatile compounds (i.e. n-pentane, 2-methyl-2-butene, MTBE) and 6% for the heavy compounds (i.e. Toluene, n-octane, p-xylene) in 20 days. These percentages fall within the tolerance range for the experiment.

Table 2.10

Concentrations of hydrocarbon compounds above source liquid

Hydrocarbon	Concentration [mg/L]	Concentration 10 Times Lower, mg/L
n-Pentane	103.2 ± 2.6	11.0 ± 1.3
2-Methyl-2-Butene	38.1 ± 1.1	4.7 ± 0.7
MTBE	5.2 ± 0.8	0.4 ± 0.2
n-Hexane	36.2 ± 1.3	7.1 ± 0.2
Benzene	5.7 ± 0.3	0.5 ± 0.02
Cyclohexane	26.3 ± 1.3	6.0 ± 0.2
Iso-Octane	28.8 ± 1.7	4.3 ± 0.2
n-Heptane	12.0 ± 0.5	2.5 ± 0.4
Toluene	8.1 ± 0.5	0.8 ± 0.1
n-Octane	3.7 ± 0.4	0.5 ± 0.1
P-Xylene	2.5 ± 0.3	0.3 ± 0.1
1,3,5-Trimethylbenzene	4.6 ± 1.3	0.5 ± 0.1

Note: These ranges were obtained by performing three different mixture batches and analyzing them three times. The numbers shown in Table 3.8 are the averages and standard deviations of the results.

2.7 Temperature and Pressure Differential in the Columns

As stated before, the objective of the experiment is to study diffusive vapor transport in the subsurface; thus, to ensure that no other type of transport occurs, the pressure differential along the length of the soil column has to be zero; even a slight pressure differential can generate advective transport which would introduce significant errors in the experimental results. Thus, to ensure that diffusion was the only transport, the pressure differential along the length of each column was monitored at all times through pressure transducers. Each column had one pressure transducer that measured the pressure differential between the top and bottom of the columns. Data from the pressure transducers was being recorded by a data logger (Omega) every 20 minutes. Also, to avoid pressure changes when replacing the vapor source solution in the bottom of the column, valves were installed in the sweep gas flow lines so that the pressure at both ends of the column would be equilibrated when replacing the vapor source. Temperature conditions also ideally need to be kept constant, but column temperatures were dependent on the ambient room temperature. The temperature was monitored through thermocouples placed at the top, middle and bottom of the columns. The soil columns are exposed to temperatures of $25 \pm 5^{\circ}\text{C}$. A change of 5°C in the ambient temperature produced an approximate change of 0.5% in the hydrocarbons vapor concentrations.

2.8 Sweep Gas Flow

A humidified sweep gas flow is passed across the top of the column at a flow of approximately 12 ml/min. To minimize loss of moisture from the columns, the gas flows from a gas cylinder to a PVC column filled with water (humidifier) where it is humidified to about 60% to avoid water condensation at the top cap in case there are room temperature changes. From the humidifier, the gas flows across the top of the column where it is mixed with hydrocarbon vapors diffusing out of the soil. The stream is then

directed to the fume hood. A humidity sensor (HM1500LF, Measurement Specialties Inc.) is placed in the outlet pipe to monitor the humidity of the gas stream. The humidity of the columns ranged from 58% to 63% during the experimental period. A schematic of this process is presented in Figure 2.6.

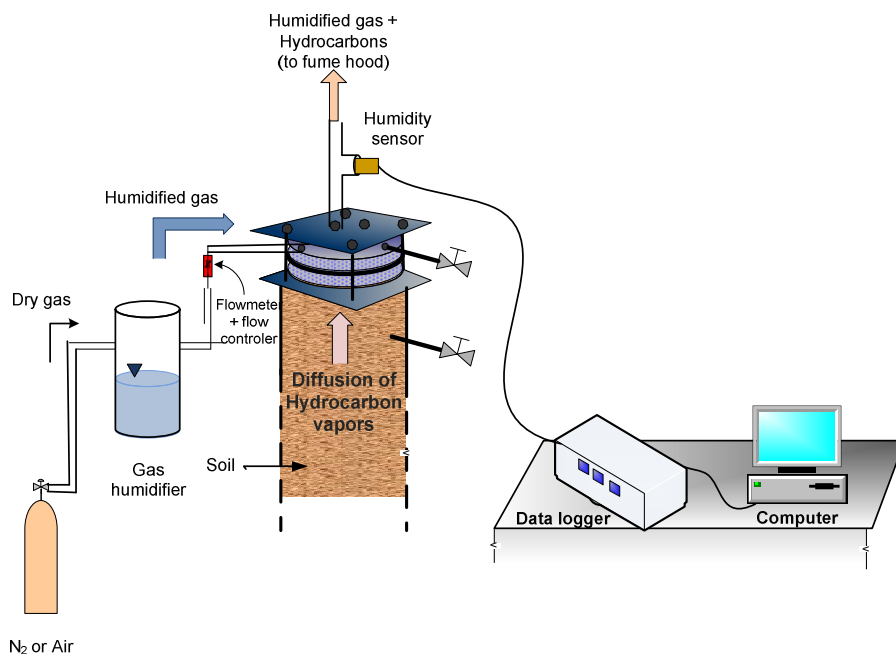


Figure 2.6. Sweep gas flow schematic

As noted in section 2.1, in experimental Phase I nitrogen is used as a sweep gas mimicking soil deep zones where oxygen is not available and steady conditions are maintained; and in Phase II, aerobic conditions in which the sweep gas is air, simulating surface conditions; and Phase III, air is also used as sweep gas; however, the vapor source concentration is lowered by 10X from the original concentration.

2.9 Shutting Down the Soil Columns

Experimental Phase III (10X lower vapor source concentration) was run for approximately 150 to 300 d depending on the soil column. Once the normalized mass flux emissions of most of the chemicals achieved near-steady conditions the soil columns

were shut down. After this, different tests were performed before and after opening each column with the objective of determine the final state of the soil and column and compare them with the initial experimental conditions.

2.9.1. Tests performed before opening the soil columns.

i) Effective diffusion coefficient test.

This test was performed when the columns were initially packed and immediately before they were opened. The procedure used was the Johnson et al. (1998) protocol described in Appendix I. The tracer gas used was helium, the volume injected was 0.4 ml and the volume withdrawn was 5 ml. The time to allow diffusion was 15 s. Results from this tests help determine changes in the soil physical characteristics.

ii) Permeability profile.

The permeability profile of the soil columns was calculated using equation 3.5.

$$K = \frac{(Q/A) \times \mu \times L}{\Delta P} \quad (3.5)$$

Where:

K = Air permeability [cm²]

Q = Air flow rate at the effluent of the soil column [cm³/s]

A = Cross-sectional area [cm²]

μ = Air dynamic viscosity at ambient air [1.8x10⁻⁵ Pa.s]

L = Length of the soil column [cm]

ΔP = Pressure differential in the soil column [Pa]

A controlled low air flow was passed from the bottom to the top of the columns during a short period of time (35 to 40 min) to avoid drying out the soil inside the column. The pressure differential between every two sampling ports (10.2 cm or 4 inch) along the length of the column was measured with an electronic pressure sensor connected to a

data logger (Omega) system. The pressure sensor was calibrated as in Luo (2009). The air flow rate at the effluent of the column was determined by collecting the effluent gas in a 10-L tedlar bag while the pressure differentials were being measured; the rate was calculated by dividing the collected gas volume over the collection time (V/t).

2.9.2 Tests performed after opening the soil columns.

Once the diffusion coefficient and permeability tests were performed, the columns were opened and soil core samples were taken every 6 inches as illustrated in Figure 2.7. Moisture content, fraction of organic carbon, and the number of colony forming units (CFU) of aerobic heterotroph bacteria and hydrocarbon degraders per gram of soil were determined for each sample. The soil core samples were taken using 1 inch copper tubing which were previously autoclaved for 20 minutes in order to take samples to be used for microbial analyses. Figure 2.8, shows the device utilized to take the soil sample cores.

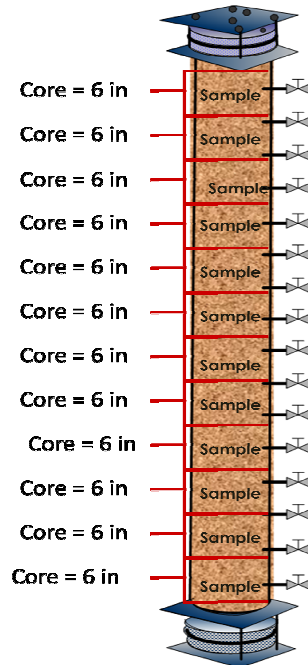


Figure 2.7. Column shut down sampling intervals

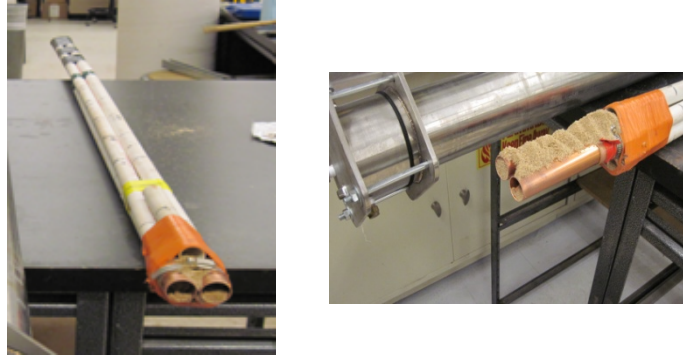


Figure 2.8. Sampling device and soil cores

i) Moisture content and fraction of organic carbon.

The moisture content and fraction of organic carbon of each core sample was determined gravimetrically as is explained in Appendix I.

ii) Microbial analyses.

In order to determine the population of heterotrophs and hydrocarbon degraders, as well as the amount of bacteria 16S rRNA genes present in the soil along the length of the soil columns, a number of microbial analyses were performed; these are listed in Table 2.11

Table 2.11

Microbial analyses

Analysis	Method
- Colony forming units (CFU) of aerobic heterotrophic bacteria (AHB)	Plating technique in tryptic soy agar (TSA)
- Petroleum hydrocarbon degrader counts	Most probable number method using Bushnell-Haas broth. N-hexane and benzene as carbon source
- Number of genes per gram of soil	Quantitative real time polymerase chain reaction (qPCR)

Plating technique

One gram of soil was added to 9 ml of phosphate buffered solution (PBS). The mixture was shaken on a shaker table for an hour in order to dislodge the bacteria into the media. Then, eight tenfold serial dilutions were made of the aqueous extract. The dilutions were then plated in tryptic soy agar (BD). The plates were incubated at room temperature for 4 to 5 days.

Most probable number (MPN)

Two grams of soil were added to 18 ml of Bushnel-Haas broth contained in a 30-ml serum bottle. The mixture was placed on a shaker table for one hour to dislodge the bacteria into the media. Then, nine tenfold dilutions were made in Bushnel-Haas broth. After diluting, 0.04 μ L of n-hexane and benzene liquid were added as carbon sources so their final concentration in the serum bottles ranged from 1 to 2 mg/L. The serum bottles were sealed and incubated at room temperature for 30 days.

To determine the CFU/g-soil, the concentration of n-hexane and benzene was measured at the beginning and at the end of the incubation period. The criteria used to determine presence of degraders was 90% of hydrocarbons disappearance. For example, if the serum bottle containing 10^{-6} dilution showed n-hexane or benzene concentrations higher than 10% of the initial value, then the concentration of degraders is 10^5 CFU/g-soil.

2.10 Quality Assurance and Quality Control

To ensure the quality of the data and to be confident in their accuracy, several measures were taken before and during the experimental period; such as performing oxygen leak tests in the columns prior to packing them (section 3.4), checking the quality of the hydrocarbon vapor source before placing it in the column (section 3.5), making sure that the pressure differential along the column remained zero (section 3.6) and calibration of instruments.

2.10.1 Apparatus.

i) GC-FID-TCD and TD-GC-MS.

The hydrocarbon and oxygen concentration analyses are performed using a GC-FID-TCD and TD-GC-MS apparatus. To ensure the quality of the analyses the machines are calibrated weekly. Also, the calibration is checked at the beginning and end of the monitoring periods. At the same time, duplicate samples were run every 10 samples as a quality control measure. The error determined ranged from 5 to 15%.

The error in the injection technique was also measured by making seven injections of the same concentration in the GC. The injection error obtained was 2%.

ii) Pressure transducer and data logger.

The pressure transducers of each column were calibrated at the beginning of the experiment. Each device was zeroed every three days to make sure of its proper functionality.

CHAPTER 3

RESULTS AND DISCUSSION

PHASE I: OXYGEN DEPLETED CONDITIONS

Petroleum hydrocarbon vapor transport through soil depends on different factors including physical and chemical properties of the vapor components; oxygen concentrations; soil physical properties such as temperature, moisture content, porosity and gas permeability. The objective of the first phase of this experiment was to determine individual compounds times to reach near-steady conditions and determine the vapor distribution and transport through different lithologies when there is no aerobic degradation reactions. In order to maintain anaerobic conditions, nitrogen was used as sweep gas at the top of the soil columns. Carbon dioxide, oxygen and methane concentrations were monitored periodically to verify that no anaerobic or aerobic biodegradation occurred during this period. Vapor mass emissions at the effluent and concentration and diffusion coefficient profiles were monitored with time on a chemical by chemical basis. Experimental results for this phase are presented in this chapter.

3.1 Soil Characterization

As described in Section 2.5, prior to packing the columns, the soils were characterized by measuring the parameters shown in Table 3.1. The difference in the physical characteristics of these two types of soils was necessary in order to later simulate diffusive vertical vapor transport through layered settings.

Table 3.1

Soil characteristics measured prior to packing the soil columns

Parameter	Sand	Granite
Bulk density ρ_b [g soil/cm ³ soil]	1.68 ± 0.01	1.73 ± 0.01
Total porosity ϕ_T , [cm ³ voids/cm ³ soil]	0.36 ± 0.01	0.41 ± 0.05
FOC % [g-OC/g-soil x 100]	0.13 ± 0.025	2.3 ± 0.06
Plasticity Index	No plasticity	6.9 ± 0.2
Air permeability (dry) [cm ²]	1.02x10 ⁻⁷ ± 1.97x10 ⁻⁹	3.20x10 ⁻⁹ ± 1.18x10 ⁻¹⁰
Helium effective diffusion coefficient (dry) [cm ² /s]	0.120 ± 0.018	0.100 ± 0.004
Moisture Content [% w/w]	2.5±0.08	10.97±0.12
Air permeability (at moisture content) [cm ²]	1.53x10 ⁻⁷ ± 1.13x10 ⁻⁸	2.10x10 ⁻¹⁰ ± 2.72x10 ⁻⁹
Helium effective diffusion coefficient (at moisture content) [cm ² /s]	0.104±0.009	0.067±0.005

3.2 Times to Reach Near-Steady State Conditions

Knowledge of the time required for soil gas profiles to reach near-steady state conditions is important when making decisions involving potential future impacts on a site and risk prediction since vapor concentrations may still be increasing or varying with time (API, 1998). The time necessary to reach near-steady conditions depends on the distance from the source, chemical properties of the compound in study (i.e. Henry's Law constant), and conditions such as the presence of surface barriers (pavement, buildings, etc.) or the stratigraphic layout of the subsurface.

Once the columns were packed, the vapor source was placed at the bottom of the columns and the effluent mass emissions were monitored. The monitoring frequency was every two to four hours for approximately 3 days, after which, it was switch to every eight hours until the emissions showed little to no increase and near-steady conditions were achieved. A chemical was considered to have reached near-steady conditions once the ratio of the slope of the emissions vs. time over the average of 3 days of data was not

changing more than one standard deviation of the data variability (See equation 3.1).






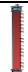
Results are given in Table 3.2.

$$\frac{\text{Slope}(\text{mass emissions}/\text{time}[3 \text{ d}])}{\text{Average of emissions } [3 \text{ d}]} = 0 \quad (3.1)$$

Table 3.2 shows that n-pentane, 2-methyl-2-butene, n-hexane, cyclohexane, iso-octane (2,2,4-trimethylpentane) and n-heptane were the first chemicals to reach near-steady conditions in all of the columns. Note that these chemicals have high Henry's Law constants and low solubilities. Other hydrocarbons such as MTBE, p-xylene and 1,3,5-trimethylbenzene (with lower Henry's Law constants), near-steady conditions were not reached even after running the experiment for 200 d. Differences in the individual times to reach near-steady conditions across the columns depended on the lithology of the soil column; thus, the columns composed with higher amounts of crushed granite (finer-grained soil) were expected to take longer to reach near-steady conditions. The order at which the columns were expected to achieve steady conditions were A<B<C<D<E<F; however the order observed was A<E<D<C<B<F. This might be due to differences in packing of the soils inside the columns.

Table 3.2

Time to reach near-steady state conditions for each chemical in each soil column

Component \ Column	Time, d					
	A - 	B - 	C - 	D - 	E - 	F - 
n-Pentane	8	22	23	11	9	31
2-Methyl-2-Butene	8	27	29	14	9	39
MTBE	44	Transient state >200 d	Transient state>200 d	Transient state>200 d	Transient State>200 d	Transient state> 200 d
n-Hexane	14	26	29	9	13	32
Benzene	12	Transient state>200 d	44	26	53	Transient state>200 d
Cyclohexane	13	31	24	16	13	32
Iso-Octane	7	34	29	18	18	33
n-Heptane	13	27	30	22	20	39
Toluene	30	Transient state >200 d	85	26	56	Transient state>200 d
n-Octane	19	73	44	36	22	49
P-Xylene	47	Transient state >200 d	Transient state>200 d	Transient state>200 d	71	Transient state>200 d
1,3,5-Trimethylbenzene	62	Transient state >200 d	Transient state>200 d	Transient state> 200 d	Transient state>200 d	Transient state>200 d

In order to determine if the results were consistent with theoretical values, the expected times to reach near-steady state were calculated using equations 3.2, 3.3 and 3.4 (API, 1998). The calculated times were compared with experimental results. This comparison is presented in Table 4.3.

$$T_r = \frac{R \cdot \phi_v \cdot L^2}{D^{eff}} \quad (3.2)$$

$$R = \left(1 + \frac{\phi_m}{H_i \cdot \phi_v} + \frac{K_i \cdot \rho_b}{\phi_v \cdot H_i} \right) \quad (3.3)$$

$$K_i = K_{oc} \cdot f_{oc} \quad (3.4)$$

Where,

T_r = Estimated time to reach near-steady conditions [d]

R = Retardation factor [unitless]

ϕ_v = Soil vapor filled porosity [cm^3 -vapor/ cm^3 -soil]

ϕ_m = Soil water filled porosity [cm^3 -water/ cm^3 -soil]

L = Soil column length [cm]

D^{eff} = Vapor effective diffusion coefficient [cm^2 /s]

H_i = Henry's law constant [cm^3 -water/ cm^3 -vapor]

K_i = sorption coefficient [L-water/Kg-soil]

K_{oc} = sorption coefficient to organic carbon [L-water/Kg-organic carbon]

f_{oc} = fraction of organic carbon [g-organic carbon/Kg soil]

Results of the comparison of theoretical and experimental times (Table 3.2) showed that Column A was the only column in which both times agreed; the rest of the columns show differences in the numbers, being the time calculated theoretically higher than the one obtained experimentally. This is due to discrepancies between the effective diffusion coefficient and soil porosities calculated from the theory vs the actual ones in the columns. Nevertheless, it is important to note that even though the times calculated theoretically are higher than the experimental times, n-pentane, 2-methyl-2-butene, n-

hexane, cyclohexane, iso-octane and n-heptane are in all the cases the chemicals expected to reach near-steady conditions before the rest of the compounds. Chemicals that did not reach near-steady conditions during the experimental period for Phase I (after 200 days) had theoretical expected times from approximately 10 months to several years. Therefore, it can be concluded that the experimental results were consistent with the theory.

Table 3.3

Comparison between the theoretical expected times to reach near steady state conditions and times obtained experimentally (Columns A, B, C)

Chemical	COLUMN A		COLUMN B		COLUMN C	
	T Experimental [d]	Tr Theory [d]	T Experimental [d]	Tr Theory [d]	T Experimental [d]	Tr Theory [d]
N-Pentane	8	4	22	232	23	144
2-methyl-2-butene	8	5	27	304	29	264
MTBE	44	44	T > 200 d	6149	T > 200 d	2886
N-Hexane	14	6	26	387	29	375
Benzene	20	20	T > 200 d	3614	44	1324
Cyclohexane	13	7	32	460	24	359
Iso-Octane	7	7	34	220	29	181
N-Heptane	13	7	27	335	30	184
Toluene	30	58	T > 200 d	9807	85	4581
N-Octane	19	7	73	184	44	61
P-Xylene	47	78	T > 200 d	2999	T > 200 d	1651
1,3,5-trimethylbenzene	62	187	T > 200 d	7517	T > 200 d	4182

Table 3.3 (Continued)

Comparison of the theoretical expected times to reach near steady-state conditions vs. times obtained experimentally (Columns D, E, F)

Chemical	COLUMN D		COLUMN E		COLUMN F	
	T Experimental [d]	Tr Theory [d]	T Experimental [d]	Tr Theory [d]	T Experimental [d]	Tr Theory [d]
N-Pentane	11	53	9	29	31	136
2-methyl-2-butene	14	93	9	38	39	339
MTBE	T > 200 d	1699	T > 200 d	813	T > 200 d	4001
N-Hexane	9	199	13	57	32	860
Benzene	26	1200	53	350	T > 200 d	2187
Cyclohexane	16	185	13	63	32	178
Iso-Octane	18	93	18	31	33	96
N-Heptane	22	162	20	36	39	176
Toluene	26	3186	56	167	T > 200 d	1657
N-Octane	36	52	22	14	49	45
P-Xylene	T > 200 d	3220	71	207	T > 200 d	2619
1,3,5-trimethylbenzene	T > 200 d	7540	T > 200 d	545	T > 200 d	3429

3.3 Normalized Flux vs. Time

The normalized flux vs time results for n-pentane, benzene and n-octane are presented in Figure 3.1. Results for the rest of the chemicals in study can be found in Appendix II.

The normalized flux was calculated as follows:

$$\text{Normalized Flux} = \frac{Q \cdot c_i / A}{D_{T,i}^{eff} \cdot c_{o,i} / L} \quad (3.5)$$

$$D_{T,i}^{eff} = \frac{Q \cdot c_i}{c_{o,i} \cdot A / L} \quad (3.6)$$

Where,

Q = Sweep gas flow [cm³/s]

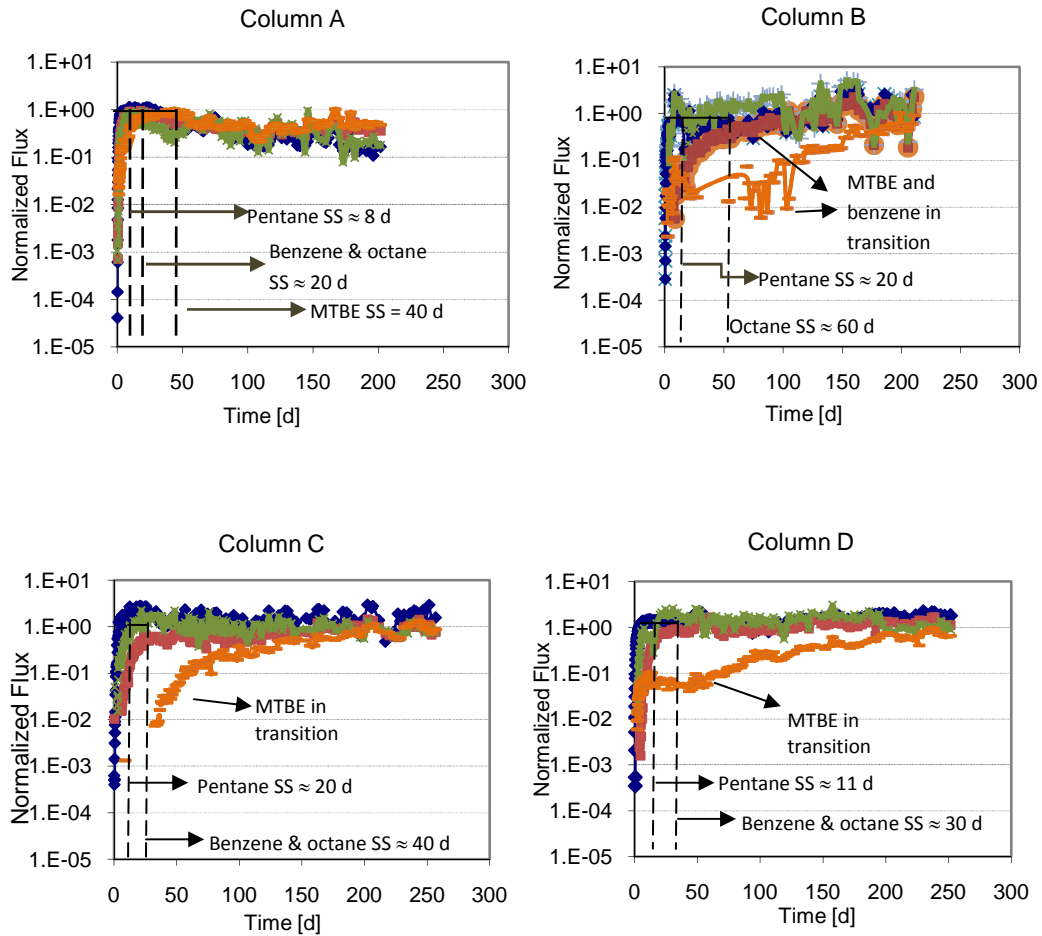
c_i = Concentration of hydrocarbon i in sweep gas leaving the column [mg/cm³]

A = Column cross sectional area [cm²]

$D_{T,i}^{eff}$ = Vapor effective diffusion coefficient of the column [cm^2/s]

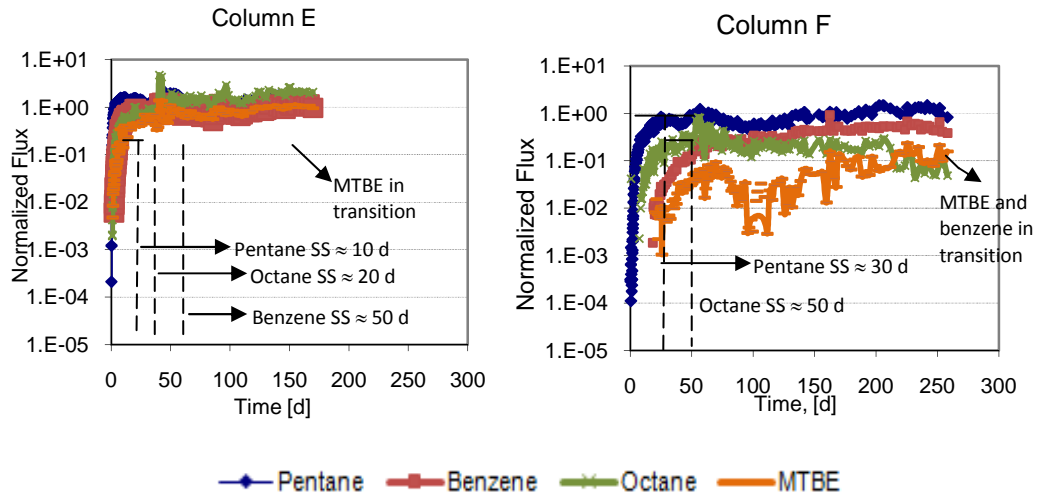
$C_{0,i}$ = Source concentration (bottom of the column) [mg/cm^3]

L = Column length [cm]



(SS = near-steady state conditions)

Figure 3.1. Normalized flux vs time. Anaerobic conditions



(SS = near-steady state conditions)

Figure 3.1. Normalized flux vs. time. Anaerobic conditions (continued)

The graphs in Figure 3.1 illustrate the transient and near-steady conditions of the chemicals with time at the effluent of the columns under anaerobic conditions.

Differences in time to reach near-steady conditions on a chemical by chemical basis and across columns can be observed.

3.3.1 Mass emissions.

A comparison of the soil hydrocarbon vapor mass emissions on a chemical by chemical basis is presented in Table 3.4. The mass emissions were calculated as follows:







$$q_i = Q \cdot C_i \tag{3.7}$$

Where,

q_i = Mass emission of vapor compound i [mg/s]

Table 3.4

Effluent mass emissions of each soil column

Columns Hydrocarbon	Mass Emissions [mg/s] x 10 ⁻⁵					
	A 	B 	C 	D 	E 	F 
N-Pentane	23.5 ± 1.7	14.5 ± 0.7	9.3 ± 1.3	27.7 ± 1.5	75.1 ± 5.9	15.0 ± 1.1
2-Methyl-2-Butene	7.7 ± 0.3	3.7 ± 0.08	1.8 ± 0.2	6.6 ± 0.2	20.2 ± 1.1	3.5 ± 0.1
MTBE	1.6 ± 0.1	0.5 ± 0.01*	0.07 ± 0.005*	0.6 ± 0.02*	0.8 ± 0.1*	0.08 ± 0.01*
N-Hexane	5.6 ± 0.3	3.3 ± 0.1	2.2 ± 0.1	5.8 ± 0.1	18.0 ± 1.0	1.9 ± 0.05
Benzene	1.2 ± 0.1	6.0 ± 0.2	0.3 ± 0.03	0.7 ± 0.02	1.6 ± 0.05	0.3 ± 0.01
Cyclohexane	5.3 ± 0.2	3.4 ± 0.05	1.9 ± 0.1	3.3 ± 0.1	14.4 ± 0.6	1.7 ± 0.04
Iso-Octane	4.0 ± 0.1	2.3 ± 0.07	1.6 ± 0.1	2.6 ± 0.1	12.1 ± 0.4	1.2 ± 0.03
N-Heptane	2.6 ± 0.1	1.5 ± 0.1	9.4 ± 0.4	2.2 ± 0.07	8.4 ± 0.6	0.7 ± 0.03
Toluene	2.9 ± 0.1	0.9 ± 0.02	0.2 ± 0.05	0.8 ± 0.04	4.3 ± 0.2	0.3 ± 0.03
N-Octane	0.7 ± 0.04	0.3 ± 0.01	0.2 ± 0.01	0.3 ± 0.01	2.1 ± 0.1	0.05 ± 0.004*
P-Xylene	0.7 ± 0.1	0.1 ± 0.01*	0.04 ± 0.002	0.1 ± 0.01	1.4 ± 0.07*	0.03 ± 0.006*
1,3,5-Trimethylbenzene	0.5 ± 0.1	0.1 ± 0.002*	0.06 ± 0.01*	0.02 ± 0.004	1.2 ± 0.08*	0.08 ± 0.006*

As seen in Table 3.4, the effluent mass emissions at the effluent decrease in a column by column basis in the order: E>A≈D>C>B>F. Note that the anticipated order was A>B>C≈D>E>F since the more fine-grained soil (crushed granite) contained in a column, the lower the emission rates, given that this soil type had a low effective diffusion coefficient. Since the columns have the same vapor source concentration, the inconsistency between the expected results and the experimental results can be attributed to differences in the soil diffusion coefficients in the lithological layers across columns. To illustrate this, Table 3.5 shows the benzene diffusion coefficients in each soil column. The diffusion coefficients were calculated from the steady anaerobic concentrations using the Fick's First Law equation (equation 3.8). As can be observed, the benzene effective diffusion coefficient of the fine grained soil varies across columns. Column E has the highest diffusion coefficient in the fine-grained soil ($8 - 9 \pm 0.4 \text{ cm}^2/\text{s}$) in comparison to the rest of the columns which explains the high mass emission rates. Column B has a low diffusion coefficient in the granite layer ($0.1 \pm 0.04 \text{ cm}^2/\text{s}$) which reduced the mass emissions of the chemicals. This explains why the emissions in Column B are not higher than Columns C and D.

Table 3.5

Benzene effective diffusion coefficient in each soil layer for each of the soil columns

Benzene Diffusion Coefficients $\times 10^{-3} [\text{cm}^2/\text{s}]$					
A	B	C	D	E	F
10 ± 3	30 ± 1	1.0 ± 0.4	30 ± 0.3	9.0 ± 0.4	2.0 ± 0.08
	0.1 ± 0.04			20 ± 0.6	
	20 ± 0.6	20 ± 0.6	1.0 ± 0.4	8.0 ± 0.2	

The mass emissions also depend on the chemical characteristics. This is observed in Table 3.4 where the most volatile chemicals (high Henry's Law constant) such as n-pentane, n-hexane and iso-octane have the highest mass emissions in each soil column; and less volatile chemicals (low Henry's Law constant) such as MTBE, benzene and 1,3,5-trimethylbenzene have the lowest mass emissions.

3.4 Concentration and Diffusion Coefficient Profiles

Vapor profile "snapshots" were taken every seven to fifteen days in order to capture changes in the vapor concentrations with time. Figure 3.2 show the plots of benzene concentration profiles in each column. Profiles of the rest of the chemicals are presented in Appendix III. As can be seen in Figure 3.2, Columns A and C show a dramatic change in the concentration between the port at the bottom of the column and the first port in the soil. This is the result of water accumulation at the bottom of the column which is a consequence of moisture condensation at the top cap due to changes in room temperature. The room temperature varied 5^o C during the day and the sweep gas had a humidity of a 100%. So, when the room temperature was high (~30^oC) the sweep gas entered into the column at a temperature lower than the room temperature (23-25^oC); as a consequence, the water in the sweep gas condensed at the top cap of the column. The condensed water dripped down into the soil causing a change in the soil moisture content which, at the same time, caused redistribution of the water in the column and accumulation of water at the bottom. A mass balance of the water in the sweep gas of Column A showed that approximately 2 ml of water per week was being condensed and dripped down into the soil. This caused the diffusion coefficient at the bottom of Columns A and C to increase affecting the vapor transport. To avoid future problems, the moisture content of the sweep gas was changed to 60% which was calculated to be sufficient to keep the soil moisture content constant and avoid condensation during the 5^o C room temperature variations.

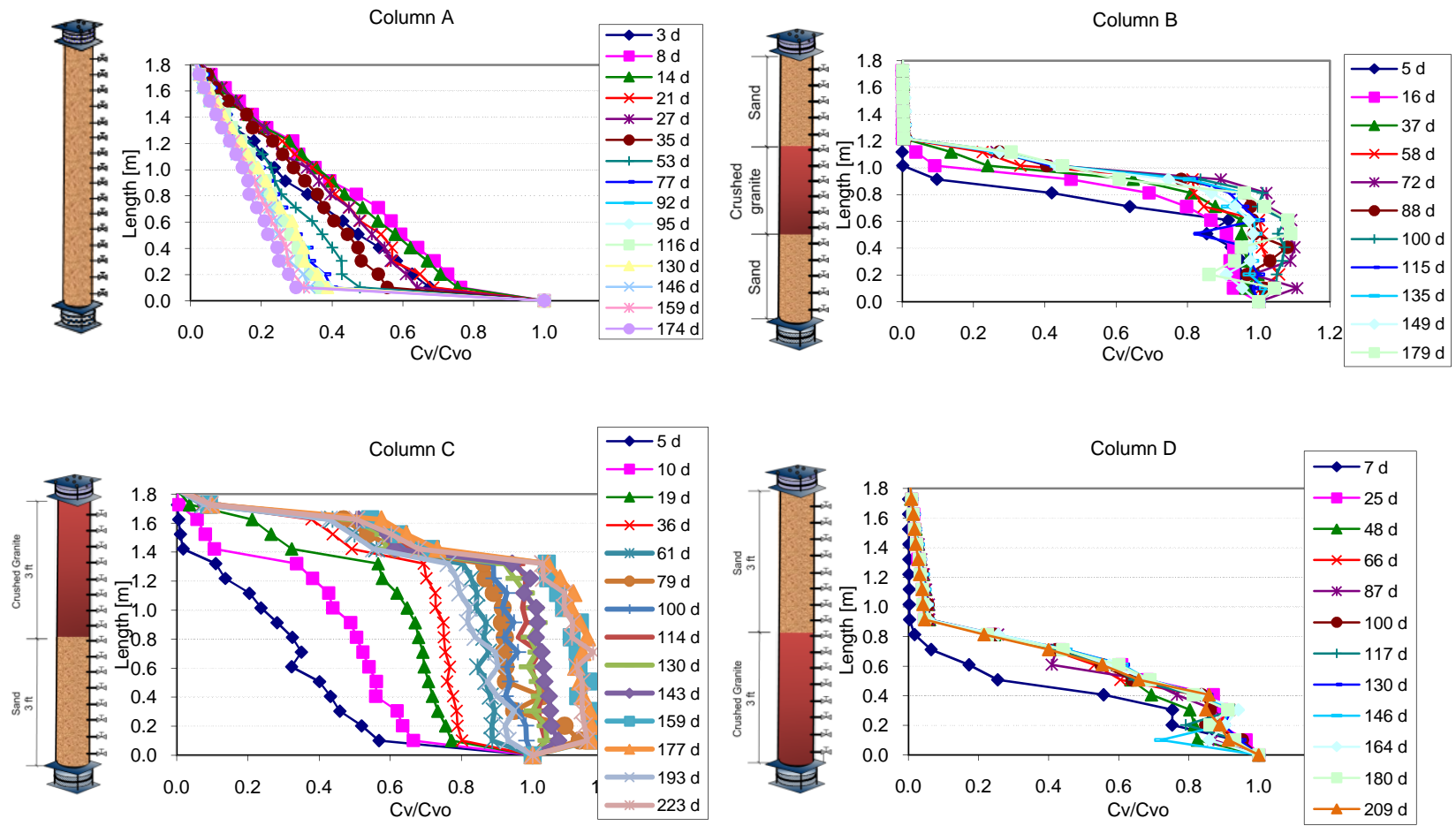


Figure 3.2. Benzene concentration vapor profiles change with time. Anaerobic conditions

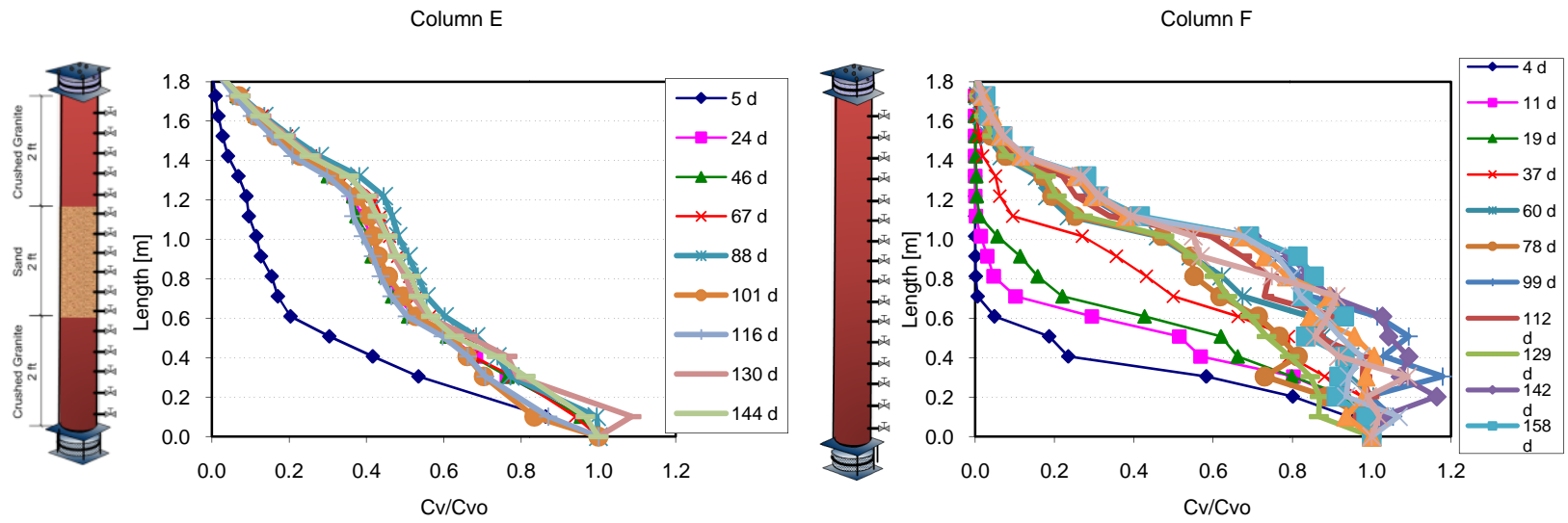


Figure 3.2. Benzene concentration vapor profiles change with time. Anaerobic conditions (Continued)

The effective diffusion coefficient profiles were calculated using Fick's First Law as follows,

$$D_{i,soil}^{eff} = \frac{Q \cdot C_i \left(\frac{\Delta L}{\Delta C_i} \right)}{A} \quad (3.8)$$

Where,

$D_{i,soil}^{eff}$ = Effective vapor diffusion coefficient of vapor hydrocarbon i [cm^2/s]

ΔL = Length of soil layer [cm]

ΔC_i = Concentration gradient of hydrocarbon i [mg/cm^3]

Figure 3.3 presents a comparison of the near-steady vapor concentration profiles for n-pentane and benzene and the corresponding calculated diffusion coefficient profiles of each column. These plots illustrate the influence of the lithology and moisture content on the effective vapor diffusion coefficient and concentration profiles over a 1.8-m soil column. As can be observed in Figure 3.3, the sand layers had the highest and least variable diffusion coefficient ($\sim 1 \times 10^{-2} \text{ cm}^2/\text{s}$) across all the columns (except near the bottom of columns A and C). The effective diffusion coefficients in the crushed granite layers were approximately an order of magnitude lower than the effective diffusion coefficients of the sand and also more variable from column to column ($\sim 1 \times 10^{-4} - 1 \times 10^{-2} \text{ cm}^2/\text{s}$). In the case of column E both types of soils had higher diffusion coefficients than the rest of the columns. This is consistent with the observed high mass emissions observed in the previous section. Column B has a very low crushed granite effective diffusion coefficient; which explains its low vapor mass emissions. The difference in the diffusion coefficients in the same soil media across columns was most likely due to differences in soil packing and/or differences in soil moisture content.

The soil gas profiles in Figure 3.2 reflect the idealized subsurface setting of each soil column. They clearly illustrate the changes in the soil effective diffusion coefficient due to lithology.

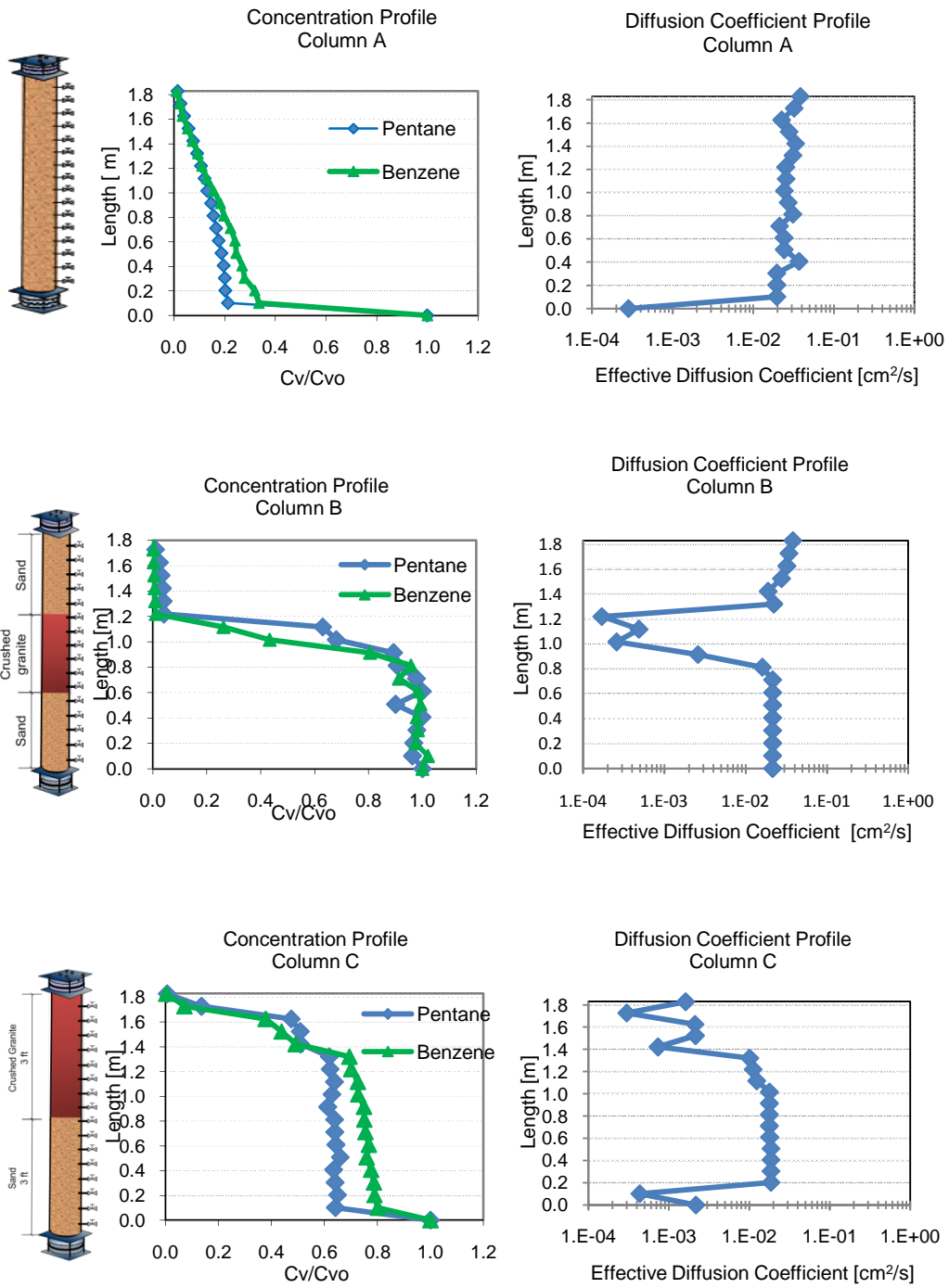


Figure 3.3. Concentration and diffusion coefficient profiles

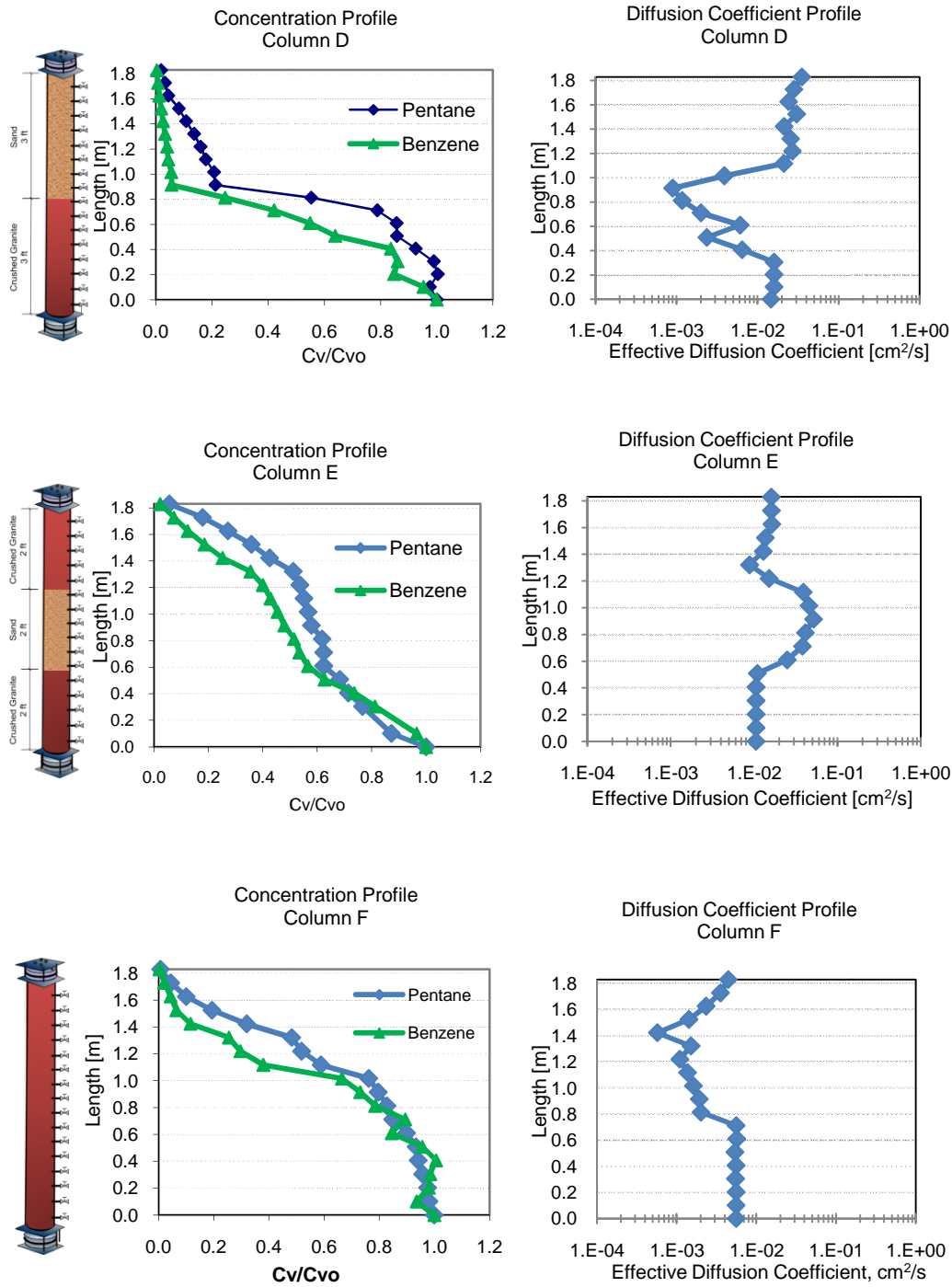


Figure 3.3. Concentration and diffusion coefficient profiles (Continued)

3.5 Carbon Dioxide, Oxygen and Methane Concentrations

To verify that aerobic or anaerobic biodegradation was not occurring during this phase of the experiment, oxygen (O₂), carbon dioxide (CO₂), and methane (CH₄) were measured over time using a TCD-FID-GC. Results from all of the columns showed that concentrations were in the range of 0.2 to 0.8 % V/V for O₂; 0.1 to 0.5 % V/V for CO₂ and less than 5 ppm of CH₄. These concentrations were constant during the anaerobic experimental period; thus, it was concluded that no degradation (aerobic or anaerobic) was took place in the soil columns during experimental Phase I.

3.6 Summary

This first phase of the soil column experiments consisted of studying vapor migration during transient and near-steady state conditions under an oxygen depleted environment in which no aerobic or anaerobic degradation occurred. The transient period was closely monitored in order to determine the times at which each hydrocarbon component reached near-steady conditions. Results showed that the near-steady conditions were first achieved by n-pentane, 2-methyl-2-butene, n-hexane, cyclohexane, and n-heptane. These results were found to be consistent with the theory. Note that these chemicals took days to weeks to achieve near-steady conditions while the rest of the compounds such as MTBE or 1,3,5-trimethylbenzene (which are less volatile hydrocarbons), took weeks to months and in some cases did not reach the near-steady state conditions during this phase experimental period (~200 d). These results confirm the effects of the hydrocarbon components physical-chemical properties on gas transport through the unsaturated zone.

Comparison of times to reach near-steady conditions across columns determine that the order at which the columns achieved near-steady conditions from the one that took the shortest period of time to the longest one is: A<E<D<C<B<F. It was expected that the columns with more amount of crushed granite had higher times to reach near-

steady conditions ($A < B < C < D < E < F$). This discrepancy might be due to differences in the soil packing across columns.

Comparison of effluent mass emissions across columns showed that the emissions decrease in the following order: $E > A \approx D > C > B > F$. This result was not consistent with what was anticipated ($A > B > C \approx D > E > F$). It was expected that the mass emissions were going to decrease accordingly to the amount of crushed granite contained in the soil columns because of the low effective diffusion coefficient in this type of soil. This discrepancy between experimental and predicted results was due to variations in the effective diffusion coefficients within the crushed granite layers across the columns. For example, in Column E, both soils, sand and crushed granite had higher diffusion coefficients than the rest of the columns ($\sim 1 \times 10^{-1}$ vs 1×10^{-2} cm^2/s for the sand and $\sim 1 \times 10^{-2}$ vs. $\sim 1 \times 10^{-3}$ cm^2/s for the crushed granite) which explains the high emission rates observed in this column. Contrastingly, Column B had a very low crushed granite effective diffusion coefficient (1×10^{-4} cm^2/s) and therefore, low vapor mass emissions. The variability of the diffusion coefficients in the same type of soil across the columns may have been due to differences in soil moisture content and soil packing.

Frequent monitoring of carbon dioxide, oxygen and methane concentrations in the columns confirmed that anaerobic or aerobic degradation was not occurring during this phase.

Soil gas vertical concentration profiles illustrated the influence of the lithology on the vapor migration along the soil columns. The near-steady condition concentration profiles were used as a base to determine aerobic degradation changes during Phases II and III (gkair as sweep gas) of the soil columns.

CHAPTER 4

RESULTS AND DISCUSSION

PHASE II: SURFACE AEROBIC CONDITIONS

Aerobic biodegradation can play a significant role in the attenuation of petroleum hydrocarbons in the vadoze zone. At a spill site, while hydrocarbon vapors move upward from the source to the soil surface, oxygen diffuses down from the atmosphere into the subsurface layers; at the regions where both meet, and in the presence of microorganisms, the hydrocarbons are partially (or completely) depleted by aerobic degradation reactions, and carbon dioxide is produced (Roggeman et al., 2001; API, 2005). In experimental Phase II, surface atmospheric conditions are simulated by switching the sweep gas from nitrogen to air. The objective is to study the effect of aerobic degradation reactions in the mass emissions and concentration profiles in the idealized scenarios represented in each soil column, as well as the determination of compound-specific degradation preferences. Therefore, changes on the effluent normalized flux, concentration profiles of petroleum hydrocarbon as well as in the CO₂ and O₂ concentrations are monitored over time in each soil column. Results of this experimental phase are discussed in this chapter.

4.1 Normalized Flux vs. Time

With the objective of observing changes in the effluent flux in the individual compounds of each column due to aerobic conditions, the normalized flux at the effluent of the columns was plotted against time. Results for n-pentane, benzene and n-octane are presented in Figure 4.1. These chemicals represent the behavior of the rest of the hydrocarbon compounds in study. Results of the rest of the chemicals can be found in Appendix II. The normalized flux for each hydrocarbon was calculated as follows:

$$Flux_{normalized} = \frac{Q.C_i/A_c}{D_i^{eff}.C_{o,i}/L} \quad (4.1)$$

Where,

Q = Sweep gas flow [cm³/s]

C_i = Concentration of hydrocarbon i at the effluent of the soil column [mg/cm³]

A_c = Column cross-sectional area [cm²]

D_i^{eff} = Total effective diffusion coefficient of hydrocarbon i [cm²/s]

C_{o,i} = Concentration of hydrocarbon i at the vapor source (bottom of the column) [mg/cm³]

L = Column length [cm]

As can be observed in Figure 4.1, as soon as the sweep gas was switched from nitrogen to air, a decrease in the individual-compound normalized fluxes was observed in most of the columns. N-Pentane showed little to zero flux attenuation in most of the columns except for Column B. The flux of Benzene (known as one of the petroleum hydrocarbons readily degradable in the presence of oxygen) was decreased in most of the columns except in Columns A and E. N-octane fluxes were attenuated in all of the columns, showing a decrease of two to four orders of magnitude in all of the columns. Based on Figure 4.1 plots, it was observed that the columns with the highest attenuation activities were columns B, C and F. In columns D, A and E only n-octane shows a significant flux attenuation. Note that during Phase I, it was observed that Columns D, A and E had the lowest mass emissions and Columns B, C and F the highest. Thus, it is possible that the flux attenuation of the columns were related to mass emissions (the highest the mass emission, the lower the flux attenuation).

After approximately 20 to 40 days (the time varies depending on the lithology, attenuation activity and chemical characteristics) an increase in the hydrocarbon normalized fluxes in all of the columns was observed. The normalized fluxes shifted back up to anaerobic near-steady condition levels. The reason for this behavior is uncertain.

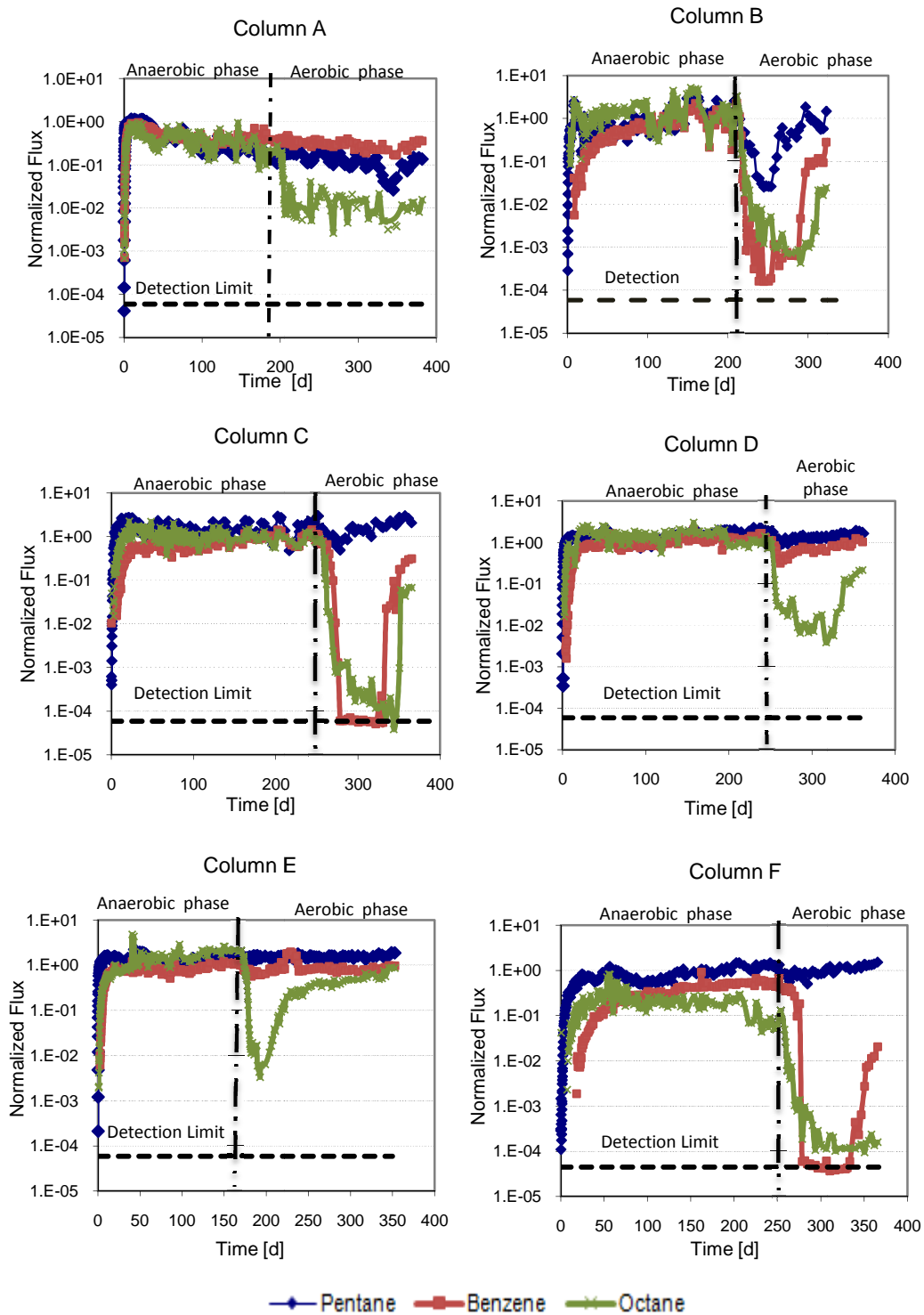


Figure 4.1. Normalized flux vs. time

4.2 Soil Vapor Profiles

4.2.1 Concentration profiles over time.

Vertical snapshots were taken approximately every 15 to 20 days. Figure 4.2 shows the concentration profile changes over time for benzene in each column. Concentration profiles of the rest of the chemicals behave similarly to benzene and they can be found in Appendix IV.

Experimental Phase II was started after approximately 200 days of running the soil columns experiment (experimental day 180 – 260 depending on the column since they were not started simultaneously). The profile taken at the beginning of Phase II (day 180 – 260 depending on the soil column is the profile before the sweep gas was switched from nitrogen to air; hence, this profile is the reference against which the rest of the concentration profiles over time are compared. In this case, the concentration profile changes over time reflect the degradation activity in each column. Consistent with the results from the effluent fluxes, columns B, C and F show a decrease in concentrations for approximately 40 days (day 300 for column B, 255 for column C and 287 for column F), after which the concentrations started to shift back towards the initial near-steady condition profiles. Concentration profiles in Columns A, D and E had little to no decrease with time.

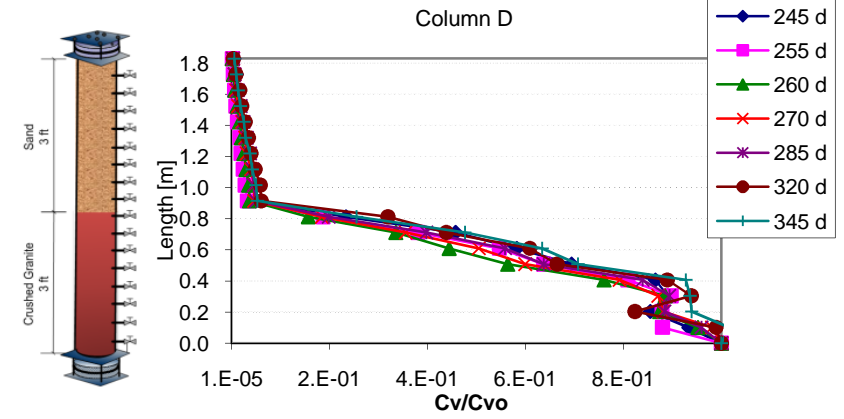
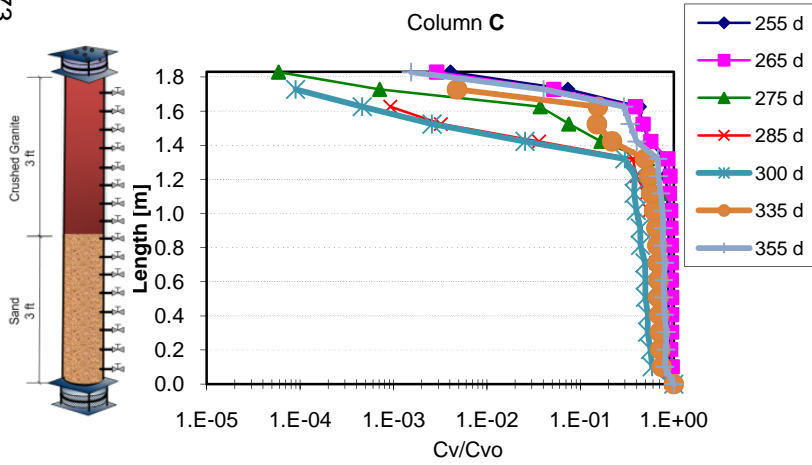
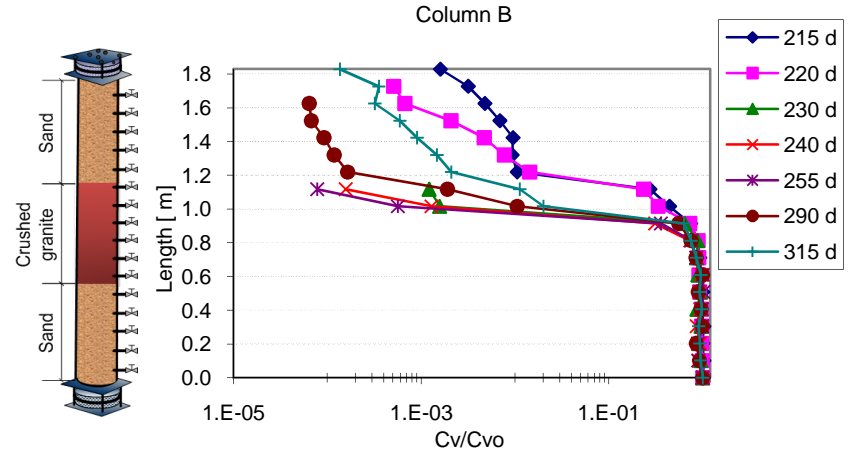
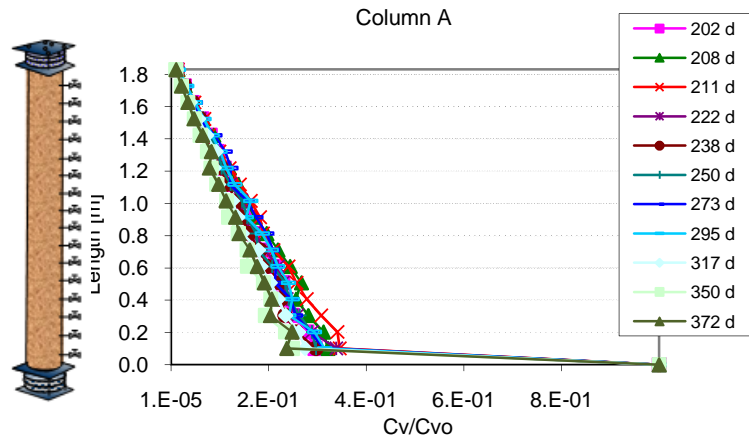


Figure 4.2. Benzene concentration vapor profiles change with time – Phase II

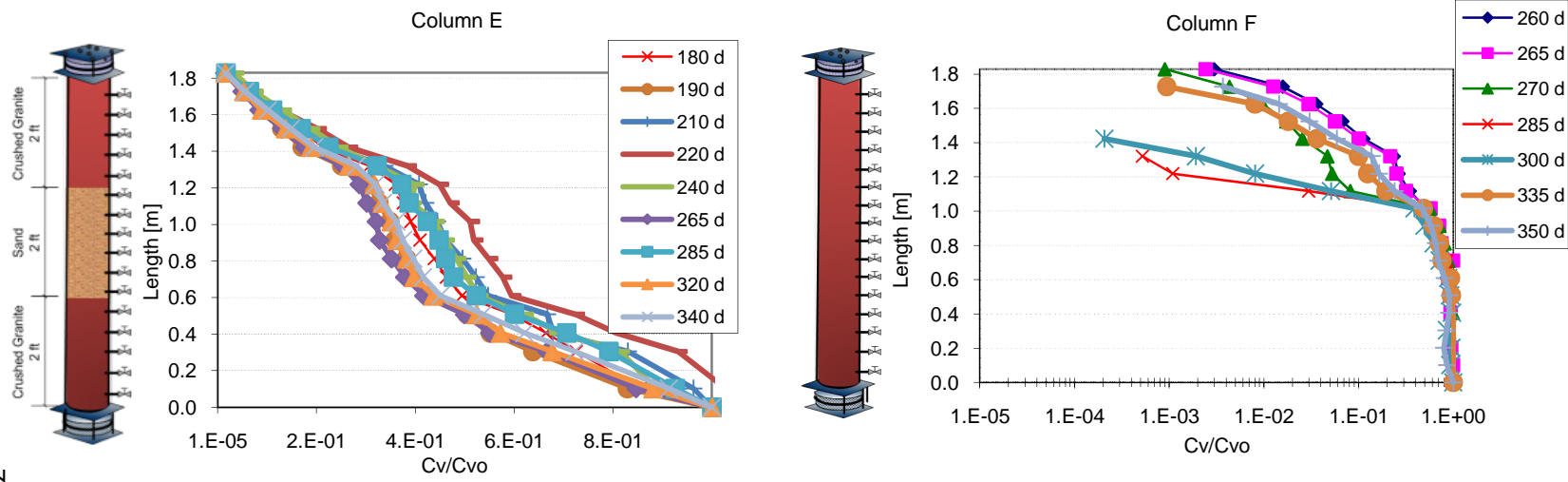


Figure 4.2. Benzene concentration vapor profiles change with time – Phase II (continuedd)

4.2.2 Oxygen and carbon dioxide concentrations.

As observed by Davis et al., 2009, O₂ concentrations decreased with depth in the impacted soils and the CO₂ concentrations increased. Both concentrations should be consistent with each other since the latter is produced by the utilization of the first. In this work, aerobic microbial degradation of the petroleum hydrocarbon vapors is coupled to the production of CO₂. Figure 4.3 shows the total vapor petroleum hydrocarbons (TPH) concentration, as well as the carbon dioxide and the oxygen concentration profiles for each column. The TPH was calculated by summing the concentrations of the 12 petroleum hydrocarbons.

Consistent with the literature (Davis et al., 2009), the CO₂ and O₂ profile plots (Figure 4.3) show that the CO₂ concentrations increased with depth while the O₂ concentrations decreased. As mentioned in the previous section, the attenuation activity of the columns stopped after approximately 40 days when the concentrations started to shift back towards the anaerobic near-steady conditions profiles. The concentrations of CO₂ and O₂ increased for approximately 75 days (day 300 – 330 depending on the column); after which, the concentrations of CO₂ started decreasing and the concentrations of O₂ stayed constant with time.

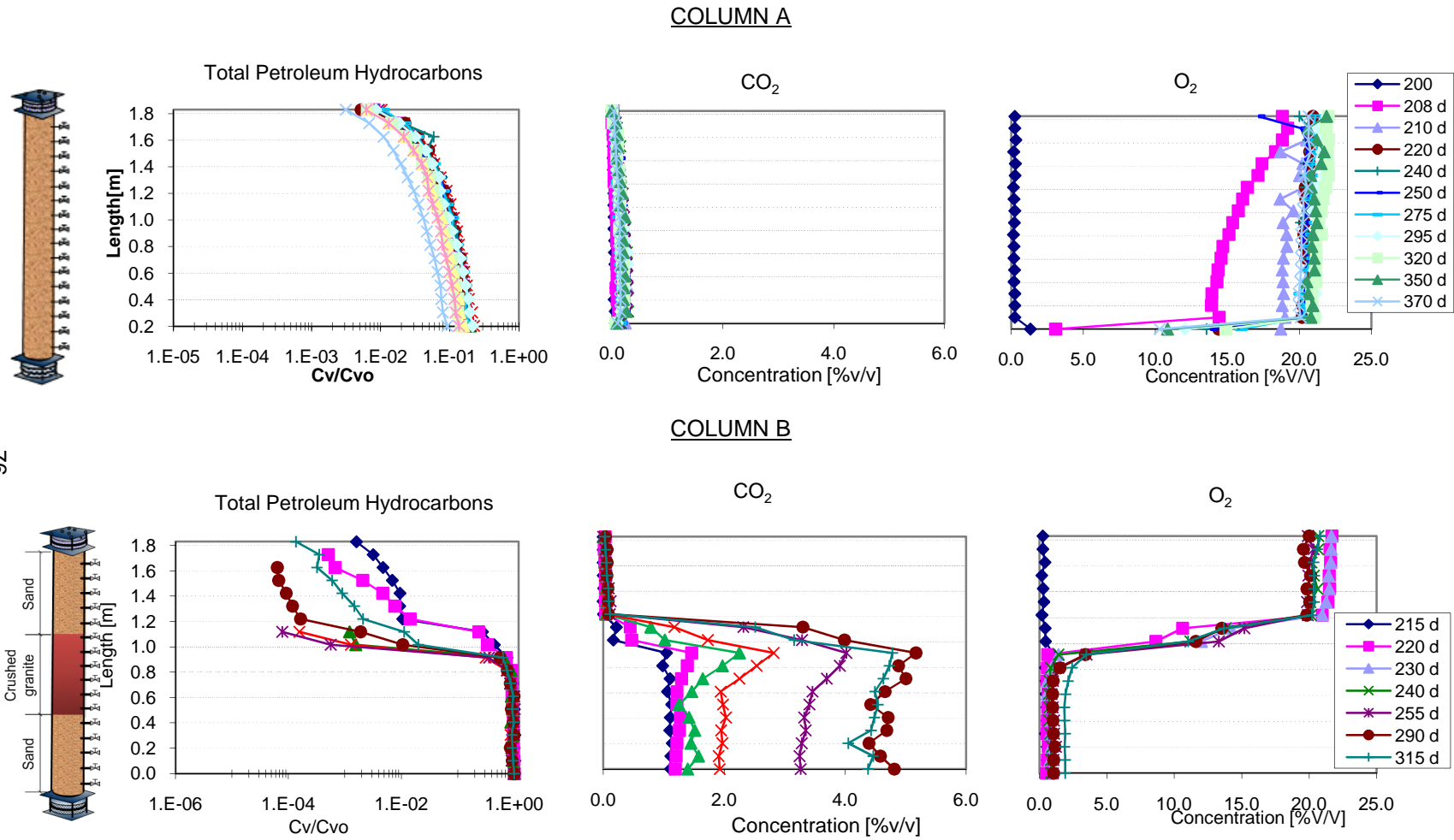


Figure 4.3. Total petroleum hydrocarbons, CO₂ and O₂ concentration profiles

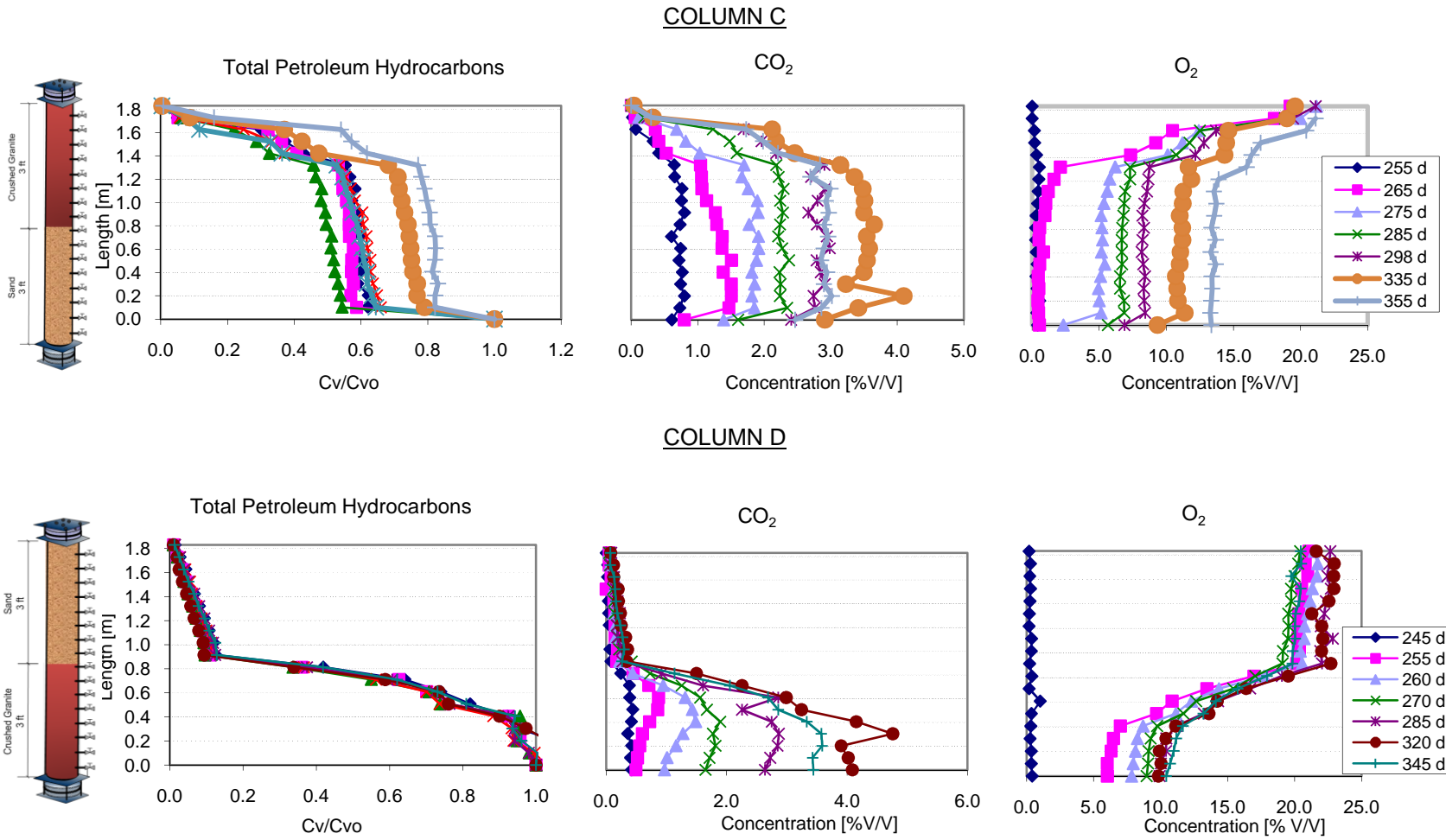


Figure 4.3. Total petroleum hydrocarbons, CO₂ and O₂ concentration profiles (continued)

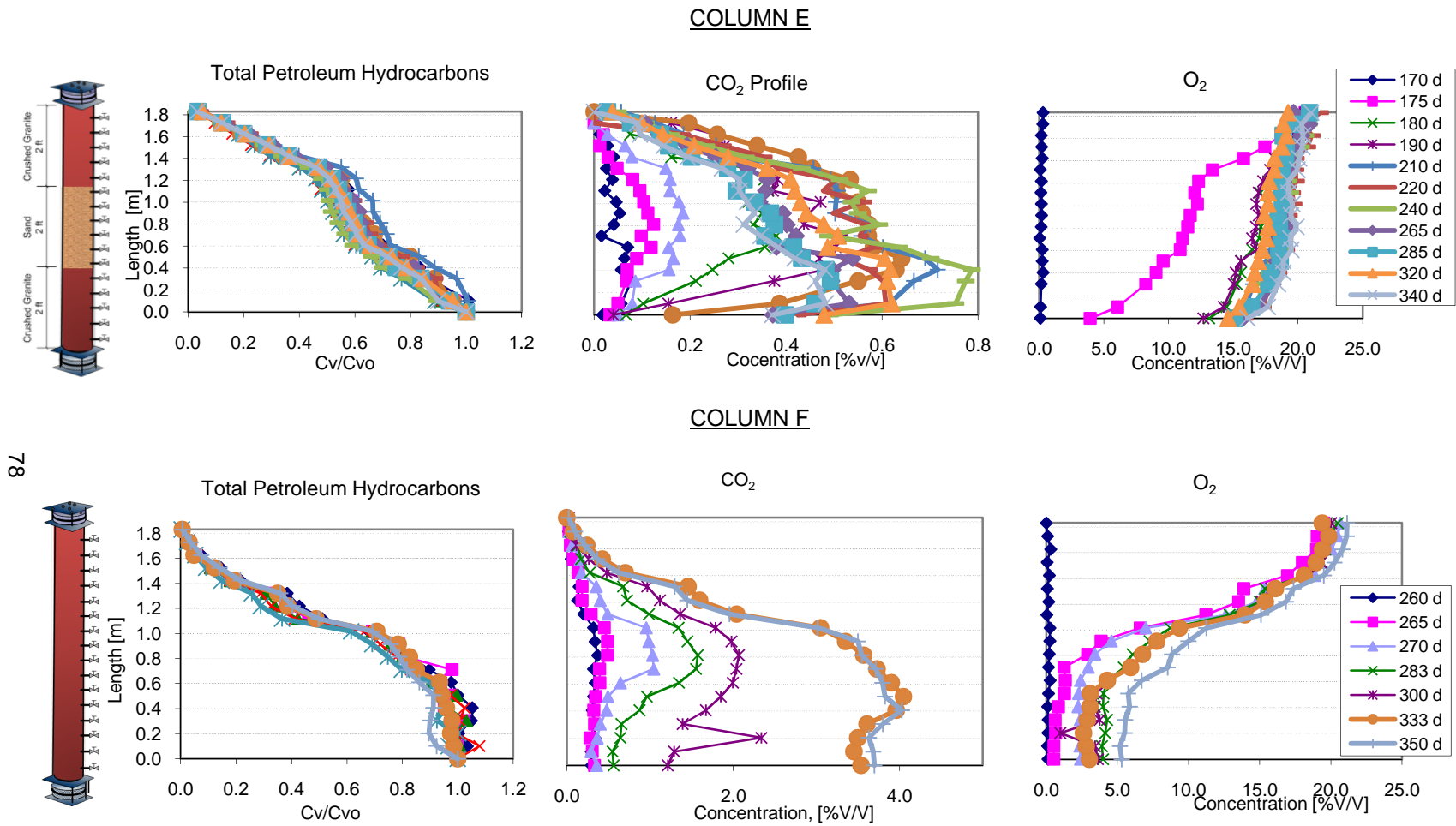


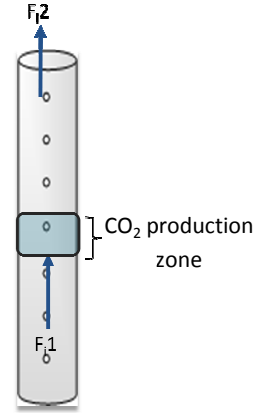
Figure 4.3. Total petroleum hydrocarbons, CO₂ and O₂ concentration profiles (continued)

In order to determine if the emission of CO₂ at the effluent was consistent with the decrease in vapor hydrocarbon concentrations, the expected CO₂ to be produced was calculated by stoichiometry using Equations 4.2, 4.3 and 4.4.. Results are presented in Table 4.1.

$$\frac{dF_i}{dz} = -k_i C_i \quad (4.2)$$

$$F_i = -D_i \frac{dC_i}{dz} \quad (4.3)$$

$$\frac{dF_i}{dz} = -D_i \frac{d^2 C_i}{dz^2} \quad (4.4)$$



Where,

F_{CO_2} = CO₂ mass emission [mg/s]

$F_{i,1}$ = Diffusive flux of hydrocarbon i below the CO₂ production zone [mg/s-cm²]

$F_{i,2}$ = Flux of hydrocarbon i at the effluent of the column [mg/s-cm²]

S_{CO_2}/S_i = moles of CO₂ per mol of hydrocarbon i

MW_{CO_2} = molecular weight of CO₂ [g/mol]







MW_i = molecular weight of hydrocarbon i [g/mol]

D_i^{eff} = Effective diffusion coefficient of hydrocarbon I [cm²/s]

Results presented in Table 4.1, show that the CO₂ emission values calculated from hydrocarbon flux decreases are higher than the ones measured directly; however, both values are roughly the same order of magnitude except for columns B and E in which the calculated numbers are one order of magnitude higher than the experimental values.

Table 4.1

Comparison of CO₂ calculated by stoichiometry vs the CO₂ measured from the soil columns

Column	CO ₂ Emission [mg/s]	
	Calculated	Experimental
A - 	1.78x10 ⁻⁴	1.81x10 ⁻⁴
B - 	1.12x10 ⁻³	1.71x10 ⁻⁴
C - 	8.89x10 ⁻⁴	1.77x10 ⁻⁴
D - 	5.44x10 ⁻⁴	3.84x10 ⁻⁴
E - 	1.31x10 ⁻³	2.65x10 ⁻⁴
F - 	6.49x10 ⁻⁴	1.05x10 ⁻⁴

Notice that all the columns have a vertical soil interval along their length at which the CO₂ fluxes increase (See Figure 4.3). This interval is referred as the “CO₂ production zones” and indicates the vertical location at which most of the aerobic degradation activity was occurring in the soil columns. The “CO₂ production zones or degradation zones” were identified by evaluating the CO₂ profiles. The length of the “degradation zone” for each column was defined by calculating the emission profile of the columns for Phase I and II using Fick’s First Law (Equation 4.3). The location along the length of the columns at which a hydrocarbon flux decrease was observed from Phase I to II determined the location and length of the “degradation zones”. Figure 4.5 shows the emission profiles for benzene for each column. The location of the “degradation zones” is marked with a rectangle. Table 4.2 shows the length range and location at which the “degradation zone” of each column was identified.

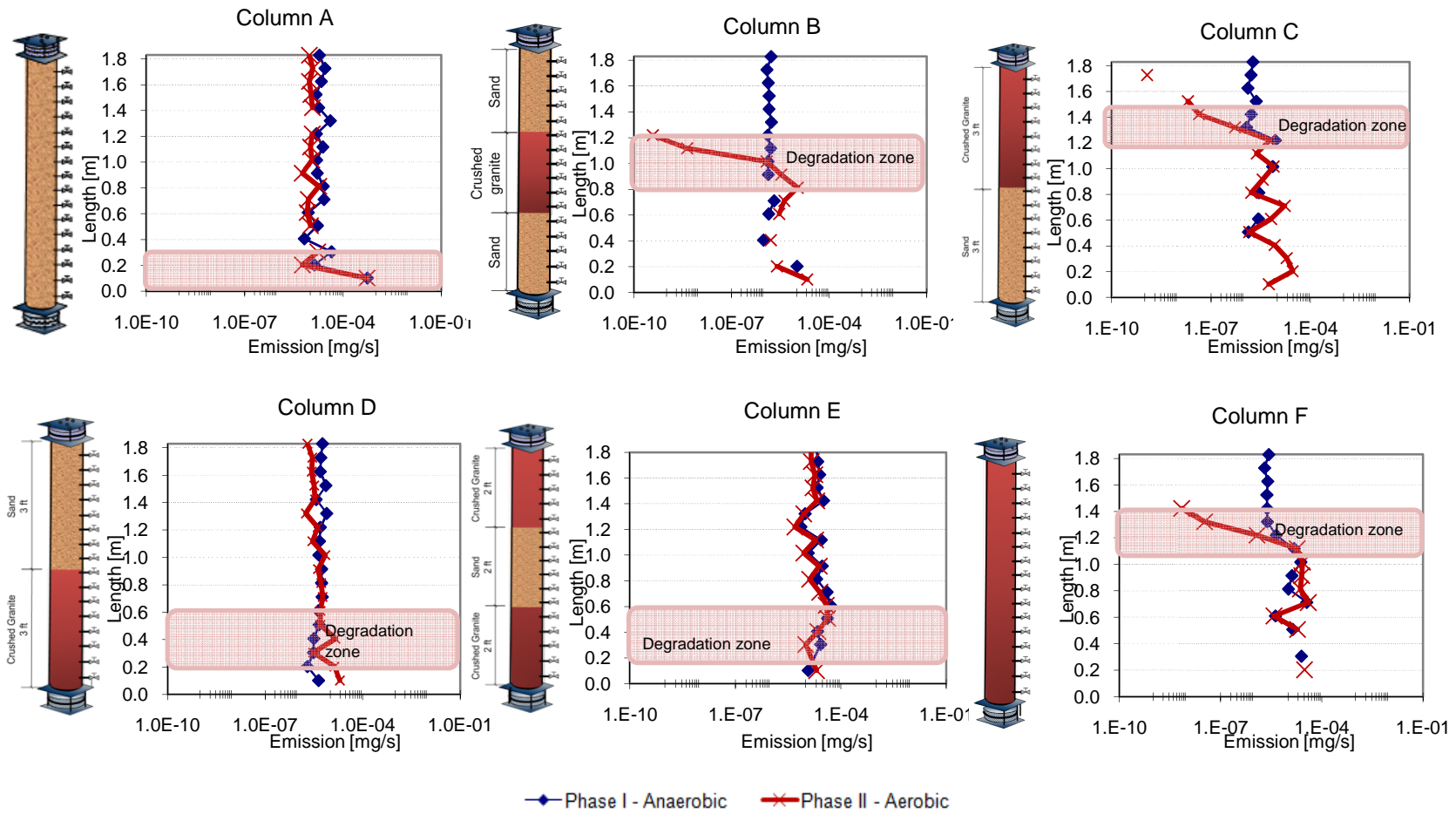


Figure 4.3. Benzene emission profiles

Table 4.2

Location of the “degradation zone” in each soil column

Column	Height above the Bottom of the Column, m	Soil Layer
A	0 – 0.2	Sand (Homogeneous sand column)
B	0.8 – 1.2	Crushed granite
C	1.2 – 1.6	Crushed granite
D	0.2 – 0.6	Crushed granite
E	0.2 – 0.6	Crushed granite
F	1.1 – 1.4	Homogeneous crushed granite column

As can be seen in Table 4.2., the degradation was most significant in the crushed granite layer of each layered column. The sand showed little to no degradation activity in comparison (see Figure 4.3).

As can be observed in Figure 4.3, the location and length of the “degradation zones” is well defined by the decrease in the hydrocarbon emissions during experimental Phase II in Columns B, C, and F. In Columns A, D and E, the emission profiles of Phase II had a very small decrease suggesting much less degradation activity during that phase.

The hydrocarbon emission decrease reflected in Figure 4.3, should correspond stoichiometrically to an increase in the CO₂ emission and a decrease in the O₂ emission with depth. This is described by equations 4.5 and 4.6. In order to determine if the concentration gradients and emissions observed in each column for the petroleum hydrocarbons are self-consistent the ratio of the CO₂ and O₂ gradients in the “degradation zones” were calculated. Results are presented in Table 4.3

$$\frac{\Delta F_{CO_2}}{\Delta F_{HC}} = \frac{S.MW_{CO_2}}{MW_{HC}} \quad (4.5)$$

$$\frac{\Delta F_{O_2}}{\Delta F_{HC}} = \frac{S.MW_{O_2}}{MW_{HC}} \quad (4.6)$$

Where,

ΔF_{HC} = Total petroleum hydrocarbons emission decrease in the “degradation zone” [mg/s]

ΔF_{CO_2} = Carbon dioxide emission increase in the “degradation zone” [mg/s]

ΔF_{O_2} = Oxygen emission decrease in the “degradation zone” [mg/s]

S = Stoichiometric factor

MW_{HC} = Total petroleum hydrocarbon molecular weight [\cong 94 g/mol]

MW_{CO_2} = Carbon dioxide molecular weight [=44 g/mol]

MW_{O_2} = Oxygen molecular weight [32 g/mol]

The values of equations 4.5 and 4.6 are approximately 3.1 g-CO₂/g-HC and 3.3 g-O₂/g-HC. As can be observed in Table 4.3 the O₂ emissions in all of the columns are reasonably balanced stoichiometrically, with the exception of Column C. The CO₂ production agrees stoichiometrically with the decrease of the total petroleum hydrocarbon emissions for Columns A, B, and D, and was lower than expected in the other columns.

Table 4.3

Flux ratio results

Column	ΔF_{HC} [mg/s]	ΔF_{CO_2} [mg/s]	ΔF_{O_2} [mg/s]	$\frac{\Delta F_{CO_2}}{\Delta F_{HC}} = 3.1$	$\frac{\Delta F_{O_2}}{\Delta F_{HC}} = 3.3$
A	5.5×10^{-5}	1.40×10^{-4}	2.02×10^{-4}	3.6	3.7
B	4.4×10^{-4}	1.3×10^{-3}	1.4×10^{-3}	2.9	3.2
C	1.6×10^{-4}	1.9×10^{-4}	3.6×10^{-4}	1.2	2.2
D	3.1×10^{-4}	9.6×10^{-3}	9.9×10^{-4}	3.5	3.2
E	1.94×10^{-4}	4.3×10^{-3}	6.8×10^{-4}	2.2	3.5
F	1.6×10^{-4}	3.1×10^{-4}	4.6×10^{-4}	2.0	2.9

4.3 Aerobic Degradation Rates and Diffusive Flux Ratios

Based on the diffusive fluxes measured during the time period when the maximum flux attenuation was observed in the soil columns, zero-order degradation rates can be calculated from the data by performing a mass balance in the soil column using the hydrocarbon fluxes below the degradation zone (Equation 4.3) and at the effluent (Equation 4.4) as follows. Results of this calculation are presented in Table 4.4.

$$V \cdot \rho_b \cdot R = (F_{i1} - F_{i2}) \cdot A_c \quad (4.7)$$

Then,

$$R = \frac{(F_{i1} - F_{i2})A_c}{\rho_b \cdot V} \quad (4.8)$$

Where,







R = Zero-order biodegradation rate [mg_i/Kg_{soil} – h]

ρ_b = Soil bulk density [g/cm³]

V = Volume of the degradation zone [cm³]

Table 4.4

Zero-order degradation rates, [mg/Kg-h]

Component	A - 	B - 	C - 	D - 	E - 	F - 
N-Pentane	7.9 ± 0.6	2.1 ± 0.2	0.2 ± 0.02*	3.0 ± 0.2*	7.3 ± 0.5	3.6 ± 0.2*
2-Methyl-2-Butene	0.8 ± 0.05	3.0 ± 0.2	2.5 ± 0.2	0.2 ± 0.01*	5.6 ± 0.3	1.0 ± 0.04
MTBE	0.4 ± 0.03	1.0 ± 0.2	0.7 ± 0.1	0.6 ± 0.1	0.2 ± 0.05*	0.3 ± 0.06
N-Hexane	0.8 ± 0.07	3.1 ± 0.2	4.9 ± 0.5	1.0 ± 0.03	1.5 ± 0.1	1.5 ± 0.1
Benzene	0.2 ± 0.02	1.5 ± 0.2	0.9 ± 0.1	0.40 ± 0.03	0.1 ± 0.01	0.16 ± 0.01
Cyclohexane	0.8 ± 0.08	1.0 ± 0.1	0.6 ± 0.04	0.1 ± 0.002*	1.1 ± 0.1*	0.4 ± 0.01*
Iso-Octane	0.7 ± 0.07	0.3 ± 0.04	0.04 ± 0.01*	0.1 ± 0.004*	0.8 ± 0.03*	0.1 ± 0.002*
N-Heptane	0.5 ± 0.1	5.0 ± 0.6	2.7 ± 0.3	1.5 ± 0.1	0.5 ± 0.1	2.3 ± 0.2
Toluene	0.7 ± 0.1	2.5 ± 0.3	2.4 ± 0.3	1.5 ± 0.1	1.1 ± 0.3*	1.03 ± 0.08
N-Octane	0.1 ± 0.05	2.3 ± 0.3	0.4 ± 0.1	1.1 ± 0.1	0.2 ± 0.03	1.1 ± 0.2
P-Xylene	0.1 ± 0.04	0.8 ± 0.3	0.9 ± 0.2	1.1 ± 0.2	0.3 ± 0.03*	0.7 ± 0.1
1,3,5-Trimethylbenzene	0.1 ± 0.02	0.2 ± 0.1	1.3 ± 0.3	0.2 ± 0.04	0.2 ± 0.02*	0.1 ± 0.02







*: Values calculated from the mass emission reduction: mass emission at the effluent during aerobic degradation phase minus the mass emission during the anaerobic phase. This was performed because the calculation of R was resulting in a negative value.

Table 4.4 shows that the zero-order degradation rates for all of the columns fall into the range from approximately 0.1 to 1.7 mg/Kg-h. No trends were detected. Hence, to have a better idea of the degradation activity of each soil column, a diffusive flux ratio of the aerobic flux when the maximum aerobic biodegradation was occurring over the anaerobic flux at steady conditions was calculated (Equation 4.7). Results are presented in Table 4.5.

$$\text{Diffusive flux ratio} = \left[\frac{\text{Aerobic effluent flux (Phase II or III)}}{\text{Steady conditions anaerobic effluent flux (phase I)}} \right] \quad (4.7)$$

Table 4.5

Diffusive flux ratio x 10²

Component	A - 	B - 	C - 	D - 	E - 	F - 
N-Pentane	44 ± 4	5 ± 0.2	57 ± 3	69 ± 1	100 ± 5	96 ± 7
2-Methyl-2-Butene	59 ± 6	4 ± 0.2	36 ± 2	44 ± 1	64 ± 3	32 ± 5
MTBE	98 ± 6	2 ± 0.5	16 ± 2	92 ± 6	95 ± 8	97 ± 14
N-Hexane	43 ± 3	0.3 ± 0.02	5 ± 0.5	33 ± 0.6	32 ± 1	3 ± 7
Benzene	68 ± 6	0.4 ± 0.1	0.06 ± 0.006	40 ± 1	76 ± 3	0.04 ± 3
Cyclohexane	44 ± 2	0.7 ± 0.06	45 ± 3	64 ± 2	79 ± 3	63 ± 5
Iso-Octane	56 ± 7	1 ± 0.08	64 ± 5	81 ± 3	80 ± 2	84 ± 3
N-Heptane	15 ± 1	0.1 ± 0.01	0.07 ± 0.005	16 ± 0.4	1 ± 0.1	0.2 ± 12
Toluene	52 ± 12	0.4 ± 0.04	0.1 ± 0.03	2 ± 0.08	41 ± 2	0.3 ± 6
N-Octane	4 ± 0.3	0.4 ± 0.04	0.5 ± 0.05	1 ± 0.1	2 ± 0.2	0.09 ± 7
P-Xylene	52 ± 17	0.2 ± 0.02	0.08 ± 0.007	0.2 ± 0.02	54 ± 2	0.4 ± 5
1,3,5-Trimethylbenzene	81 ± 7	0.09 ± 0.009	0.4 ± 0.08	0.7 ± 0.1	76 ± 7	0.2 ± 14

Results from Table 4.5 show that n-heptane and n-octane had the lowest diffusive flux ratios, followed by the aromatic hydrocarbons such as benzene, toluene and p-xylene. The compounds with the highest diffusive ratios and therefore, the most recalcitrant were n-pentane, MTBE, iso-octane and cyclohexane. These results are qualitatively consistent with a large lysimeter experiment made by Pasteris et al. (2001)

where it was observed that long chain alkanes such as n-octane and n-hexane were rapidly degraded; MTBE showed recalcitrance compared to other fuel vapors. Also, DeVaul et al. (2004) found in their diffusive soil column experiment that both MTBE and Iso-octane are recalcitrant compounds and degraded at slower rates than the BTEX (benzene, toluene, ethylbenzene and xylene) vapors.

Results from Table 4.4, as well as the plots in Figures 4.1, 4.2 and 4.3, demonstrated that the different columns have different degradation activities; with column B being the one with the highest aerobic degradation activity since almost all of the chemicals have the lowest diffusive flux ratios, followed by columns C and F. The columns with the lowest aerobic degradation activity, and high diffusive flux ratios, were columns A and E. Column A was composed only by sand which, as noted before, presented little degradation activity. Column E had higher diffusion coefficients and air filled porosities than the rest of the columns (Chapter 3), as a consequence, the aerobic degradation activity is low in comparison to the rest of the columns. Column E results are consistent with the study made by Kristensen et al. (2010) who determined that natural attenuation of petroleum hydrocarbons in the vadose zone depends on the physical soil environment (and not the depth) which influences the gas exchange and the pore-scale microbial metabolism; in their study, they evaluated the degradation of benzene in different textured soil samples and found that aerobic degradation was better in sandy loams (Air-filled porosity = 0.093 L-pores/L-soil Diffusivity = $0.021 \text{ cm}^2 \cdot \text{s}^{-1}$ -soil/ $\text{cm}^2 \cdot \text{s}^{-1}$ -air) than in fine sand (Air-filled porosity = 0.21 L-pores/L-soil, Diffusivity = $0.031 \text{ cm}^2 \cdot \text{s}^{-1}$ -soil/ $\text{cm}^2 \cdot \text{s}^{-1}$ -air). They concluded that air-filled porosity is a key factor for intrinsic biodegradation potential in the field.

4.4 Summary

With the objective of studying the effect of the lithology and aerobic biodegradation activity, as well as compound-specific degradation preferences, aerobic conditions were established in the soil columns. In this phase, effluent mass emissions and vapor hydrocarbon, CO₂ and O₂ profiles were determined. In this study, aerobic degradation is coupled with CO₂ production and mass emissions flux reductions. Results show that there are clear differences in the attenuation for different chemicals; based on the diffusive flux ratios calculated in Table 5.4, the degradation of the petroleum hydrocarbon vapor in this study can be ranked as follows:

Long-branched alkanes (n-heptane, n-octane) > *aromatics* (benzene, toluene, p-xylene, 1,3,5-trimethylbenzene) > *alkenes* (2-methyl-2-butene) > *cyclic alkanes* (cyclohexane) > *volatile alkanes* (n-hexane, n-pentane) > *high molecular weight-alkanes* (iso-octane) > *ether* (MTBE)

This ranking is consistent with the one presented by Leahy et al. (1990) and discussed in Chapter 1, as well as, results obtained by Pasteris et al. (2002) and DeVaul et al. (2004) in which alkanes such as n-hexane, n-octane and BTEX compounds are completely degraded and compounds such as MTBE and iso-octane show recalcitrance.

Based on the total petroleum hydrocarbon vapor, CO₂ and O₂ concentration profiles as well as the diffusive flux ratios (Table 4.4), the columns can be ordered starting from the one that showed the highest mass flux reductions to the lowest as follows: B>C>F>D>A>E.

The CO₂ and O₂ concentration profiles are consistent with what was observed in previous studies (Pasteris et al., 2001; Wilson et al., 2005; Davis et al., 2009); in which the O₂ concentrations decreases with the depth and the CO₂ concentrations increases.

During the time in which fluxes and concentrations were decreasing with time, a “degradation zone or CO₂ production zone” was identified in each soil column. This is the location along the length of the columns at which the maximum CO₂ concentrations were

detected and where the mass emission of hydrocarbon decrease with respect to the flux at near-steady conditions and no reaction. Results suggested that the “degradation zones” of each column were located in the finer-grained soil (crushed granite) and over a narrow interval. This is consistent with findings by Kristensen et al. (2010) who observed that the finest-grained soils showed better aerobic degradation activity than the coarser ones.

Zero-order degradation rates results were in the range from 0.1 to 1.7 mg/kg-h for all the chemicals in all of the columns and no trends were identified;

After 20 to 40 days of running the columns aerobically, the hydrocarbon vapor concentrations and fluxes started to shift back to the anaerobic near-steady conditions levels indicating that the degradation reactions were decreasing. In order to determine if the high hydrocarbon concentrations of the vapor source were a factor for this behavior, the hydrocarbon concentrations in the source were decreased ten times of original levels. Results of this experiment are presented in the next chapter (Chapter 5).

CHAPTER 5

RESULTS AND DISCUSSION

PHASE III: DECREASE OF VAPOR HYDROCARBON SOURCE UNDER AEROBIC SURFACE CONDITIONS

The objective of this experimental phase was to determine the effect of a reduced vapor source concentration in the vapor hydrocarbon mass emissions, soil gas distribution and biodegradation activity of the soil. To do this, the source vapor concentration was decreased by 10X and aerobic conditions were maintained (air as sweep gas). As in the previous chapter, the concentration of petroleum hydrocarbon vapors, CO₂ and O₂, as well as the mass emissions were monitored over time. Results are discussed in this chapter.

5.1 Normalized Flux vs. Time

The normalized flux of the columns effluent was plotted against time. The normalized flux was calculated using Equation 4.1. Results for n-pentane, benzene and n-octane are presented in Figure 5.1. Results for the rest of the chemicals can be found in Appendix II. As can be observed in Figure 5.1, the normalized effluent flux of most of the columns showed a higher decrease when the source concentration was lowered by 10X (Phase III) than during the aerobic phase (Phase II) with the exception of Column E. Column E showed little to no change in the normalized fluxes. As observed in previous Chapters this column displayed the highest effluent mass emission rates and the lowest degradation activity. The normalized fluxes in Column A decreased for approximately 40 days (experiment day 470), after which they started to shift back up towards the anaerobic near-steady condition levels; however, after 30 days (day 550), the fluxes decreased again until they reach near-steady conditions. The normalized fluxes of Columns B, C, D and F showed a decrease of approximately one (benzene) to three (n-octane) lower than the effluent normalized fluxes of Phase II. All of the columns reached

near-steady conditions after approximately 100 – 120 days of running this conditions (10X reduced concentrations under aerobic conditions).

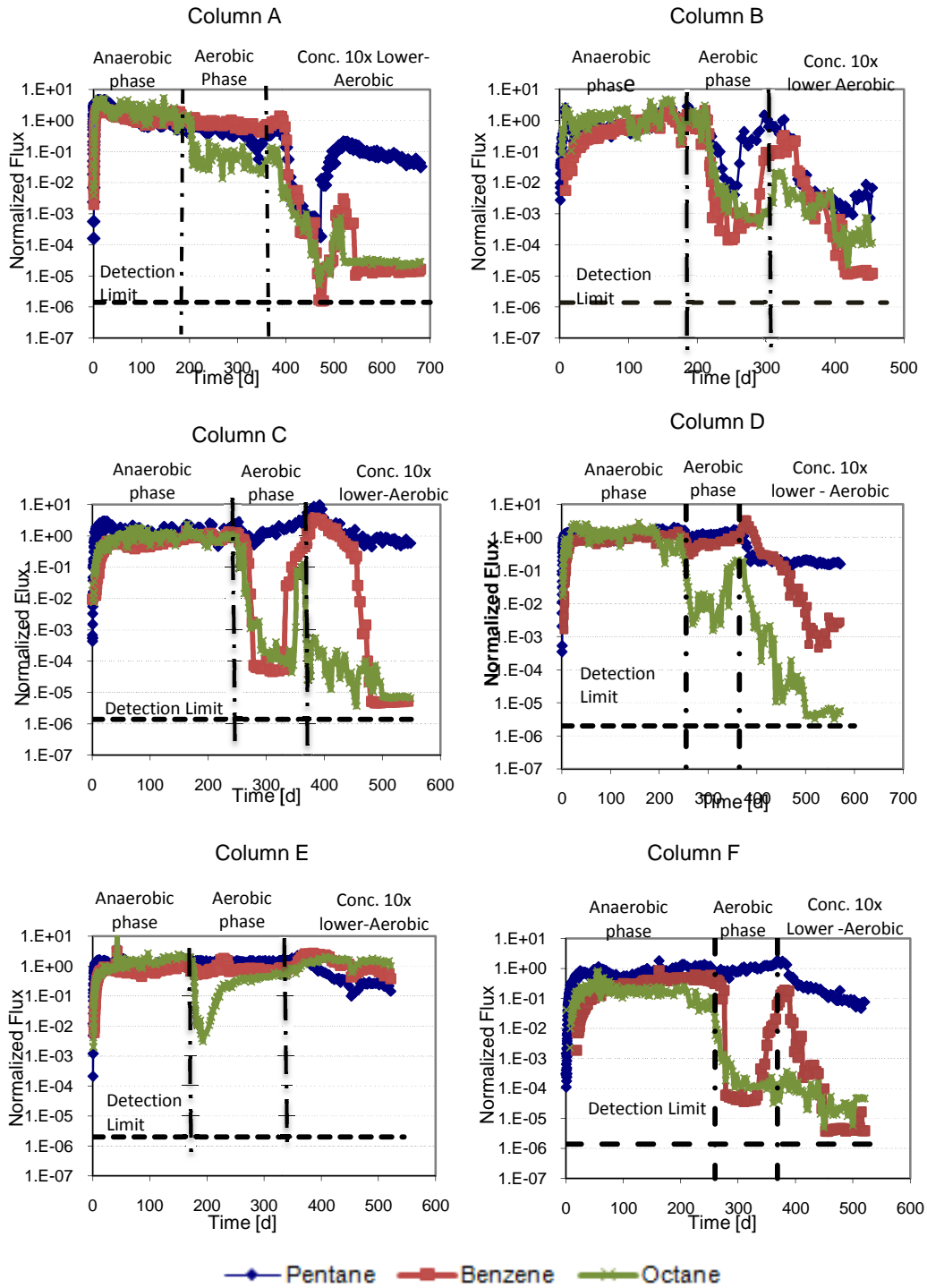


Figure 5.1. Normalized flux vs. time

5.2 Soil Vapor Profiles

5.2.1 Concentration profiles over time

As in the previous chapters (Chapter 3 and 4), vertical snapshots were taken approximately every 15 to 20 days; Figure 5.2 show the normalized concentration profiles to the vapor source concentration (C/C_0) for benzene of each column and how its profile change with time. Concentration profiles of the rest of the chemicals behave similar to benzene and they can be found in Appendix V.

Experimental Phase III was started approximately at day 345 - 370 (day vary with the columns since they were not started at the same time), the concentration profiles taken in these days were considered the reference point against which the rest of profiles are compared. As can be observed in Figure 5.2, after 30 to 55 days, the concentrations of benzene in most of the columns (except Column A) were higher than the reference the initial profile; this is because the columns were in transition from a high concentration vapor source to a lower one. Column A reflects the behavior observed in the effluent fluxes (Figure 5.1): the concentrations decrease for about 50 days (day 520), stayed constant during day 540, and then at day 575 the normalized concentrations increased; however, the concentrations decreased again at day 600 and no concentrations increments were observed after that, reaching near-steady conditions at day 650. The concentration profiles of the rest of the columns (B, C, D and E) show a decrease in normalized concentrations with time. The columns were run for approximately 200 days. These results suggest that attenuation of petroleum hydrocarbons was increased once the vapor source concentration was lowered by 10X.

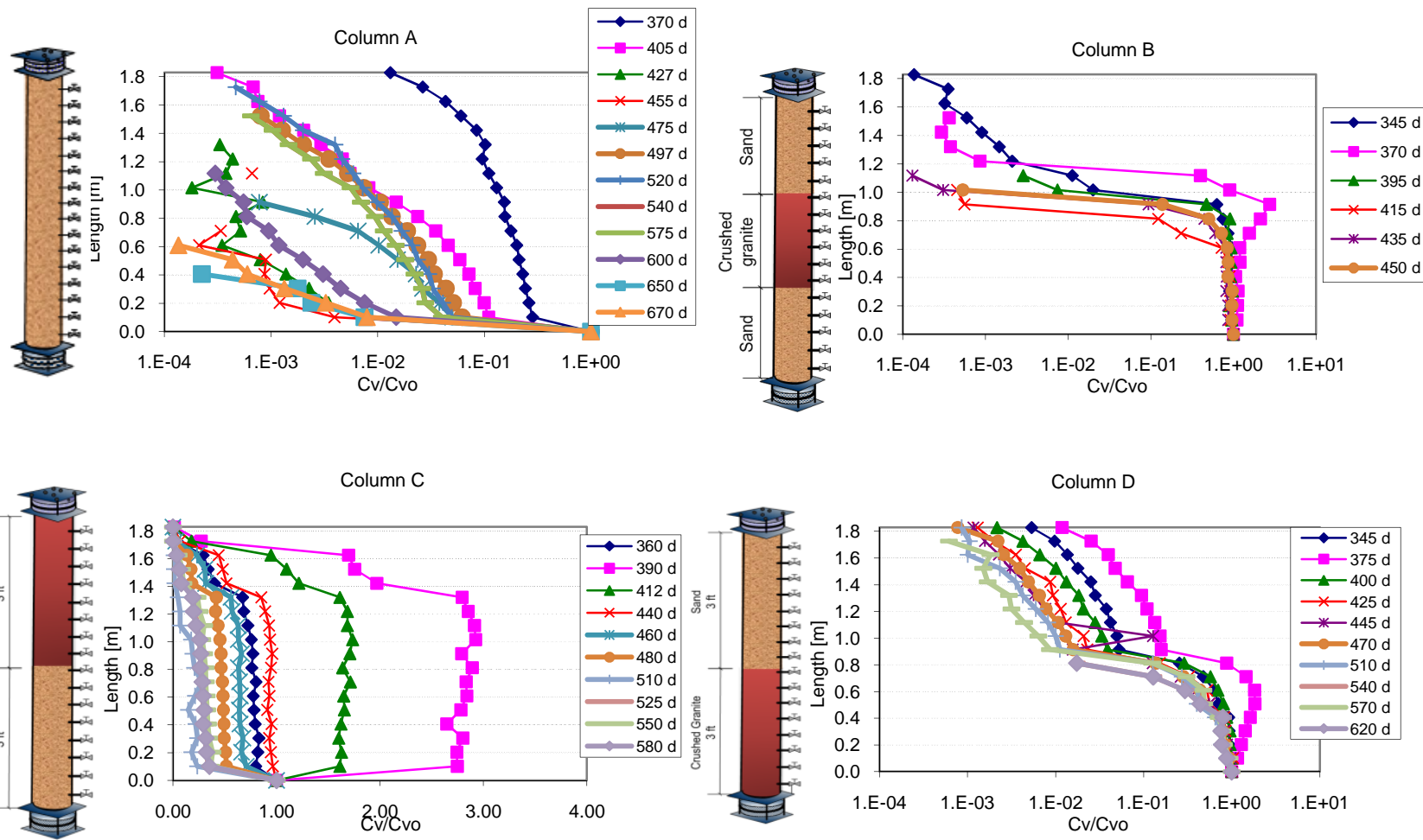


Figure 5.2. Benzene concentration profiles over time – Phase III

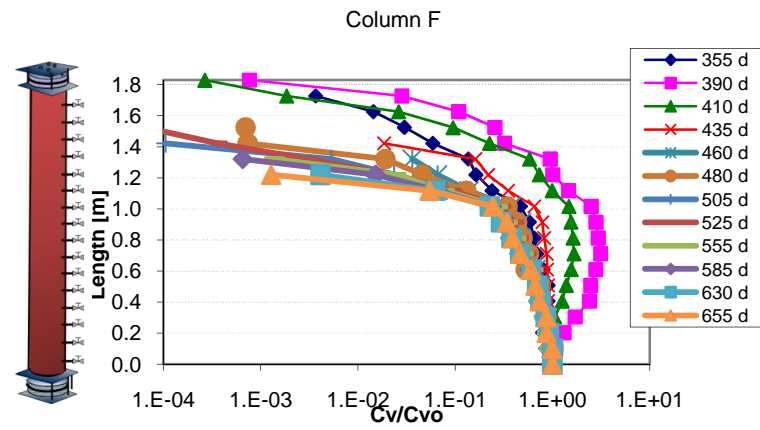
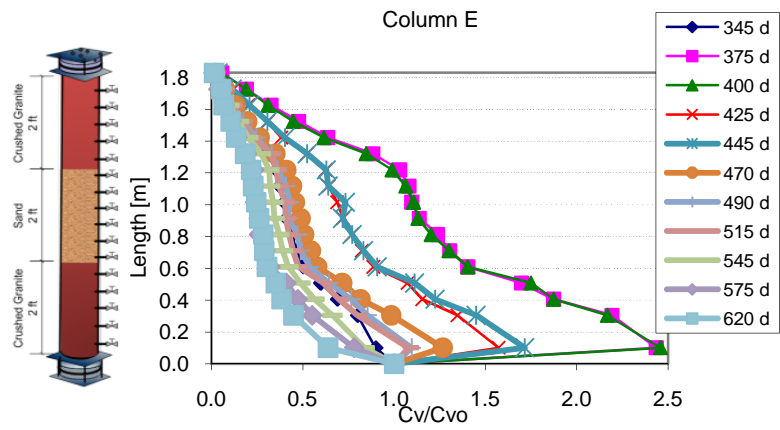


Figure 5.2. Benzene concentration profiles over time – Phase III (continued)

5.2.2 Oxygen and carbon dioxide profiles

Figure 5.3 shows the total petroleum hydrocarbon (TPH), CO₂ and O₂ concentration profiles of each column. As in Chapter 4, the aerobic microbial degradation of the petroleum hydrocarbon vapors is coupled to the production of CO₂. The TPH concentrations are the sum of the 12 petroleum hydrocarbon concentrations in study.

The CO₂ concentration profiles showed a decrease in the concentrations with time. The decrease is due to the lower hydrocarbon concentrations in the soil columns which means there is less substrate for the microorganisms to oxidize into CO₂ and water. The O₂ concentration profiles show an increase in the oxygen concentrations at the bottom of the columns. This is because the columns have been exposed to constant atmospheric oxygen conditions for more than 450 days and the oxygen has been diffusing down towards the bottom of the columns without escaping to the atmosphere.

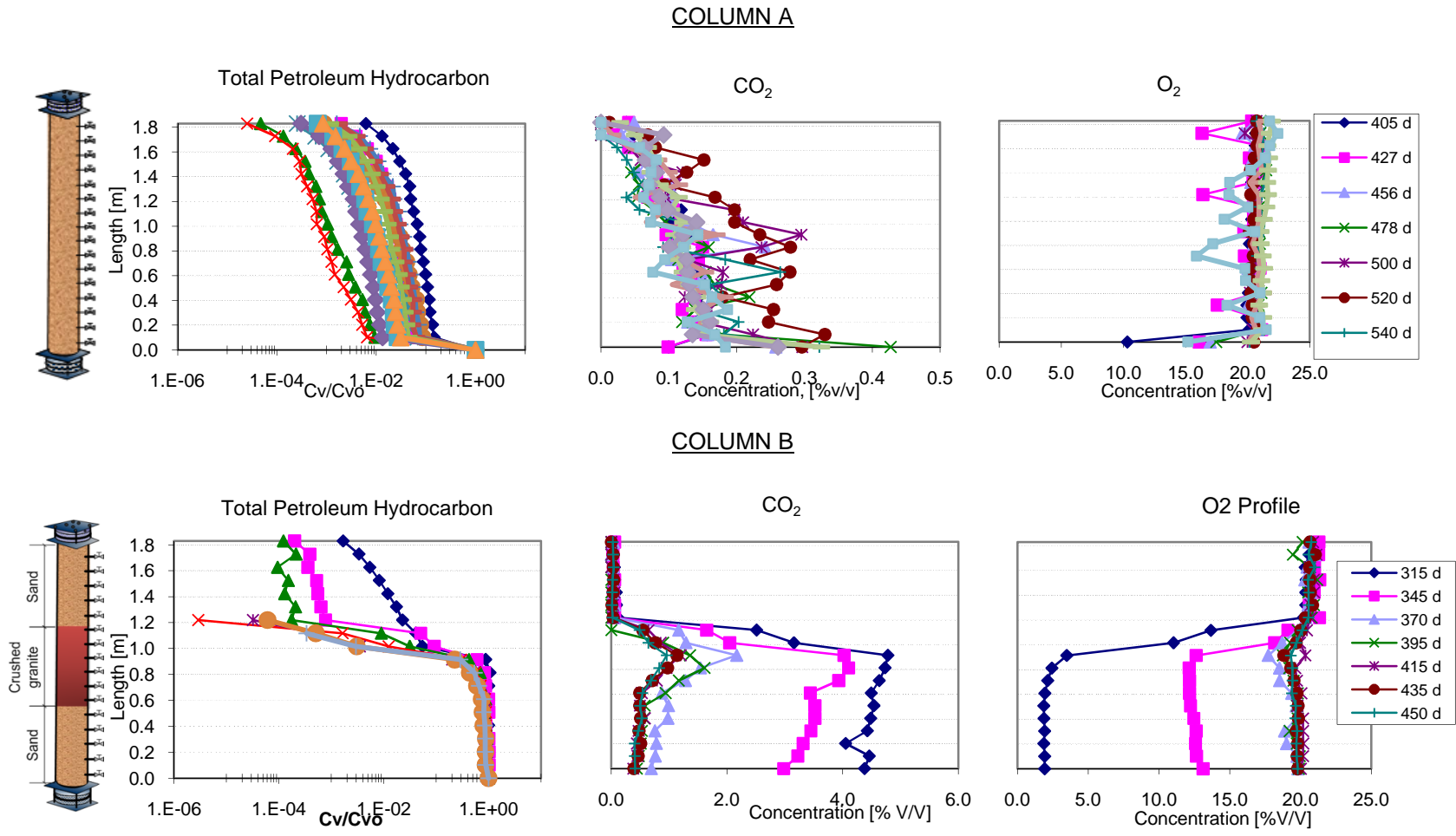


Figure 5.3. Total petroleum hydrocarbons, CO₂ and O₂ concentration profiles

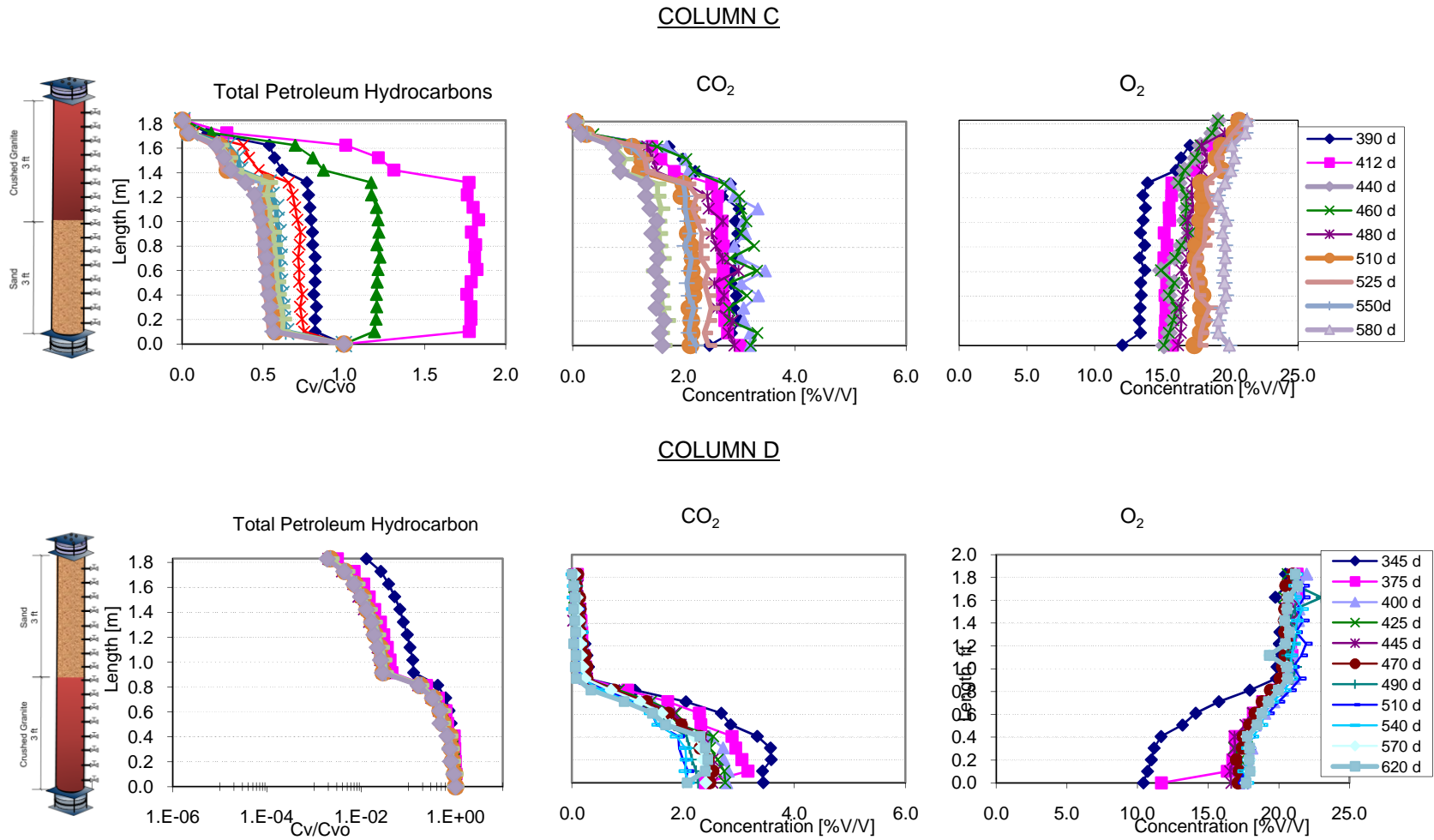


Figure 5.3. Total petroleum hydrocarbons, CO₂ and O₂ concentration profiles (continued)

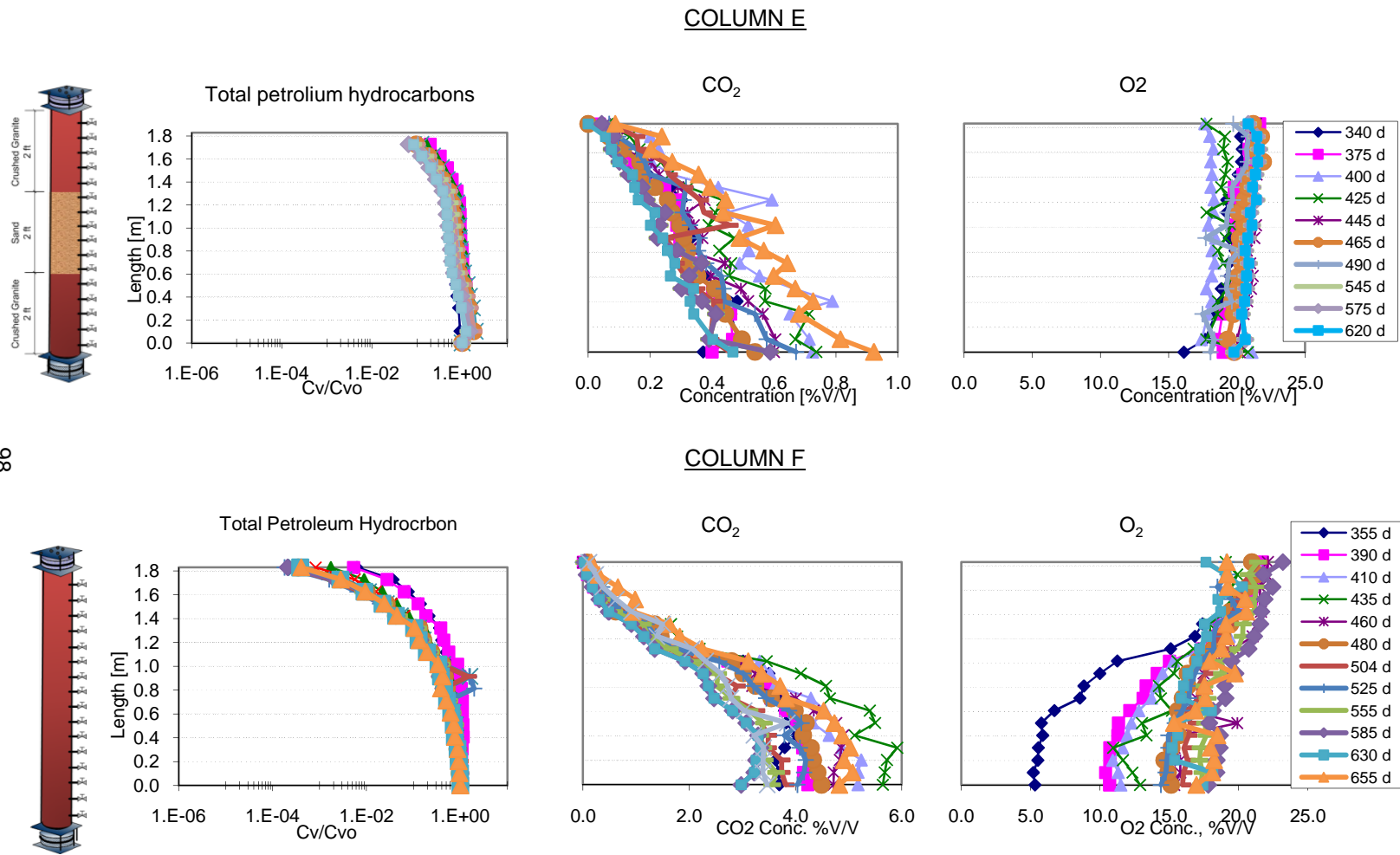








Figure 5.3. Total petroleum hydrocarbons, CO₂ and O₂ concentration profiles (continued)

As in Chapter 4, the CO₂ effluent emissions are compared with the expected CO₂ calculated from stoichiometry. Results are shown in Table 5.1. The calculated values were determined using Equations 4.2, 4.3 and 4.4.

Table 5.1

Comparison of CO₂ calculated mass emissions by stoichiometry vs. CO₂ mass emissions measured from the soil columns (experimental)

Column	CO ₂ Emission, mg/s	
	Calculated	Experimental
A - 	5.2x10 ⁻⁴	1.8±0.3x10 ⁻⁴
B - 	4.5x10 ⁻⁴	1.3±0.4x10 ⁻⁴
C - 	5.7x10 ⁻⁴	2.2±0.4x10 ⁻⁴
D - 	2.0x10 ⁻³	2.1±0.8x10 ⁻⁴
E - 	2.7x10 ⁻³	2.4±0.5x10 ⁻⁴
F - 	4.8x10 ⁻⁴	3.2±0.4x10 ⁻⁴

Results in Table 5.1 showed that the calculated CO₂ emission values using hydrocarbon data are higher than the ones obtained experimentally. However, in most of the columns the values are in the same order of magnitude except for Columns D and E in which higher CO₂ experimental values were expected.

Note that the CO₂ profiles in Figure 5.3, showed that the “CO₂ production zones” were in approximately the same length interval of the columns as in Phase II (See Chapter 4). In order to confirm this, the flux profiles were calculated and compared to the flux profiles of Phases I and II (See Figure 5.4). The “degradation zones” are defined by a hydrocarbon mass emission decrease along the length of the soil columns.

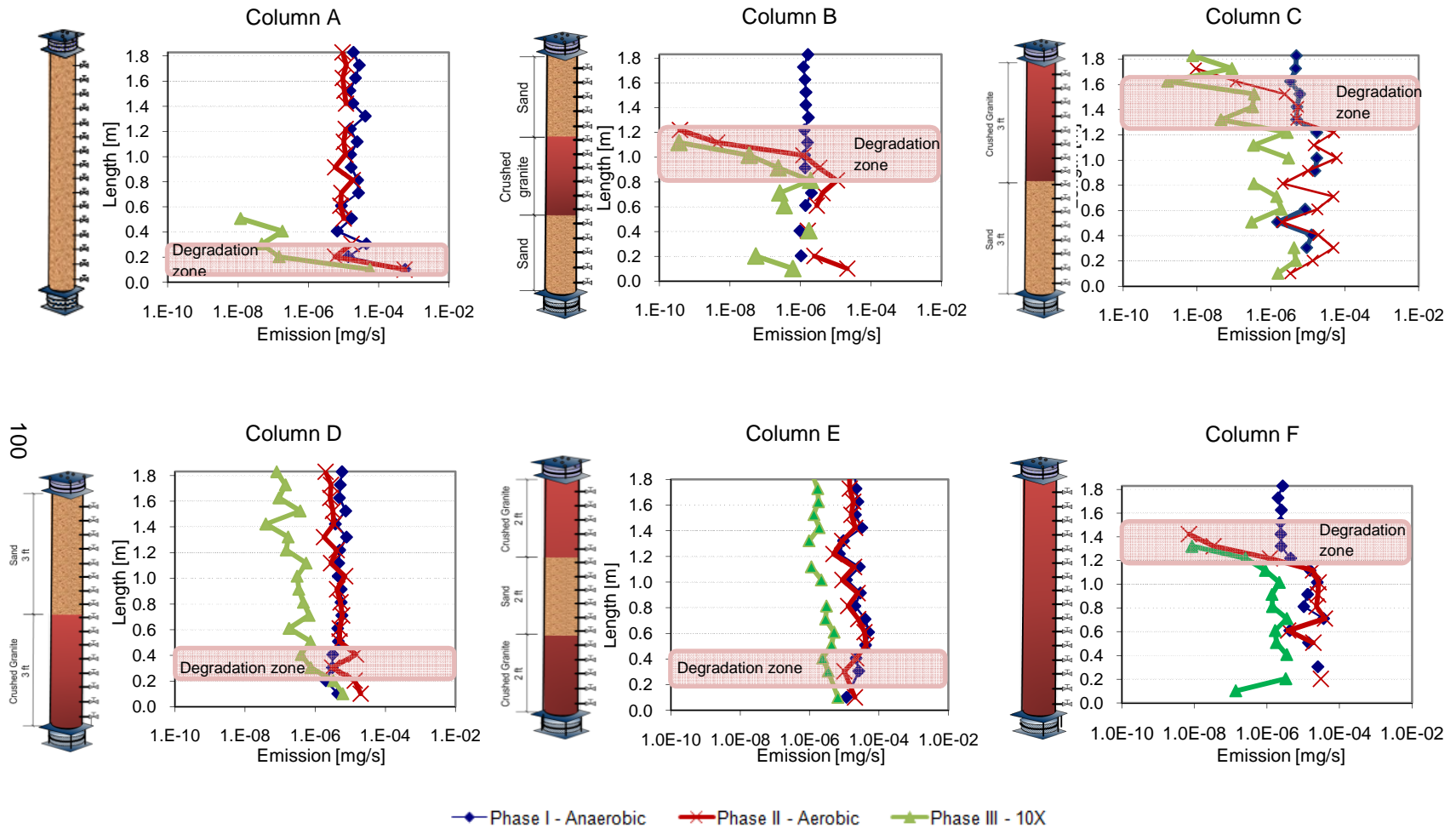


Figure 5.4. Benzene emission profiles (continued)

Table 5.2 presents a comparison of the location of the “degradation zone” determined during experimental Phase II vs the “degradation zone” in experimental Phase III. As can be observed, the “degradation zone” for both phases are in the same location.

Table 5.2

Comparison of the location of the “degradation zone” in each soil column during Phases II and III

Column	Length From the Bottom of the Column, m	
	Phase II	Phase III
A	0 – 0.2	0 – 0.3
B	0.8 – 1.2	0.8 – 1.2
C	1.2 – 1.6	1.2 – 1.6
D	0.2 – 0.6	0 – 0.5
E	0.2 – 0.6	0.1 – 0.4
F	1.1 – 1.4	1.0 -1.4

As in Chapter 4, the mass emission reduction in the “biodegradation zone” has to correspond stoichiometrically to an increase in the CO₂ mass emission and a decrease in the O₂ mass emission. Table 5.3 show results of the comparison of the ratios of the change in CO₂ and O₂ mass emissions over the change in the total petroleum hydrocarbon mass emissions. As can be observed, the fluxes show good agreement with the stoichiometry; therefore, it can be concluded that the total petroleum hydrocarbon flux reductions can be attributed mostly to aerobic degradation.

Table 5.3

Flux ratio results

Column	ΔF_{HC} [mg/s]	ΔF_{CO_2} [mg/s]	ΔF_{O_2} [mg/s]	$\frac{\Delta F_{CO_2}}{\Delta F_{HC}} = 3.1$	$\frac{\Delta F_{O_2}}{\Delta F_{HC}} = 3.3$
A	1.2×10^{-5}	4.3×10^{-5}	4.41×10^{-5}	3.5	3.6
B	2.1×10^{-4}	7.3×10^{-4}	6.6×10^{-4}	3.5	3.2
C	7.6×10^{-5}	2×10^{-4}	2.3×10^{-4}	2.7	3.1
D	1.72×10^{-4}	6.1×10^{-4}	5.3×10^{-4}	3.6	3.1
E	8.1×10^{-4}	2.3×10^{-3}	2.89×10^{-3}	2.9	3.6
F	1.1×10^{-4}	3.5×10^{-4}	3.0×10^{-4}	3.3	2.9

5.3 Aerobic Degradation Rates and Mass Emission Reduction







5.3.1 Zero-Order degradation rate constants.

In order to determine if the zero-order degradation rates were different from the ones calculated in the aerobic phase, the zero-order degradation rates were calculated using equation 5.5. Results are presented in Table 5.4.

The results in Table 5.4 show that, similar to the aerobic phase, the zero-order degradation rates do not show any preferred aerobic degradation trend. The values are in the range from approximately 0.001 to 2 mg/Kg-h which is a similar range to the one obtained during Phase II. This results suggest that even though the source is ten times lower than in Phase II, both phases have similar zero-order degradation rates.

Table 5.4

Zero-order degradation rates, mg/Kg-h

Component	Column					
	A - 	B - 	C - 	D - 	E - 	F - 
Pentane	10.4± 1.8	1.6 ± 0.1	8.18 ± 1.2	2.2 ± 0.9	7.4 ± 0.5	0.7 ± 0.08
2-Methyl-2-Butene	0.02 ± 0.004	1.2 ± 0.07	0.4 ± 0.04	2.7 ± 0.1	2.1 ± 0.1	0.3 ± 0.08
MTBE	0.06 ± 0.004	0.2 ± 0.03*	0.2 ± 0.02*	4.6 ± 0.3	0.004± 0.001*	0.3 ± 0.06*
Hexane	0.01± 0.002	1.4 ± 0.1	0.9 ± 0.1	4.2 ± 1.5	3.7 ± 0.3	0.5 ± 0.02
Benzene	0.02 ± 0.003	0.1 ± 0.1	0.05 ± 0.02	0.9 ± 0.05	0.06 ± 0.02	0.04± 0.002
Cyclohexane	0.006±3x10 ⁻⁴	1.6 ± 0.1	0.2 ± 0.02	1.7 ± 0.05	5.0 ± 0.3	0.4 ± 0.08
Iso-Octane	0.004±0.0008	0.9 ± 0.1	0.6 ± 0.1	1.2 ± 0.07	5.63 ± 0.4	2.1 ± 0.2
Heptane	0.002±8x10 ⁻⁵	1.2 ± 0.2	0.2 ± 0.03	5.5 ± 0.5	5.2 ± 0.4	0.2 ± 0.01
Toluene	0.003 ± 0.001	0.3 ± 0.2	0.1 ± 0.04	2.4 ± 0.1	2.2 ± 0.2	0.2 ± 0.001
Octane	5±0.1x10 ⁻⁴	0.2 ± 0.1	0.02 ± 0.04	1.0 ± 0.07	2.4 ± 0.2	0.1 ± 0.04
P-Xylene	5±2x10 ⁻⁴	0.1 ± 0.02	0.05 ± 0.003	1.0 ± 0.1	0.8 ± 0.1	0.2 ± 0.07
1,3,5-Trimethylbenzene	2±0.2x10 ⁻⁴ *	0.1 ± 0.07	0.1 ± 0.04	1.9 ± 0.4	0.3 ± 0.04	0.01 ± 0.002*







*: Values calculated from the mass emission reduction: mass emission at the effluent during aerobic degradation conditions minus the mass emission during the oxygen depleted conditions.

5.3.2 Diffusive flux ratio.

In order to determine the decrease in flux for each column, and therefore the attenuation of the individual compounds during Phase III, the diffusive ratio for was calculated using Equation 5.7. The results are shown in Table 5.4.

Table 5.5

Diffusive flux ratio x 10²

Component \ Column	A - 	B - 	C - 	D - 	E - 	F - 
Pentane	0.7±0.07	0.01±0.007	4.8±0.02	2.1±0.04	2.0±0.1	1.74±0.07
2-Methyl-2-Butene	0.16±0.02	3±0.02x10 ⁻³	4.6±0.02	2.2±0.04	3.9±0.2	8x10 ⁻⁴
MTBE	1.0±0.06	0.05±0.007	18.8±3.0	16.3±0.7	23.1±1.6	0.6±0.1
Hexane	6±1x10 ⁻³	0.02±0.006	0.5±0.005	0.5±0.1	7.13±2.1	1±0.07x10 ⁻⁴
Benzene	2±0.2x10 ⁻⁴	8.0±0.03 x10 ⁻⁵	4.5±0.1 x10 ⁻⁵	0.02±0.006	7.4±0.3	7.9±0.2x10 ⁻⁵
Cyclohexane	0.92±0.04	0.04±0.002	8.2±0.05	7.8±0.1	10.7±0.3	1.5±0.05
Iso-Octane	2.7±0.3	0.08±0.002	10.2±0.7	7.9±0.02	24.7±0.2	0.07±0.002
Heptane	1.0±0.05 x10 ⁻³	8.0±1.0x10 ⁻³	2.0±0.1 x10 ⁻⁴	1.0±0.3 x10 ⁻³	15.1±1.6	4±1x10 ⁻⁴
Toluene	2.0±4.0x10 ⁻³	5.0±0.3x10 ⁻³	2.7x10 ⁻⁵	0.05±0.01	8.15±0.3	0.02±0.001
Octane	3.0±1.0x10 ⁻⁴	2.0±0.7x10 ⁻³	9.9x10 ⁻⁵	2±0.2x10 ⁻⁴	25.1±1.6	4±1x10 ⁻³
P-Xylene	5±0.05x10 ⁻³	8.0±1.0x10 ⁻⁴	7.0±0.2	4±1x10 ⁻³	25.1±0.8	0.2±0.08
1,3,5-Trimethylbenzene	9.0±1.0x10 ⁻³	0.04±0.01	0.01±0.003	0.3±0.1	99.2±1.8	0.03±0.006

The results in Table 5.5 suggests that phase III had a higher decrease in the normalized mass emissions than phase II. When comparing the diffusive flux ratios across columns, Column B displayed the highest attenuation activity as in the previous phase; however, the column with the second lowest diffusive flux ratios was column A, followed by columns F, C and D ordered from lowest to highest. Column E displays the highest diffusive flux ratios, indicating little to no decrease in the mass flux emissions. This is consistent with results plotted in Figure 5.1 (column E).

Also, in this case, not only n-heptane and n-octane had the highest flux attenuations but also benzene and toluene. Recalcitrant compounds such as n-pentane, MTBE and iso-octane, showed lower diffusive flux ratios than in the previous case (phase II).

Since the mass emission reduction analysis shown in Table 5.3 demonstrated that the decrease in the emissions could be attributed to aerobic degradation, it can be concluded that aerobic attenuation of hydrocarbon compounds (including recalcitrant chemicals) can be achieved when they are present at low concentrations.

5.4 Summary

With the objective of observing the effects of the vapor source concentration in the aerobic degradation activity of the columns, the concentration of the vapor source was decreased ten times the original concentration. Results show a decrease in the effluent normalized fluxes and concentrations in most of the chemicals across the columns except for column E. Figure 5.5 presents a comparison of the normalized fluxes for all of the chemicals for each experimental phase.

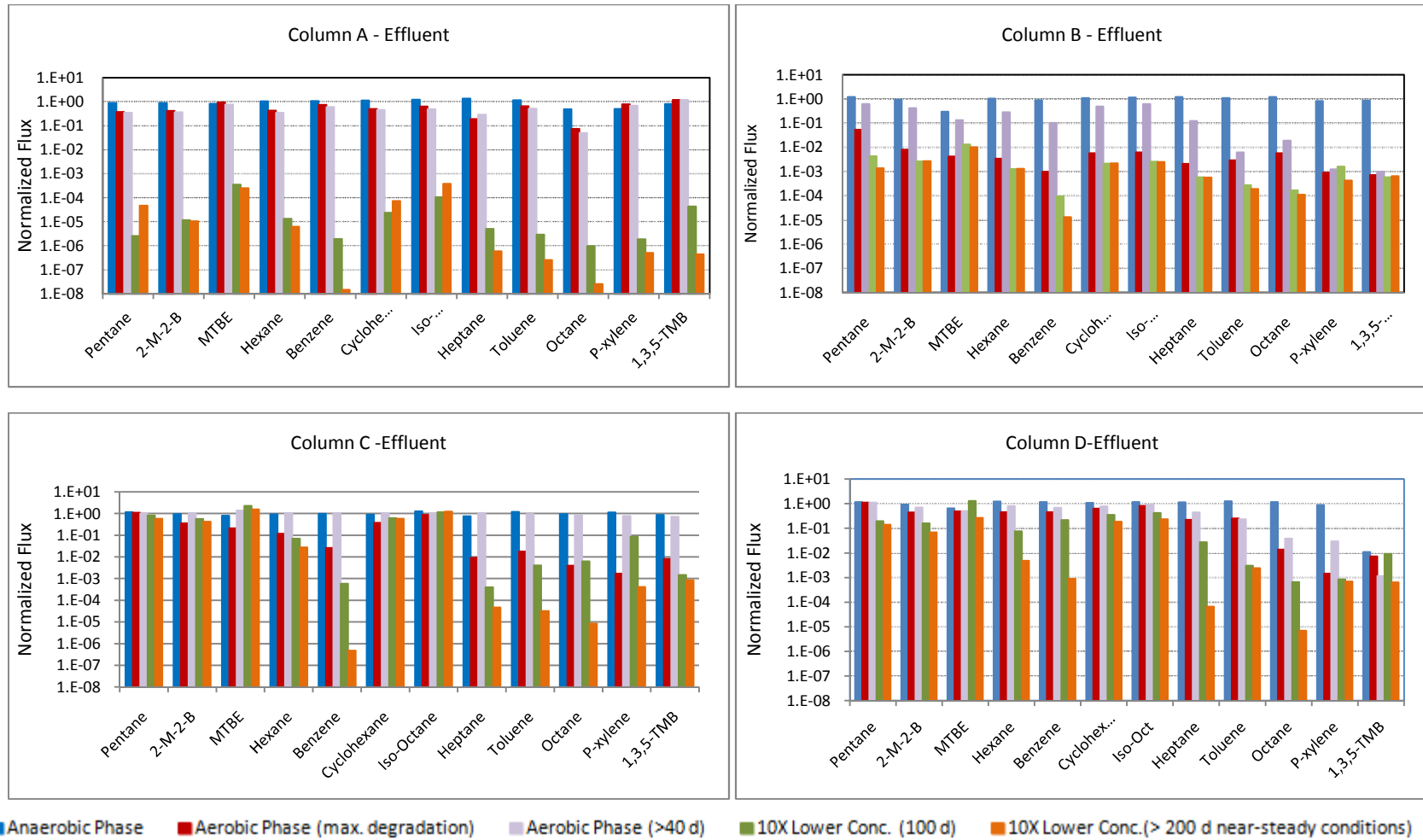
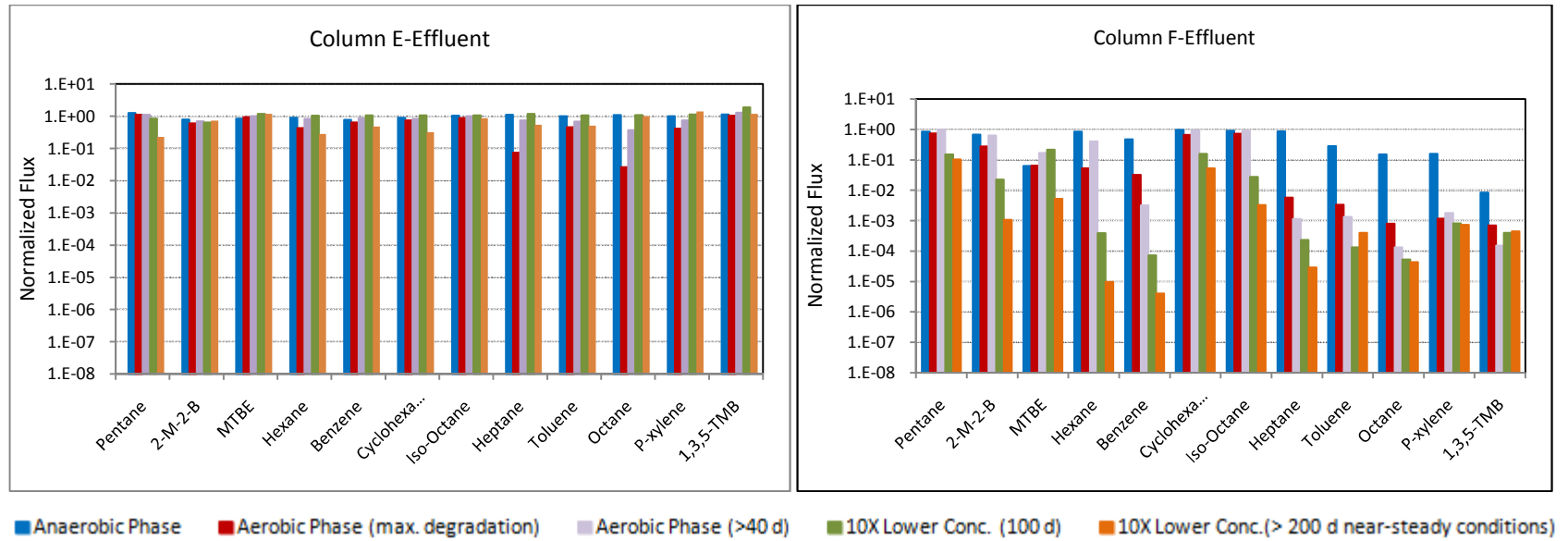


Figure 5.5. Comparison of the normalized flux of each chemical during the three conditions studied in the soil columns



(Note: 2-M-2-B = 2-methyl-2-butene and 1,3,5-TMB = 1,3,5-trimethylbenzene)

Figure 5.5. Comparison of the normalized flux of each chemical during the three conditions studied in the soil columns (continue)

The plots show that a reduction in the normalized flux of most of the chemicals took place in all of the columns during experimental Phase III. Fluxes of recalcitrant compounds such as MTBE and iso-octane were also decreased in most of the columns except in Columns C and E. Column A showed a large decrease in the petroleum hydrocarbon concentrations and fluxes during approximately 50 days of starting Phase III; after which, an increase in the fluxes of n-pentane, cyclohexane and iso-octane were observed, the rest of the chemicals did not show flux increases. Column E had little to no change in the normalized fluxes during the whole experimental period.

Phase III CO₂ profile plots showed that the CO₂ concentrations decreased with time in all of the columns. This behavior was expected since the hydrocarbon concentrations along the length of the columns were lower (due to lower source concentrations), thus the microbial communities had less substrate to convert to CO₂. However, as the flux profiles results showed (Figure 5.4) the “degradation zones” location of each column were the same as in Phase II.

As in Phase II, the diffusive flux ratios of each chemical with respect to the mass emissions of the anaerobic phase were calculated. The results suggested that the compounds that showed the highest mass flow attenuation are n-heptane, n-octane followed by benzene. Also, In this case, the columns can be ordered starting from the one that showed the highest mass flux reduction to the lowest as follows: B>F>A>D>C>E, which is different from the previous phase (B>C>F>D>A>E). In this case, column A showed a higher attenuation activity than during Phase II and Column C had a lower attenuation activity. However, Columns B and E were the columns with the highest and lowest flux decreases in both experimental phases.

Based on analysis made in Table 5.3, in which the reduction in the total petroleum hydrocarbon fluxes corresponded stoichiometrically to an increase in the CO₂ mass emissions and a decrease in the O₂ mass emissions, the flux attenuations observed during this experimental phase can be attributed to aerobic degradation

reactions. And since during this experimental phase (Phase III) the mass flux attenuation relative to the anaerobic phase, increased once when the vapor source concentration was decreased ten times from the original concentrations. Thus, it can be concluded that the aerobic attenuation activity of the soil was increased once the vapor source concentration was decreased ten times.

CHAPTER 6

POST-EXPERIMENT CHARACTERIZATION

6.1 Soil Properties

Once vapor concentrations reached near-steady conditions in Phase III (10X lower concentration vapor source), the soil columns were shut down by withdrawing the vapor source mixture from the bottom and stopping the sweep gas flow. Before opening the soil columns, helium effective diffusion coefficients as described in Appendix I and permeability were measured to determine the state of the soil columns at the end of the experiment and compare them with initial conditions. The columns were then opened and core samples were taken every 15.2 cm (6 inch). Soil moisture content and fraction of organic carbon (foc) were measured for each sample to compare them with the moisture content and foc of the soil before the columns were packed.

Figure 6.1 show the helium effective diffusion coefficient profiles with time. A decrease in the helium effective diffusion coefficient indicates an increase of the soil moisture content and therefore, a decrease in the soil vapor volume fraction. The plots in Figure 6.1 show little to no changes in the helium effective diffusion coefficient for the crushed granite layers, except at the top of column F, where the diffusion coefficient is higher, indicating a decrease in the soil moisture content, and at the bottom of column D, where the helium effective diffusion coefficient shows a decrease with time indicating that the moisture content of the soil increased with time during the experimental period. Similarly, the sand layers only display differences at the top of Columns B and D where the helium diffusion coefficient is higher at the end of the experiment by a factor of 2 in the case of Column B and 1.2 for Column D, indicating a decrease in the soil moisture content at the top of these columns.

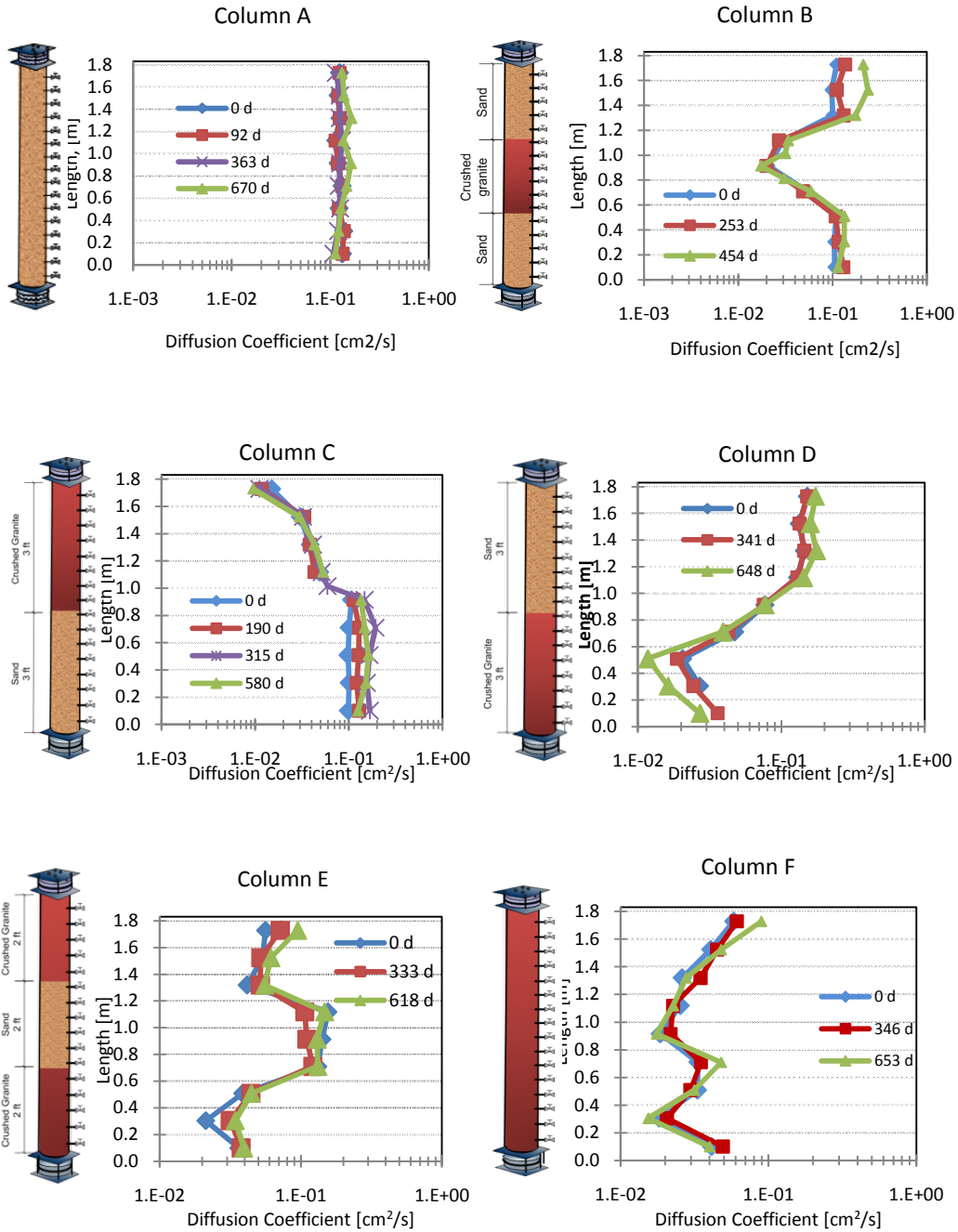








Figure 6.1 Helium Effective Diffusion Coefficient Profiles

Figure 6.2 shows the moisture content, permeability and fraction of organic carbon (FOC) profiles in each soil column. The profiles represented by the dashed lines are the values of each parameter measured before the soil was packed into the columns. The error in these measurements is 1% for the soil moisture content, 5% for the permeability and 0.2% for the foc.

Prior to packing, the moisture content of the sand and crushed granite were $2.5 \pm 0.03\%$ W/W and $11.0 \pm 0.1\%$ w/w respectively. The post-test moisture content profiles show that there was water redistribution during the experimental period since most of the columns show lower moisture contents at the top (except columns C and E) and higher moisture contents at the bottom than the initial values. To confirm this, the total water content in the soil was calculated at the beginning and at the end of the experiment. Results are presented in table 6.1.

Table 6.1

Initial vs. final water content in the soil [g-water/g-soil]

Column	A - 		B - 		C - 		D - 		E - 		F - 	
Value	Initial	Final	Initial	Final	Initial	Final	Initial	Final	Initial	Final	Initial	Final
Water Content [Kg]	1.1	0.87	0.17	0.05	3.7	3.6	0.27	0.04	1.1	0.93	5.2	4.8
			1.0	1.1					0.19	0.07		
			0.17	0.14	0.86	0.88	1.5	1.6	0.97	1.2		
SUM	1.1	0.87	1.3	1.3	4.6	4.5	1.8	1.6	2.3	2.2	5.2	4.8

As can be observed in Table 6.1 and consistent with the moisture profiles, the post-test water mass at the top of columns A, B, D, and F is lower than the pre-test mass. However, the total mass of water post and pre-experiment are similar to each other, indicating the occurrence of water redistribution along the length of the soil columns.

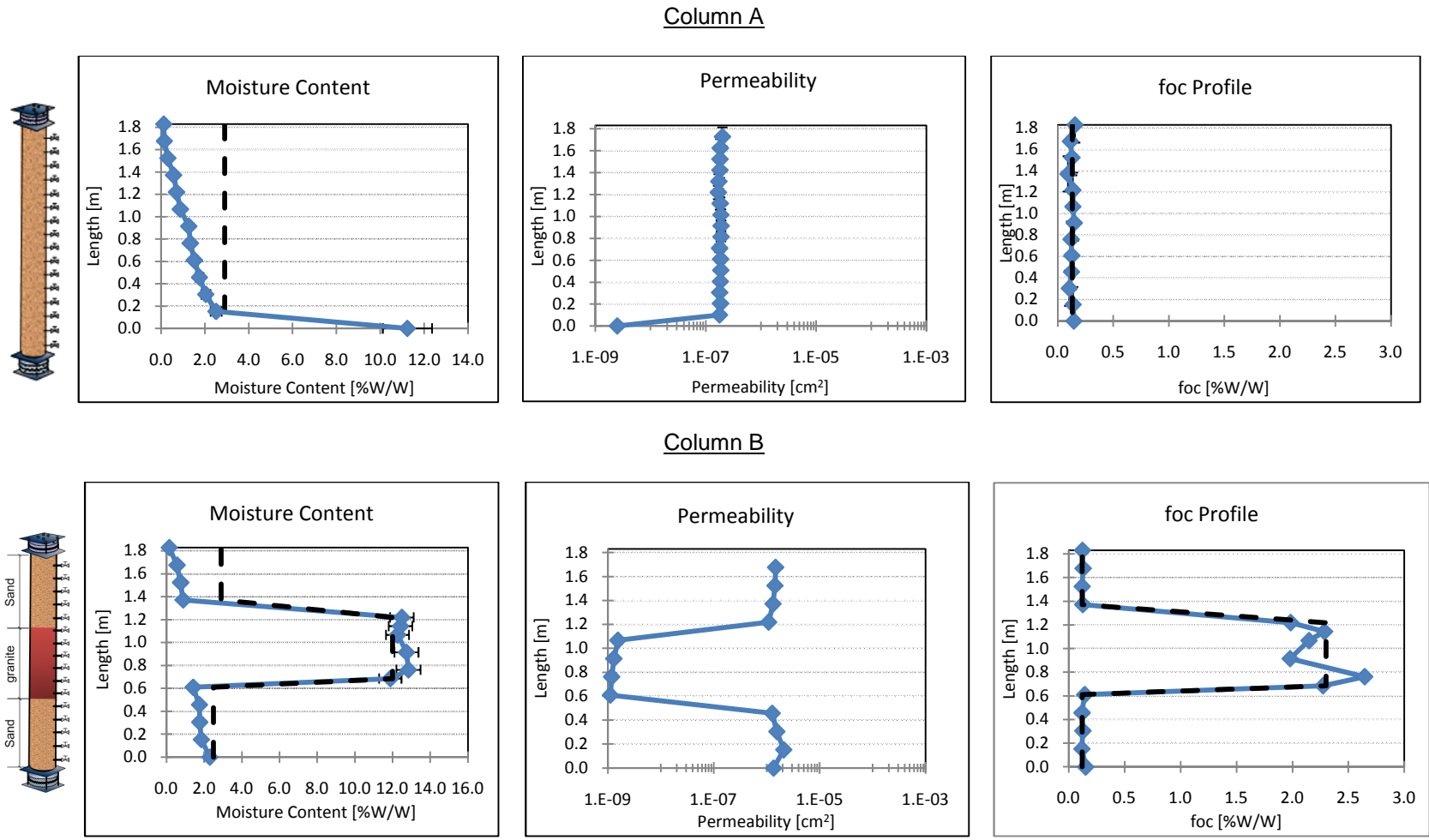


Figure 6.2. Moisture content, permeability and FOC profiles (--- soil initial conditions prior to packing the soil columns)

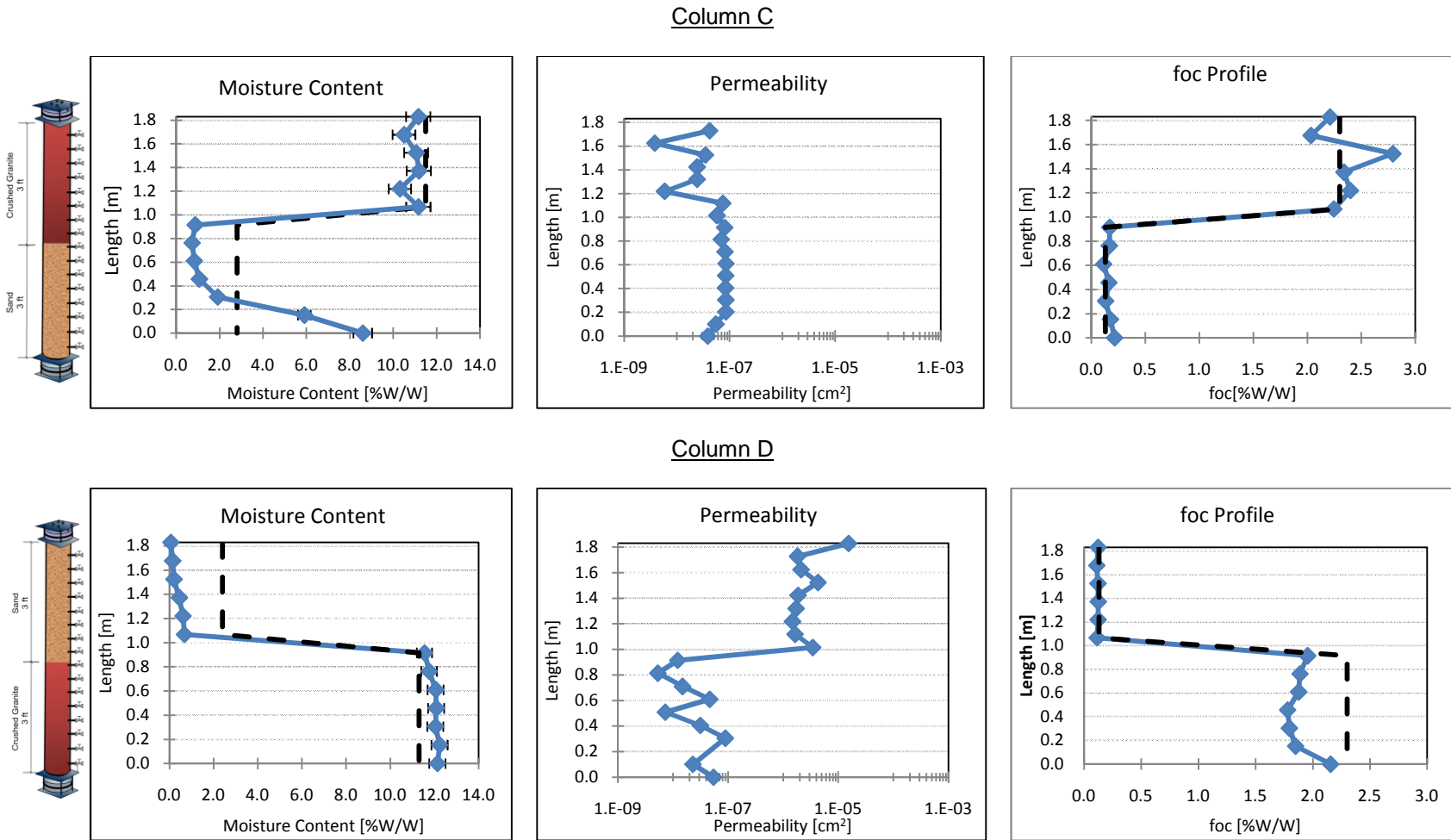


Figure 6.2. Moisture content, permeability and FOC profiles (- - - soil conditions prior to packing the soil columns) (continued)

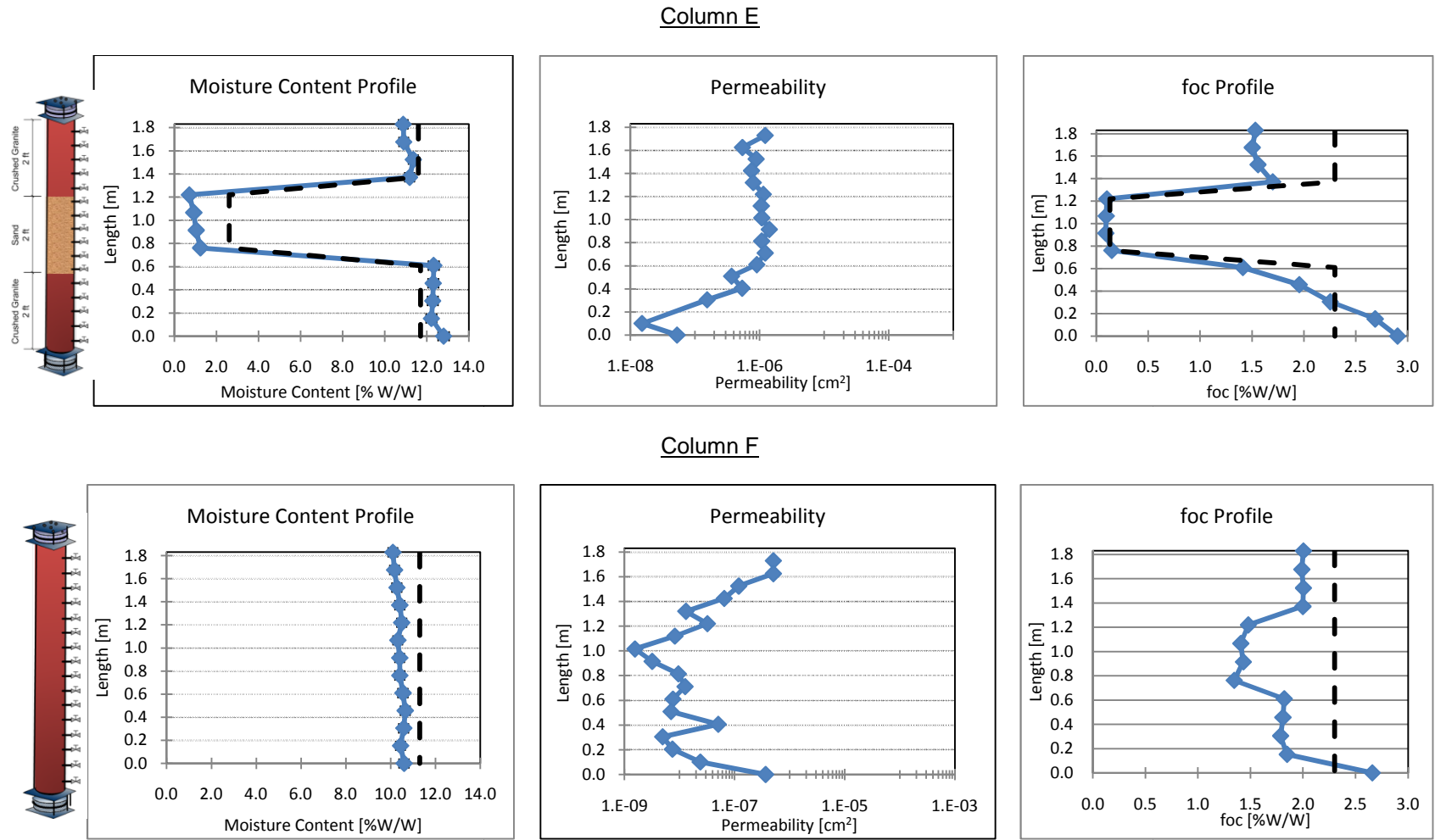








Figure 6.2. Moisture content, permeability and FOC profiles (--- soil initial conditions prior to packing the soil columns) (continued)

Consistent with what was observed in the near-steady conditions concentration profiles of Columns A and C, where the concentration gradient at the bottom of the column is higher than the rest of the layer (Chapters 3), higher moisture contents were observed in these column sections indicating water accumulation. The water was being accumulated below sampling port 1 (first sampling port above the source), therefore, the helium diffusion test was not able to detect it.

In order to determine how the redistribution of water impact the vapor transport, the post-experiment water filled porosity was calculated based on the water content of the soil and compared to pre-experiment values. Results are presented in Table 6.2.

Table 6.2

Water filled porosity [$\text{cm}^3\text{-water}/\text{cm}^3\text{-soil}$] based on the water mass in the soil columns

Column	A - 		B - 		C - 		D - 		E - 		F - 	
Value	Initial	Final	Initial	Final	Initial	Final	Initial	Final	Initial	Final	Initial	Final
Water filled porosity, $\text{cm}^3\text{water}/\text{cm}^3\text{-soil}$	0.04	0.03	0.04	0.01	0.20	0.19	0.04	0.01	0.23	0.21	0.20	0.18
			0.23	0.24					0.04	0.02		
			0.04	0.03	0.05	0.05	0.23	0.22	0.23	0.24		

Theoretically, the change in water filled porosity at the top of columns B, D and E resulted in an increase of the helium effective diffusion coefficient of 1 to 4%. To determine this, a sensitivity test analysis was performed using equation I.6 in Appendix I.

Initial foc of the sand was $0.04 \pm 0.002\%$ and of the granite was $0.5 \pm 0.03\%$. As can be observed in the profiles, both soils show little to no change in the foc during the experimental period.

6.2 Microbial Analyses

The number of colony forming units (CFU) present on a substrate (in this case, soil) is generally determined to gain information on the biodegradation potential of the substrate, to test the efficiency of bioremediation and/or determine the microbial activity of contaminated sites; however, it is important to note that only a small fraction of microorganisms (<1 to 10%) can be cultivated and grown in laboratory media since the growth requirements for many microbial strains is unknown. Therefore, plate counts underestimate the true population density present in the substrate (Margesin et al., 2003). Thus, in this study, results of the microbial analyses performed reflect only the culturable population of microorganisms. The qPCR tests provide the number of gene copies per gram of all the microorganisms present in the soil sample; thus, the results should be similar or higher than the CFU/g-soil of aerobic heterotrophic bacteria (AHB).

Profiles of the bacteria 16S rRNA gene copies per gram of soil, as well as the amount of CFU/g-soil of AHB and hydrocarbon degraders are presented in Figure 6.3. The CFU/g-soil of AHB and degraders has an error in the range of 5 to 15% and the qPCR values have an error of 5 to 18.8%.

As can be observed in Figure 6.3, the profiles of AHB are consistent with the bacteria 16srRNA genes since in most of the cases (except at the bottom of column E) both curves have the same shape and the gene copies/g-soil are slightly higher or equal to the AHB CFU/g-soil. Results show that in most of the columns, the crushed granite had higher CFU and gene copies per gram of soil than the sand except for column D, in which the crushed granite has approximately the same amount of genes and CFU per gram of soil than in the sand.

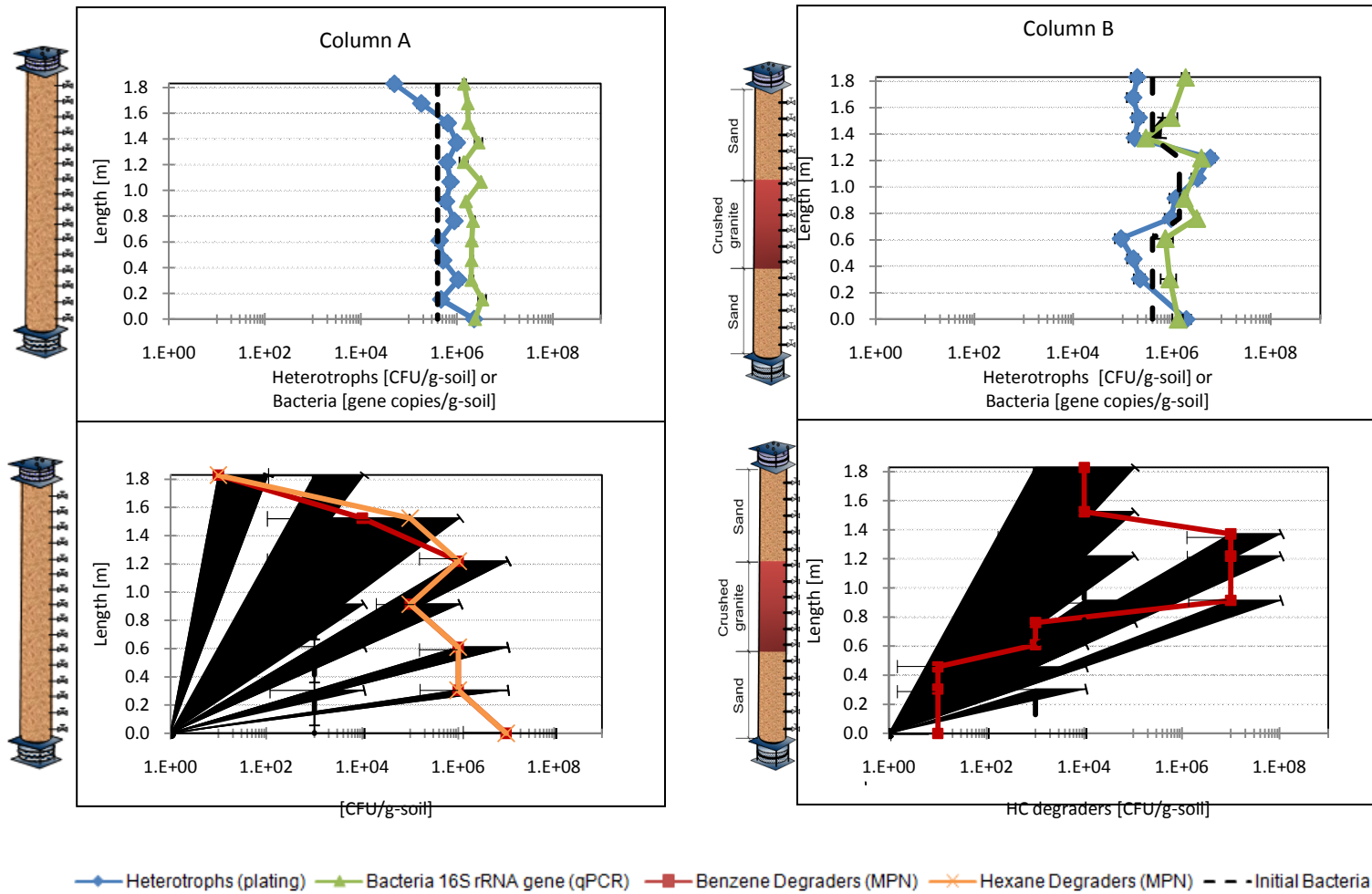


Figure 6.3. Microbial populations in the soil columns

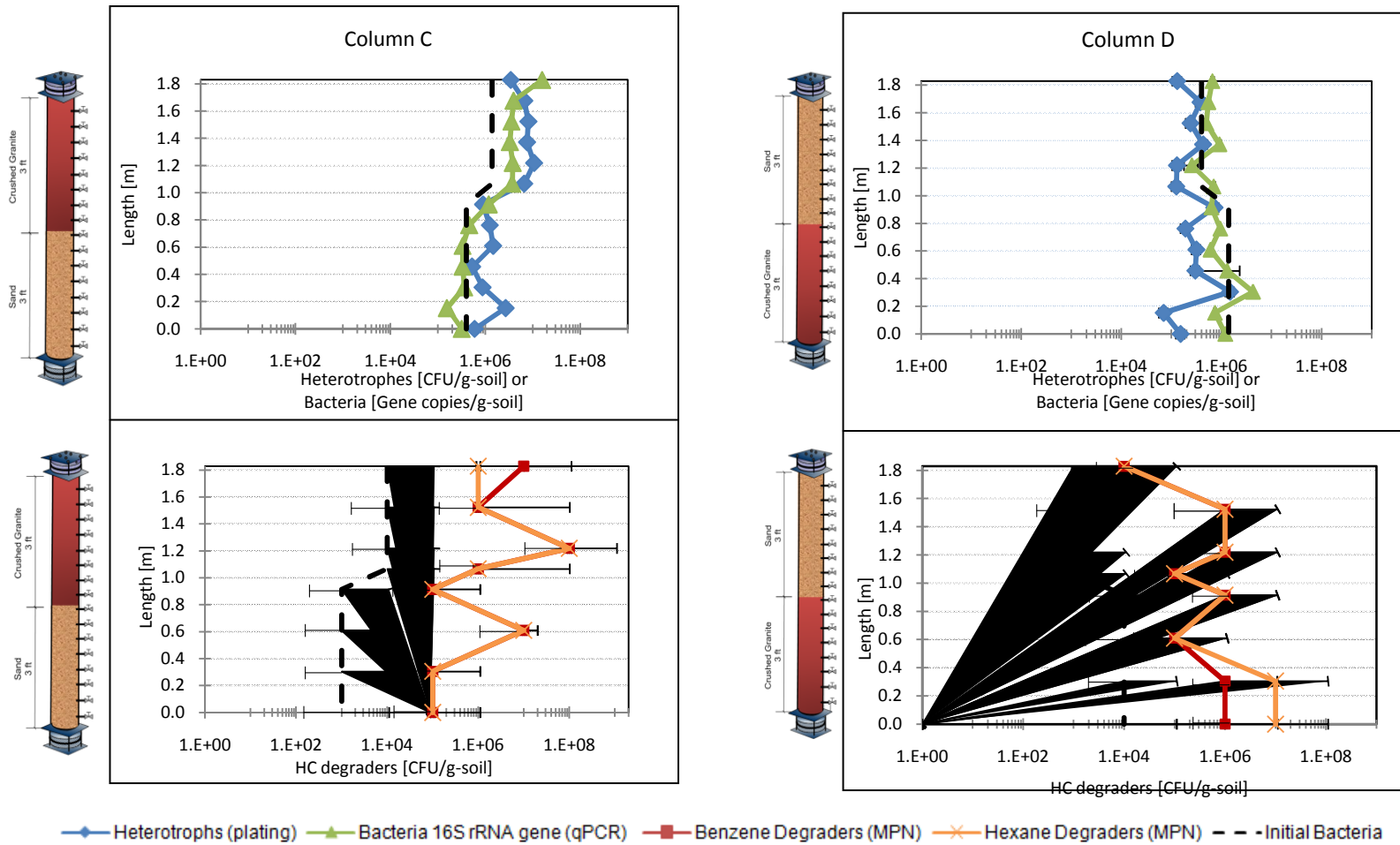


Figure 6.3. Microbial populations in the soil columns (continued)

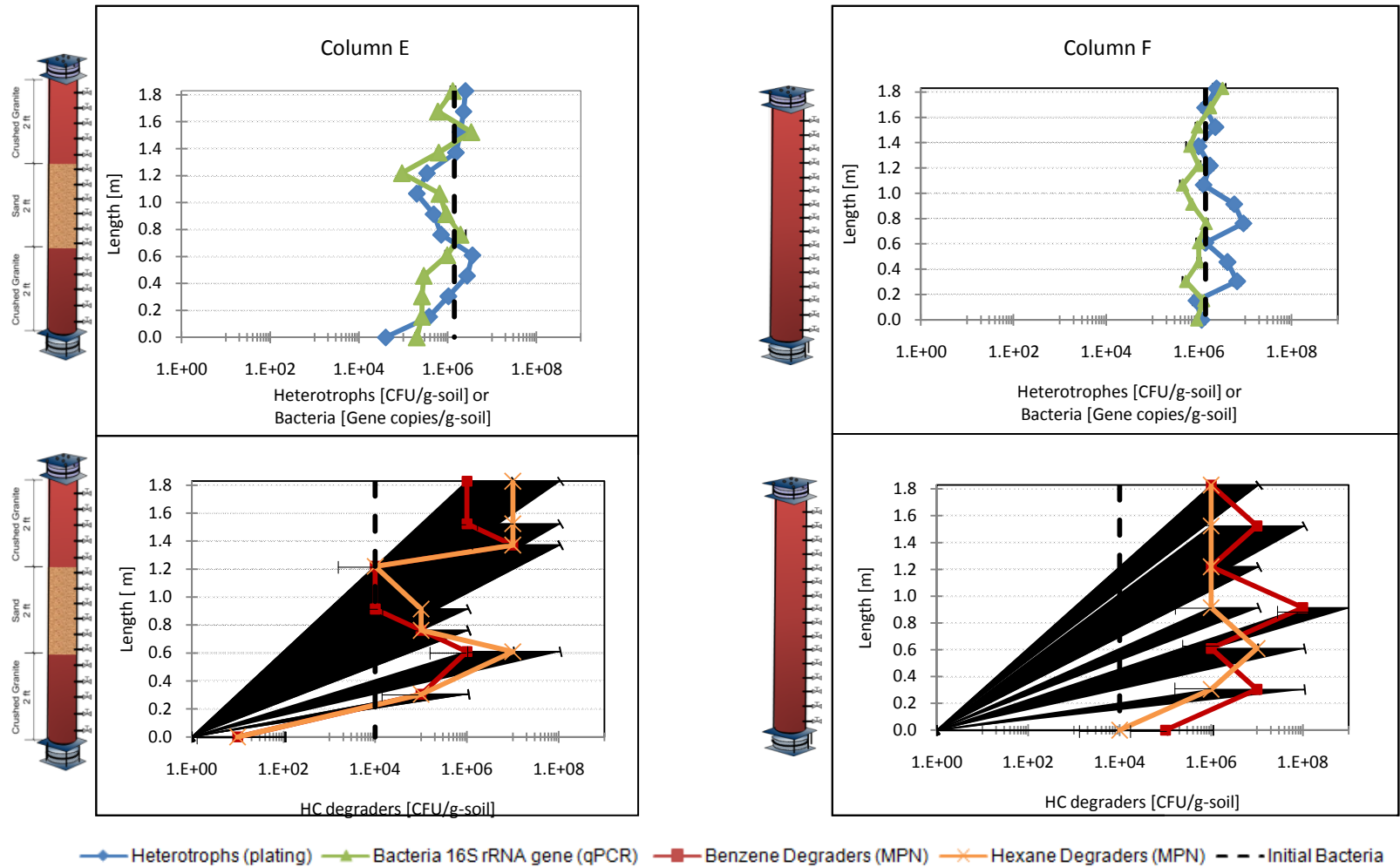


Figure 7.3. Microbial populations in the soil columns (continued)

DeVaul et al. (2004) performed a soil column experiment (1.2 by 0.08 m) in which it was observed that the soil, after being exposed to hydrocarbon vapors, had populations of 10^2 CFU/g-soil of benzene degraders at the top of the column (1.05 m), 10^6 CFU/g-soil in the middle of the column (0.45 – 0.75 m) and 10^8 CFU/g-soil at the bottom of the column. In this experiment, similarly to DeVaul et al. (2004), the aerobic hydrocarbon degraders population at the top of the column ($1 \pm 3 \times 10^4 - 1 \pm 3 \times 10^6$ CFU/g-soil) was lower than in the middle ($1 \pm 3 \times 10^6 - 1 \pm 3 \times 10^8$ CFU/g-soil); however, the number of degraders at the bottom of the columns was even lower than at the top of the columns ($1 \pm 3 \times 10^1 - 1 \pm 3 \times 10^5$ CFU/g-soil) except for Columns A and D. These columns had their “degradation zones” at the bottom (0 – 0.3 m), therefore, it is reasonable that the number of degraders is higher ($1 \pm 3 \times 10^6 - 1 \pm 3 \times 10^7$) in this soil interval.

As explained in Chapter 5, during the experiment aerobic phases II and III, a “degradation zone” was identified in each column. It was expected that the maximum number of hydrocarbon degraders be located in these zones. Therefore, the location of the “degradation zone” and the location where the maximum number of CFU/g-soil of degraders were observed were compared in Table 6.3. As can be observed both locations match in all of the columns.

Table 6.3

Comparison of the location of the degradation zone vs. location of the maximum number of CFU/g-soil of hexane and benzene degraders in the soil columns

Column	Length from the bottom of the column [m]		Soil type
	Degradation zone	Length where the maximum number of CFU/g-soil of hexane and benzene degraders was observed	
A	0 – 0.3	0 – 0.3	Sand (Homogeneous sand column)
B	0.8 – 1.2	0.8 – 1.2	Crushed granite
C	1.2 – 1.6	1.1 – 1.3	Crushed granite
D	0 – 0.5	0.0 - 0.3	Crushed granite
E	0.2 – 0.4	0.4 – 0.7	Crushed granite
F	1.0 -1.4	0.3 – 0.6	Homogeneous crushed granite column

6.3. Summary

The experiment was terminated after most of the chemicals had reached near-steady conditions during experimental phase III. This was performed by removing the vapor source solution from the bottom and stopping the sweep gas flow. Before opening the columns, the effective diffusion coefficient and permeability were measured. The effective diffusion coefficient profiles were compared with the values at different stages of the experiment. Then, the columns were opened and core samples were taken every 15.2 cm (6 inch.) to determine the post-experiment moisture content and foc profiles. Finally, microbial analyses such as qPCR, the plating technique and MPN were used to determine the number of bacteria 16S rRNA gene/g-soil and the number of CFU/g-soil for AHB (plating) and hydrocarbon degraders (MPN) present along the soil column length.

Soil moisture content profiles and water mass balance pre and post-experiment (Figure 6.1 and Table 6.1), show that water redistributed during the experimental period as most the columns showed an increase in moisture content at the bottom and a

decrease at the top. Exceptions were Columns C and E that maintained initial moisture content levels at the top.

Consistent with what it was observed in the vapor concentration profiles during near-steady conditions, columns A and C had significantly increased moisture contents at the bottom, indicating that water accumulated at the bottom of these columns.

In order to determine how the change in moisture content at the top of the columns affected the vapor transport in the soil, the water filled porosities were calculated based on the mass of water content in each soil column. Using these values a sensitivity analysis on the helium effective diffusion coefficients was performed using equation I.6 (Appendix I). Results showed that the helium effective diffusion coefficient is increased by 1 to 4% in Columns B, D and E as a result of the decrease of the water filled porosities at the top.

Results from the plating technique and qPCR determine that the number of CFU and gene copies per gram of soil were higher in the crushed granite material than in the sand. However, in Column D both soils had approximately the same microbial concentrations.

The profiles of CFU/g-soil of hydrocarbon degraders showed that the number of microorganisms degraders at the bottom of most of the columns were lower than in the rest of the columns length. Columns A and D however, showed that the highest degrader CFU/g- soil were found at the bottom (0 – 0.3 m). The reason for this, is that these two columns had their “degradation zones” at the bottom (0 – 0.3 m).

With the objective of determining if the maximum number of degraders were located at the same column length of the “degradation zones” of each column, a comparison of the location where the maximum microbial population along the length of the columns vs. the location of the “degradation zone” of each column was performed (Table 6.3). Results indicated that the maximum benzene and hexane degraders

population were found at the locations where the “degradation zones” were identified in each column.

CHAPTER 7

MATHEMATICAL MODEL SIMULATION OF THE SOIL COLUMNS EXPERIMENT

With the objective of determining the first-order degradation rate constants of the aerobic degradation reactions that occurred in the soil column experiment, the Luo (2009) modified version of the Abreu-Johnson (2005) three-dimensional transient mathematical model was used. The 3-D transient mathematical model has the capability of simulating the vapor transport of multiple chemicals in multiple layer settings, multiple source zones, wind load effect on the pressure distribution and biodegradation kinetics such as zero-order, first-order and monod kinetics. Some of the model outputs include: three-dimensional normalized concentration profiles, soil gas mass emissions, three-dimensional pressure distribution and indoor air concentrations (when there is a building on the soil surface). The model has been previously utilized to explore the influences of natural factors such as different soil characteristics, oxygen content in the soil, as well as the effects of the location and size of the source zone, bio-attenuation, wind load and barometric pressure fluctuation on the subsurface gas distribution and indoor air concentrations (Abreu et al., 2005; Luo et al., 2009).

In order to determine the first-order constants, the 3-D transient numerical model was used to perform a 1-D simulation of the near-steady conditions for the three phases of this study. Simulations for each soil column were performed. The twelve petroleum hydrocarbons included in the vapor source were simulated simultaneously; the source zone was located 1.8 m (6 ft) below the soil surface and the pressure differential along the vertical length of the soil column was set to zero. Since the soil column experiment is a study of the vapor transport and aerobic degradation in the vadose zone, the simulation was performed for cases in which no building was located at the soil surface. Once this conditions were established, the next three steps were performed:

- I. Model domain and effective diffusion coefficients determination. This is performed by simulating the near-steady conditions of experimental Phase I and fitting the simulation output to the experimental results
- II. First-order degradation rates are determined by trial and error using the model domain and effective diffusion coefficients obtained from Step I, then the simulation output was fitted to the near-steady state results of experimental Phase III.
- III. Simulation of the near-steady conditions of experimental Phase II was performed using the model domain and the first-order degradation rate constants obtained from simulating experimental Phases I and III (Steps I and II).

7.1 Step I: Model Domain and Effective Diffusion Coefficients. Simulation of Experimental Phase I

7.1.1 Input parameters.

During Phase I, no degradation reactions occurred, therefore, the simulation only includes the diffusive vapor transport of the twelve petroleum hydrocarbon compounds through the soil columns.

i) Soil characteristics.

The soil columns contained 1 to 3 soil layers built from two types of soils; each soil layer had its own physical characteristics such as, moisture content and effective diffusion coefficients. Experimental results demonstrated that these characteristics varied even within the same soil type. Thus, for modeling purposes the soil columns were divided in small soil vertical sections (approximately 0.10 m thick) so differences in the soil characteristics could be accounted for. The soil sections were chosen according to the experimental effective diffusion coefficient profiles. Figure 7.1 show a schematic of

the model domain utilized for one of the soil columns. As can be seen in Figure 7.1, smaller soil sections (0.034 m) are applied mainly at the boundary where the two types of soils converge in order to increase the accuracy of the simulation more accurate results.

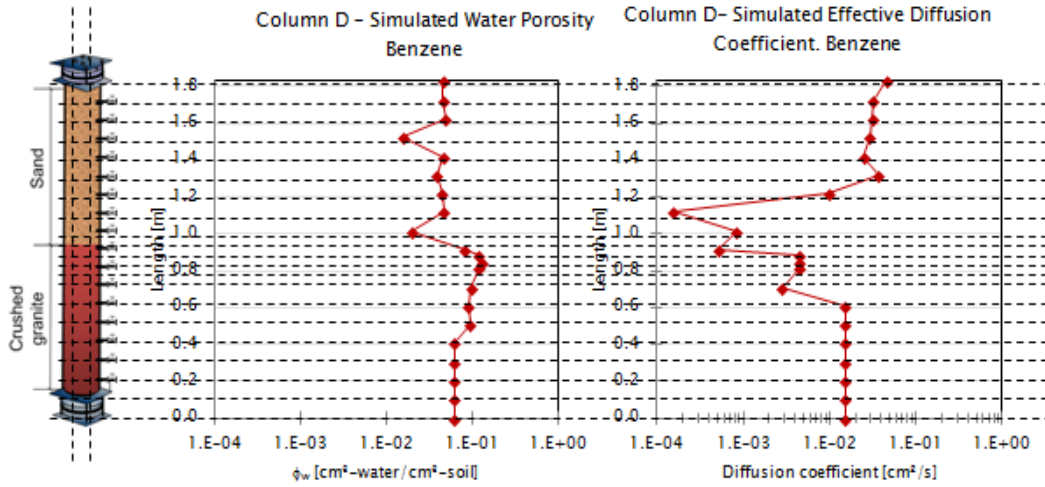


Figure 7.1. Model domain schematic

The 3-D transient model calculates the vapor diffusion coefficient in each of the soil sections using the Millington-Quirk equation (Equation 7.1). The total and water filled porosity are necessary inputs to perform this calculation. In this case, to make the simulation more accurate, the soil total and water filled porosities were calculated from the effective diffusion coefficients determined experimentally (See Chapter 4, Figure 4.3) using Equations 7.1 and 7.2. Table 7.1 shows the results, which were inputs in each simulation.

$$D_v^{eff} = D_i^{air} \cdot \frac{\phi_v^{3.33}}{\phi_T^2} + \frac{D_i^{H2O}}{H_i} \cdot \frac{\phi_{H2O}^{3.33}}{\phi_T^2} \quad (7.1)$$

$$\phi_{H2O} = \phi_T - \phi_v \quad (7.2)$$

Where,

D_v^{eff} = Effective vapor diffusion coefficient [cm²/s]

D_i^{air} = Diffusion coefficient of component i in air [cm²/s]

$D_i^{H_2O}$ = Diffusion coefficient of component i in water [cm^2/s]

ϕ_v = Vapor filled porosity [cm^3 vapor/ cm^3 soil]

ϕ_{H_2O} = Water filled porosity [cm^3 water/ cm^3 soil]

ϕ_T = Total porosity [cm^3 voids/ cm^3 soil]

H_i = Henry's law constant

The soil bulk density utilized for the model is the one measured for each type of soil at the beginning of the experiment (1.68 g/cm^3 for sand and 1.73 g/cm^3 for the crushed granite). The foc and permeability values in each soil section were measured from the 6-in soil core samples taken at the end of the experiment (See Figure 2.7, Chapter 2). Table 7.1 shows the calculated soil total porosity and water filled porosities used as inputs.

ii) Chemical characteristics.

The twelve petroleum hydrocarbon chemicals utilized in the vapor source for the soil column experiments were simulated simultaneously. The model requires the chemicals source, initial soil and atmosphere concentrations as well as their physical characteristics such as the Henry's law constants. These inputs are presented in Tables 7.2.

Table 7.1

Calculated total and water filled porosities for the simulation of each soil column

Soil Section	Column A				Column B				Column C			
	Length from bottom, m	Soil Type	ϕ_T , cm ³ voids/cm ³ soil	ϕ_{H_2O} , cm ³ H ₂ O/cm ³ soil	Length from bottom m	Soil Type	ϕ_T , cm ³ voids/cm ³ soil	ϕ_{H_2O} , cm ³ H ₂ O/cm ³ soil	Length from bottom, m	Soil Type	ϕ_T , cm ³ voids/cm ³ soil	ϕ_{H_2O} , cm ³ H ₂ O/cm ³ soil
1	0.03	Sand	0.22	0.15	0.61	Sand	0.36	0.04	0.10	Sand	0.20	0.12
2	0.07	Sand	0.22	0.14	0.71	Granite	0.41	0.21	0.20	Sand	0.85	0.01
3	0.10	Sand	0.22	0.11	0.81	Granite	0.41	0.17	0.30	Sand	0.85	0.01
4	0.14	Sand	0.42	0.02	0.91	Granite	0.41	0.29	0.41	Sand	0.65	0.11
5	0.17	Sand	0.42	0.05	1.02	Granite	0.41	0.32	0.51	Sand	0.22	0.04
6	0.20	Sand	0.42	0.02	1.07	Granite	0.41	0.30	0.61	Sand	0.55	0.03
7	0.30	Sand	0.53	0.12	1.12	Granite	0.41	0.30	0.71	Sand	0.96	0.003
8	0.41	Sand	0.53	0.07	1.16	Granite	0.41	0.30	0.81	Sand	0.45	0.1
9	0.51	Sand	0.70	0.08	1.19	Granite	0.41	0.30	0.91	Sand	0.55	0.05
10	0.61	Sand	0.55	0.04	1.21	Sand	0.36	0.08	1.02	Granite	0.50	0.05
11	0.71	Sand	0.53	0.06	1.32	Sand	0.53	0.005	1.12	Granite	0.5	0.14
12	0.81	Sand	0.45	0.04	1.42	Sand	0.39	0.001	1.22	Granite	0.41	0.06
13	0.91	Sand	0.75	0.11	1.52	Sand	0.48	0.02	1.32	Granite	0.41	0.15
14	1.02	Sand	0.65	0.08	1.62	Sand	0.55	0.04	1.42	Granite	0.41	0.28
15	1.12	Sand	0.55	0.04	1.73	Sand	0.55	0.03	1.52	Granite	0.41	0.20
16	1.22	Sand	0.55	0.06	1.83	Sand	0.76	0.07	1.62	Granite	0.41	0.27
17	1.32	Sand	0.50	0.03					1.65	Granite	0.41	0.26
18	1.42	Sand	0.65	0.08					1.69	Granite	0.41	0.21
19	1.52	Sand	0.55	0.06					1.73	Granite	0.41	0.29
20	1.62	Sand	0.45	0.03					1.83	Granite	0.41	0.22
21	1.73	Sand	0.50	0.03								
22	1.83	Sand	0.50	0.03								

Table 7.1 (continue)

Calculated total and water filled porosities for the simulation of each soil column (Continue)

Soil Section	Column D				Column E				Column F			
	Length from bottom, m	Soil Type	ϕ_T , cm ³ voids/ cm ³ soil	ϕ_{H_2O} cm ³ H ₂ O/ cm ³ soil	Length from bottom, m	Soil Type	ϕ_T , cm ³ voids/ cm ³ soil	ϕ_{H_2O} cm ³ H ₂ O/ cm ³ soil	Length from bottom, m	Soil Type	ϕ_T , cm ³ voids/ cm ³ soil	ϕ_{H_2O} cm ³ H ₂ O/ cm ³ soil
1	0.41	Granite	0.41	0.10	0.41	Granite	0.46	0.06	0.10	Granite	0.41	0.06
2	0.51	Granite	0.41	0.22	0.51	Granite	0.41	0.07	0.71	Granite	0.41	0.12
3	0.61	Granite	0.41	0.22	0.61	Sand	0.47	0.05	0.81	Granite	0.41	0.17
4	0.71	Granite	0.41	0.23	0.71	Sand	0.55	0.05	0.91	Granite	0.41	0.27
5	0.81	Granite	0.41	0.26	0.81	Sand	0.58	0.05	1.02	Granite	0.41	0.16
6	0.85	Granite	0.41	0.27	0.91	Sand	0.69	0.04	1.12	Granite	0.41	0.26
7	0.88	Granite	0.41	0.26	1.02	Sand	0.62	0.05	1.22	Granite	0.41	0.25
8	0.91	Sand	0.41	0.14	1.12	Granite	0.56	0.03	1.32	Granite	0.41	0.23
9	1.02	Sand	0.64	0.02	1.22	Granite	0.41	0.08	1.42	Granite	0.41	0.29
10	1.12	Sand	0.44	0.05	1.32	Granite	0.41	0.14	1.52	Granite	0.41	0.25
11	1.22	Sand	0.45	0.04	1.42	Granite	0.41	0.09	1.63	Granite	0.41	0.22
12	1.32	Sand	0.47	0.04	1.52	Granite	0.41	0.09	1.73	Granite	0.41	0.19
13	1.42	Sand	0.39	0.05	1.62	Granite	0.41	0.08	1.83	Granite	0.41	0.16
14	1.52	Sand	0.46	0.02	1.73	Granite	0.41	0.08				
15	1.62	Sand	0.46	0.05	1.83	Granite	0.41	0.09				
16	1.73	Sand	0.50	0.05								
17	1.83	Sand	0.50	0.05								

130

Table 7.2

Chemical characteristics inputs for simulating experimental phase I

Chemical	H_i^a cm ³ -H ₂ O/ cm ³ -vapor	K_{oc}^a , g/g-oc	$D^{air\ a}$, cm ² /s	$D^{H_2O} \times 10^{-6\ a}$, cm ² /s	Atmospheric concentration, g/cm ³	Initial soil concentration, g/cm ³	Source gas concentration x10 ⁻⁶ g/cm ³ (experimental phases I and II)
N-Pentane	41.15	4.1	0.086	8.1	0.0	0.0	96.2
2-Methyl-2-butene	3.55	130.8	0.086	8.9	0.0	0.0	28.2
MTBE	0.03	12.3	0.079	7.5	0.0	0.0	4.6
N-Hexane	58.13	1250	0.071	7.8	0.0	0.0	25.3
Benzene	0.18	58.9	0.088	1.0	0.0	0.0	3.8
Cyclohexane	6.14	482	0.078	8.4	0.0	0.0	20.4
Iso-octane	107.27	3.43	0.062	6.2	0.0	0.0	18.6
N-Heptane	78.07	2400	0.065	7.0	0.0	0.0	14.9
Toluene	0.21	182	0.082	8.6	0.0	0.0	4.8
N-octane	89.84	1600	0.051	6.6	0.0	0.0	2.5
P-xylene	0.21	389	0.077	8.4	0.0	0.0	1.5
1,3,5-trimethylbenzene	0.24	1200	0.068	7.2	0.0	0.0	1.5
CO ₂	1.2	0.0	0.16	16.7	7.5x10 ⁻⁷	0.0	NA
Oxygen	31.6	0.0	0.2	24.1	2.8x10 ⁻⁴	0.0	NA

^a: Source: CRC handbook and Perry's Chemical Engineering Handbook

The procedure followed to fit the simulation output to the experimental results of Phase I is illustrated in Figure 7.2.

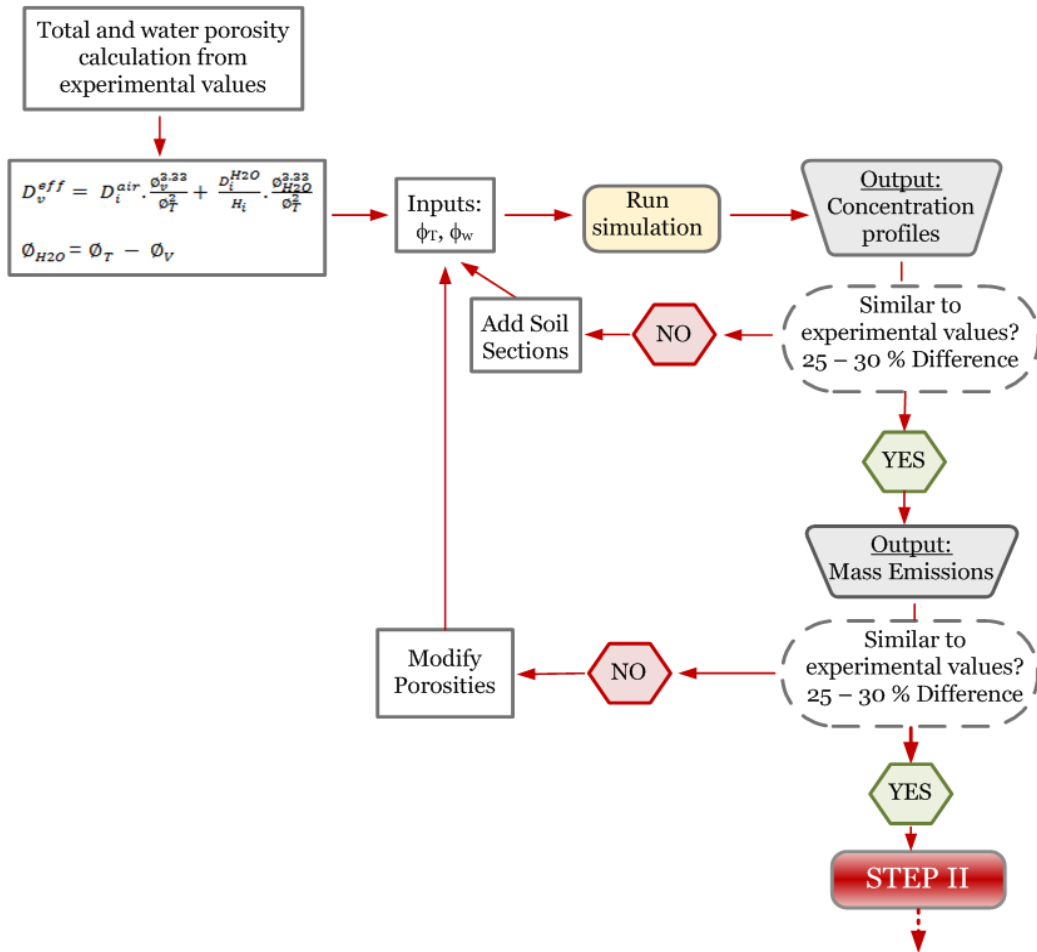


Figure 7.2. Step I: model domain and effective diffusion coefficients calculation.

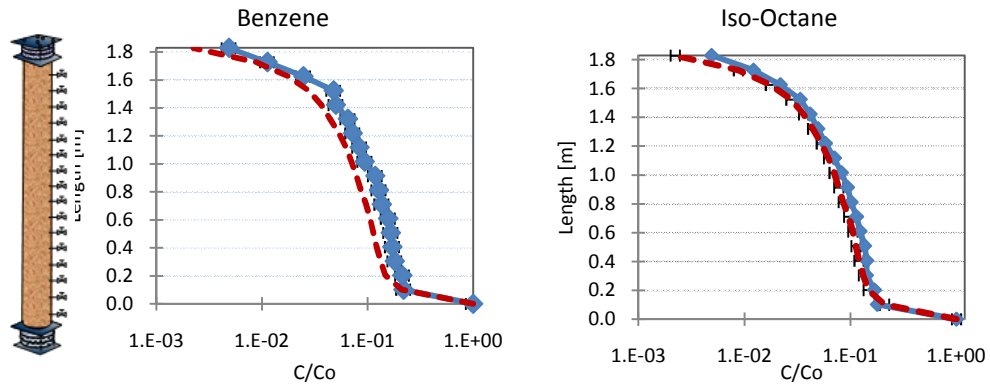
Simulation fitted to near-steady conditions of experimental Phase I.

(Note: 25 to 30% difference was used to take into account the variability of the experimental results)

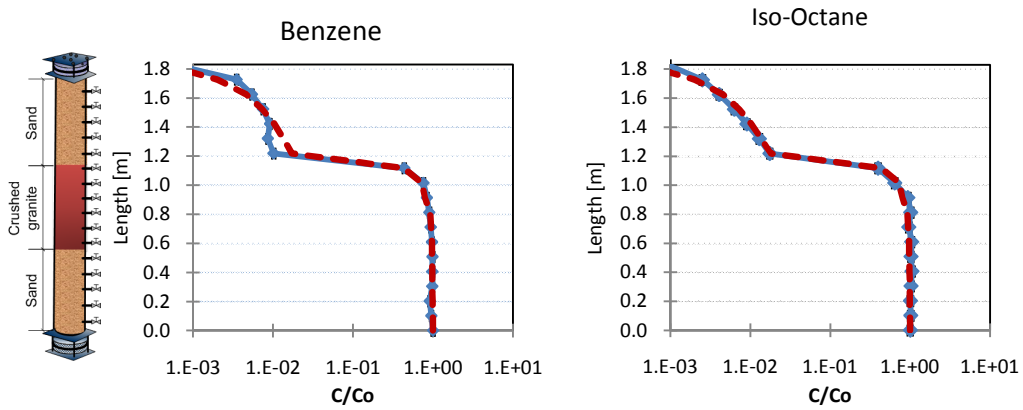
7.1.2 Simulation results.

Figure 7.3 shows the simulated gas profiles for benzene and iso-octane for each one of the columns, as well as their comparison to the experimental results. Plots of the rest of the components can be found in Appendix VI.

Column A



Column B



Column C

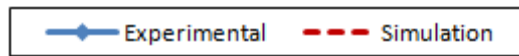
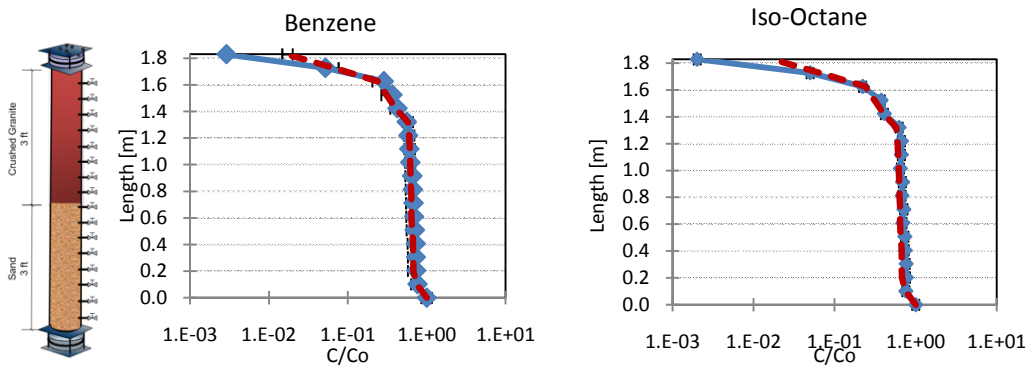
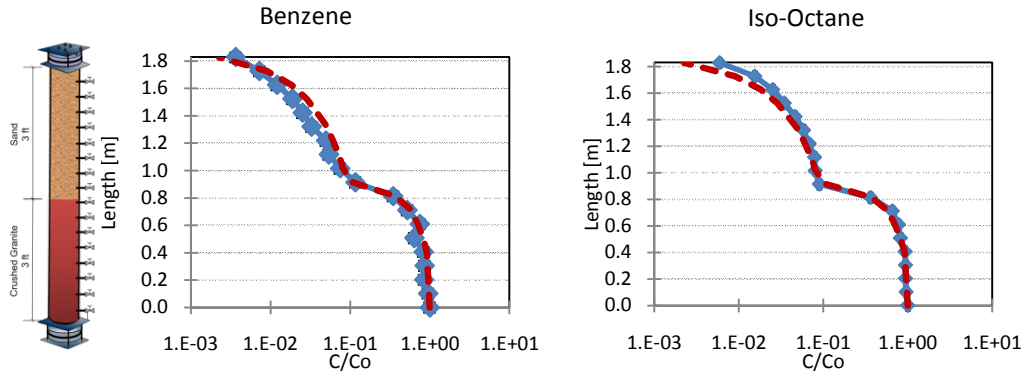
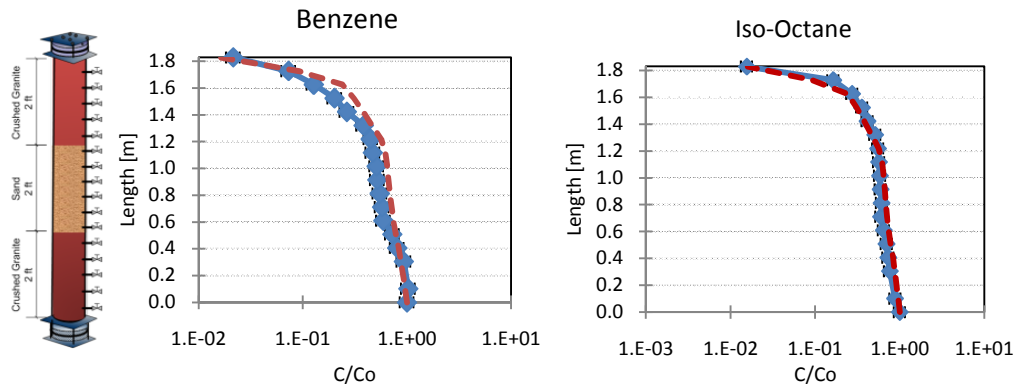


Figure 7.3. Oxygen depleted phase simulation profile results at near-steady conditions and their comparison to the experimental results

Column D



Column E



Column F

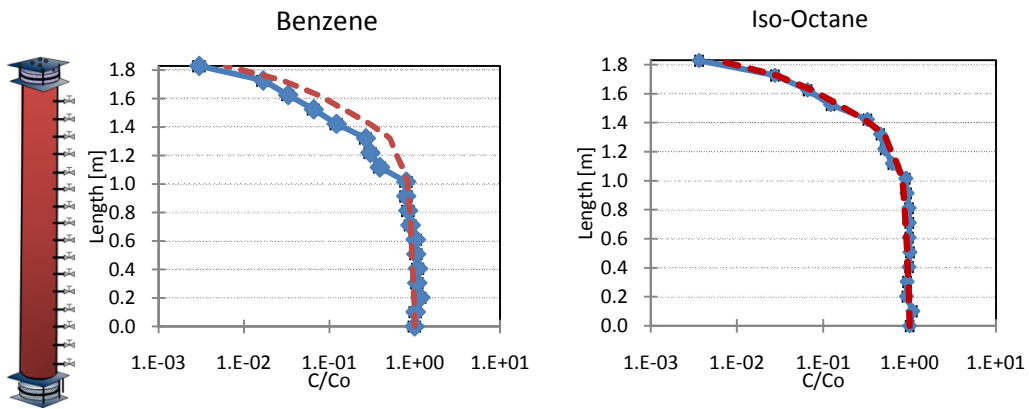


Figure 7.3. Oxygen depleted phase simulation profile results at near-steady conditions and their comparison to experimental results (Continued)

As can be observed in Figure 7.3 the simulation profiles fit the experimental profiles. However, since the curves can be easily constructed with the soil characteristics and diffusion coefficients, it is necessary to confirm that all of the outputs are consistent with the experimental results. To do this, the simulated effluent mass emissions were compared to the ones obtained experimentally. Both numbers had to be similar to each other in order to confirm that the modeled results fit the experimental data. Table 7.3 presents the comparison of the model mass emissions outputs to the experimental mass emission of each soil column.

Table 7.3

Comparison of mass emissions: experimental vs simulation during phase I (anaerobic phase)

Compound	Column A x10 ⁻⁸ [g/s]		Column B x10 ⁻⁸ [g/s]		Column Cx10 ⁻⁸ [g/s]	
	Experiment	Simulation	Experiment	Simulation	Experiment	Simulation
N-Pentane	23.5 ± 1.7	22.9	7.6 ± 0.7	7.1	14.5 ± 1.3	13.6
2-Methyl-2-Butene	7.7 ± 0.3	8.4	2.2 ± 0.08	2.7	3.9 ± 0.2	4.0
MTBE	1.6 ± 0.1	1.2	0.2 ± 0.01*	0.4	0.5 ± 0.02*	0.6
N-Hexane	5.6 ± 0.3	6.6	2.2 ± 0.1	2.2	3.3 ± 0.1	3.5
Benzene	1.2 ± 0.1	1.2	0.3 ± 0.2	0.3	0.6 ± 0.03	0.7
Cyclohexane	5.3 ± 0.2	5.9	2.0 ± 0.05	2.0	3.4 ± 0.1	3.5
Iso-Octane	4.0 ± 0.1	4.5	1.6 ± 0.07	1.5	2.3 ± 0.1	2.4
N-Heptane	2.6 ± 0.1	2.9	0.94 ± 0.1	0.99	1.1 ± 0.4	1.5
Toluene	2.9 ± 0.1	2.1	0.2 ± 0.02*	0.7	0.2 ± 0.05	0.7
N-Octane	0.7 ± 0.04	0.7	0.01 ± 0.01	0.02	0.2 ± 0.01	0.2
P-Xylene	0.7 ± 0.1	0.7	0.04 ± 0.001*	0.04	0.06 ± 0.002*	0.3
1,3,5-Trimethylbenzene	0.5 ± 0.1	0.5	0.08 ± 0.002*	0.08	0.1 ± 0.01*	0.3

* Chemical did not reach near-steady conditions

Table 7.3

Comparison of mass emissions: experimental vs simulation during phase I (anaerobic phase) (continue)

Compound	Column D x10 ⁻⁸ [g/s]		Column E x10 ⁻⁸ [g/s]		Column F x10 ⁻⁸ [g/s]	
	Experiment	Simulation	Experiment	Simulation	Experiment	Simulation
N-Pentane	25.0 ± 1.5	22.5	87.6 ± 5.9	86.7	14.6 ± 1.1	12.9
2-Methyl-2-Butene	6.6 ± 0.2	6.9	20.2 ± 1.1	26.2	3.4 ± 0.1	3.4
MTBE	0.6 ± 0.02*	0.99	0.8 ± 0.1*	3.5	0.09 ± 0.01*	0.5
N-Hexane	5.8 ± 0.1	5.2	18.3 ± 1.0	19.5	1.9 ± 0.05	2.0
Benzene	0.7 ± 0.02	0.9	1.6 ± 0.05	3.6	0.3 ± 0.01	0.4
Cyclohexane	3.3 ± 0.1	4.6	14.4 ± 0.6	17.3	1.7 ± 0.04	1.7
Iso-Octane	2.6 ± 0.1	3.1	12.1 ± 0.4	12.4	1.2 ± 0.03	1.2
N-Heptane	2.2 ± 0.07	2.2	8.4 ± 0.6	8.4	0.7 ± 0.03	0.8
Toluene	0.5 ± 0.04	0.3	4.3 ± 0.2*	6.8	0.3 ± 0.03	0.5
N-Octane	0.3 ± 0.01	0.4	2.09 ± 0.1	2.09	0.05 ± 0.004*	0.2
P-Xylene	0.1 ± 0.01*	0.4	1.0 ± 0.07*	1.0	0.03 ± 0.006*	0.2
1,3,5-Trimethylbenzene	0.02 ± 0.004*	0.3	1.4 ± 0.08*	1.4	0.08 ± 0.006*	0.2

* Chemical did not reach near-steady conditions

Since most of the simulated mass emissions shown in Table 7.3 have similar values to the experimental results, it confirms that the simulation gave a good fit to the experimental results. The simulated mass emissions of MTBE, P-Xylene and 1,3,5-trimethylbenzene are higher than the experimental values in most of the columns (Columns B, C, D, E and F). These chemicals did not reach near-steady conditions during the anaerobic experimental period; thus, the experimental mass emissions are lower than the simulation results.

7.2 Step II: First-Order Degradation Rate Constants. Simulating Experimental Phase III

7.2.1 Model inputs.

To simulate this experimental phase, the same model domain and soil section characteristics determined during the simulation of phase I were used (See Figure 7.1 and Table 7.1). In this case, the vapor source concentration is 10 times lower than the anaerobic case and aerobic degradation reactions are occurring. Hence, CO₂ is simulated together with the twelve petroleum hydrocarbon compounds of the vapor source. Table 7.4 presents the constituents properties included in the input files for the simulation of this phase.

In order to determine if the simulation results were a good fit of the experimental data, the following outputs had to match the experimental results:

- (i) individual compound gas emissions,
- (ii) CO₂ emissions, and
- (iii) CO₂ concentration profiles

A schematic of the procedure followed to perform this simulation is shown in Figure 7.4.

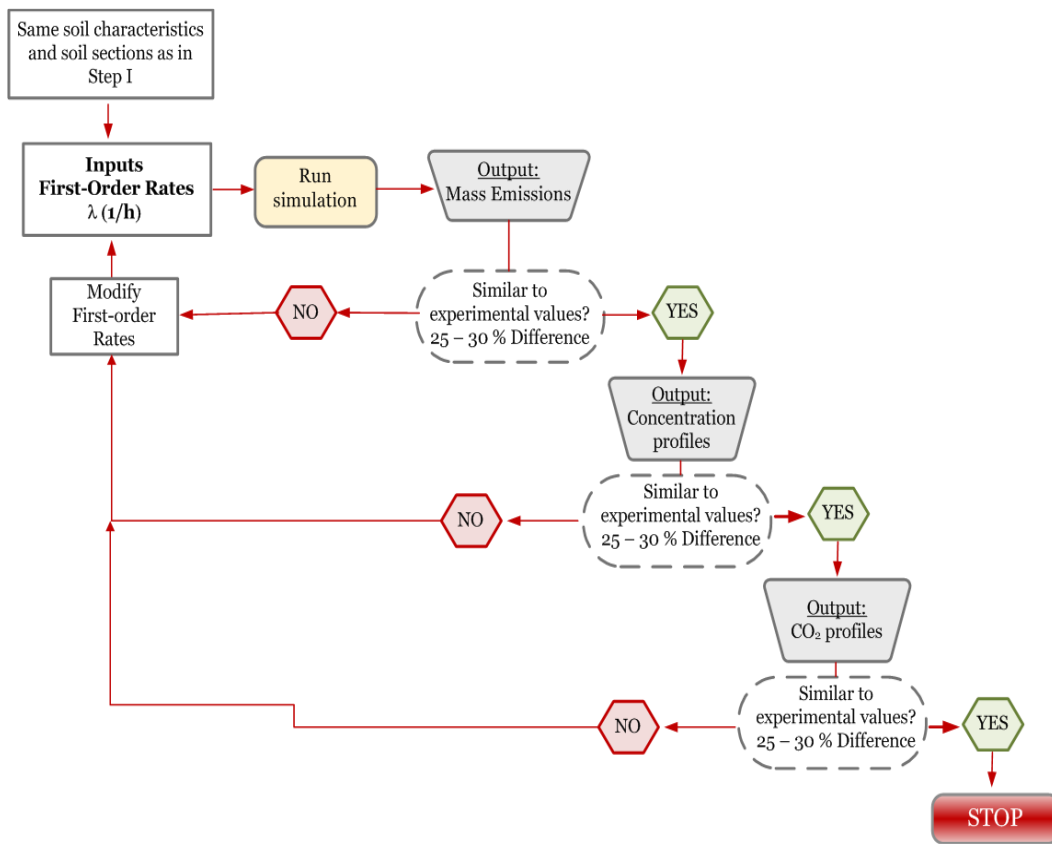


Figure 7.4. Step II: First-order degradation rate constants calculation. Simulation outputs

fitted to near-steady conditions results from experimental Phase III.

(Note: 25 to 30% difference was used to take into account the variability of the experimental results)

Table 7.4

Chemical characteristic inputs for simulating experimental phase III

Chemical	H_i^a cm ³ -H ₂ O/ cm ³ -vapor	K_{oc}^a , g/g-oc	D^{air}^a , cm ² /s	$D^{H_2O} \times 10^{-6}^a$, cm ² /s	Atmospheric concentration, g/cm ³	Initial soil concentration, g/cm ³	Source gas concentration x10 ⁻⁷ g/cm ³
N-Pentane	41.15	4.1	0.086	8.1	0.0	0.0	101.1
2-Methyl-2-butene	3.55	130.8	0.086	8.9	0.0	0.0	33.7
MTBE	0.03	12.3	0.079	7.5	0.0	0.0	4.3
N-Hexane	58.13	1250	0.071	7.8	0.0	0.0	54.0
Benzene	0.18	58.9	0.088	1.0	0.0	0.0	4.6
Cyclohexane	6.14	482	0.078	8.4	0.0	0.0	54.2
Iso-octane	107.27	3.43	0.062	6.2	0.0	0.0	24.2
N-Heptane	78.07	2400	0.065	7.0	0.0	0.0	26.5
Toluene	0.21	182	0.082	8.6	0.0	0.0	8.8
N-octane	89.84	1600	0.051	6.6	0.0	0.0	6.5
P-xylene	0.21	389	0.077	8.4	0.0	0.0	3.8
1,3,5-trimethylbenzene	0.24	1200	0.068	7.2	0.0	0.0	5.7
CO ₂	1.2	0.0	0.16	16.7	7.5x10 ⁻⁷	0.0	0.0
Oxygen	31.6	0.0	0.2	24.1	2.8x10 ⁻⁴	0.0	0.0

^a: Source: CRC handbook and Perry's Chemical Engineering Handbook

i) Reaction rates

As noted above, the 3-D transient model has the capability of simulating zero-order, first-order and monod kinetics; in this case, first-order kinetics gave a better fit to the degradation process in the experiment than zero-order or monod.

The model requires first-order rate constants for each chemical in each soil sections as inputs. These values were determined by trial and error as follows: initial first-order rate values were obtained from the literature for similar experiments (Devauil et al., 2004; DeVauil, 2007). The same reaction rate constants were applied to all the soil sections. Then, the model was run and the outputs compared to the experimental data. Subsequently, the first-order rates values were modified based on the simulation output results and their comparison to the experimental data results, soil characteristics and location of the “degradation zone” and the model was rerun (See Figure 7.4). The simulation first-order rates were adjusted until the simulation output results matched the individual compound mass emissions, CO₂ mass emissions and CO₂ profiles. Table 7.5 shows the first-order degradation rate constants obtained from simulating the experimental results of Phase III.

As can be observed in Table 7.5, most of the rate constants are in the range presented by DeVauil (2007), especially those located inside the “degradation zones”. In most cases, the first-order rate constants outside the “degradation zones” are below the ranges, since little to no degradation occurs in these zones.

7.2.2 Simulation results.

The model normalized gas profile results for n-pentane, MTBE, benzene, n-octane, as well as the CO₂ and O₂ normalized concentration profiles and their comparison to experimental data are presented in Figure 7.5. Results for the remaining constituents are presented in Appendix VI.

Table 7.5

First-order degradation rates along the length of the column for each compound

	COLUMN A [1/d]											
Length, m	N-Pentane	2-Methyl-2-Butene	MTBE	N-Hexane	Benzene	Cyclohexane	Iso-Octane	N-Heptane	Toluene	N-Octane	P-Xylene	1,3,5-TMB ^a
Literature value			0.047 ^b	$2.4 \times 10^2 - 1.9 \times 10^4$ ^c	1.2–360 ^c	$2.4 \times 10^2 - 1.9 \times 10^4$ ^c	$2.4 \times 10^2 - 7.5 \times 10^2$ ^b	$2.4 \times 10^2 - 1.9 \times 10^4$ ^c	0.14 - 288 ^{b,c}	$2.4 \times 10^2 - 1.9 \times 10^4$ ^c	0.23 – 63.1 ^{b,c}	$2.4 \times 10^2 - 1.9 \times 10^4$ ^c
1.02-1.83	1.4x10 ³	60.0	0.14	1.8x10 ³	12.0	24.0	1.0x10 ²	3.9x10 ³	10.8	3.7x10 ³	0.6	7.2
0.10-1.02	3.2x10 ³	38.4	0.19	1.9x10 ³	0.48	24.0	1.0x10 ²	75.4	8.4	3.6x10 ³	0.6	0
0 – 0.10	3.2x10 ³	1.1x10 ²	0.19	2.0x10 ³	16.8	33.6	1.6x10 ²	4.3x10 ³	14.4	5.7x10 ³	1.68	21.6

142

	COLUMN B [1/d]											
Length, m	N-Pentane	2-Methyl-2-Butene	MTBE	N-Hexane	Benzene	Cyclohexane	Iso-Octane	N-Heptane	Toluene	N-Octane	P-Xylene	1,3,5-TMB ^a
Literature value			0.047 ^b	$2.4 \times 10^2 - 1.9 \times 10^4$ ^c	1.2–360 ^c	$2.4 \times 10^2 - 1.9 \times 10^4$ ^c	$2.4 \times 10^2 - 7.5 \times 10^2$ ^b	$2.4 \times 10^2 - 1.9 \times 10^4$ ^c	0.14 - 288 ^{b,c}	$2.4 \times 10^2 - 1.9 \times 10^4$ ^c	0.23 – 63.1 ^{b,c}	$2.4 \times 10^2 - 1.9 \times 10^4$ ^c
1.22-1.83	3.7x10 ³	4.8	0.0	2.4	0.0	2.4	0.0	0.17	0.0	1.7x10 ²	0.0	0.3
1.12-1.22	3.7x10 ³	7.2	0.48	82.6	8.6	2.4	55.8	3.2x10 ²	1.3	6.3x10 ²	0.36	0.9
1.0 2-1.12	4.6x10 ³	51.6	4.1	1.0x10 ³	9.1	1.6x10 ²	1.6x10 ²	6.2x10 ²	5.6	6.9x10 ²	0.48	2.0
0.91-1.02	3.0x10 ³	61.2	0.41	7.4x10 ²	1.9	89.5	5.6x10 ²	3.3x10 ²	2.3	9.0x10 ²	0.48	2.2
0.61–0.91	8.7x10 ²	37.2	0.0	2.6x10 ²	2.2	0.0	0.0	29.8	0.0	4.5x10 ²	0.0	1.4
0-0.61	8.7x10 ²	6.7	0.0	7.3x10 ²	0.24	0.0	0.0	41.7	0.0	5.1x10 ²	0.0	0.0

■ Degradation zone; ^a: 1,3,5-Trimethylbenzene; ^b: DeVaul et al., (2004); ^c: DeVaul (2007).

Table 8.5

First-order degradation rates along the length of the column for each compound (Continue)

Length, m	COLUMN C [1/s]											
	N-Pentane	2-Methyl-2-Butene	MTBE	N-Hexane	Benzene	Cyclohexane	Iso-Octane	N-Heptane	Toluene	N-Octane	P-Xylene	1,3,5-TMB ^a
Literature value			0.047 ^b	$\frac{2.4 \times 10^2}{1.9 \times 10^4}$ ^c	1.2–360 ^c	$\frac{2.4 \times 10^2}{1.9 \times 10^4}$ ^c	$\frac{2.4 \times 10^2}{7.5 \times 10^2}$ ^b	$\frac{2.4 \times 10^2}{1.9 \times 10^4}$ ^c	0.14 - 288 ^{b,c}	$\frac{2.4 \times 10^2}{1.9 \times 10^4}$ ^c	0.23 - 63.1 ^{b,c}	$\frac{2.4 \times 10^2}{1.9 \times 10^4}$ ^c
1.42-1.83	2.9X10 ²	2.9	0.05	1.6X10 ²	4.3	4.8	4.8	8.2x10 ²	4.8	7.3x10 ²	0.0	1.2
0.91-1.42	2.9X10 ²	2.9	0.48	1.6X10 ²	4.3	4.8	4.8	8.2x10 ²	4.8	1.4x10 ³	0.0	3.6
0.10–0.91	12.0	0.0	0.0	0.0	0.0	0.0	1.2	3.1	0.0	12.0	1.9x10 ²	1.4
0-0.10	60.0	0.0	0.0	96.0	0.48	0.05	1.2	51.1	0.48	12.0	1.9x10 ²	1.4

Length, m	COLUMN D [1/s]											
	N-Pentane	2-Methyl-2-Butene	MTBE	N-Hexane	Benzene	Cyclohexane	Iso-Octane	N-Heptane	Toluene	N-Octane	P-Xylene	1,3,5-TMB ^a
Literature			0.047 ^b	$\frac{2.4 \times 10^2}{1.9 \times 10^4}$ ^c	1.2–360 ^c	$\frac{2.4 \times 10^2}{1.9 \times 10^4}$ ^c	$\frac{2.4 \times 10^2}{7.5 \times 10^2}$ ^b	$\frac{2.4 \times 10^2}{1.9 \times 10^4}$ ^c	0.14 - 288 ^{b,c}	$\frac{2.4 \times 10^2}{1.9 \times 10^4}$ ^c	0.23 - 63.1 ^{b,c}	$\frac{2.4 \times 10^2}{1.9 \times 10^4}$ ^c
0.91-1.83	4.9x10 ²	0.0	0.0	2.0x10 ²	0.008	13.2	0.0	8.0x10 ²	0.74	1.1x10 ³	0.0	1.3
0.41–0.91	7.3x10 ²	6.0	0.05	2.4x10 ²	0.008	13.2	88.8	1.1x10 ³	0.96	1.6x10 ³	0.48	1.3
0-0.41	7.8x10 ²	73.2	0.13	2.9x10 ²	2.16	74.4	89.6	2.2x10 ²	21.6	1.6x10 ³	0.67	5.3

■ Degradation zone; ^a: 1,3,5-Trimethylbenzene. ^b: DeVuall et al. (2004). ^c: DeVuall et al. (2007).

Table 8.5

First-order degradation rates along the length of the column for each compound (Continue)

Length, m	COLUMN E [1/s]											
	N-Pentane	2-Methyl-2-Butene	MTBE	N-Hexane	Benzene	Cyclohexane	Iso-Octane	N-Heptane	Toluene	N-Octane	P-Xylene	1,3,5-TMB ^a
Literature value			0.047 ^b	$2.4 \times 10^2 - 1.9 \times 10^4$ ^c	1.2–360 ^c	$2.4 \times 10^2 - 1.9 \times 10^4$ ^c	$2.4 \times 10^2 - 7.5 \times 10^2$ ^b	$2.4 \times 10^2 - 1.9 \times 10^4$ ^c	0.14 - 288 ^{b,c}	$2.4 \times 10^2 - 1.9 \times 10^4$ ^c	0.23 - 63.1 ^{b,c}	$2.4 \times 10^2 - 1.9 \times 10^4$ ^c
1.21-1.83	1.2×10^2	7.2	0.0	1.3×10^2	0.008	13.2	2.4	51.1	0.0	7.8×10^2	0.0	0.0
0.61-1.21	2.9×10^3	1.3×10^2	0.0	1.2×10^2	0.008	13.2	2.4	51.1	0.0	24.0	7.2×10^{-3}	0.0
0-0.61	5.6×10^3	1.3×10^2	1.4×10^{-5}	7.8×10^2	2.2	74.4	60	2.4×10^2	6.7×10^{-4}	7.8×10^2	0.11	2.4×10^{-7}

144

Length, m	COLUMN F [1/s]											
	N-Pentane	2-Methyl-2-Butene	MTBE	N-Hexane	Benzene	Cyclohexane	Iso-Octane	N-Heptane	Toluene	N-Octane	P-Xylene	1,3,5-TMB ^a
Literature			0.047 ^b	$2.4 \times 10^2 - 1.9 \times 10^4$ ^c	1.2–360 ^c	$2.4 \times 10^2 - 1.9 \times 10^4$ ^c	$2.4 \times 10^2 - 7.5 \times 10^2$ ^b	$2.4 \times 10^2 - 1.9 \times 10^4$ ^c	0.14 - 288 ^{b,c}	$2.4 \times 10^2 - 1.9 \times 10^4$ ^c	0.23 - 63.1 ^{b,c}	$2.4 \times 10^2 - 1.9 \times 10^4$ ^c
1.02-1.83	3.7×10^2	26.4	0.08	6.2×10^2	1.7	5.3	3.9×10^2	99.1	1.2	3.7×10^2	0.11	0.65
0.81–1.02	4.8×10^2	26.4	0.11	6.2×10^2	6.0	12.8	4.4×10^2	99.1	1.2	3.7×10^2	0.10	1.2
0 – 0.81	8.9	20.4	0.0	1.5×10^2	1.2	3.8	96.0	31.2	0.96	60.0	0.0	0.01

■ Degradation zone; ^a: 1,3,5-Trimethylbenzene; ^b: DeVaul et al. (2004); ^c: DeVaul et al. (2007).

Column A

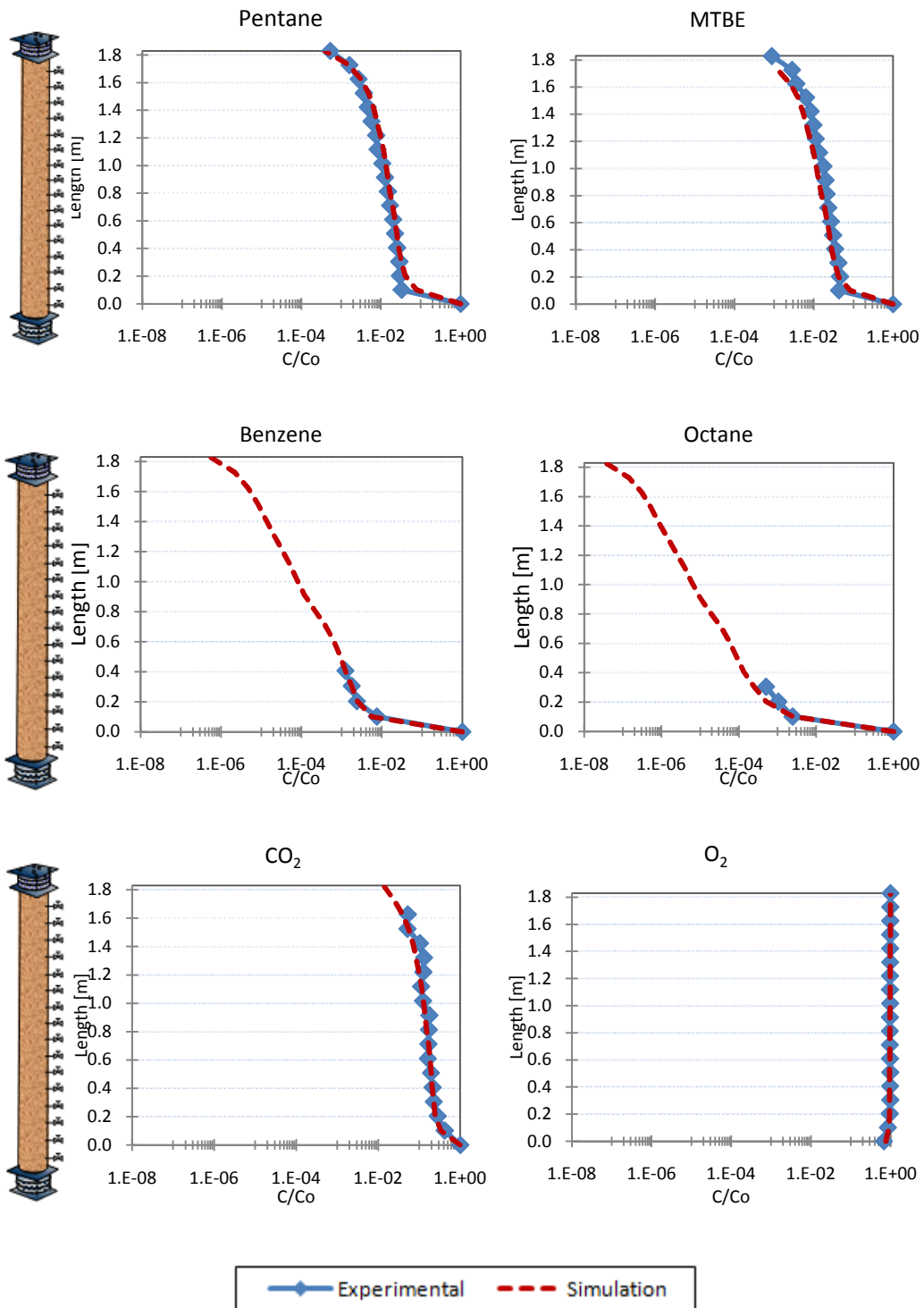


Figure 7.5. Simulated vs experimental profiles. Experimental Phase III

Column B

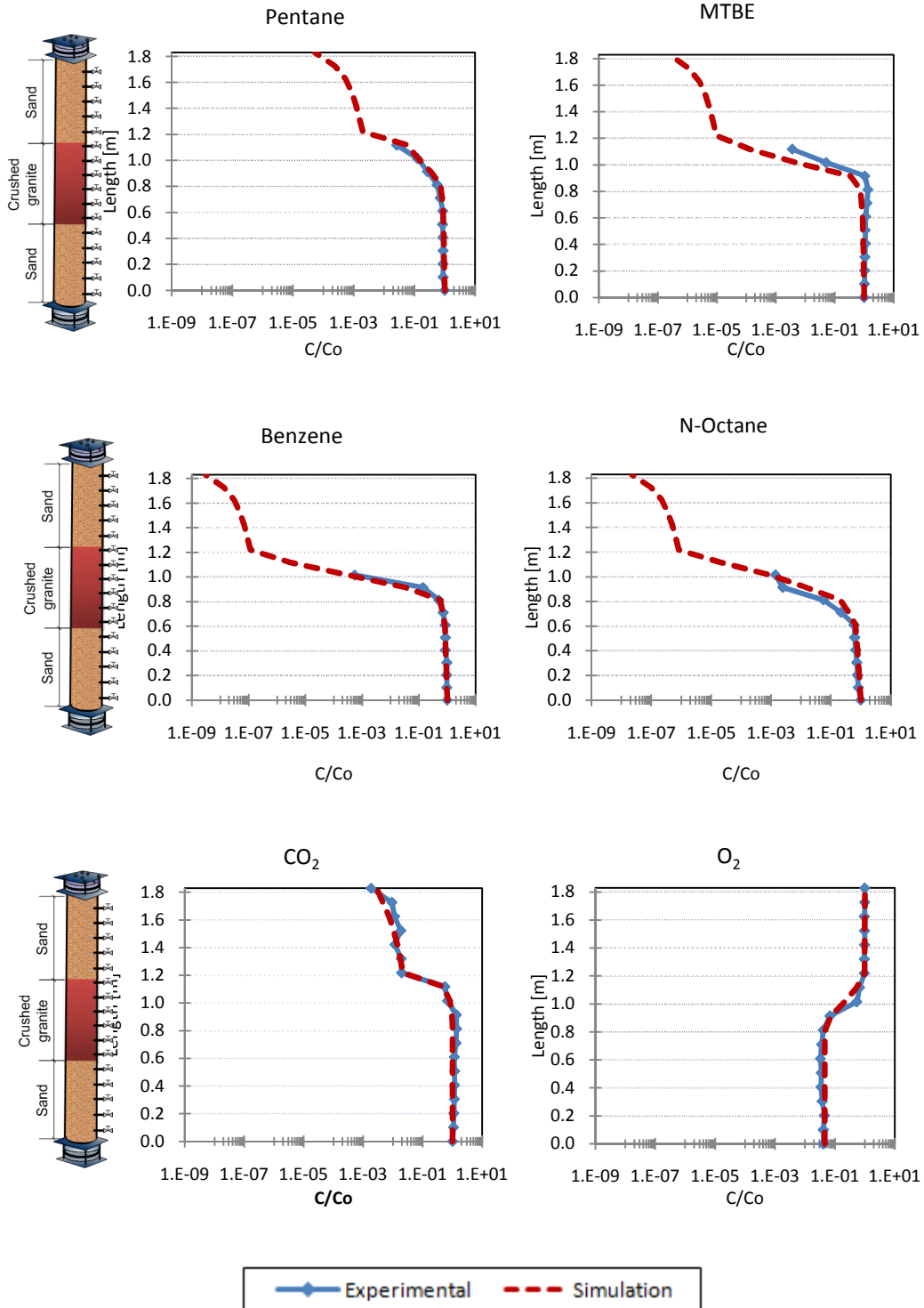


Figure 7.5. Simulated vs experimental profiles. Experimental Phase III (Continue)

Column C

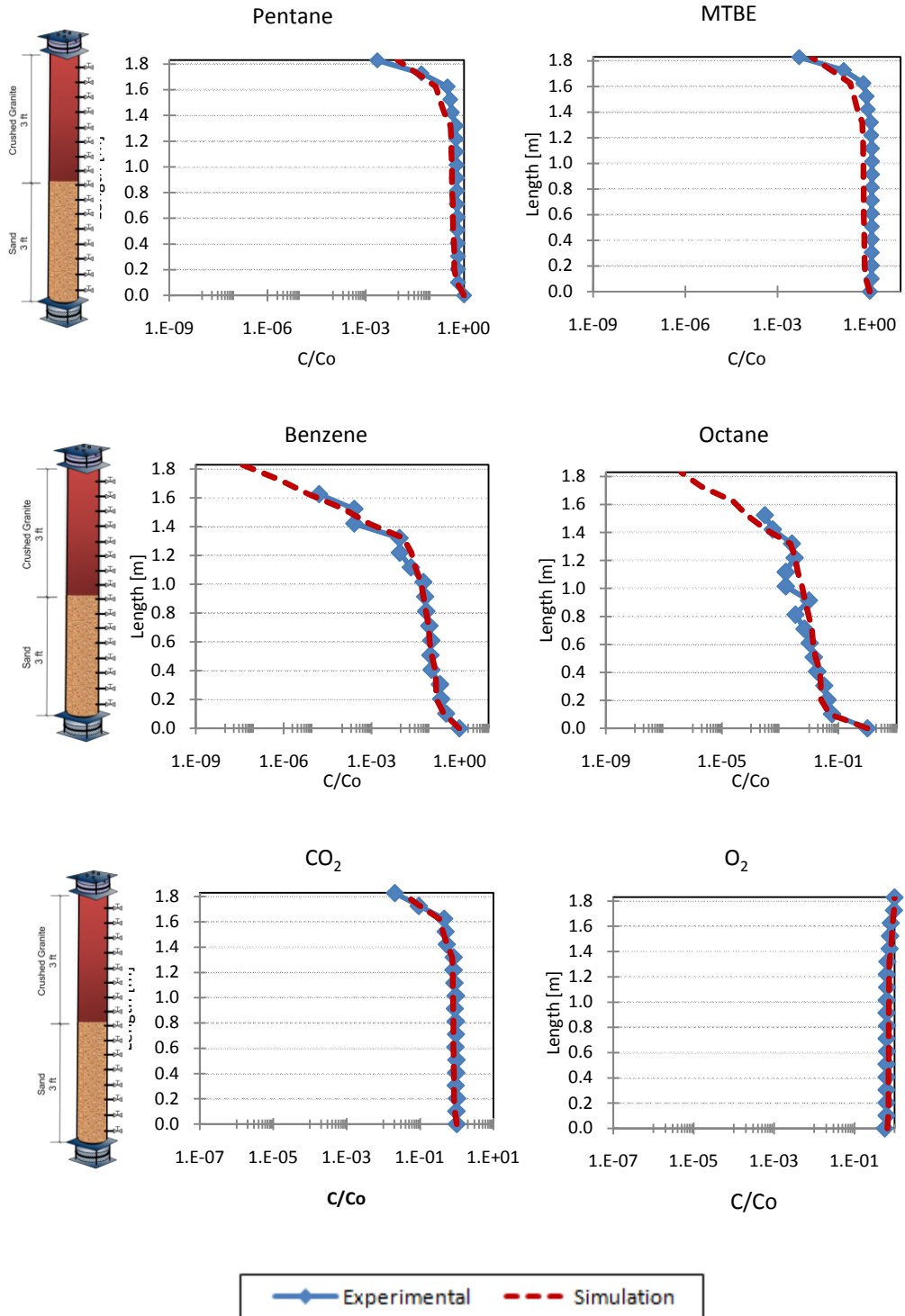


Figure 7.5. Simulated vs experimental profiles. Experimental Phase III (Continue)

Column D

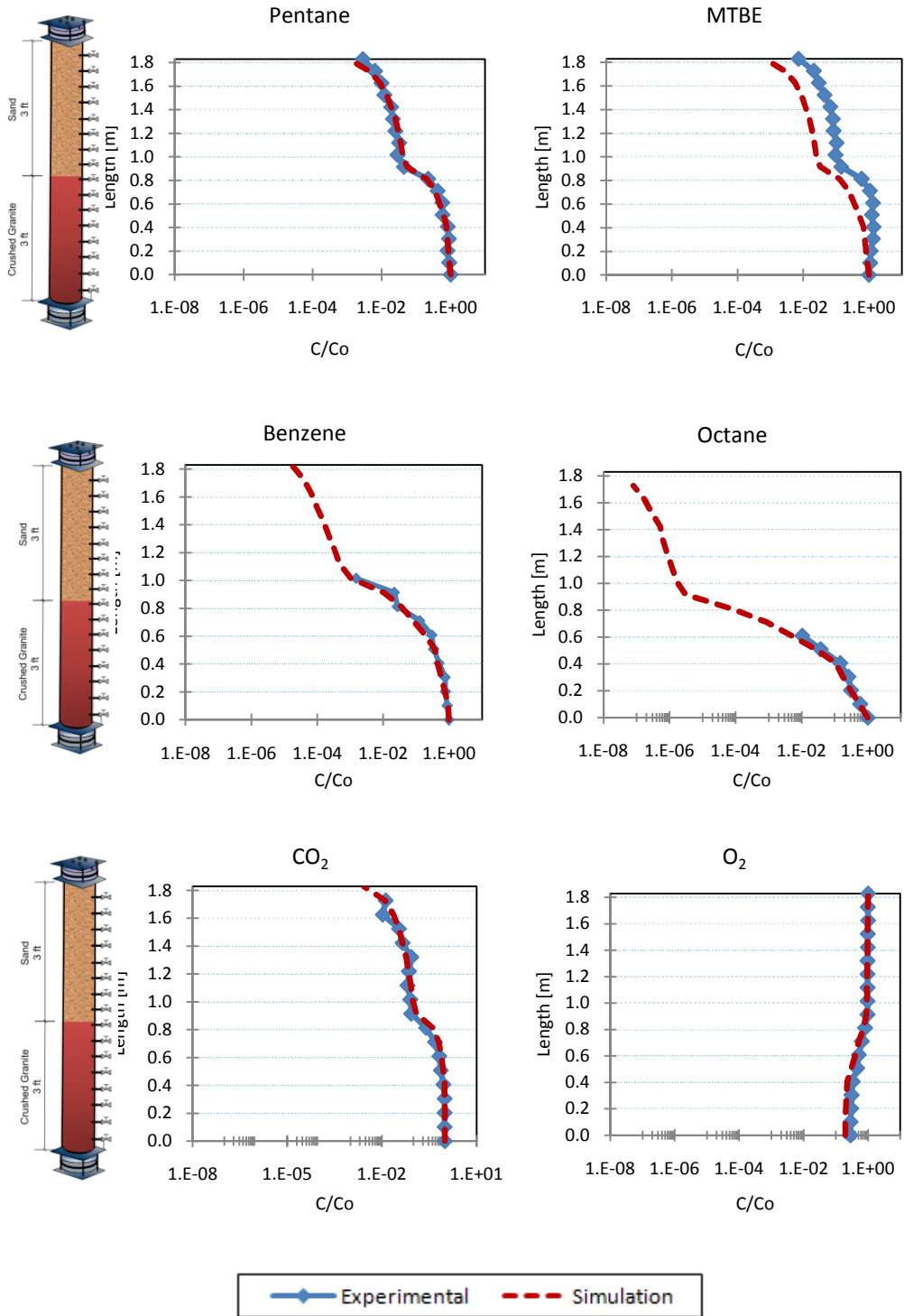


Figure 7.5. Simulated vs experimental profiles. Experimental Phase III (Continue)

Column E

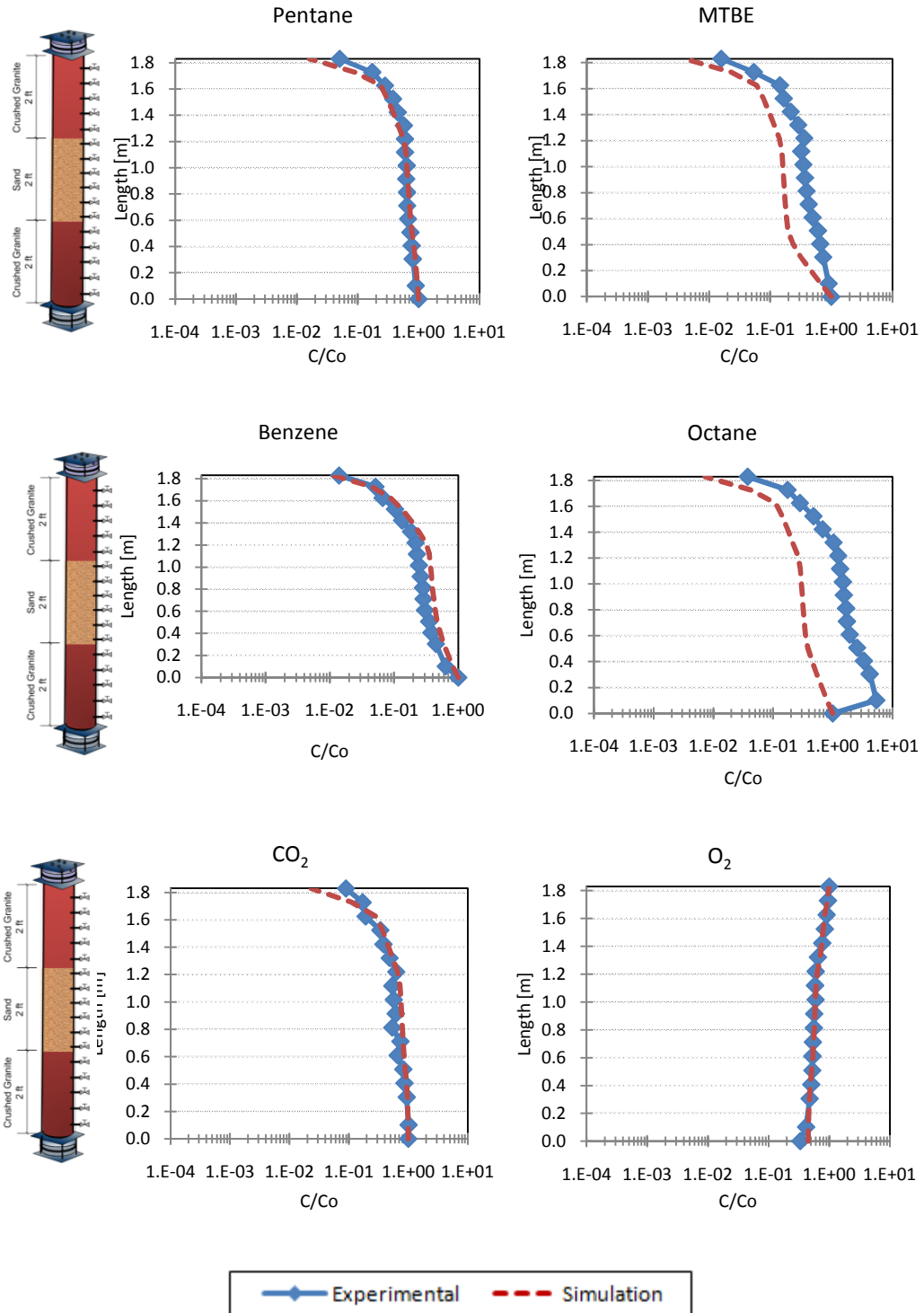


Figure 7.5 Simulated vs experimental profiles. Experimental Phase III (Continue)

Column F

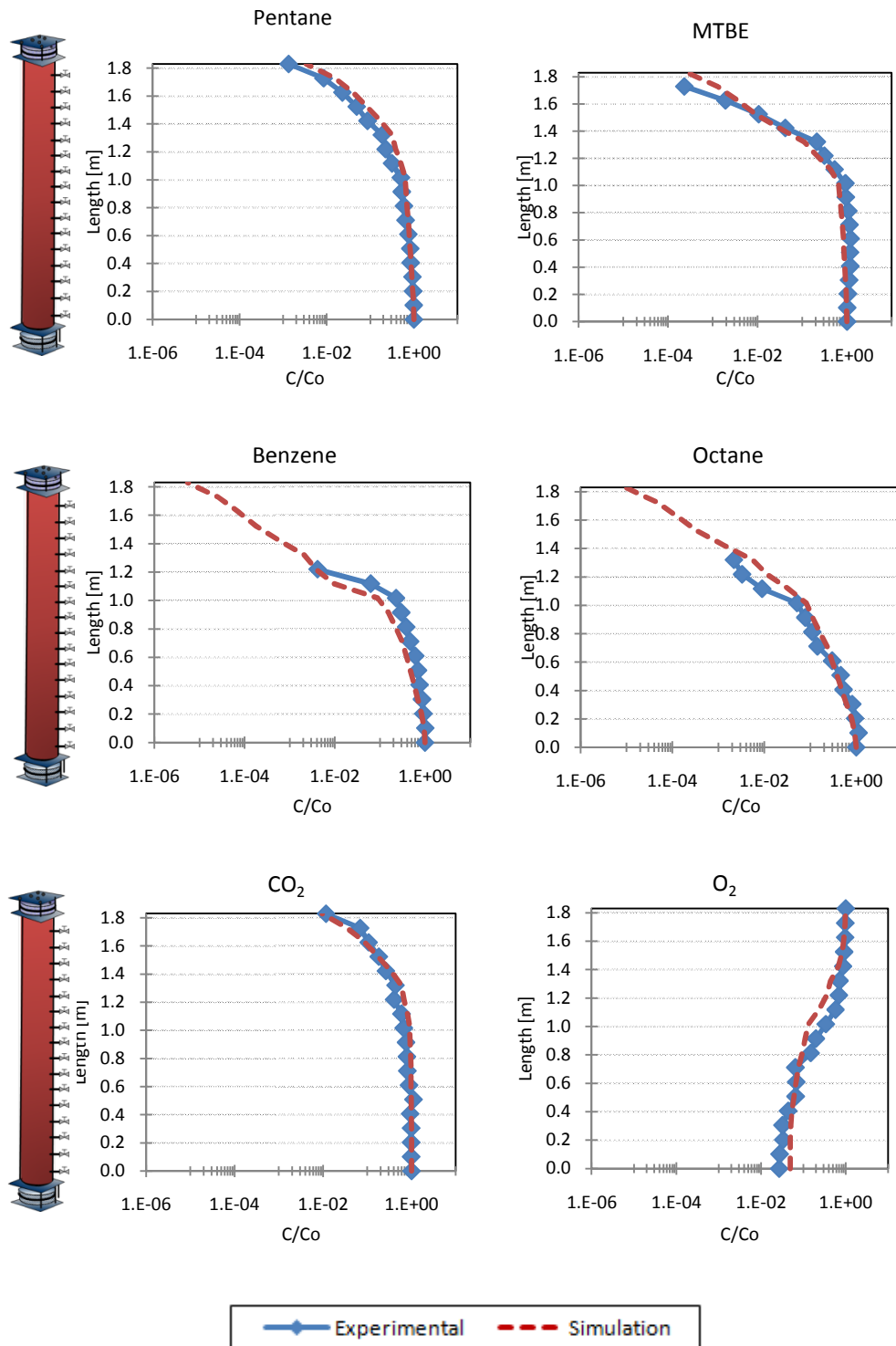


Figure 7.5. Simulated vs experimental profiles. Experimental Phase III (continued)

As can be observed in Figure 7.5, the CO₂ gas profiles show a good match between simulated and experimental results confirming that the simulated results are matching the experimental data. Also, the individual compound profiles present a good fit, except for the constituents that did not reach near-steady conditions during this experimental phase such as MTBE in Columns C, D and E as well benzene and n-octane in column E.

Table 6.6 presents the comparison of the simulated effluent mass emission to the experimental values. As shown in Table 7.6, simulated mass emissions were similar to the experimental. Therefore it was concluded that the simulation results fitted the experimental results.

Table 7.6

Comparison of mass emissions: experimental vs simulation for experimental phase III

Compound	Column A [g/s]		Column B [g/s]		Column C [g/s]	
	Experiment	Simulation	Experiment	Simulation	Experiment	Simulation
N-Pentane	$5.5 \pm 0.2 \times 10^{-9}$	5.5×10^{-9}	$9.7 \pm 0.1 \times 10^{-12}$	7.6×10^{-12}	$4.5 \pm 0.4 \times 10^{-9}$	4.5×10^{-9}
2-Methyl-2-Butene	$1.2 \pm 0.1 \times 10^{-10}$	3.3×10^{-10}	$5.2 \pm 0.1 \times 10^{-13}$	4.4×10^{-13}	$1.2 \pm 0.06 \times 10^{-9}$	1.2×10^{-9}
MTBE	$1.7 \pm 0.1 \times 10^{-10}$	1.4×10^{-10}	$3.2 \pm 0.05 \times 10^{-13}$	3.9×10^{-13}	$5.7 \pm 1.3 \times 10^{-10*}$	4.0×10^{-10}
N-Hexane	$3.4 \pm 0.05 \times 10^{-12}$	5.8×10^{-12}	$3.9 \pm 0.02 \times 10^{-12}$	4.4×10^{-12}	$1.0 \pm 0.2 \times 10^{-10}$	1.0×10^{-10}
Benzene	$2.2 \pm 0.01 \times 10^{-14}$	4.3×10^{-14}	$2.1 \pm 0.03 \times 10^{-15}$	2.5×10^{-15}	$1.4 \pm 0.4 \times 10^{-15}$	1.5×10^{-15}
Cyclohexane	$4.8 \pm 0.09 \times 10^{-10}$	2.1×10^{-10}	$7.5 \pm 0.2 \times 10^{-12}$	6.3×10^{-12}	$2.0 \pm 0.1 \times 10^{-9}$	1.3×10^{-9}
Iso-Octane	$1.1 \pm 0.04 \times 10^{-9}$	4.1×10^{-9}	$1.2 \pm 0.02 \times 10^{-11}$	1.9×10^{-11}	$2.3 \pm 0.5 \times 10^{-9}$	3.2×10^{-9}
N-Heptane	$3.3 \pm 0.1 \times 10^{-13}$	2.8×10^{-13}	$7.0 \pm 0.1 \times 10^{-13}$	5.9×10^{-13}	$2.4 \pm 0.1 \times 10^{-14}$	2.3×10^{-14}
Toluene	$6.3 \pm 0.4 \times 10^{-13}$	4.7×10^{-13}	$1.1 \pm 0.04 \times 10^{-13}$	1.7×10^{-13}	$2.3 \pm 0.2 \times 10^{-15}$	2.8×10^{-15}
N-Octane	$2.2 \pm 0.04 \times 10^{-14}$	1.6×10^{-14}	$2.6 \pm 0.2 \times 10^{-14}$	2.1×10^{-14}	$2.4 \pm 0.1 \times 10^{-15}$	2.4×10^{-15}
P-Xylene	$3.4 \pm 0.09 \times 10^{-13}$	3.1×10^{-13}	$3.3 \pm 0.2 \times 10^{-15} *$	2.2×10^{-17}	$3.1 \pm 1.8 \times 10^{-14}$	2.3×10^{-14}
1,3,5-Trimethylbenzene	$5.1 \pm 0.2 \times 10^{-13}$	2.5×10^{-13}	$2.2 \pm 0.2 \times 10^{-13} *$	2.8×10^{-16}	$2.1 \pm 0.8 \times 10^{-13}$	1.8×10^{-13}
CO ₂	$2.2 \pm 0.1 \times 10^{-7}$	5.8×10^{-7}	$3.3 \pm 0.1 \times 10^{-7}$	5.5×10^{-7}	$2.2 \pm 0.1 \times 10^{-7}$	2.2×10^{-7}

Table 7.6

Comparison of mass emissions: experimental vs simulation (continue)

Compound	Column D [g/s]		Column E [g/s]		Column F [g/s]	
	Experiment	Simulation	Experiment	Simulation	Experiment	Simulation
N-Pentane	$4.2 \pm 0.8 \times 10^{-9}$	4.1×10^{-9}	$1.8 \pm 0.09 \times 10^{-8}$	2.0×10^{-8}	$1.8 \pm 0.5 \times 10^{-9}$	1.3×10^{-9}
2-Methyl-2-Butene	$1.2 \pm 0.1 \times 10^{-9}$	1.6×10^{-9}	$7.9 \pm 0.06 \times 10^{-9}$	7.9×10^{-9}	$2.8 \pm 0.2 \times 10^{-13}$	2.9×10^{-13}
MTBE	$2.2 \pm 0.3 \times 10^{-10}$	2.6×10^{-10}	$1.4 \pm 0.03 \times 10^{-9}$	1.4×10^{-9}	$2.7 \pm 0.01 \times 10^{-12*}$	2.7×10^{-12}
N-Hexane	$2.1 \pm 1.0 \times 10^{-10}$	2.1×10^{-10}	$1.4 \pm 0.2 \times 10^{-8}$	1.7×10^{-8}	$2.6 \pm 0.3 \times 10^{-14}$	2.1×10^{-14}
Benzene	$1.6 \pm 0.05 \times 10^{-12}$	2.0×10^{-12}	$1.3 \pm 0.04 \times 10^{-9}$	1.7×10^{-10}	$2.1 \pm 0.4 \times 10^{-15}$	2.0×10^{-15}
Cyclohexane	$1.6 \pm 0.05 \times 10^{-9}$	1.6×10^{-9}	$1.6 \pm 0.08 \times 10^{-8}$	2.0×10^{-8}	$2.4 \pm 0.4 \times 10^{-10}$	2.1×10^{-10}
Iso-Octane	$2.0 \pm 0.07 \times 10^{-9}$	2.3×10^{-9}	$3.0 \pm 0.08 \times 10^{-8}$	4.0×10^{-8}	$3.3 \pm 0.4 \times 10^{-12}$	2.9×10^{-12}
N-Heptane	$2.4 \pm 0.5 \times 10^{-13}$	2.4×10^{-13}	$1.3 \pm 0.2 \times 10^{-8}$	1.7×10^{-8}	$2.7 \pm 0.2 \times 10^{-14}$	2.1×10^{-14}
Toluene	$3.7 \pm 0.1 \times 10^{-12}$	3.6×10^{-12}	$2.4 \pm 0.05 \times 10^{-9}$	1.2×10^{-9}	$1.8 \pm 0.2 \times 10^{-13}$	1.8×10^{-13}
N-Octane	$7.2 \pm 0.1 \times 10^{-15}$	7.6×10^{-15}	$3.5 \pm 0.03 \times 10^{-9}$	2.5×10^{-9}	$2.1 \pm 0.2 \times 10^{-14}$	2.2×10^{-14}
P-Xylene	$1.7 \pm 0.1 \times 10^{-14}$	2.2×10^{-14}	$3.5 \pm 0.1 \times 10^{-9}$	3.5×10^{-9}	$4.14 \pm 0.2 \times 10^{-13}$	5.5×10^{-13}
1,3,5-Trimethylbenzene	$8.3 \pm 0.4 \times 10^{-13}$	8.5×10^{-13}	$1.4 \pm 0.1 \times 10^{-8}$	1.6×10^{-9}	$3.7 \pm 0.4 \times 10^{-13}$	3.8×10^{-13}
CO ₂	$1.6 \pm 0.1 \times 10^{-6}$	1.4×10^{-6}	$3.5 \pm 0.1 \times 10^{-7}$	2.8×10^{-7}	$3.10 \pm 0.1 \times 10^{-7}$	8.72×10^{-7}

* Chemical did not reach near-steady conditions

7.3. Simulation of Experimental Phase II: Aerobic Conditions

Results of Phase II (aerobic phase, see Chapter 4) indicated that near-steady conditions were not achieved during the experimental period. In this phase, it was observed that the effluent normalized mass emissions, as well as, the vapor concentration profiles decreased due to aerobic degradation for approximately 25 to 40 days after which, the effluent mass emissions and concentrations started to increase back to the anaerobic near-steady condition values. Due to the change in concentrations with time, the individual hydrocarbons did not reach-near steady conditions during the experimental Phase II. Thus, with the objective of determining how the vapor concentration profiles and mass emissions would look like in case near-steady conditions were reached during this aerobic phase, experimental phase II was simulated

7.3.1 Model inputs.

The same model domain, effective diffusion coefficients, soil characteristics and first-order degradation rates determined in Steps I and II (Sections 7.1 and 7.2) were used to perform this simulation, except that in this case, the concentration of the chemicals in the vapor source were the same as in Phase I and ten times higher than the concentrations in Phase III.

7.3.2 Model results.

Figure 7.6 presents the simulation vapor concentration profiles for benzene, CO₂ and O₂. This profiles are compared to the experimental gas profiles when the concentrations reached minimum levels (lowest mass emissions during Phase II); and to the experimental gas profiles at the end of the experimental period when attenuation activity had stopped (Final emission). The mass emissions results from the model were also compared to the experimental mass emissions when they were at their minimum levels and the ones at the end of the experimental phase period. This comparison is presented in Table 7.7.

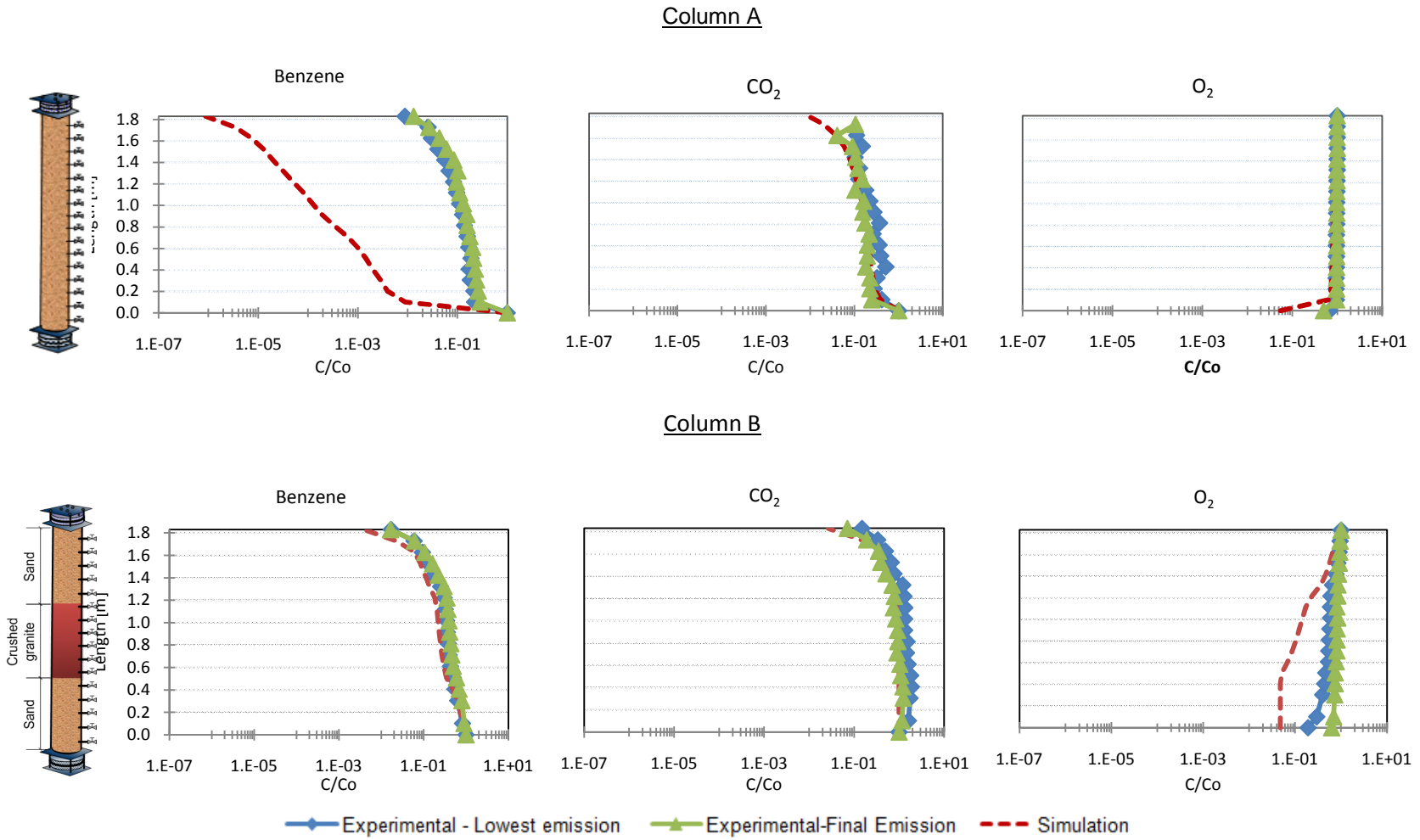


Figure 7.6. Experimental vs. Simulated vapor concentration profiles

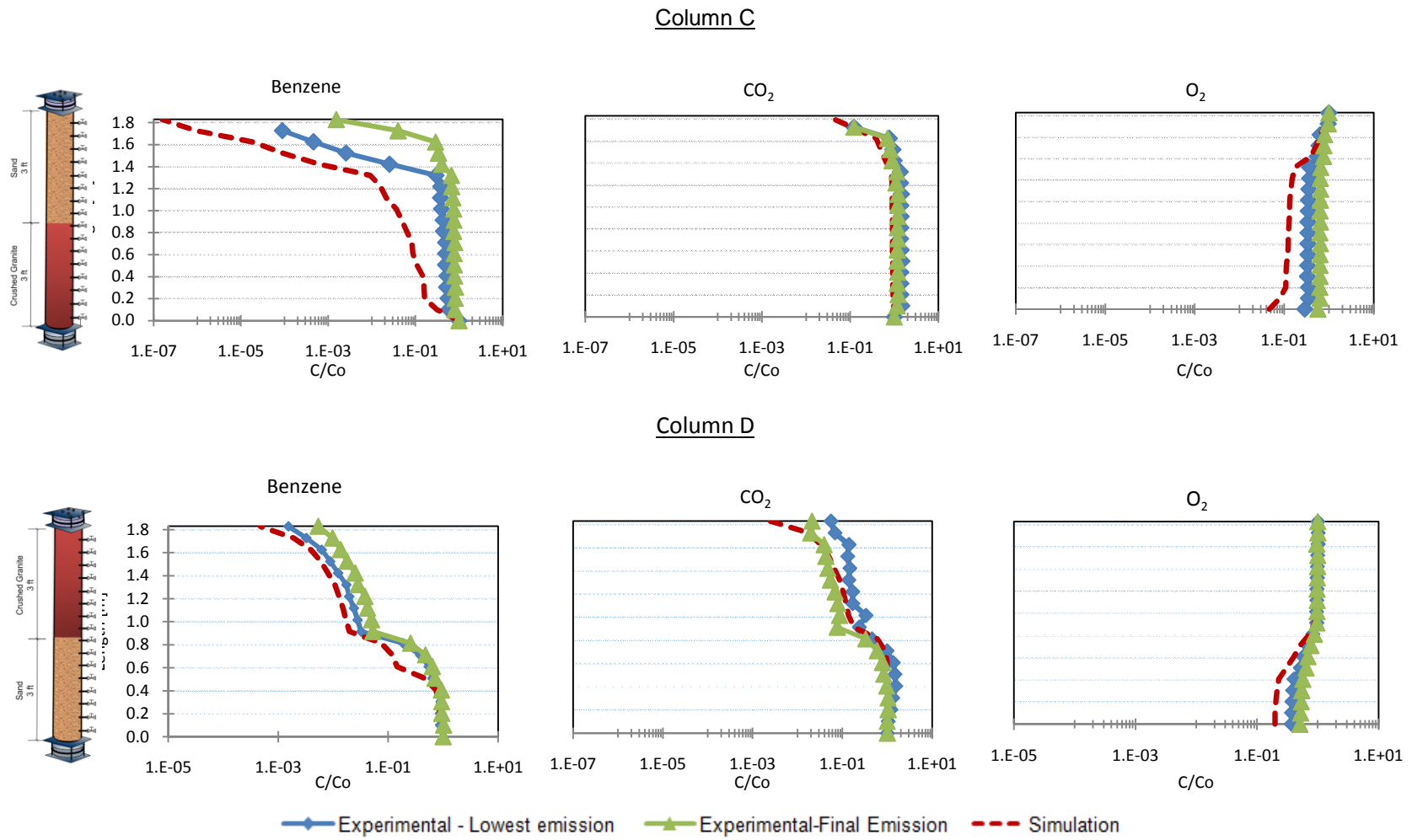


Figure 7.6. Experimental vs. Simulated vapor concentration profiles (continued)

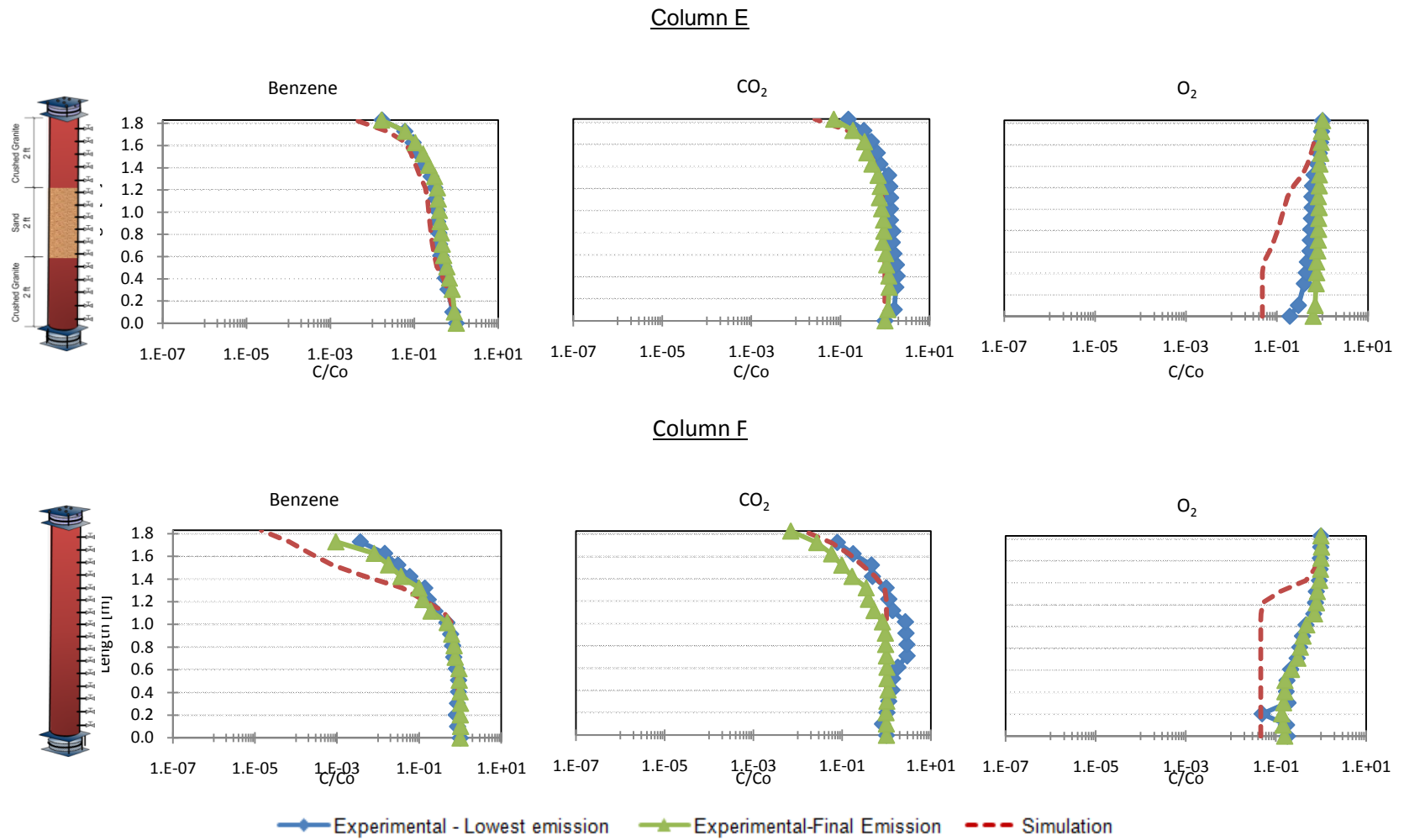


Figure 7.6. Experimental vs. Simulated vapor concentration profiles (continued)

Table 7.7

Comparison of mass emissions: experimental vs simulation for experimental phase II

Compound	Column A [g/s]			Column B [g/s]			Column C [g/s]		
	Experiment		Simulation	Experiment		Simulation	Experiment		Simulation
	lowest emission	**Final emission		Lowest emission	**Final emission		Lowest emission	**Final emission	
N-Pentane	$1.7 \pm 0.5 \times 10^{-8}$	$1.9 \pm 0.5 \times 10^{-8}$	4.7×10^{-8}	$2.5 \pm 0.2 \times 10^{-9}$	$1.4 \pm 0.2 \times 10^{-7}$	1.7×10^{-9}	$4.7 \pm 0.02 \times 10^{-8}$	$2.4 \pm 0.02 \times 10^{-7}$	4.0×10^{-8}
2-Methyl-2-Butene	$1.3 \pm 0.1 \times 10^{-8}$	$3.0 \pm 0.1 \times 10^{-8}$	2.8×10^{-9}	$1.6 \pm 0.01 \times 10^{-11}$	$1.2 \pm 0.01 \times 10^{-8}$	4.1×10^{-10}	$2.9 \pm 0.05 \times 10^{-9}$	$2.4 \pm 0.05 \times 10^{-8}$	7.9×10^{-8}
MTBE	$1.20.03 \pm \times 10^{-8}$	$1.8 \pm 0.03 \times 10^{-8}$	1.6×10^{-9}	$1.0 \pm 0.05 \times 10^{-12}$	$3.6 \pm 0.05 \times 10^{-10}$	2.2×10^{-11}	$1.3 \pm 0.05 \times 10^{-10}$	$2.4 \pm 0.05 \times 10^{-9}$	2.8×10^{-9}
N-Hexane	$4.6 \pm 0.1 \times 10^{-9}$	$2.6 \pm 0.1 \times 10^{-8}$	3.6×10^{-11}	$1.0 \pm 0.2 \times 10^{-11}$	$6.9 \pm 0.2 \times 10^{-9}$	3.6×10^{-9}	$4.7 \pm 0.1 \times 10^{-10}$	$1.3 \pm 0.1 \times 10^{-8}$	5.0×10^{-10}
Benzene	$6.5 \pm 0.02 \times 10^{-9}$	$9.2 \pm 0.02 \times 10^{-9}$	4.0×10^{-12}	$2.1 \pm 0.05 \times 10^{-13}$	$3.4 \pm 0.05 \times 10^{-10}$	2.9×10^{-11}	$2.3 \pm 0.05 \times 10^{-13}$	$1.3 \pm 0.05 \times 10^{-9}$	1.6×10^{-14}
Cyclohexane	$9.6 \pm 0.1 \times 10^{-9}$	$2.7 \pm 0.1 \times 10^{-8}$	2.0×10^{-8}	$4.2 \pm 0.01 \times 10^{-11}$	$8.1 \pm 0.01 \times 10^{-9}$	4.0×10^{-10}	$2.9 \pm 0.03 \times 10^{-9}$	$1.8 \pm 0.03 \times 10^{-8}$	4.8×10^{-9}
Iso-Octane	$1.1 \pm 0.1 \times 10^{-8}$	$2.2 \pm 0.1 \times 10^{-8}$	2.1×10^{-8}	$3.3 \pm 0.2 \times 10^{-11}$	$6.7 \pm 0.2 \times 10^{-9}$	1.4×10^{-9}	$3.3 \pm 0.01 \times 10^{-9}$	$1.6 \pm 0.01 \times 10^{-8}$	1.5×10^{-8}
N-Heptane	$1.4 \pm 0.1 \times 10^{-9}$	$1.0 \pm 0.1 \times 10^{-8}$	1.1×10^{-11}	$2.4 \pm 0.1 \times 10^{-12}$	$8.4 \pm 0.1 \times 10^{-10}$	8.1×10^{-10}	$2.3 \pm 0.2 \times 10^{-13}$	$1.3 \pm 0.2 \times 10^{-11}$	4.0×10^{-12}
Toluene	$1.2 \pm 0.1 \times 10^{-8}$	$1.3 \pm 0.1 \times 10^{-8}$	6.1×10^{-11}	$6.1 \pm 0.1 \times 10^{-12}$	$4.7 \pm 0.1 \times 10^{-12}$	5.6×10^{-11}	$9.7 \pm 0.2 \times 10^{-13}$	$3.3 \pm 0.2 \times 10^{-10}$	2.6×10^{-14}
N-Octane	$9.9 \pm 0.1 \times 10^{-11}$	$2.4 \pm 0.1 \times 10^{-10}$	1.1×10^{-13}	$2.7 \pm 0.1 \times 10^{-13}$	$5.9 \pm 0.1 \times 10^{-12}$	5.9×10^{-12}	$1.2 \pm 0.05 \times 10^{-13}$	$1.1 \pm 0.05 \times 10^{-10}$	8.5×10^{-14}
P-Xylene	$1.3 \pm 0.04 \times 10^{-10}$	$3.1 \pm 0.04 \times 10^{-9}$	2.4×10^{-12}	$2.1 \pm 0.1 \times 10^{-13}$	$7.7 \pm 0.1 \times 10^{-14}$	3.6×10^{-13}	$2.3 \pm 0.1 \times 10^{-13}$	$7.43 \pm 0.1 \times 10^{-12}$	7.1×10^{-13}
1,3,5-Trimethylbenzene	$3.1 \pm 0.2 \times 10^{-9}$	$6.6 \pm 0.2 \times 10^{-9}$	6.6×10^{-13}	$1.2 \pm 0.01 \times 10^{-13}$	$5.3 \pm 0.01 \times 10^{-13}$	3.8×10^{-13}	$1.4 \pm 0.2 \times 10^{-12}$	$1.4 \pm 0.2 \times 10^{-12}$	1.5×10^{-12}
CO ₂	$2.2 \pm 0.2 \times 10^{-7}$	$1.8 \pm 0.2 \times 10^{-7}$	2.8×10^{-07}	$2.2 \pm 0.2 \times 10^{-7}$	$1.8 \pm 0.2 \times 10^{-7}$	8.9×10^{-7}	$8.4 \pm 0.2 \times 10^{-7}$	$3.5 \pm 0.2 \times 10^{-7}$	1.3×10^{-6}

Table 7.7

Comparison of mass emissions: experimental vs simulation for experimental phase II (continue)

Compound	Column D [g/s]			Column E [g/s]			Column F [g/s]		
	Experiment		Simulation	Experiment		Simulation	Experiment		Simulation
	lowest emission	**Final emission		Lowest emission	**Final emission		Lowest emission	**Final emission	
N-Pentane	$2.5 \pm 0.2 \times 10^{-7}$	$5.0 \pm 0.2 \times 10^{-7}$	8.3×10^{-8}	$8.3 \pm 0.5 \times 10^{-7}$	$1.2 \pm 0.5 \times 10^{-6}$	2.7×10^{-7}	$1.3 \pm 0.2 \times 10^{-7}$	$2.7 \pm 0.2 \times 10^{-7}$	2.3×10^{-8}
2-Methyl-2-Butene	$1.6 \pm 0.01 \times 10^{-8}$	$5.5 \pm 0.01 \times 10^{-8}$	2.3×10^{-8}	$9.6 \pm 0.3 \times 10^{-8}$	$1.4 \pm 0.3 \times 10^{-7}$	1.1×10^{-7}	$5.7 \pm 0.04 \times 10^{-9}$	$2.4 \pm 0.04 \times 10^{-8}$	4.6×10^{-11}
MTBE	$2.7 \pm 0.1 \times 10^{-9}$	$4.0 \pm 0.1 \times 10^{-9}$	4.3×10^{-9}	$8.9 \pm 0.05 \times 10^{-9}$	$1.2 \pm 0.05 \times 10^{-8}$	2.2×10^{-8}	$2.1 \pm 0.06 \times 10^{-10}$	$4.3 \pm 0.06 \times 10^{-10}$	6.8×10^{-11}
N-Hexane	$1.0 \pm 0.03 \times 10^{-8}$	$4.5 \pm 0.03 \times 10^{-8}$	3.4×10^{-9}	$3.2 \pm 0.08 \times 10^{-8}$	$1.6 \pm 0.08 \times 10^{-7}$	9.1×10^{-8}	$1.2 \pm 0.06 \times 10^{-10}$	$8.9 \pm 0.06 \times 10^{-9}$	2.8×10^{-12}
Benzene	$1.2 \pm 0.03 \times 10^{-9}$	$4.5 \pm 0.03 \times 10^{-9}$	2.0×10^{-9}	$9.7 \pm 0.01 \times 10^{-9}$	$1.4 \pm 0.01 \times 10^{-8}$	2.9×10^{-9}	$1.7 \pm 0.03 \times 10^{-13}$	$7.5 \pm 0.03 \times 10^{-11}$	3.4×10^{-12}
Cyclohexane	$1.8 \pm 0.02 \times 10^{-8}$	$3.6 \pm 0.02 \times 10^{-8}$	1.8×10^{-8}	$9.1 \pm 0.06 \times 10^{-8}$	$1.2 \pm 0.06 \times 10^{-7}$	8.5×10^{-8}	$5.8 \pm 0.01 \times 10^{-9}$	$2.0 \pm 0.01 \times 10^{-8}$	4.4×10^{-9}
Iso-Octane	$1.6 \pm 0.04 \times 10^{-8}$	$2.9 \pm 0.04 \times 10^{-8}$	1.5×10^{-8}	$9.9 \pm 0.03 \times 10^{-8}$	$1.1 \pm 0.03 \times 10^{-7}$	1.1×10^{-7}	$5.9 \pm 0.01 \times 10^{-9}$	$1.6 \pm 0.01 \times 10^{-8}$	8.4×10^{-11}
N-Heptane	$1.7 \pm 0.1 \times 10^{-10}$	$1.0 \pm 0.1 \times 10^{-8}$	3.7×10^{-11}	$9.1 \pm 0.1 \times 10^{-11}$	$5.9 \pm 0.1 \times 10^{-8}$	6.0×10^{-8}	$1.5 \pm 0.1 \times 10^{-12}$	$1.5 \pm 0.1 \times 10^{-11}$	8.4×10^{-10}
Toluene	$2.1 \pm 0.1 \times 10^{-12}$	$3.6 \pm 0.1 \times 10^{-9}$	6.1×10^{-11}	$1.2 \pm 0.3 \times 10^{-8}$	$2.5 \pm 0.3 \times 10^{-8}$	4.4×10^{-8}	$1.3 \pm 0.1 \times 10^{-13}$	$1.3 \pm 0.1 \times 10^{-13}$	2.3×10^{-11}
N-Octane	$4.7 \pm 0.05 \times 10^{-12}$	$2.6 \pm 0.05 \times 10^{-10}$	1.0×10^{-12}	$6.8 \pm 0.03 \times 10^{-11}$	$7.5 \pm 0.03 \times 10^{-9}$	9.0×10^{-9}	$2.1 \pm 0.1 \times 10^{-13}$	$1.8 \pm 0.1 \times 10^{-13}$	3.1×10^{-12}
P-Xylene	$2.2 \pm 0.1 \times 10^{-14}$	$2.3 \pm 0.1 \times 10^{-10}$	3.9×10^{-12}	$1.7 \pm 0.03 \times 10^{-9}$	$9.9 \pm 0.03 \times 10^{-9}$	1.4×10^{-8}	$2.1 \pm 0.1 \times 10^{-13}$	$6.1 \pm 0.1 \times 10^{-13}$	6.9×10^{-11}
1,3,5-Trimethylbenzene	$1.2 \pm 0.1 \times 10^{-12}$	$4.4 \pm 0.1 \times 10^{-13}$	7.5×10^{-12}	$4.8 \pm 0.02 \times 10^{-9}$	$1.3 \pm 0.02 \times 10^{-8}$	1.0×10^{-8}	$1.5 \pm 0.2 \times 10^{-13}$	$3.3 \pm 0.2 \times 10^{-13}$	4.7×10^{-12}
CO ₂	$3.3 \pm 0.2 \times 10^{-7}$	$2.9 \pm 0.2 \times 10^{-7}$	2.3×10^{-6}	$3.4 \pm 0.2 \times 10^{-7}$	$1.3 \pm 0.2 \times 10^{-7}$	7.5×10^{-6}	$3.1 \pm 0.2 \times 10^{-7}$	$2.7 \pm 0.2 \times 10^{-7}$	1.3×10^{-6}

As can be observed in Figure 7.6 the simulated benzene vapor profiles showed lower concentrations in all of the columns than both experimental vapor profiles. The CO₂ simulated profiles showed lower concentrations than the CO₂ profile when mass emissions were at their minimum levels and higher than the CO₂ concentrations at the end of the experimental period when the aerobic biodegradation activity of the soil had stopped. In the case of O₂, the profiles show that the simulated values are lower than the ones obtained experimentally especially at the bottom of each column.

Table 7.7 shows that consistent with what it was observed for the CO₂ concentration profiles, the simulated mass emissions for most of the chemicals were higher than the lowest emission during the experimental phase and lower than the emission at the end of the Phase II. Exceptions to this is Column A that showed a low degradation activity during phase II, therefore the experimental concentrations and mass emissions were significantly higher than the simulated results.

7.4 Summary

With the objective of determining the first-order degradation rate constants of the individual compounds being studied in the soil column experiments, the Luo (2009) version of the Abreu-Jhonson (2005) 3-D transient mathematical model was used to perform 1-D simulations. The rate constants were determined following two steps: (i) simulation of near-steady conditions of experimental Phase I to determine the model domain and effective diffusion coefficients and (ii) simulation of the near-steady conditions of experimental Phase III, in which the model domain and effective diffusion coefficients determined in step I are used calculate the first-order degradation rate constants. Finally, the first-order degradation rate constants were used to simulate experimental Phase II to study the vapor profiles and mass emissions if near-steady conditions would have been reached during this phase; results are compared to experimental results.

The criteria used to determine when the simulation outputs were giving a good fit to the experimental results is the following:

- *Phase I:* the simulated mass emissions at the effluent had to match the experimental mass emissions.
- *Phase II:* the output mass emissions, CO₂ mass emissions and CO₂ concentration profiles had to be similar to the experimental mass emissions.

As can be observed in Figures 7.3 and 7.6 as well as in Tables 7.3 and 7.5, the simulated concentration profiles and effluent mass emission gave a good fit to the experimental results.

The first-order degradation rate constants obtained from the simulation were in the range of values published by DeVaul (2007). Note that in all of the soil columns for most of the chemicals the highest rate constants were located at the “degradation zones”. Also, the first-order degradation rates showed different values for the same chemical in the same material; the rate constant depended mostly of the location where of the “degradation zone”.

Results from the simulation of experimental phase II, showed that the concentration profiles for benzene are lower than the experimental profiles when the minimum mass emissions were detected and when the concentrations were going back to anaerobic near-steady conditions levels. However, comparison of the simulated mass emissions to the experimental values showed that for most of the chemicals, the simulated results had higher mass emissions than the ones obtained during the bio-attenuation period of phase II and lower than the mass emission at the end of the experimental phase when aerobic biodegradation reactions had stopped. Exception are MTBE and 1,3,5-trimethylbenzene that showed higher simulated mass emissions than the experimental ones. These chemicals did not reach near-steady conditions during the whole experimental period.

CHAPTER 8

CONCLUSIONS AND RECOMMENDATIONS

Vapor intrusion pathway assessments involve the interpretation of soil gas profiles and these represent the combined effects of soil stratigraphy, moisture content, biodegradation, surface conditions, and source concentrations. Thus in this work, the diffusive vapor migration and aerobic biodegradation of petroleum hydrocarbon vapors in the vadose zone was studied by means of a laboratory soil column experiment. Six 1.8-m soil columns representing different geological settings were prepared using 40-60 mesh sand (medium-grained soil) and 16-minus mesh decomposed granite (fine-grained soil). The experiment was performed in three phases: (i) Phase I: anaerobic phase, (ii) Phase II: aerobic phase and (iii) Phase III: vapor source concentration was decreased ten times the original concentrations under aerobic conditions. At the end of the experiment, soil core samples were taken and the physical characteristics and microbial population of the soil were analyzed. Finally, the soil column experiment was simulated using a three-dimensional transient mathematical model to determine first-order degradation rate constants consistent with the profiles.

This chapter provides a summary of conclusions drawn from the experiment, as well as some recommendations for future research based on the results obtained in this study.

8.1 Conclusions

When performing an assessment of the vapor intrusion pathway, it is important to know if the soil gas profiles have reached near-steady conditions. During Phase I, the transient migration and the time required to travel 2 m was observed. These results were consistent with the theory and indicated that independent of the lithology, chemicals with similar characteristics to n-pentane, 2-methyl-2-butene, n-hexane, cyclohexane, iso-octane and n-heptane would be the quickest to achieve near-steady conditions. These

chemicals have high Henry's Law constants and low solubilities. The times to near-steady conditions varied from days to weeks for the other chemicals; and the times for chemicals with low Henry's Law constants such as MTBE or 1,3,5-trimethylbenzene were estimated to vary from months to years (MTBE and 1,3,5-trimethylbenzene did not reach near-steady conditions during the 200 days anaerobic phase period). The time for each chemical to achieve near-steady conditions across different soil columns was not only dependent on the chemical characteristics but also the soil characteristics such as moisture content, effective diffusion coefficient and bulk density.

Vapor concentration profiles at near-steady conditions during experimental Phase I (no aerobic degradation reactions were occurring) reflected the idealized subsurface settings in each column. This result suggests that during a vapor intrusion assessment, subsurface gas profiles, can provide information about subsurface conditions for cases where near-steady conditions have been reached and there is little to no degradation taking place. This could include locations with zones of high/low effective diffusion coefficients due to stratigraphy or changes in the soil moisture content.

During Phase I, it was expected that the columns composed mostly by low-grained soil (crushed granite) were going to have lower mass emissions than the ones composed by medium-grained soil (sand) in the following order: $A > B > C \approx D > E > F$. Results indicated that the order was $E > A \approx D > C > B > F$. Column E had higher effective diffusion coefficients than the rest of the columns which produced higher mass emissions. Differences in the diffusion coefficients of soil layers of the same material across the soil columns were due to differences in the packing of the soil in the columns. Changes in the soil moisture content also lead to changes in the soil vapor transport. In the experiment, a water mass balance analysis determined that water redistributed along the length of the soil columns, changing in that way, the soil moisture content of each soil layer. The soil moisture content at the top of the columns was lower than initial conditions which lead to an increase of 1 to 4% in the helium effective diffusion coefficients. This is important to

take into account when evaluating gas results from a spill site since some of the variability in data can be due to changes in the moisture content of the soil followed by rain events and water distribution in the soil matrix (Davis et al., 2005; Lundegard et al., 2008; Folkes, 2009; Luo et al., 2009; EPA, 2012).

Results from diffusive flux ratios determined during experimental phases II and III (Tables 4.5 and 5.5), indicated that the long-chain alkanes such as n-heptane and n-octane are the preferred compounds to be aerobically attenuated, followed by aromatic hydrocarbons such as benzene, toluene and p-xylene. In addition, it was found that the most recalcitrant components were n-pentane, iso-octane and MTBE. These results can explain the presence of compounds such as iso-octane or absence of n-heptane or n-octane on a weathered hydrocarbon spill site.

Previous studies (Scopa et al., 2006) have shown that the diversity of the soil microbial community decrease in the presence of high concentrations of petroleum hydrocarbon compounds (5,000 – 10,000 mg/Kg). In this study, a decrease in the effluent normalized mass emissions was observed once the sweep gas was switched from nitrogen to air. However, during Phase II, the hydrocarbon mass emissions shifted back to near-anaerobic levels after approximately 40 days. During Phase III when the vapor source concentrations were lowered ten time from the original concentrations, the normalized mass emissions decreased more than in Phase II at near-steady conditions.

In this work, aerobic microbial degradation of the petroleum hydrocarbon vapors was closely coupled to the production of CO₂. The profiles showed that there were CO₂ production zones over narrow intervals (0.2 – 0.4 m) along the length of each soil column, indicating that aerobic biodegradation was occurring in these locations. The vertical length of the “degradation zones” was defined by studying the hydrocarbon flux profiles. The hydrocarbon flux decreased at the locations where the aerobic degradation reactions took place. These “degradation zones” were mostly identified in the finer-grained soil (crushed granite) across the columns. These results were consistent with

findings by Kristensen et al. (2010) who observed that the finest-grained soils showed better aerobic degradation activity than the coarser ones. Microbial population analyses showed that the highest number of CFU/g-soils of hydrocarbon degraders could be found at this “degradation zones. These results suggest that the soil gas profiles alone can be a good indicator of biodegradation activity and microbial analyses are not necessary.

A number of conceptual models have been developed by studying the aerobic degradation of hydrocarbon vapor in the vadose zone. Roggemans et al. (2001), identified four behaviors:

- Behavior A: aerobic biodegradation occurs over a narrow interval of soil; above that interval no hydrocarbons are detected, and the soil has high concentrations of O₂ and CO₂. Below the bio-attenuation interval no CO₂ or O₂ are detected.
- Behavior B: aerobic biodegradation occur along the whole length of the soil column and it is limited by the degradation rates.
- Behavior C: aerobic degradation consumed the usable oxygen in the soil gas and the oxygen re-supply is lower than the oxygen consumption rate, so little to no oxygen concentrations are detected in the subsurface
- Behavior D: biodegradation occurs close to the vapor source. This occurs when the soil has a higher diffusion resistant zone immediately above the vapor source.

The aerobic degradation behavior of the soil columns did not fall into any of Roggemans et al. (2001) conceptual models, indicating that a new conceptual model can be added to the list. In the soil columns, bio-attenuation occurred over a narrow interval as in Behavior A. However, in this case, the petroleum hydrocarbon concentrations are detected above the bio-attenuation zone along with CO₂ and O₂. Also, concentrations of O₂ and CO₂ could be detected below the bio-attenuation zone. Figure 8.1 shows two of

the conceptual models of Roggemans et al (2001) compared to the soil column experiment conceptual model.

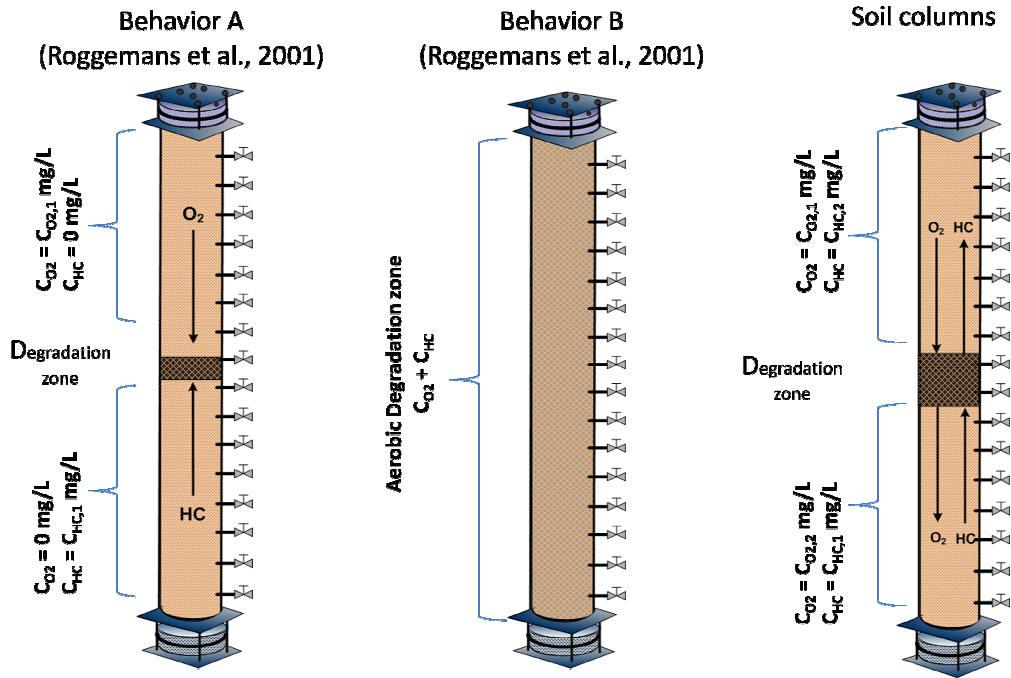


Figure 8.1. Roggemans et al. (2001) vs. soil columns experiment biodegradation behavior

There are many studies that have evaluated the biodegradation of petroleum hydrocarbons in the vadose zone (Hers et al., 2000; Pasteris et al., 2002; Höhener et al., 2006; DeVaul et al., 2004; DeVaul, 2007). Hence, there is a wide range of published values for first-order biodegradation rate constants, and these depend on the soil characteristics, such as nutrient content and moisture content. First-order degradation kinetics are commonly used to define aerobic degradation reactions of the petroleum hydrocarbon, not only due to simplicity but also they had been found to match adequately experimental and field results. In this case, the first-order degradation constants for the twelve petroleum hydrocarbons studied were estimated by performing a 1-D simulation of the near-steady conditions of the soil column experiment using the Luo (2009) version

of the Abreu-Johnson (2006) 3-D transient mathematical model. First-order rates ranged from 0.0 to $5.7 \times 10^3 \text{ d}^{-1}$ across the chemicals in this study (Table 8.5, Chapter 8). This rate constants fall into the range identified by DeVaul et al. (2007). It is important to note, that since the “degradation zones” were occurring over a narrow interval of soil (0.2 -0.3 m), in each column, different first-order degradation rates were estimated for the same material and same chemical at different positions in the columns.

Based on the soil column experiment results, it is concluded that assessment of the vapor intrusion pathway at petroleum hydrocarbon sites should include the measurement of physical soil characteristics, vapor concentration profiles and O_2 and CO_2 profiles. The soil physical characteristics such as soil stratigraphy, moisture content, total porosity, permeability and effective diffusion coefficient are key to predicting vapor transport through the vadose zone. The concentration profiles reflect vadose zone conditions (zones of different effective diffusion coefficients due to moisture content or different lithology) in all cases. The vapor profiles provide information about whether or not aerobic degradation is occurring on a particular site and where it is occurring.

8.2 Recommendations

Vapor fate and transport

- The soil column experiment was limited to the study of diffusive vapor transport. The study can be extended to observe the effect of advective transport in the soil columns. This can be achieved by creating a positive and/or negative pressure differential inside the soil columns, in that way the impacts of advective transport in the vapor hydrocarbon concentrations profiles, mass emissions and aerobic biodegradation can be determined. Degradation kinetics can be determined using the 3-D transient mathematical model used in this research project.

- This experiment provided a good insight of the transport and biodegradation of petroleum hydrocarbon vapors over a 1.8 m soil columns with different lithological settings. The experiment could be repeated for a mix of chlorinated compounds to study if biodegradation can be significant for vapor migration attenuation of those compounds.
- An important factor that affects the diffusive vapor transport and biodegradation through the vadose zone is the soil moisture content. This effect can be studied by setting up soil columns (they can be small <1 m long by 2 in wide) packed with homogeneous soils, each column will have different moisture content. Similar to this experiment, a mixture of petroleum hydrocarbons can be used as a vapor source and the columns could be run for anaerobic and aerobic conditions.

Maximum petroleum hydrocarbon concentrations that can be degraded

- Biodegradation rates of petroleum hydrocarbon vapor can vary widely depending on the soil and chemical characteristics, presence of nutrients and microorganisms. However, Scopa et al (2000) determined that soil with hydrocarbon concentrations of approximately 5,000 mg/Kg had low microbial diversity and aerobic degradation activity than soils with lower hydrocarbon concentrations. Thus, analysis of the threshold at which hydrocarbons have a toxic effect on the soil microbial populations is important. This can give an insight together with O₂ concentrations in the soil of why biodegradation does not occur or stops. The analysis can be performed using small soil columns, each having different vapor source concentrations.

Microbial populations

- Microbial test analysis results (MPN test) showed that the number of CFU/g-soil of benzene and n-hexane degraders did not match in some of the soil column locations (Figure 6.3). It would be interesting to expand this study further and determine the number of CFU/g-soil of degraders that prefer specific petroleum hydrocarbons, identified them and determine their location along the length of a soil column.

REFERENCES

- Abreu, L.D., Johnson, P. C. (2005). Effect of vapor source-building separation and building construction on soil vapor intrusion as studied with a three-dimensional numerical model. *Environmental Science & Technology*, 39(12), 4550-4561. Doi: 10.1021/es049781k
- Abreu, L.D., Johnson, P.C. (2006). Simulating the effect of aerobic biodegradation on soil vapor intrusion into buildings: influence of degradation rate, source concentration, and depth. *Environmental Science & Technology*. 40, 2304 – 2315.
- Adams, J.F., Reddy, K.R. (2003). Extent of benzene biodegradation in saturated soil column during air sparging. *Ground Water Monitoring and Remediation*, 23(3), 85-94
- Agency for Toxic Substances & Disease Registry (ASTDR). www.astdr.cdc.gov. Consulted October 2008
- Abreu, L. D. (2005). *A transient three-dimensional numerical model to simulate vapor intrusion into buildings*. Dissertation, Arizona State University. Tempe, AZ.
- Allard, P. F. (2007). *Vapor intrusion: Emerging regulations and evaluation methods*. Third Annual Gatekeeper Regulatory Roundup Conference. February 20-21. GEC, Phoenix, AZ.
- American Petroleum Institute (API). *Collecting and Interpreting Soil Gas Samples from the Vadose Zone. A Practical Strategy for Assessing the Subsurface Vapor-to-Indoor Air Migration Pathway at Petroleum Hydrocarbon Sites*. Regulatory and Scientific Affairs. Publication No. 4741. November 2005.
- American Petroleum Institute (API). *Assessing the Significance of Subsurface Contaminant Vapor Migration to Enclosed Spaces. Site-Specific Alternatives to Generic Estimates*. Health and Environmental Sciences Department. Publication No. 4674. December 1998.
- Andre, L., Dedziorek, M. A.M., Bourg, A. C.M., Haeseler, F., Blanchet, D. (2009). A novel experimental procedure to investigate the biodegradation of NAPL under unsaturated conditions. *Journal of Hydrology*, 370, 1 – 8. Doi: 10.1016/j.jhydrol.2009.01.031
- Baker, R. J., Baehr, A. L., & Lahvis, M. A. (2000). Estimation of hydrocarbon biodegradation rates in gasoline-contaminated sediment from measured respiration rates. *Journal of Contaminant Hydrology*, 41(1-2), 175-192. Doi: 10.1016/S0169-7722(99)00063-7

- Barbee, G. C. (1994). Fate of chlorinated aliphatic hydrocarbons in the vadose zone and ground water. *Ground Water Monitoring and Remediation*, 14(1), 129-140. Doi:10.1111/j.1745-6592.1994.tb00098.x
- Batterman, S., Kulshrestha, A., Cheng, H. (1995). Hydrocarbon vapor transport in low moisture soils. *Environmental Science and Technology*, 29(1), 171 -180
- Boopathy, R. (2004). Anaerobic biodegradation of no. 2 diesel fuel in soil: a soil column study. *Bioresource Technology*, 94(2), 143-151. Doi: 10.1016/S0960-8524(03)00371-7
- Borden, R. C., & Bedient, P. B. (1986). Transport of dissolved hydrocarbons influenced by oxygen-limited biodegradation .1. theoretical development. *Water Resources Research*, 22(13), 1973-1982. Doi: 10.1029/WR022i013p01973
- Bozkurt, O., Pennell, K.G., Suuberg, E.M. (2009). Simulation of the vapor intrusion process for nonhomogeneous soils using a three-dimensional numerical model. *Ground Water Monitoring and Remediation*, 29(1), 92 -104
- Broholm, M., Christophersen, M., Maier, U., Stenby, E., Hoehener, P., & Kjeldsen, P. (2005). Compositional evolution of the emplaced fuel source in the vadose zone field experimet at airbase vaerlose, denmark. *Environmental Science & Technology*, 39, 8251. Doi: 10.1021/es048557s
- Carrol, K. C., Taylor, R., Gray, E., Brusseau, M.L. (2009). The impact of composition on the physical properties and evaporative mass transfer of a PCE-diesel immiscible liquid. *Journal of Hazardous Materials*, 164, 1074-1081. Doi:10.1016/j.jhazmat.2008.09.003
- Clifton, L. M. (2008). Effect of dissolved oxygen manipulation on the benzene flux from a low permeability soil layer. (Master of Science, Arizona State University)
- Conant, B. H., Gilham, R. W., & Mendoza, C. A. (1996). Vapor transport of trichloroethylene in the unsaturated zone: Field and numerical modeling investigations. *Water Resources Research*, 32(1), 9-22. Doi: 10.1029/95WR02965
- Davis, G. B., Patterson, B. M., & Trefry, M. G. (2009). Evidence for instantaneous oxygen-limited biodegradataion of petroleum hydrocarbon vapors in the subsurface. *Ground Water Monitoring and Remediation*, 29(1), 126-137. Doi: 10.1111/j.1745-6592.2008.01221.x
- Davis, G. B., Rayner, J. L., Trefry, M. G., Fisher, S. J., & Patterson, B. M. (2005). Measurement and modeling of temporal variations in hydrocarbon vapor behavior in

a layered soil profile. *Vadose Zone Journal*, 4(2), 225-239.
Doi: 10.2136/vzj2004.0029

DeVaul, G. E. (2007). Indoor vapor intrusion with oxygen-limited biodegradation for a subsurface gasoline source. *Environmental Science & Technology*, 41(9), 3241-3248

DeVaul, G.E., Ettinger, R.A., Salanitro, J.P., Gustafson, J.B. *Transport and aerobic degradation of gasoline vapor constituents in a diffusive soil column – theory and experiments*. Technical Progress Report. Petroleum Environmental research Forum (PERF). 2004-2005

DeVaul, G. E., Ettinger, R., & Gustafson, J. (2002). Chemical vapor intrusion from soil or groundwater to indoor air: Significance of unsaturated zone biodegradation of aromatic hydrocarbons. *Soil and Sediment Contamination*, 11(4), 625-641.
Doi: 10.1080/20025891107195

Eklund, B. M., & Simon, M. A. (2007). Concentration of tetrachloroethylene in indoor air at a former dry cleaner facility as a function of subsurface contamination: a case study. *Air and Waste Management Association*, 57, 753-760. Doi: 10.3155/1047-3289.57.6.753

English, C. W., & Loehr, R. C. (1991). Degradation of organic vapors in unsaturated soils. *Journal of Hazardous Materials*, 28(1-2), 55-63. Doi: 10.1016/0304-3894(91)87005-M

English, C. W. (1991). Removal of organic vapors in unsaturated soil. (Doctoral, University of Texas at Austin, Austin, TX, United States (USA)). (University Microfilms, Ann Arbor, MI, United States (USA))

Federal Contaminated Site Risk Assessment in Canada Part 1: *Guidance on Human Health Preliminary Quantitative Risk Assessment (PQRA)*, (2004)

Fine, P., Graber, E.R., Yaron, B. (1997). Soil interactions with petroleum hydrocarbons: abiotic processes. *Soil Technology*, 10, 133 -153

Fischer, M.L., Bentley, A.J., Dunkin, K.A., Hodgson, A.T., Nazaroff, W.W., Sextro, R.G., Daisey, J.M. (1996). Factors affecting indoor air concentrations of volatile organic compounds at a site of subsurface gasoline contamination. *Environmental Science and Technology*, 30(10), 2948 -2957

Fitzpatrick, N. A., & Fitzgerald, J. J. (2002). An evaluation of vapor intrusion into buildings through a study of field data. *Soil and Sediment Contamination*, 11(4), 603-623. Doi: 10.1080/20025891107186

- Folkes, D., Wertz, W., Kurtz, J., & Kuehster, T. (2009). Observed spatial and temporal distributions of CVOCs at colorado and new york vapor intrusion sites. *Ground Water Monitoring and Remediation*, 29(1), 70-80. Doi: 10.1111/j.1745-6592.2009.01216.x
- Garbesi, K., Sextro, R.G. (1989). Modeling and field evidence of pressure-driven entry of soil gas into a house through permeable below-grade walls. *Environmental Science and Technology*, 23(12), 1481 – 1487. Doi:10.1021/es00070a005
- Greene, E.A., Kay, J.G., Jaber, K., Stehmeier, L.G., Voordouw, G. (2000). Composition of soil microbial communities enriched on a mixture of aromatic hydrocarbons. *Applied and Environmental Microbiology*, 66(12), 5282 – 5289
- Haynes, W. M., Lide, D.R. (2011-2012). *CRC handbook of chemistry and physics*. 92nd ed. Boca Raton, FL.; CRC Press. Retrieved from <http://hbcnetbase.com.ezproxy1.lib.asu.edu/>
- Hers, I., Atwater, J., Li, L., Zapf-Gilje R. (2000). Evaluation of vadose zone biodegradation of BTX vapours. *Journal of Contaminant Hydrology*, 46, 233 -264
- Hers, I., Zapf-Gilje, R., Johnson, P.C., Li, L. (2003). Evaluation of the Johnson and Ettinger model for prediction of indoor air quality. *Ground Water Monitoring and Remediation*, 23(2), 119 -133. Doi: 10.1111/j.1745-6592.2003.tb00784.x
- Hoehener, P., Duwig, C., Pasteris, G., Kaufmann, K., Dakhel, N., & Harms, H. (2003). Biodegradation of petroleum hydrocarbon vapors; laboratory studies on rates and kinetics in unsaturated alluvial sand. *Journal of Contaminant Hydrology*, 66(1-2), 93-115
- Hohener, P., Dakhel, N., Christophersen, M., Broholm, M., & Kjeldsen, P. (2006). Biodegradation of hydrocarbon vapors: Comparison of laboratory studies and field investigations in the vadose zone at the emplaced fuel source experiment, airbase vaerloese, denmark. *Journal of Contaminant Hydrology*, 88(3-4), 337-358
- Interstate Technology & Regulatory Council (ITRC) (2007). Vapor intrusion pathway: a practical guideline. *Technical and Regulatory Guidance*.
- Jin, Y., Streck, T., & Jury, W. A. (1994). Transport and biodegradation of toluene in unsaturated soil. *Journal of Contaminant Hydrology*, 17(2), 111-127

- Johnson, P. C. (2005). Identification of application-specific critical inputs for the 1991 Johnson and Ettinger vapor intrusion algorithm. *Ground Water Monitoring and Remediation*, 25(1), 63-78
- Johnson, P. C., Bruce, C., Johnson, R. L., & Kemblowski, M. W. (1998). In situ measurement of effective vapor-phase porous media diffusion coefficients. *Environmental Science & Technology*, 32(21), 3405-3409
- Johnson, P. C., Ettinger, R. A. (1991). Heuristic model for predicting the intrusion rate of contaminant vapors into buildings. *Environmental Science & Technology*, 25(8), 1445-1452. Doi: 10.1021/es00020a013
- Johnson, P. C., Ettinger, R. A., Kurtz, J., Bryan, R., & Kester, J. E. (2002). Migration of soil gas vapors to indoor air: determining vapor attenuation factors using a screening-level model and field data from the CDOT-MTL Denver, Colorado site. *American Petroleum Institute (API)*, (16), 1-10
- Johnson, P. C., Kemblowski, M. W., & Colthart, J. D. (1990). Quantitative analysis for the cleanup of hydrocarbon-contaminated soils by in-situ soil venting. *Ground Water*, 28(3), 413-429
- Johnson, P. C., Kemblowski, M. W., & Johnson, R. L. (1999). Assessing the significance of subsurface contaminant vapor migration to enclosed spaces: Site-specific alternatives to generic estimates. *Journal of Soil Contamination*, 8(3), 389-421
- Johnson, P. C., Stanley, C. C., Kemblowski, M. W., Byers, D. L., & Colthart, J. D. (1990). A practical approach to the design, operation, and monitoring of in-situ soil-venting system. *Ground Water Monitoring and Remediation*, 10(2), 159-178. Doi:10.1111/j.1745-6592.1990.tb00347.x
- Karapanagioti, H. K., Gaganis, P., & Buganos, V. N. (2003). Modeling attenuation of volatile organic mixtures in the unsaturated zone: Codes and usage. *Environmental Modeling & Software*, 18, 329-337. Doi: 10.1016/S1364-8152(02)00108-1
- Keith, L. H. (1991). *Environmental sampling and analysis: a practical guide*. United States: Lewis Publishers, Inc.
- Kristensen, A.H., Poulsen, T.G., Mortensen, L., Moldrup, P. (2010). Variability of soil potential for biodegradation of petroleum hydrocarbons in a heterogeneous subsurface. *Journal of Hazardous Materials*. 179, 573 – 580.
- Lahvis, M. A., Baehr, A. L., & Baker, R. J. (1999). Quantification of aerobic biodegradation and volatilization rates of gasoline hydrocarbons near the water

- table under natural attenuation conditions. *Water Resources Research*, 35(3), 753-765. Doi: 10.1029/1998WR900087
- Laubacher, R. C., Bartholomae, P., Velasco, P., & Reisinger, H. J. (1997). An evaluation of the vapor profile in the vadose zone above a gasoline plume. *Proceedings of the VWWA/API. Conference on Petroleum Hydrocarbons and Organic Chemicals in Ground Water - Prevention, Detection & Restoration*, 396-409
- Leahy, J. G., & Colwell, R. R. (1990). Microbial Degradation of Hydrocarbons in the Environment. *Microbiological Reviews*, 54(3), 305-315
- Li, H., Zhang, Y., Kravchenko, I., Xu, H., Zhang, C. (2007). Dynamic changes in microbial activity and community structure during biodegradation of petroleum compounds: a laboratory experiment. *Journal of Environmental Sciences*, 19, 1003 – 1013
- Little, J. C., & Daisey, J.M., Nazaroff, W.W. (1992). Transport of subsurface contaminants into buildings: An exposure pathway for volatile Organics. *Environmental Science & Technology*, 26, 2058-2066. Doi: 10.1021/es00035a001
- Lundegard, P. D., Johnson, P. C., & Dahlen, P. (2008). Oxygen transport from the atmosphere to soil gas beneath a slab-on-grade foundation overlying petroleum-impacted soil. *Environmental Science & Technology*, 42, 5534-5540. doi:10.1021/es070607g
- Luo, H., Dahlen, P., Johnson, P. C., Peargin, T., & Creamer, T. (2009). Spatial variability of soil-gas concentrations near and beneath a building overlying shallow petroleum hydrocarbon-impacted soils. *Ground Water Monitoring and Remediation*, 29(1), 81-91. Doi: 10.1111/j.1745-6592.2008.01217.x
- Luo, H. (2009). Field and modeling studies of soil vapor migration into buildings at petroleum hydrocarbon impacted sites. (Doctoral in Philosophy, Arizona State University)
- Marguesin, R., Labbe, D., Schinner, F., Greer, C.W., Whyte, L.G. (2003). Characterization of hydrocarbon-degrading microbial populations in contaminated and pristine alpine soils. *Applied and Environmental Microbiology*, 69(6), 3085-3092. Doi: 10.1128/AEM.69.6.3085-3092.2003
- Massmann, J., Farrier, D.F. (1992). Effects of atmospheric pressures on gas transport in the vadose zone. *Water Resources Research*. 28(3), 777 – 791.
- McHugh, T. E., Connor, J. A., Ahmad, F. (2004). An empirical analysis of the groundwater-to-indoor-air exposure pathway: The role of background concentrations in indoor air. *Environmental Forensics*, 5, 33-44. Doi: 10.1080/15275920490424024

- McHugh, T., Kuder, T., Ahmad, Fiorenza, S., Gorder, K., Dettenmaier, E., Philp, P. (2011). Application of CSIA to distinguish between vapor intrusion and indoor sources of VOCs. *Environmental Science and Technology*, 45(14), 5952-5958
- Militon, C., Boucher, D., Vachelard, C., Perchet, G., Barra, V., Troquet, J., Peyretailade, E., Peyret, P. (2010). Bacterial community changes during bioremediation of aliphatic hydrocarbon-contaminated soil. *FEMS Microbiology Ecology*, 74, 669-681. Doi: 10.1111/j.1574-6941.2010.00982.x
- Neale, N., Hughes, J. B., & Ward, C. H. (2000). Impacts of unsaturated zone properties on oxygen transport and aquifer reaeration. *Ground Water*, 38(5), 784-794. Doi: 10.1111/j.1745-6584.2000.tb02714.x
- Nazaroff, W.W., Lewis, S.R., Doyle, S.M., Moed, B.A., Nero, A.V. (1987). Experiments on pollutant transport from soil into residential basements by pressure-driven airflow. *Environmental Science and Technology*, 21(5), 459 – 466. Doi:10.1021/es00159a006
- Ong, S.K., Culver, T.B., Lion, L.W., Shoemaker, C.A. (1992). Effects of soil moisture and physical-chemical properties of organic pollutants on vapor-phase transport in the vadose zone. *Journal of contaminant hydrology*, 11, 273 – 290
- Ostendorf, D. W., & Kampbell, D. H. (1991). Biodegradation of hydrocarbon vapors in the unsaturated zone. *Water Resources Research*, 27(4), 453-462. Doi: 10.1029/91WR00111
- Ostendorf, D. W., & Kampbell, D. H. (1990). Bioremediated soil venting of light-hydrocarbons. *Hazardous Waste & Hazardous Materials*, 7(4), 319-334. Doi: 10.1089/hwm.1990.7.319
- Pasteris, G., Werner, D., Kaufmann, K., Hohener, P. (2002). Vapor phase transport and biodegradation of volatile fuel compounds in the unsaturated zone: a large scale lysimeter experiment. *Environmental Science and Technology*, 36(1), 30-39
- Patterson, B. M., & Davis, G. B. (2009). Quantification of vapor intrusion pathways into a slab-on-ground building under varying environmental conditions. *Environmental Science & Technology*, 43, 650-656. Doi: 10.1021/es801334x
- Pennell, K.G., Bozkurt, O., Suuberg, E.M. (2009). Development and application of a three-dimensional finite element vapor intrusion model. *Journal of the Air & Waste Management Association*, 59, 447 – 460. Doi: 10.3155/1047-3289.59.4.447

- Perry, R.H., Green, D.W. (2008). *Perry's chemical engineering handbook*. 8th ed. New York; McGraw-Hill.
- Popp, N., Schlomann, M., Mau, M. (2006). Bacterial diversity in the active stage of a bioremediation system for mineral oil hydrocarbon-contaminated soils. *Microbiology*, 152, 3291-3304. Doi: 10.1099/mic.0.29054-0
- Powers, S. E., Villaume, J. F., & Ripp, J. A. (1997). Multivariate analyses to improve understanding of NAPL pollutant sources. *Ground Water Monitoring and Remediation*, 17(2), 130-140
- Roggemans S., Bruce, C. L., Johnson, P. C., & Johnson, R. L. (2001). Vadose zone natural attenuation of hydrocarbon vapors: An empirical assessment of soil gas vertical profile data. *American Petroleum Institute (API)*, (15), 1-12
- Sanders, P. F., & Hers, I. (2006). Vapor intrusion in homes over gasoline-contaminated ground water in Stanford, New Jersey. *Ground Water Monitoring and Remediation*, 26(1), 63-72. Doi: 10.1111/j.1745-6592.2006.00048.x
- Sanders, P. F., & Stern, A. H. (1994). Calculation of soil cleanup criteria for carcinogenic volatile organic-compounds as controlled by the soil-to-indoor air exposure pathway. *Environmental Toxicology and Chemistry*, 13(8), 1367-1373. Doi: 10.1897/1552-8618(1994)13[1367:COSECF]2.0.CO2
- Scopa, A., Salzano, G., Scrano, L., Bufo, S.A., Bonomo, M.G. (2006). Preliminary assessment of microbial community recovery after an accidental oil spill by molecular analysis. *Fresenius Environmental Bulletin*, 15(7), 675 – 681
- Solano-Serena, F., Marchal, R., Huet, T., Lebeaulty, J. M., & Vandecasteele, J. -. (2000). Biodegradability of volatile hydrocarbons of gasoline. *Applied Microbiology and Biotechnology*, 54, 121-125
- Tillman Jr., F. D., Weaver, J. W. (2007). Temporal moisture content variability beneath and external to a building and the potential effects on vapor intrusion risk assessment. *Science of the Total Environment*, 379(1), 1-15. Doi: 10.1016/j.scitotenv.2007.02.003
- Tillman F.D., Weaver, J.W. (2005). Review of research on vapor intrusion. U.S. Environmental Protection Agency. Office of Research and Development. Washington, DC
- United States Environmental Protection Agency EPA. (2012). *Conceptual Model Scenarios for the Vapor Intrusion Pathway*. Office of Solid Waste and Emergency Response. Washington, DC.

United States Environmental Protection Agency EPA. (2011). *Petroleum Hydrocarbons and Chlorinated Hydrocarbons Differ in their Potential for Vapor Intrusion*. Office of Underground Storage Tanks. Washington, DC.

United States Environmental Protection Agency EPA. (2011). *Background Indoor Air Concentrations of Volatile Organic Compounds in North American Residences (1990-2005): a Compilation of Statistics for Assessing Vapor Intrusion*. Office of Solid Waste and Emergency Response. Washington, DC.

United States Environmental Protection Agency EPA. (2002). *OSWER draft guidance for evaluating the vapor intrusion to indoor air pathway from groundwater and soils (subsurface vapor intrusion guidance)* EPA

Wilson, J.T, Adair, C., Kaiser, P.M., Kolhatkor, R. (2005). Anaerobic biodegradation of MTBE at a gasoline spill site. *Ground Water Monitoring and Remediation*. 25(3), 103-115. Doi: 10.1111/j.1745-6592.2005.00032.x

Yu, S., Unger, A. J., & Parker, B. (2009). Simulating the fate and transport of TCE from groundwater to indoor air. *Journal of Contaminant Hydrology*, 107, 140-161. Doi: 10.1016/j.jconhyd.2009.04.009

APPENDIX I
PROCEDURE TO DETERMINE SOIL CHARACTERISTICS

PROCEDURE FOR SOIL CHARACTERISTICS DETERMINATION

i) Soil Moisture Content

The soil moisture content is one of the key variables of the experiment. It is necessary to keep it constant and homogeneous along the column and during the experimental period to ensure that the vapor diffusion conditions are constant at all times and consequently, ensure that the vapor flux profiles do not change due to moisture content variations.

Tests prior packing the columns were conducted to determine the best moisture conditions in which the soils are able to maintain constant moisture content without presenting vertical water redistribution. The tests were performed using three 4" by 12" PVC soil columns (See Figure I.1). The PVC columns were sealed at the bottom by a PVC cap in which a copper tubing port coupled with three-way nylon Luer-type plastic valve (Kentos, Glass Company, Vineland, NJ) is attached. This port had various uses such as sampling port and water injection port for porosity tests. In the middle of the body of the column there is one stainless steel needle sample port (0.16"x4", Popper) coupled with three-way nylon Luer-type plastic valve as shown in Figure 2.3. The tests consisted in packing the three columns with the soil in study (20-40 mesh sand or crushed granite) at predetermined moisture contents. The top of the PVC columns were sealed with parafilm tape (VWR). Subsequently, diffusion coefficient measurements were performed at the middle port following the procedure explained in section iv below. The columns were then left for 24 hours. After 24 hours, new diffusion coefficient tests were performed and soil samples from the top, middle and bottom of the column were taken to determine the moisture content by using the standard moisture content test ASTM D2216-05 and in that manner, find out if there had been moisture redistribution along the soil column. The standard moisture content method consists on placing the soil samples in aluminum foil cups (Cole-Parmer Instruments Co.) that have been previously weighted in an analytical balance. The samples are weighted and placed in an oven at 110°C for

approximately 24 hours. After 24 hours, the samples are placed on a desiccator to let them cool down and then are weighted. The moisture content is then determined by the equation:

$$\text{Moisture content } [\% W/W] = \frac{(\text{Initial soil weight [g]} - \text{Final soil weight [g]})}{\text{Initial soil weight (g)}} \times 100 \quad (1.1)$$

These tests determined that the moisture contents at which the soils did not experiment vertical water redistribution were 2.5% w/w for the 20-40 mesh sand and 11% w/w for the crushed granite.

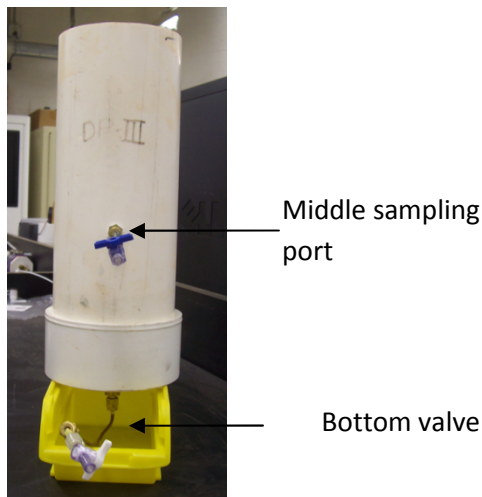


Figure 1.1. Four inch. by twelve inch PVC soil column

ii) Bulk Density ρ_b

The soil bulk density for each type of soil to was obtained during the moisture content tests. The volume of soil placed in the 4"x12" PVC soil columns was known. The soil in the columns was weighted once it was packed in the PVC columns. Thus, the bulk density was determined using the equation:

$$\rho_b = \frac{\text{Soil Weight (g)}}{\text{Soil Volume (ml)}} \quad (1.2)$$

iii) Fraction of Organic Carbon (FOC)

The FOC was determined by taking three dry soil samples in aluminum foil cups (VWR), weighting them and placing them in the oven at 110 °C overnight so the moisture content of the soil is eliminated. Then, the samples were reweighted and placed on a furnace muffle (thermolyne 6000) at 350°C to eliminate the organic carbon contained in the soil. The samples are left to cool down to ambient temperature on a desiccator and weighted again. The FOC is determined as follows:

$$FOC \% w/w = \frac{(Dried\ soil\ weight\ [g] - soil\ weight\ after\ furnace\ [g])}{Dried\ soil\ weight\ [g]} \times 100 \quad (1.3)$$

iv) Air Permeability

The air permeability test was performed on dry soil samples and samples containing the moisture content to be used to pack the columns. The apparatus utilized was an “air permeameter” designed at ASU (See Figure 1.2 below). The tests are performed by placing a soil sample in the cylinder. A constant specific air flow rate is passed through the soil and measured with air flow meters (Dwyer). Once the flow rate is determined and constant, the pressure differential between the upstream and downstream of the sample is measured by means of Magnahelic pressures gauges. Then, the air permeability is calculated by the equation:

$$K = \frac{v \times \mu \times L}{\Delta P} \quad (1.4)$$

Where:

K = Air permeability [cm²]

v = Air velocity passing through the soil [cm/s] (v = Q/A, air flow rate [cm³/s]/cross-sectional area [cm²])

μ = Air dynamic viscosity at ambient air (25°C) [Pa.s]

L = Length of the cylinder used to place the sample [cm]

ΔP = Pressure differential between upstream and downstream of the soil sample when air is flown through it [Pa]

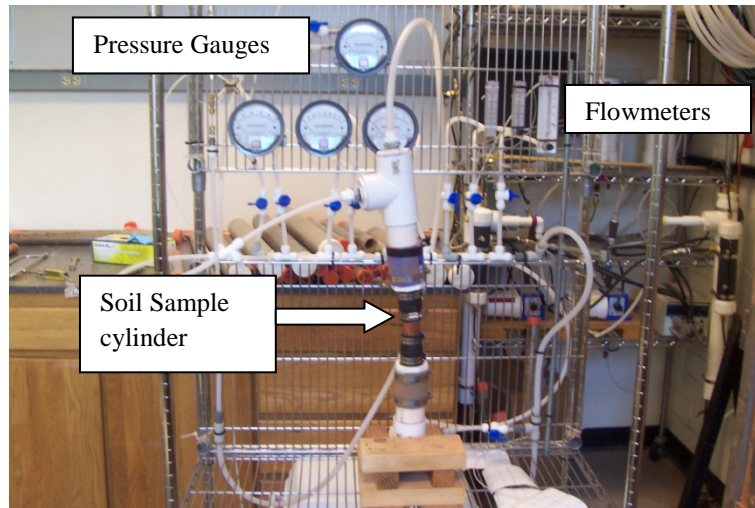


Figure 1.2. ASU air permeameter

v) Total Porosity, ϕ_T

The total porosity was determined by using the water saturation method. The method consists on adding water to the soil until saturation is reached; then, the porosity is calculated with the equation:

$$\phi_T = \frac{\text{Volume of water [cm}^3\text{]}}{\text{Volume of soil [cm}^3\text{]}} \quad (1.5)$$

To do this, the apparatus shown in Figure 2.5 was utilized. The water was driven by gravity from the burette to the bottom of the 4" by 12" PVC column. Water was introduced in a slow rate to avoid trapping any air in the soil pores and obtain an accurate measurement. As a quality control measure, the test was repeated three times for each type of soil.

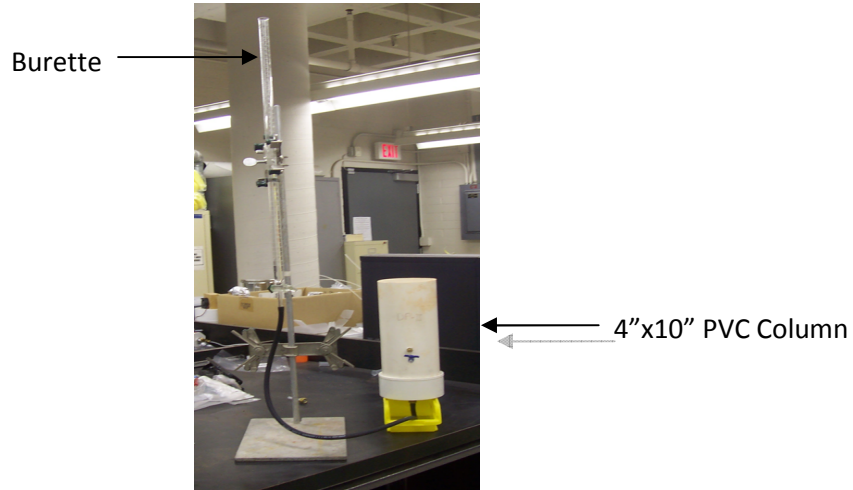


Figure I.3. Total porosity determination set-up

vi) Effective Diffusion Coefficient, D^{eff}

Diffusion coefficient tests are performed following the Johnson et al. (1998) protocol. The method consists in determining the mass fraction of tracer gas recovered after injecting a known concentration tracer into the soil, waiting for a predetermined period of time, and withdrawing a known volume of gas. The effective diffusion coefficient is then calculated by trial and error from the equations:

$$\eta = \frac{c_v V_{out}}{c_v^0 V_{in}} = \left(\frac{3V_{out}}{V_{in}} \right) \int_0^1 \frac{\xi^2}{2} \left\{ \text{erf} \left[\left(\left(\frac{V_{in}}{V_{out}} \right)^{1/3} + \xi \right) \beta^{1/2} \right] + \text{erf} \left[\left(\left(\frac{V_{in}}{V_{out}} \right)^{1/3} - \xi \right) \beta^{1/2} \right] \right\} d\xi - 3V_{out}V_{in}01\xi2\pi\beta\exp-V_{in}V_{out}1/3-\xi2\beta-\exp-V_{in}V_{out}1/3+\xi2\beta d\xi \text{ Eq. I.6}$$

$$\beta = \left[\frac{\theta_v^{1/3}}{D_v^{\text{eff}}} \right] \left[\frac{1}{4t_s} \right] \left[\frac{3V_{out}}{4\pi} \right]^{2/3} \quad (I.6)$$

Where,

η = Mass fraction of recovered tracer gas

C_v = Tracer gas recovered concentration

C_v^0 = Tracer gas initial concentration

V_{out} = Withdrawn volume from the soil

V_{in} = Volume injected into the soil

θ_v = Soil vapor filled porosity

t_s = Predetermine diffusive waiting time between injection and withdraw of tracer gas

(ξ = dummy function)

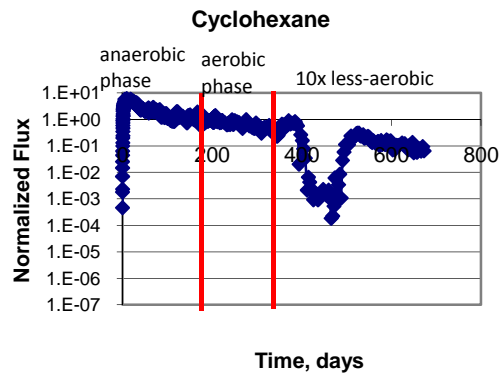
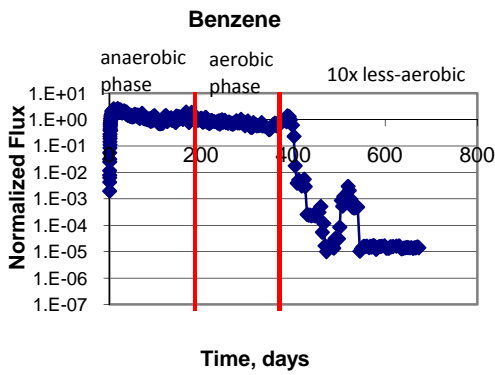
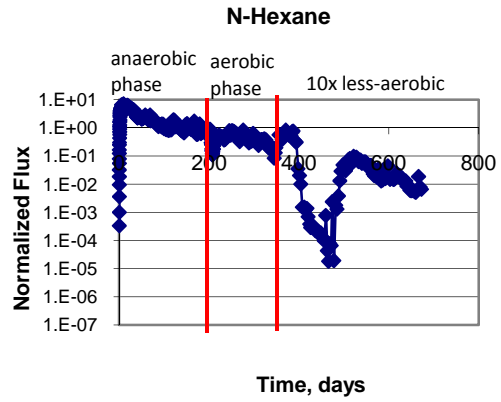
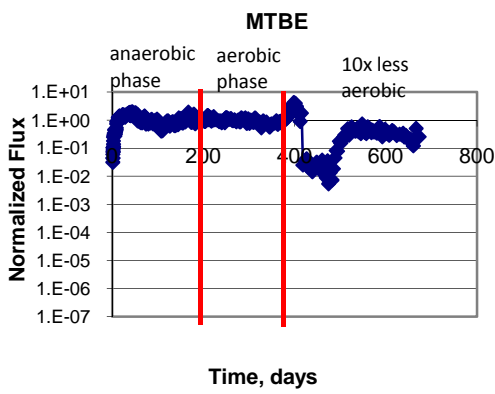
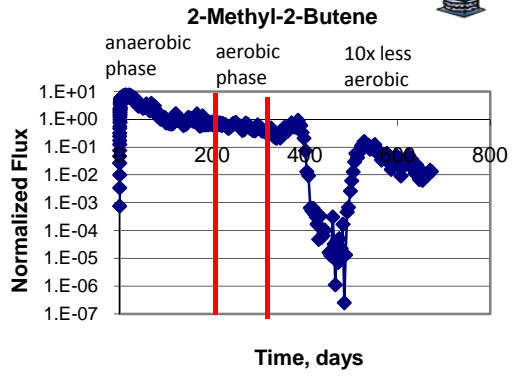
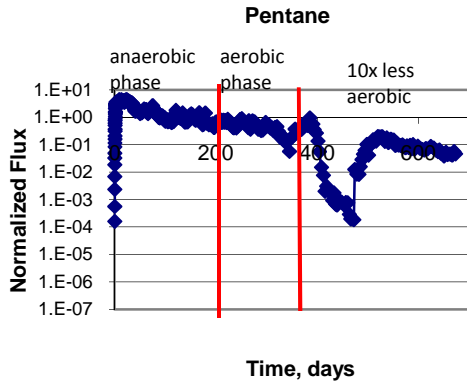
(Johnson et al., 1998)

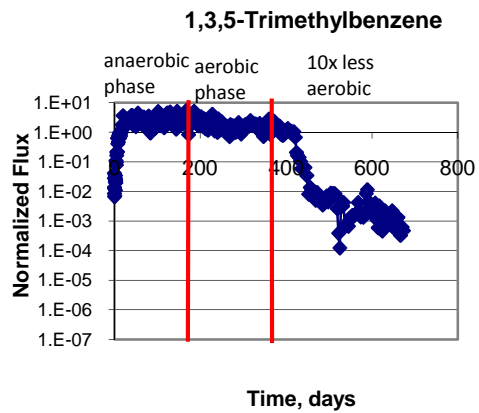
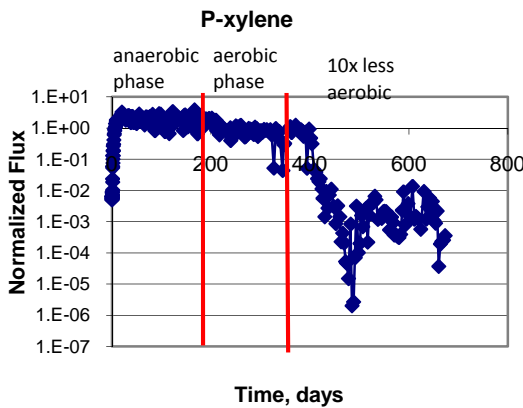
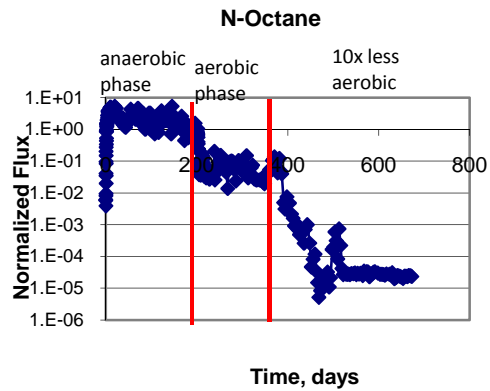
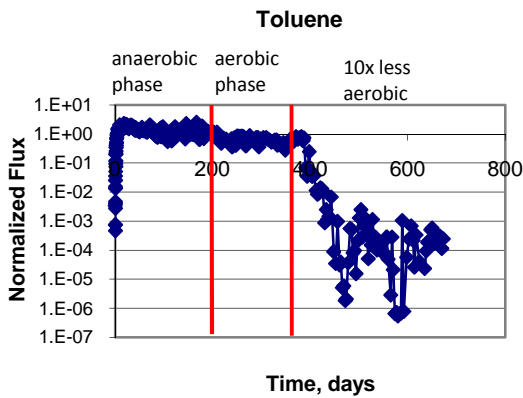
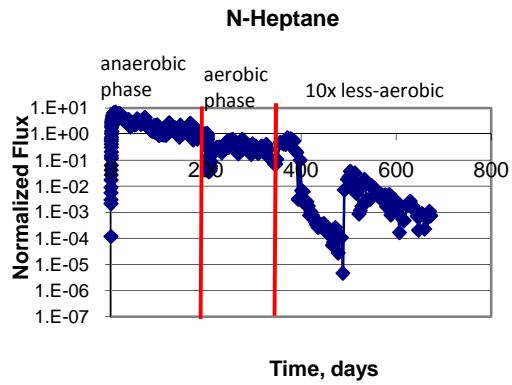
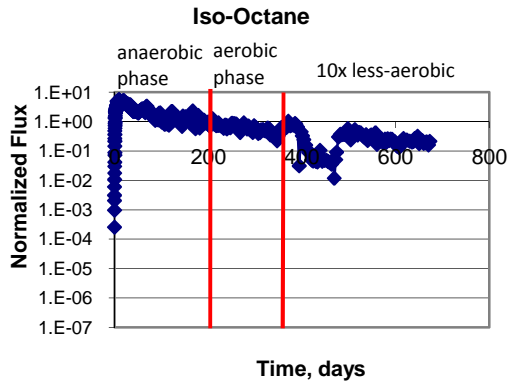
In this case, the carrier gas utilized was helium (He). The injected volume into de soil (V_{in}) was 0.4 mls, the volume withdrawn (V_{out}) was 5 mls; and the period of time at which the gas is left in the soil (t_s) was 15 seconds. The helium concentration in the soil samples was determined by means of a gas chromatograph (SRI 8610C, SRI instruments) equipped with a thermal conductivity detector (TCD) and two molsieve-5 m. columns joint together (Alltech Associates, Inc., Deerfield, IL., USA). The sample is injected into a 1 ml loop, which takes the samples into the column. The carrier gas is nitrogen (N_2) at a flow of 21.6 ml/min and the temperature is kept constant at 80°C. As explained in section i), effective diffusion coefficient tests were performed prior packing the stainless steel columns using the 4"x12" PVC soil columns during the moisture content tests.

During the experimental period, effective diffusion coefficient measurements were performed prior placing the hydrocarbon source in the stainless steel columns and at the end of the experimental period of each column.

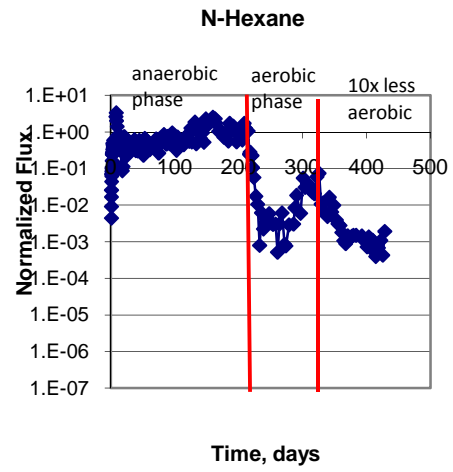
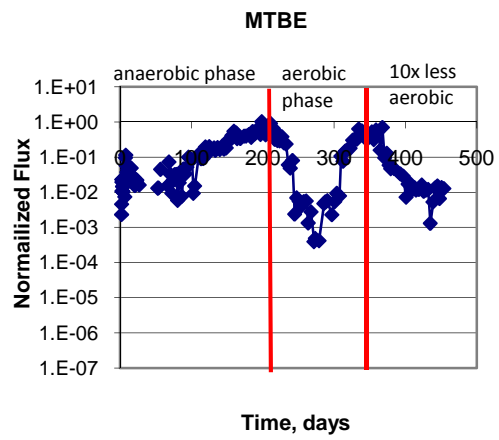
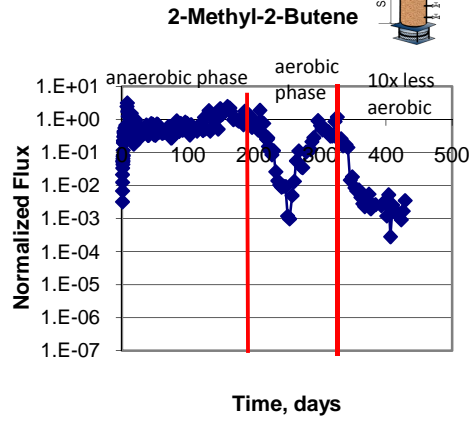
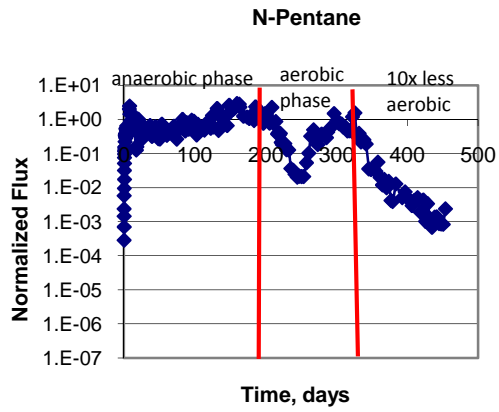
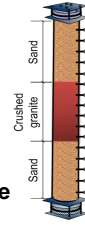
APPENDIX II
EFFLUENT NORMALIZED FLUX VS. TIME

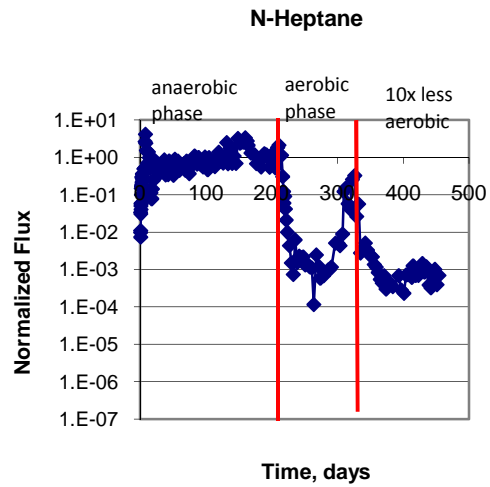
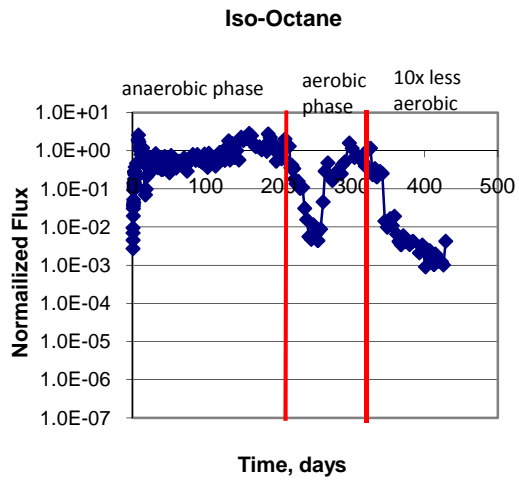
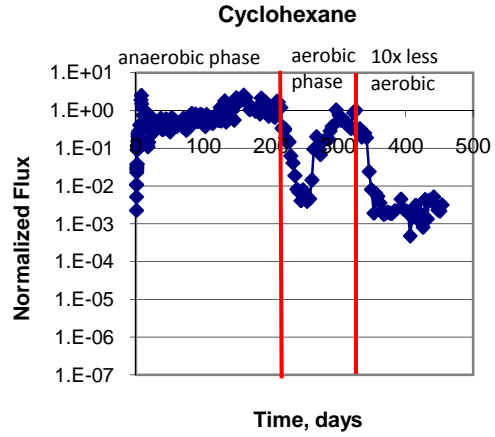
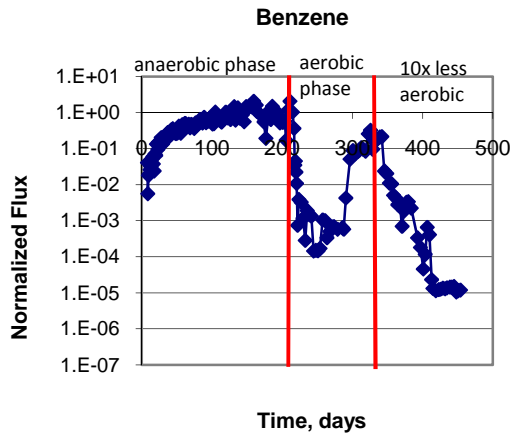
COLUMN A – EFFLUENT NORMALIZED FLUX VS TIME

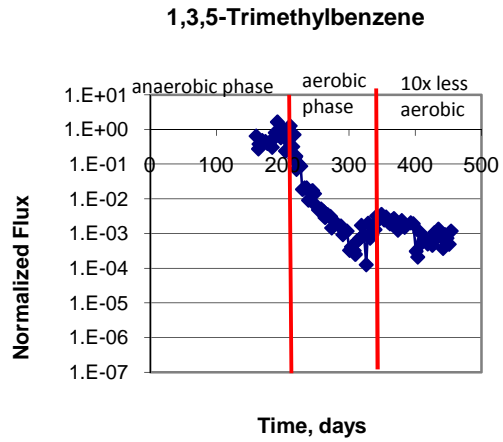
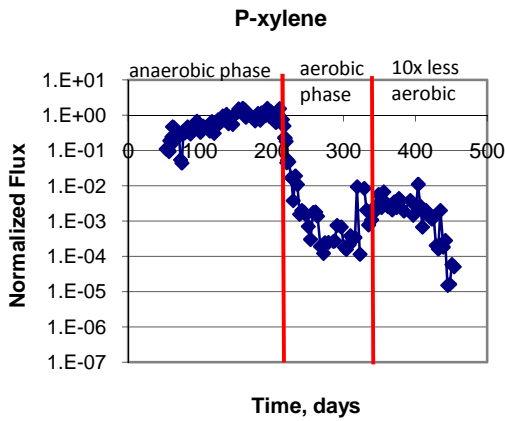
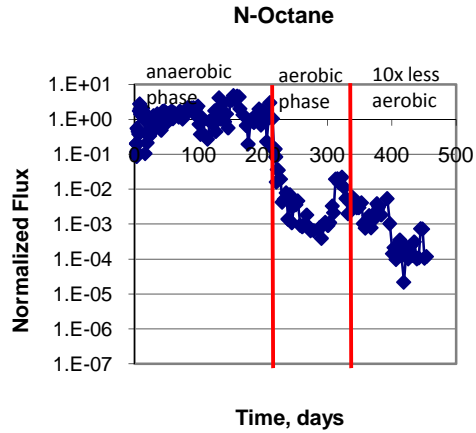
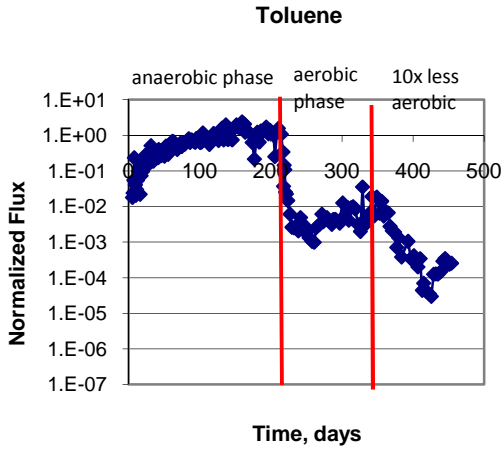




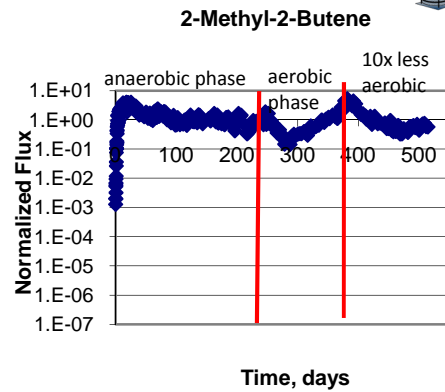
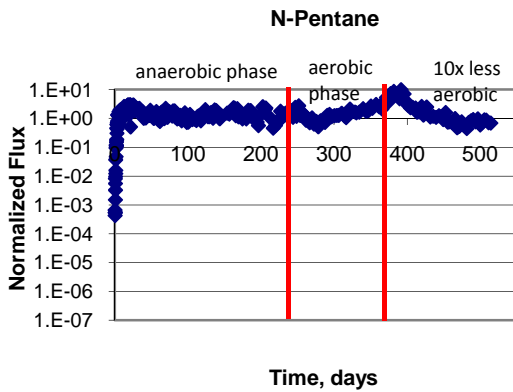
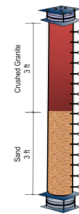
COLUMN B EFFLUENT – NORMALIZED FLUX VS TIME

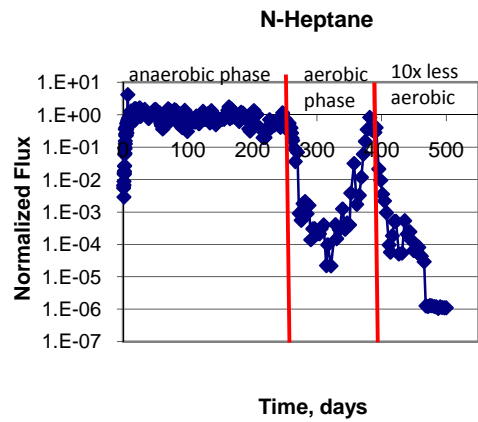
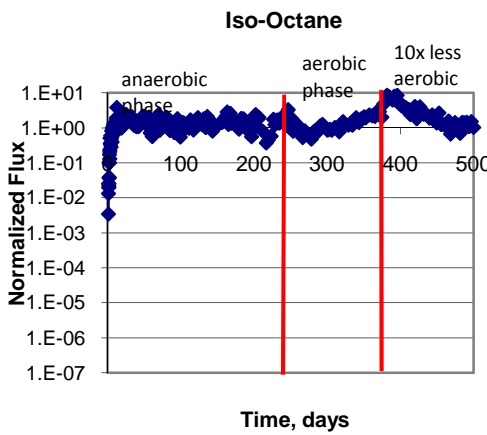
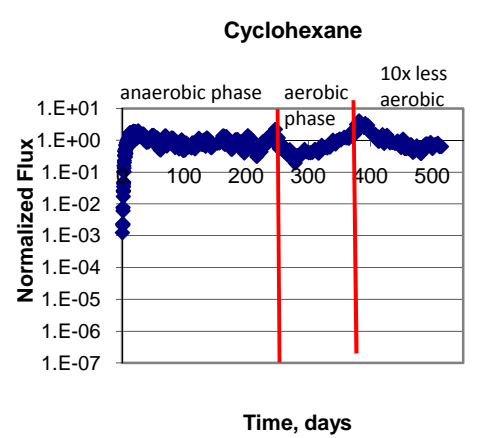
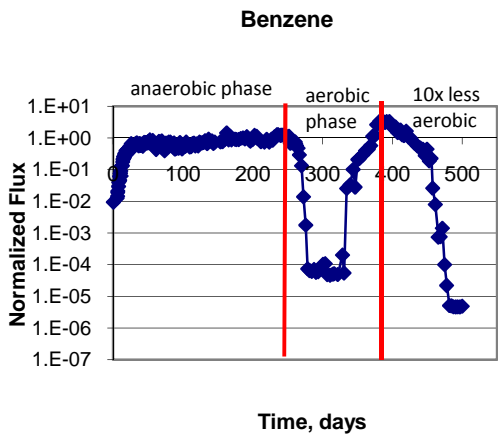
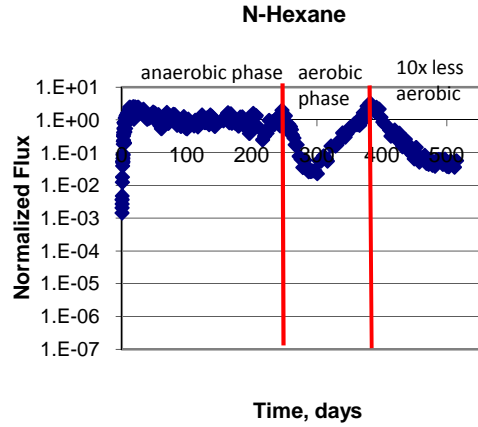
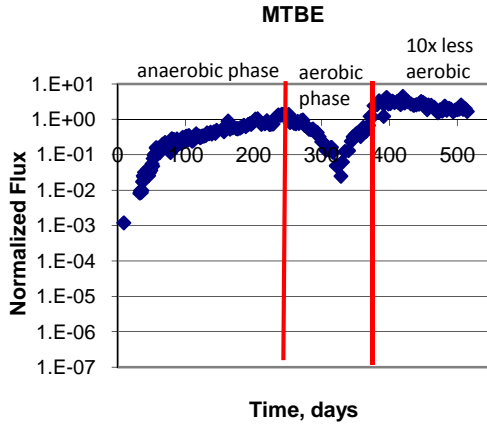


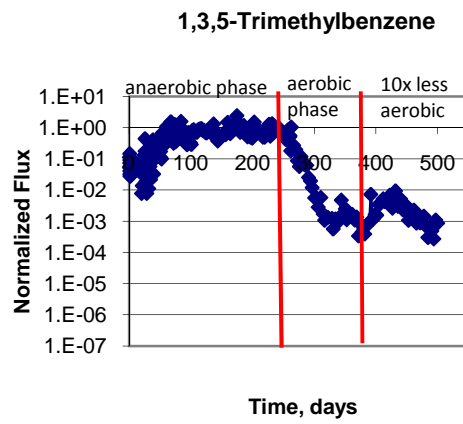
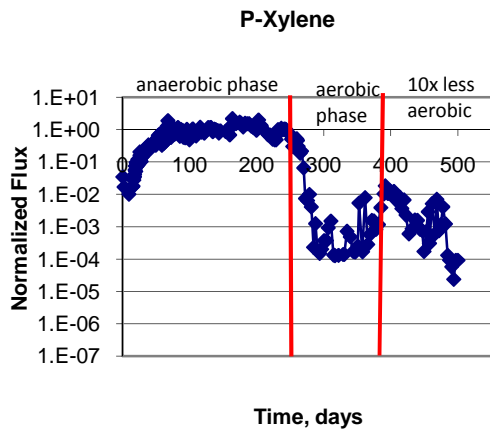
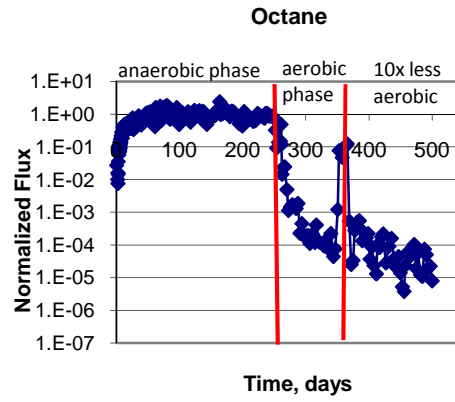
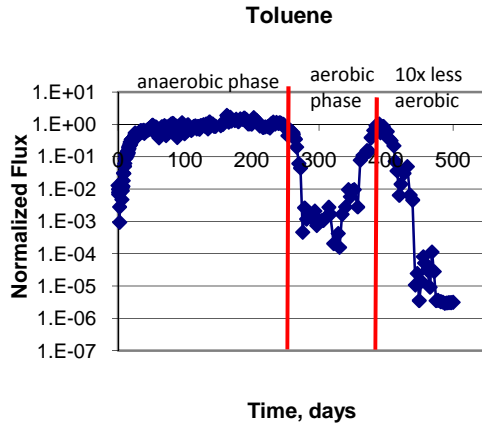




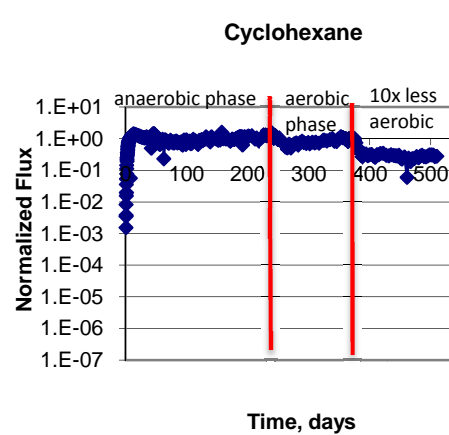
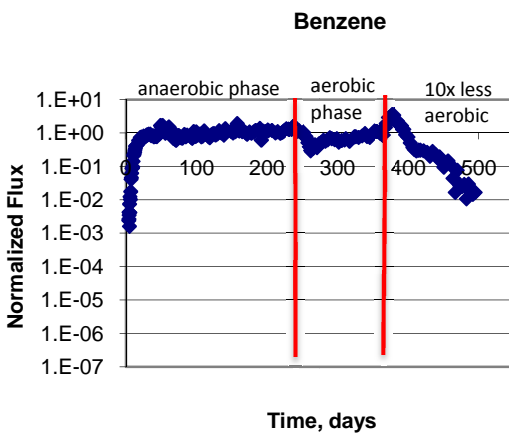
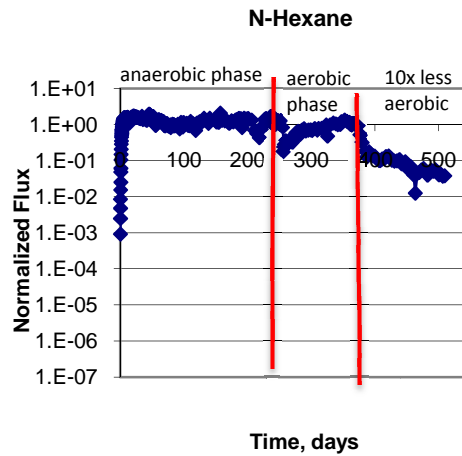
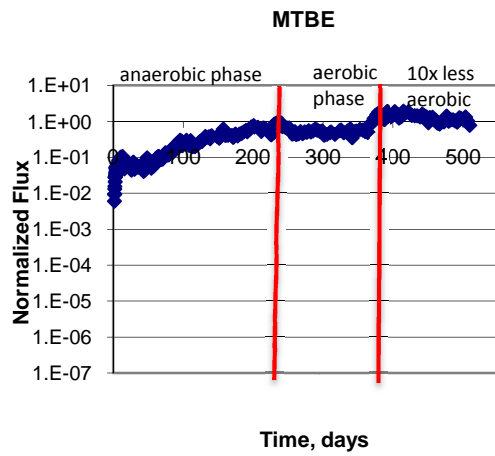
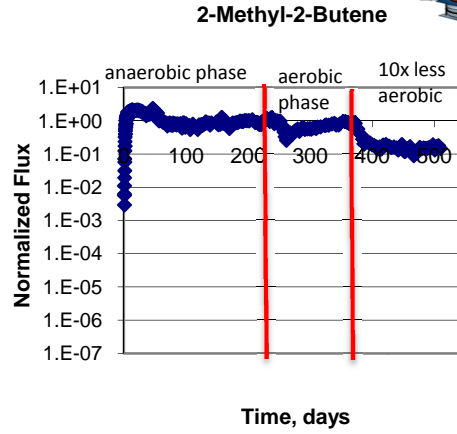
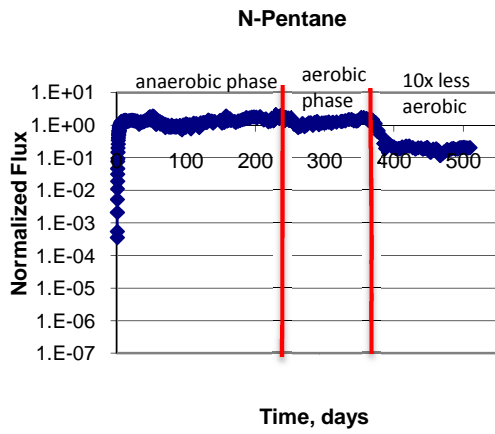
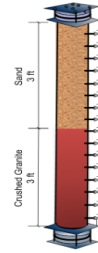
COLUMN C EFFLUENT – NORMALIZED FLUX VS TIME



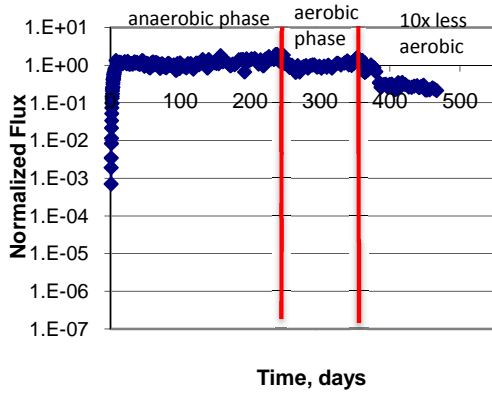




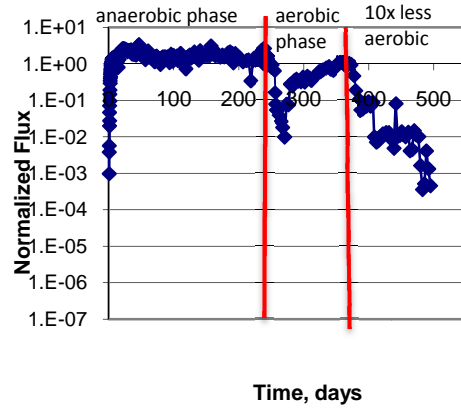
COLUMN D EFFLUENT – MASS EMISSIONS VS TIME



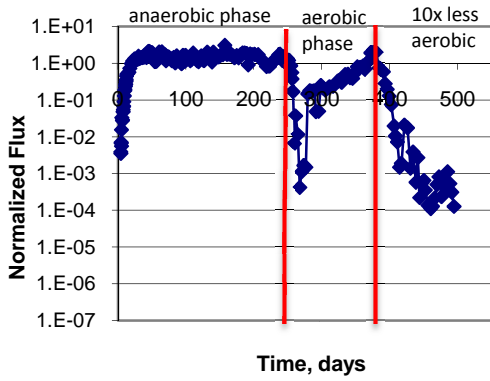
Iso-Octane



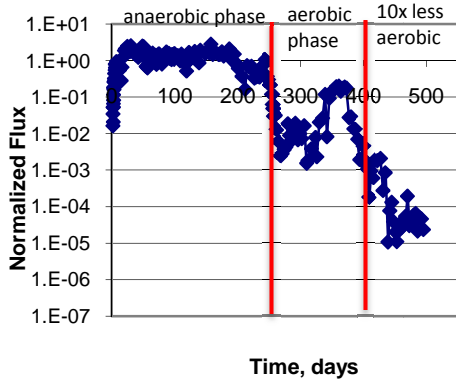
N-Heptane



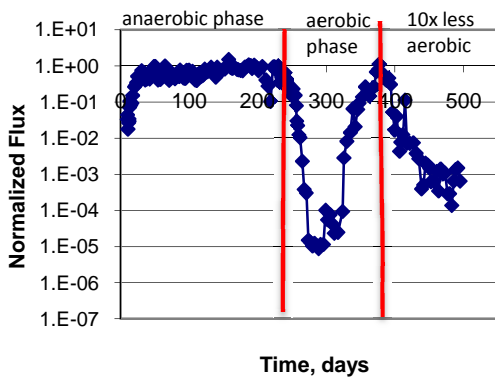
Toluene



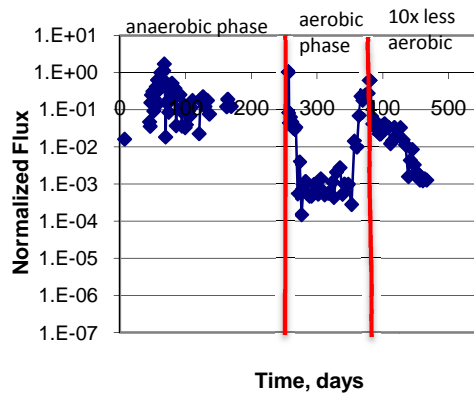
N-Octane



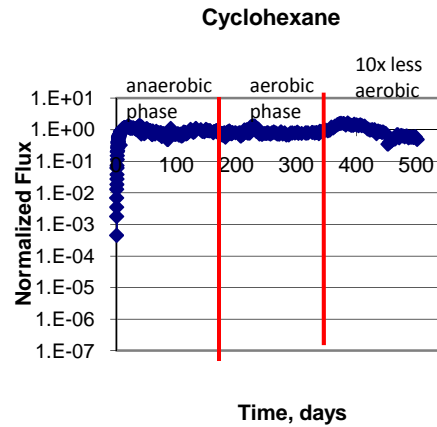
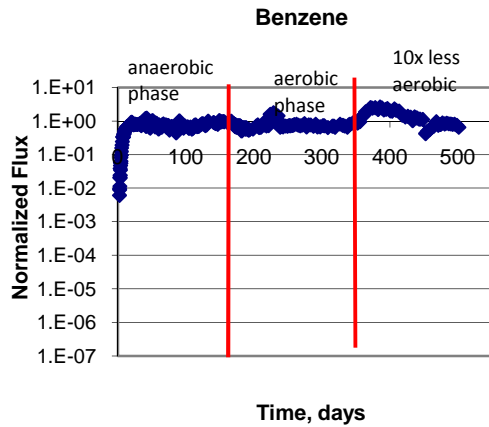
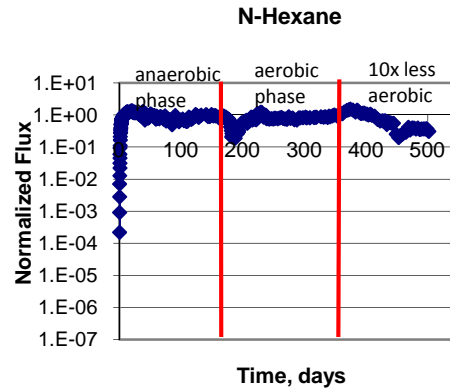
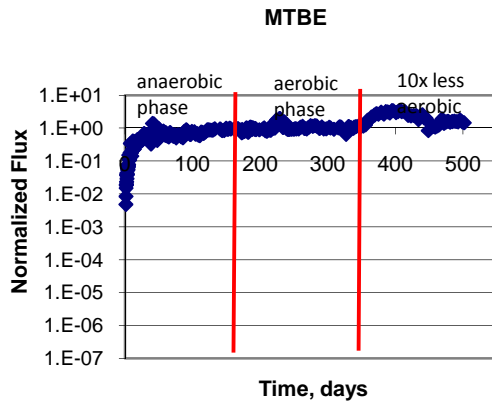
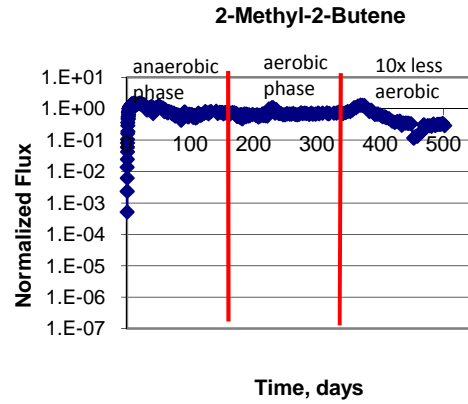
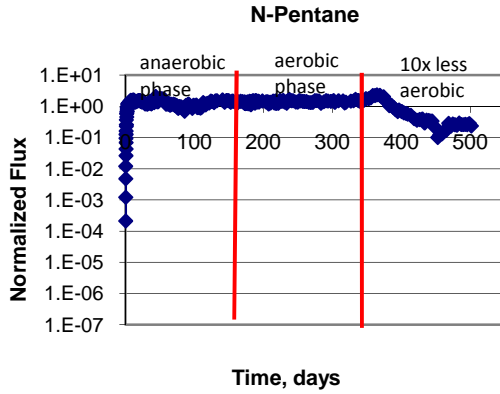
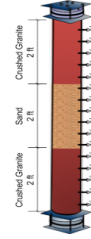
P-xylene

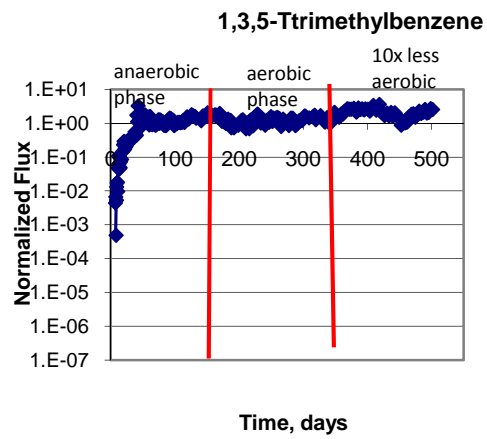
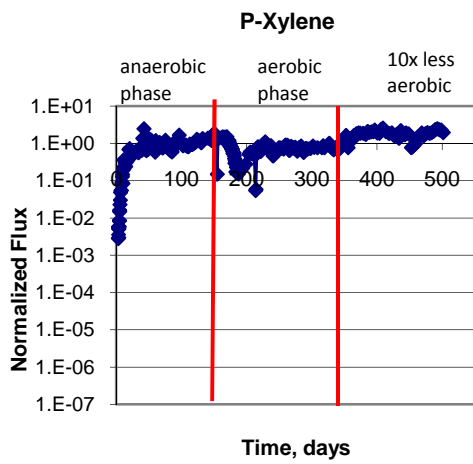
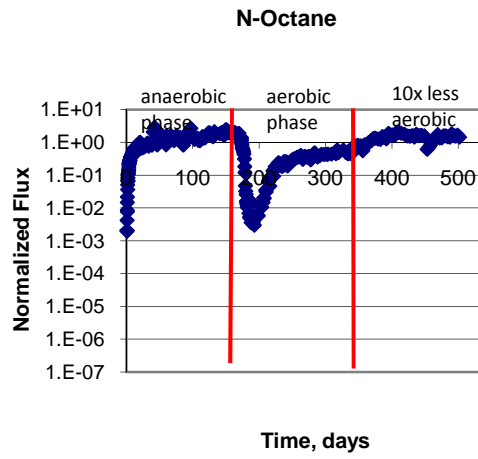
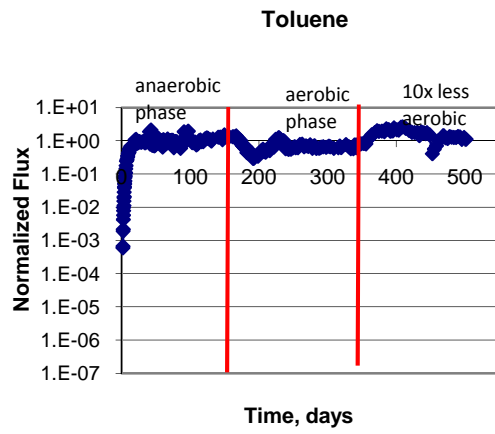
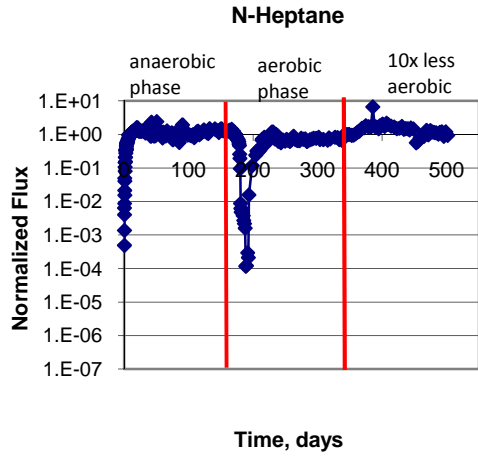
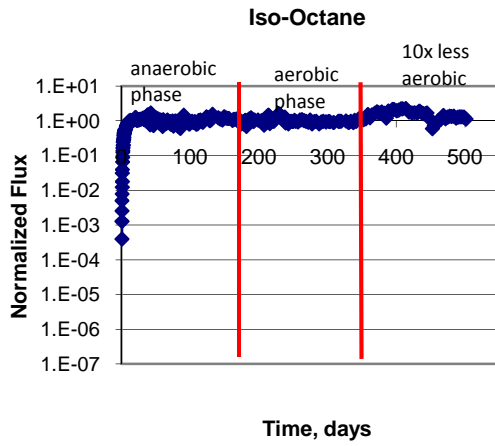


1,3,5-Trimethylbenzene

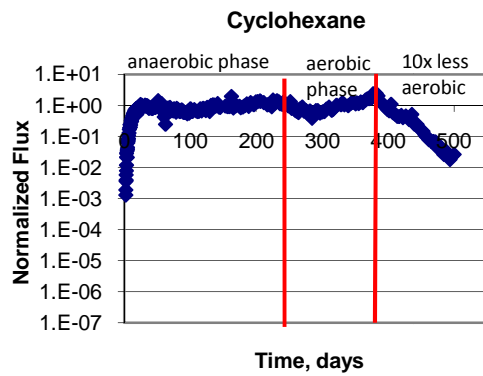
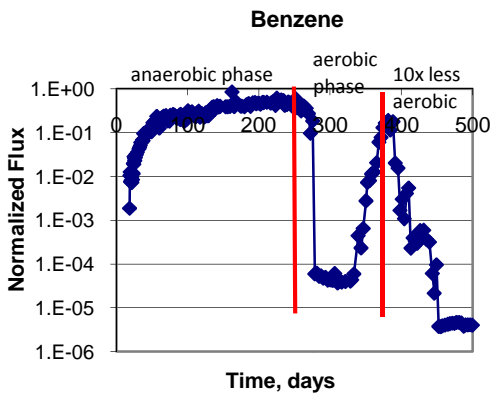
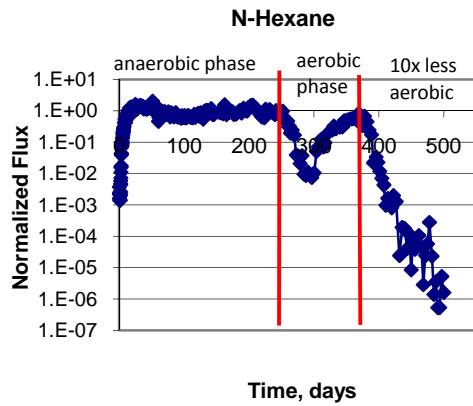
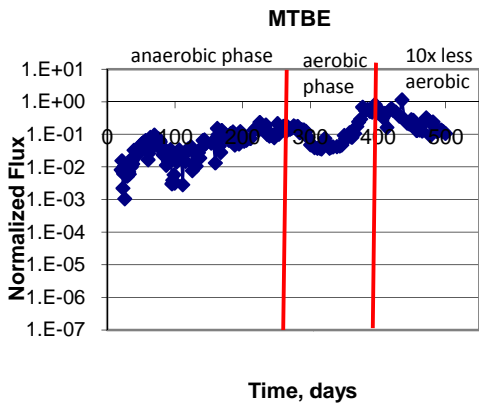
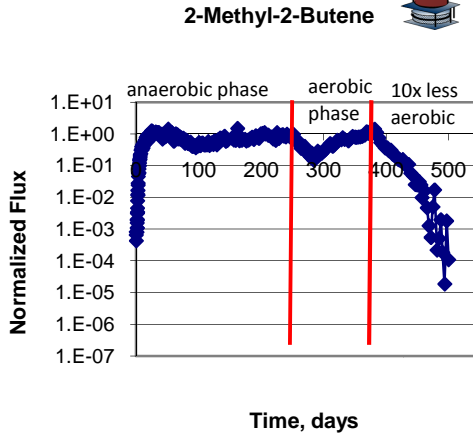
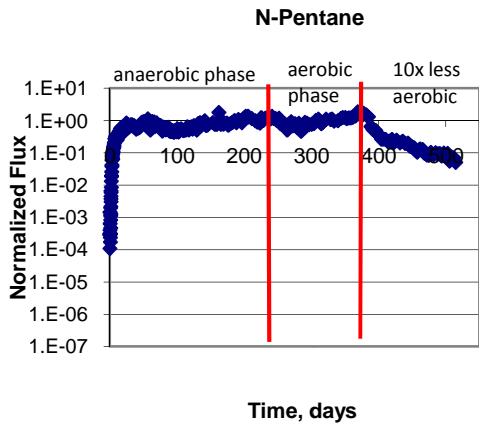


COLUMN E EFFLUENT – NORMALIZED MASS EMISSION VS TIME

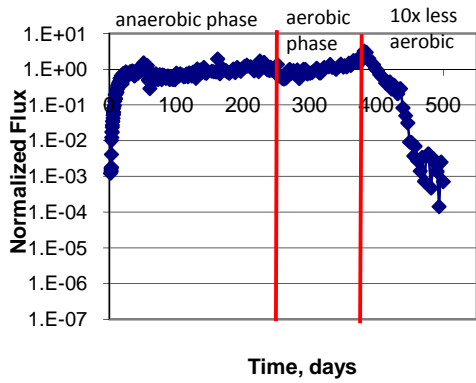




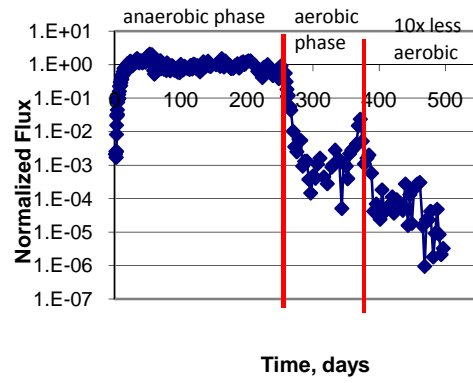
COLUMN F EFFLUENT – MASS EMISSION VS TIME



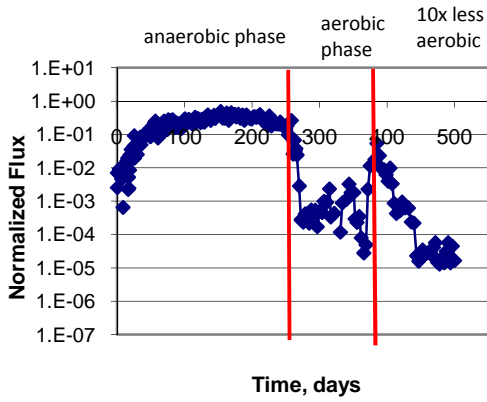
Iso-Octane



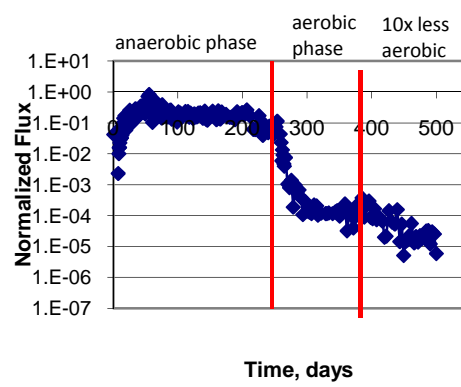
N-Heptane



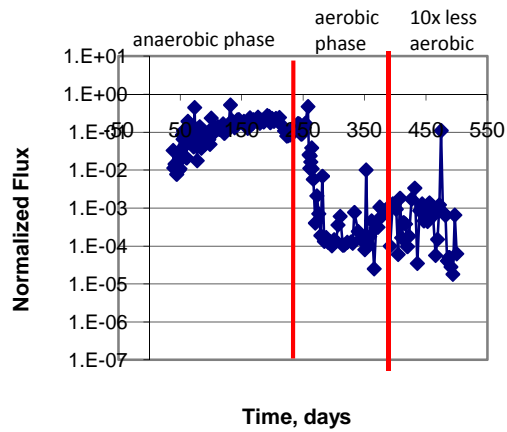
Toluene



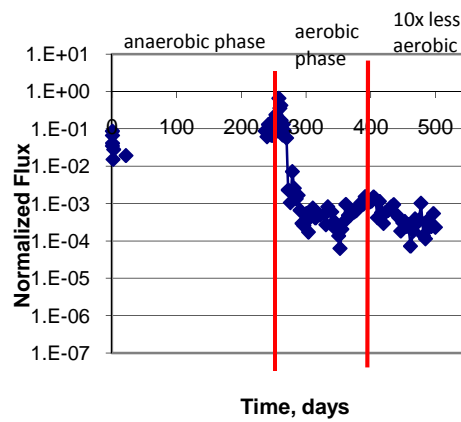
N-Octane



P-xylene

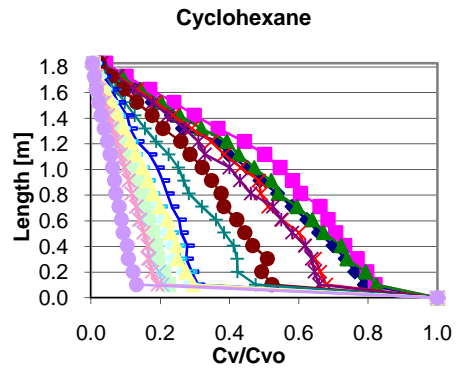
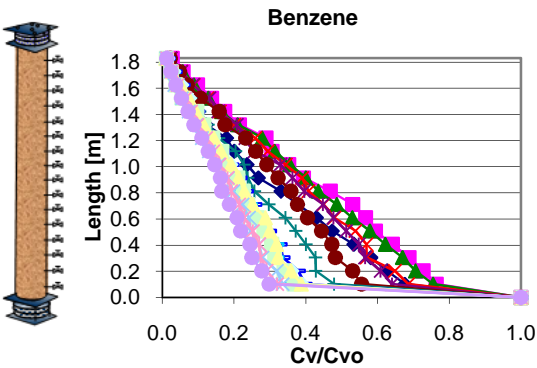
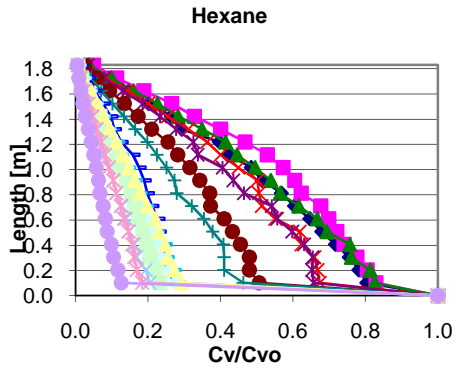
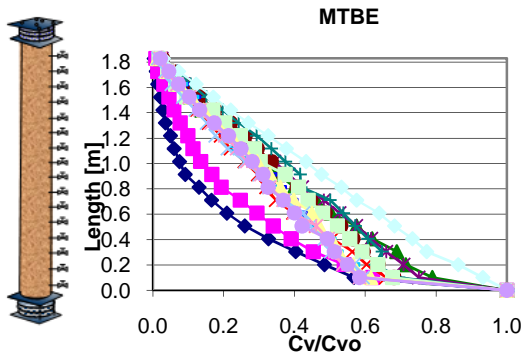
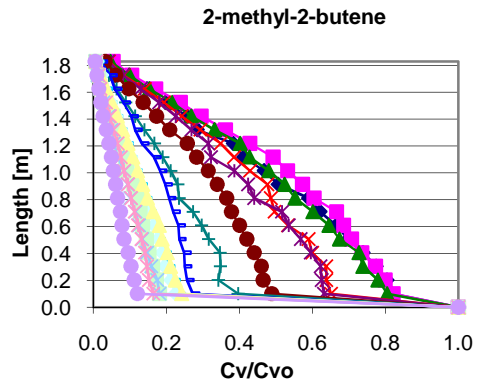
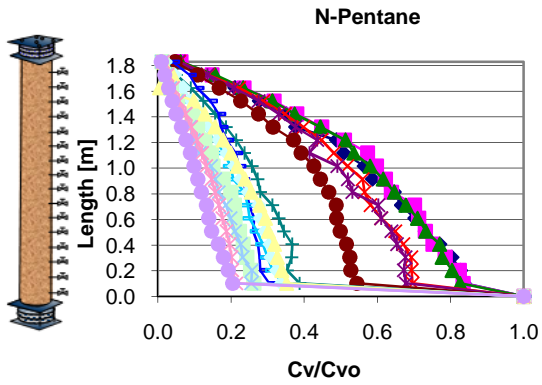
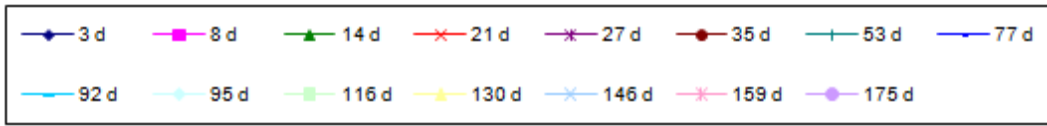


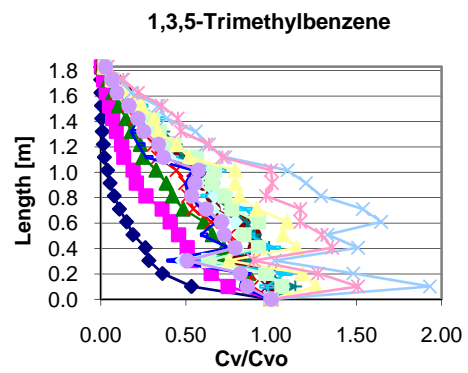
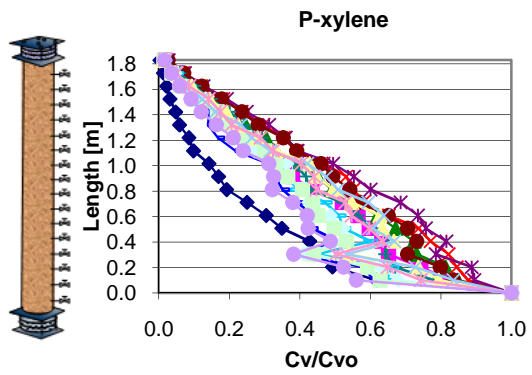
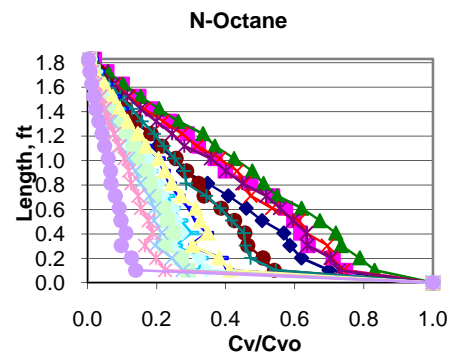
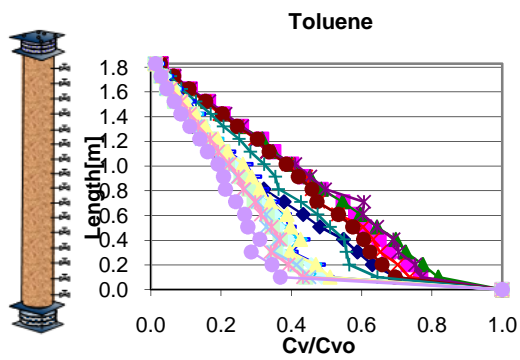
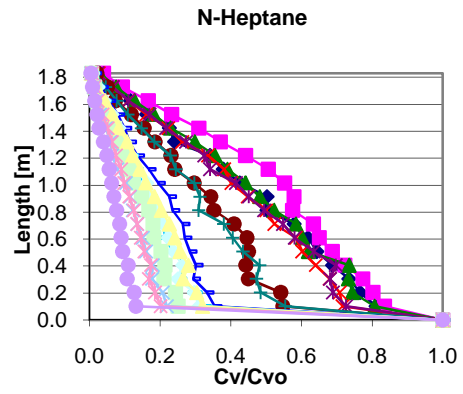
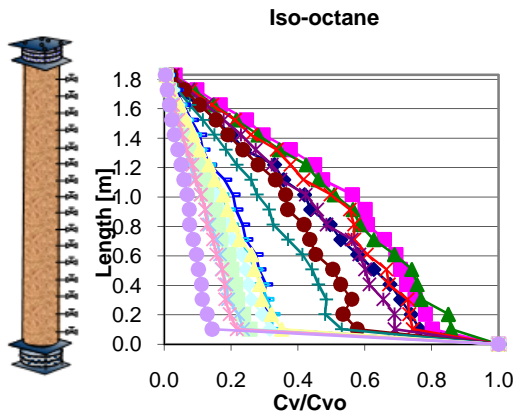
1,3,5-Trimethylbenzene



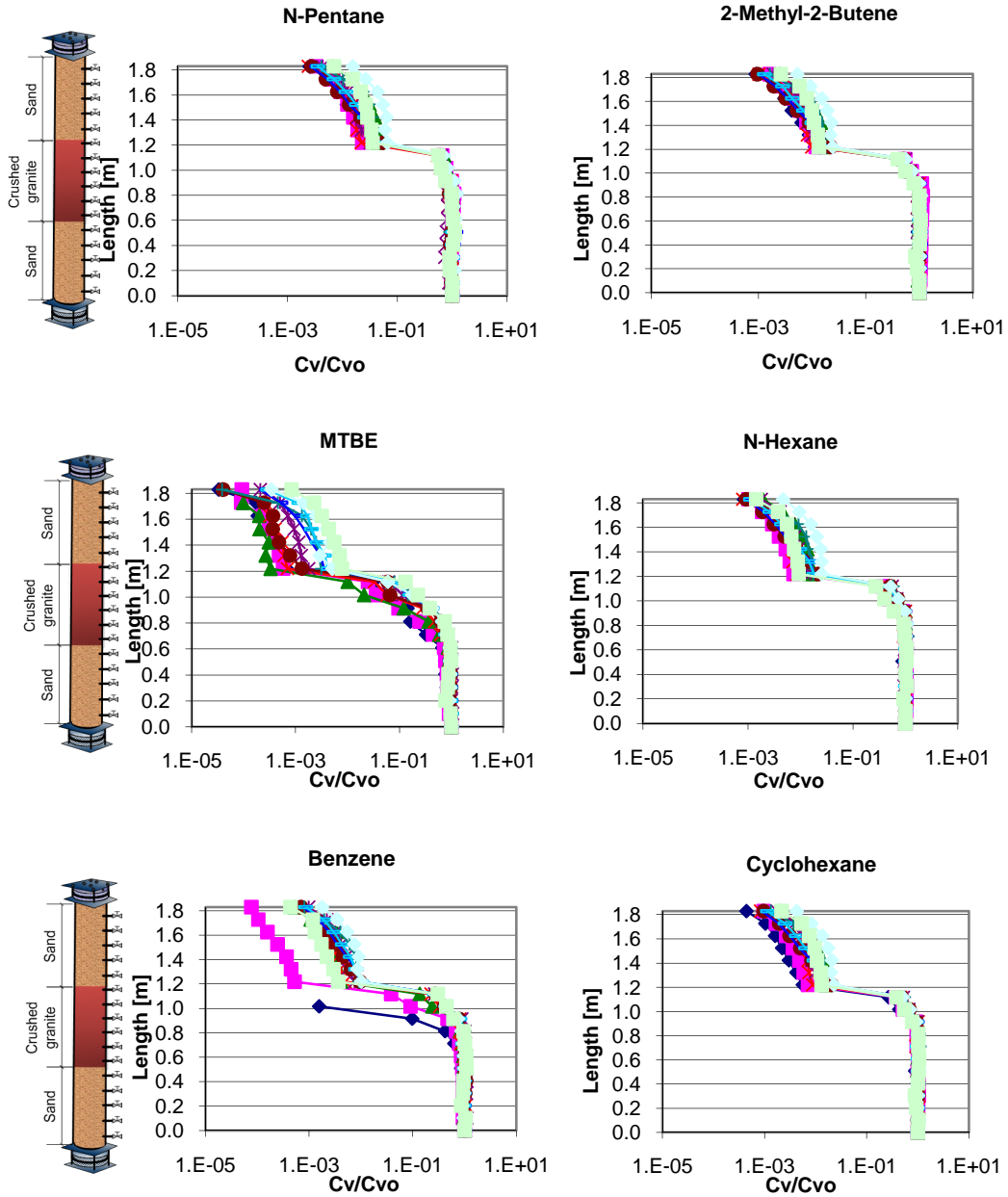
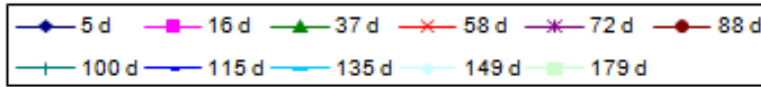
APPENDIX III
VAPOR CONCENTRATION PROFILES.
ANAEROBIC PHASE

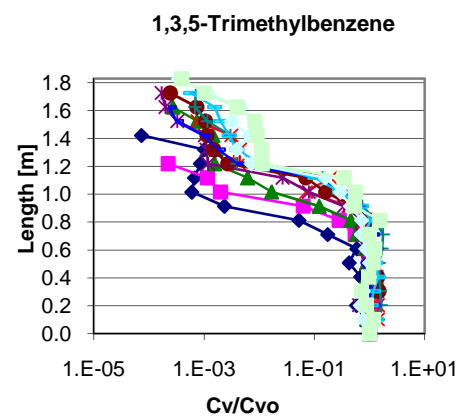
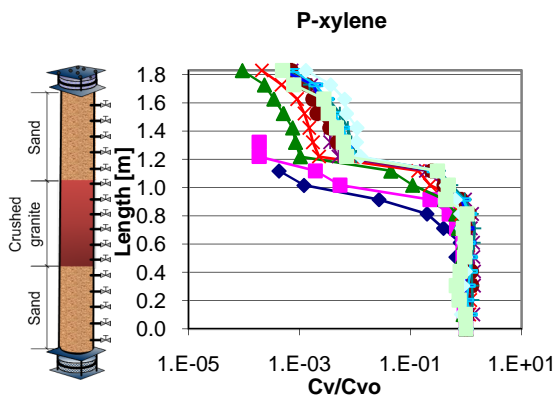
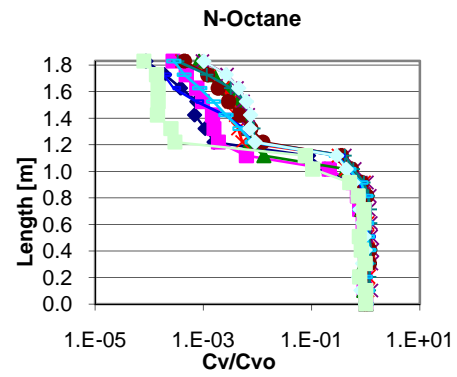
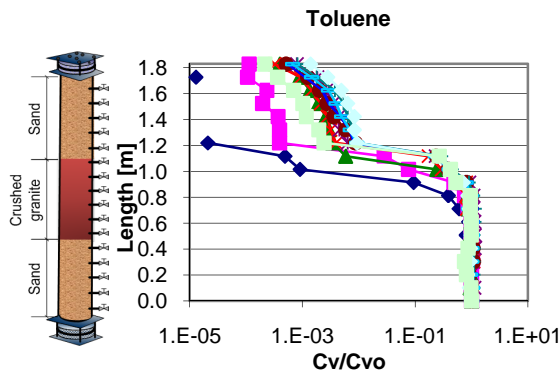
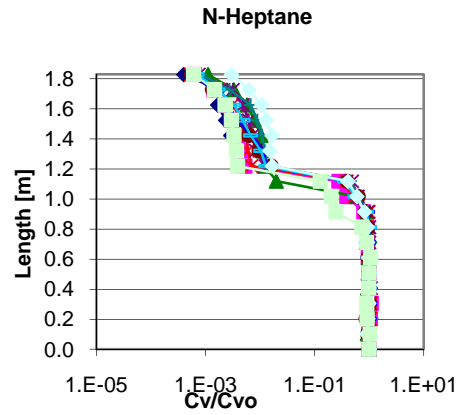
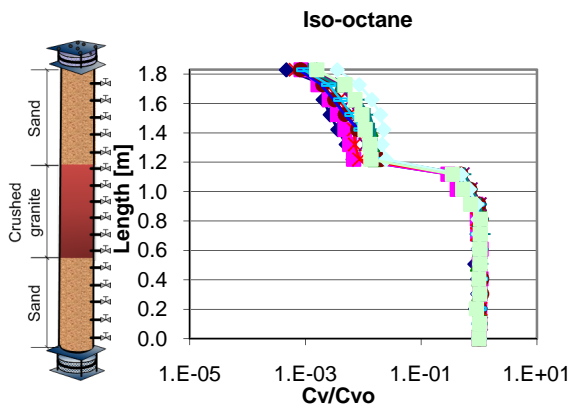
COLUMN A – ANAEROBIC PROFILES



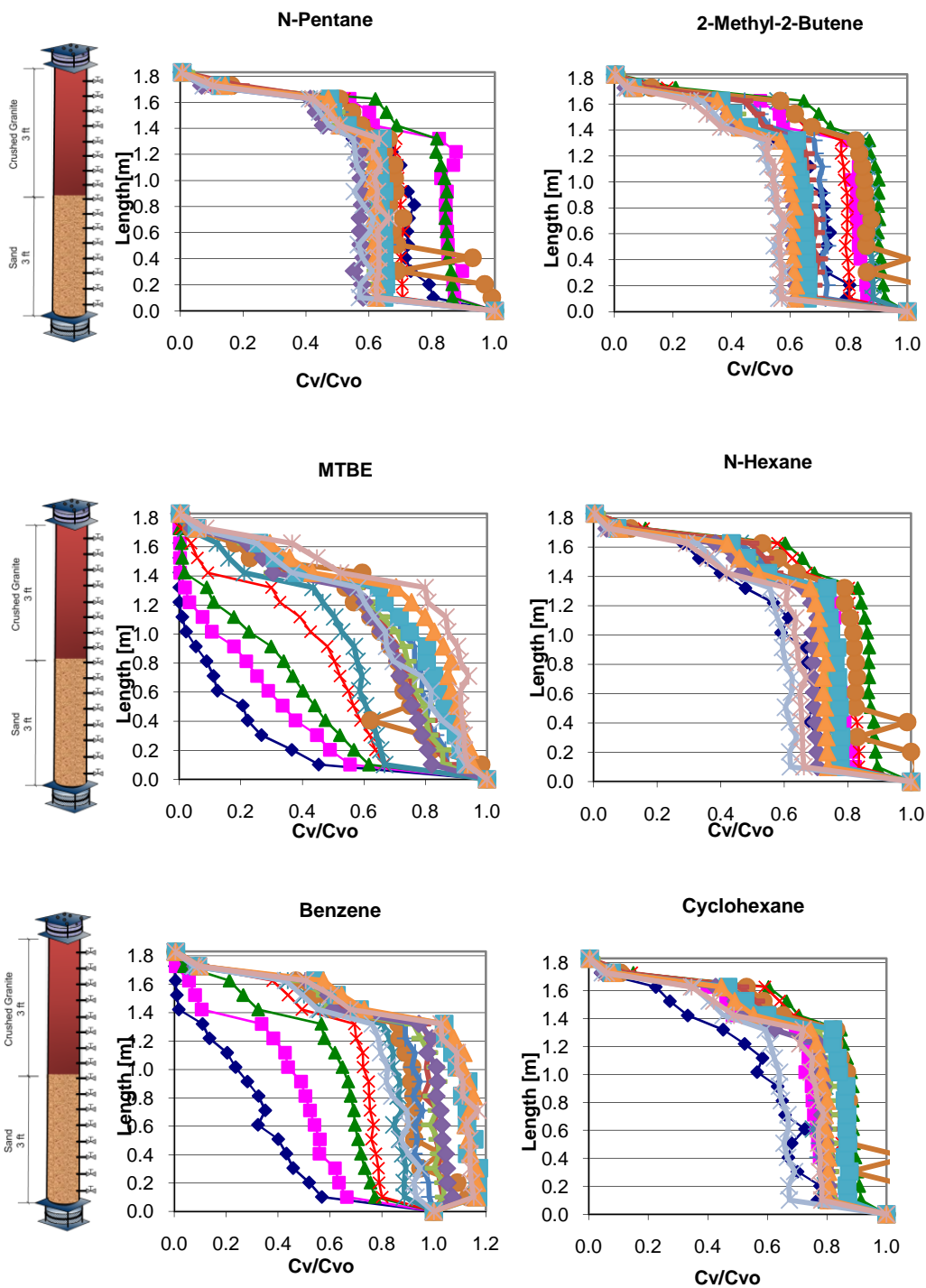


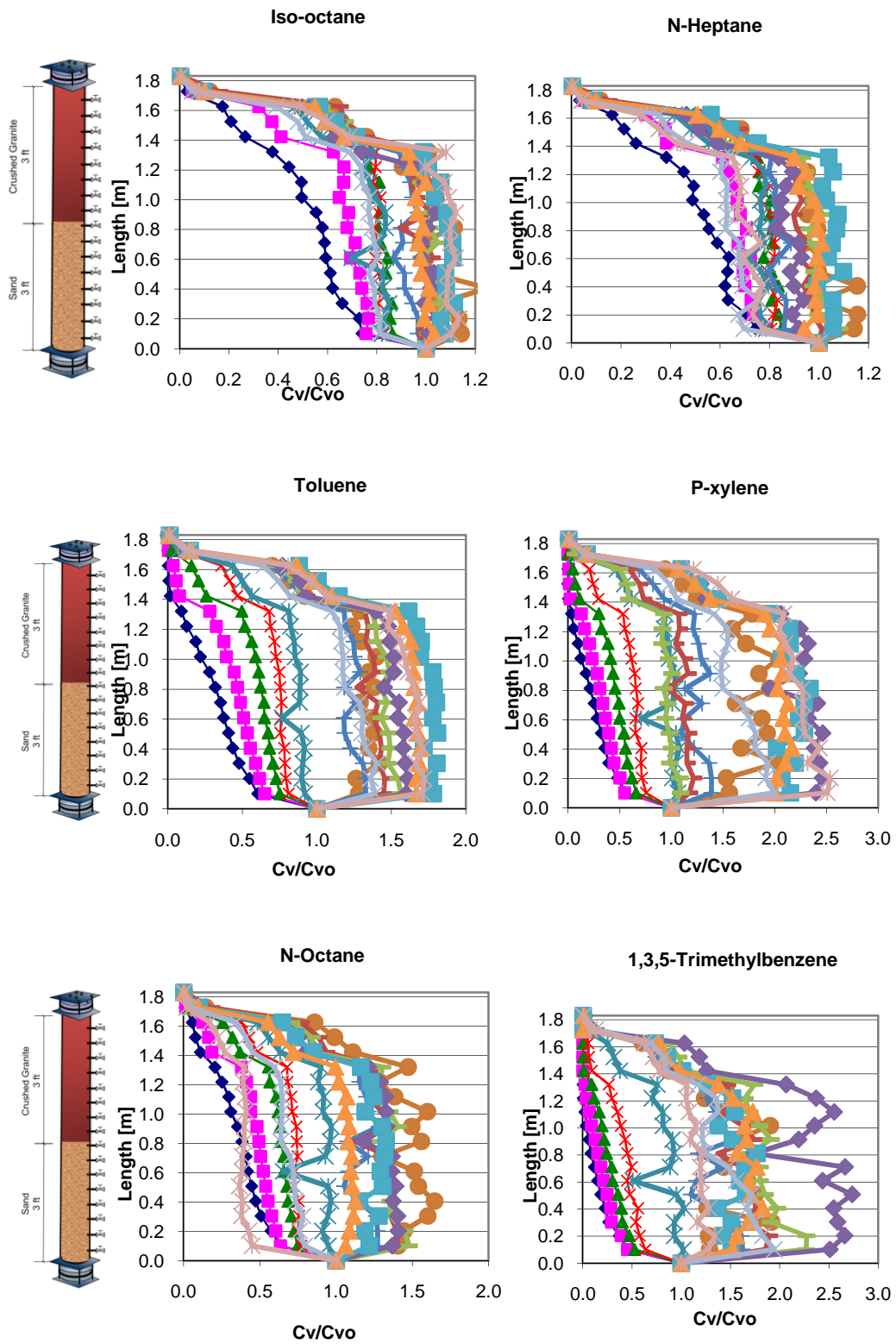
COLUMN B – ANAEROBIC PROFILES



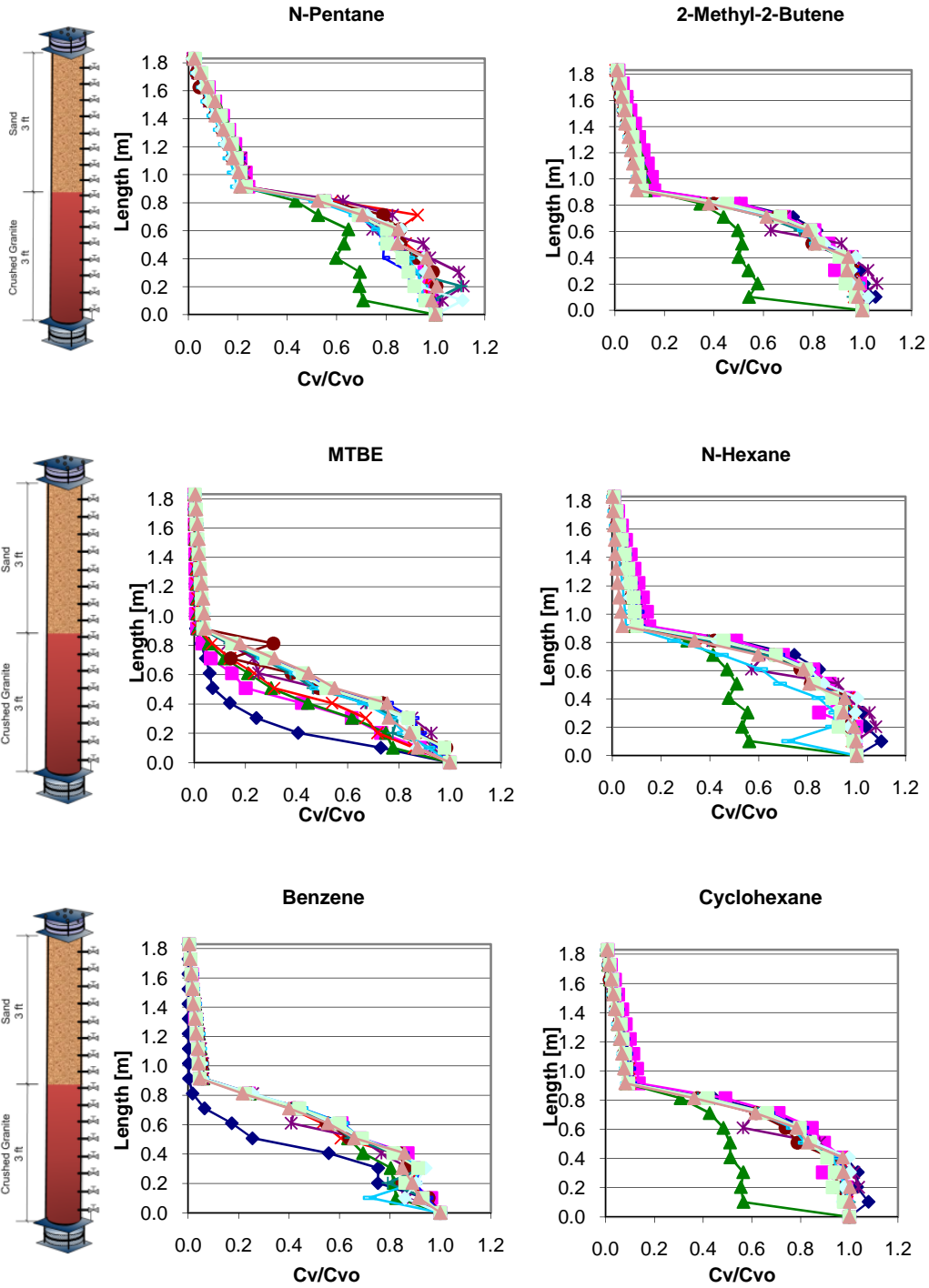
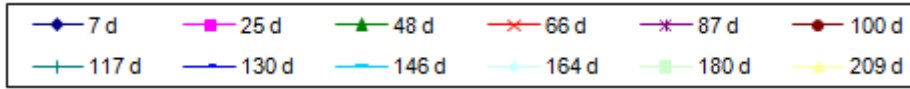


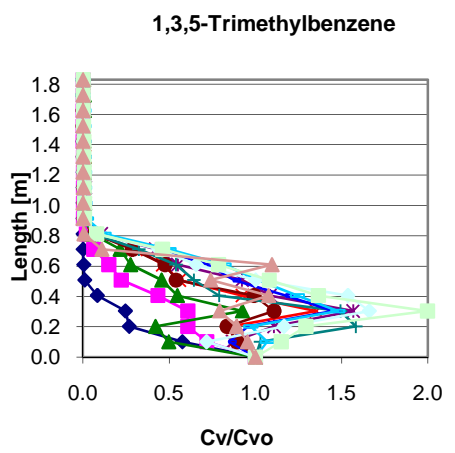
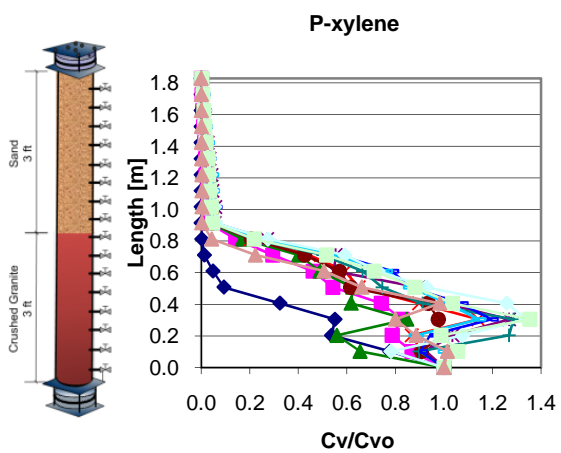
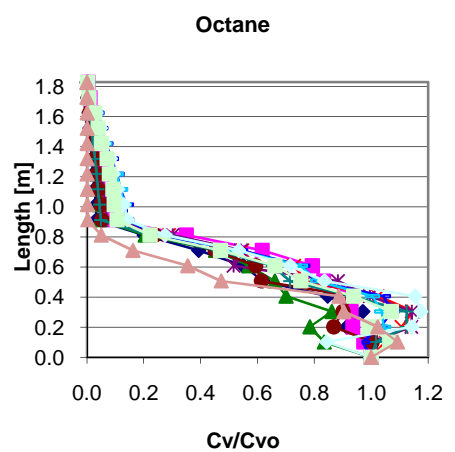
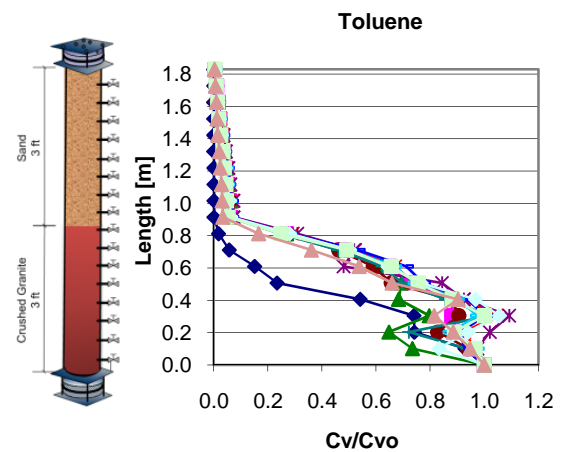
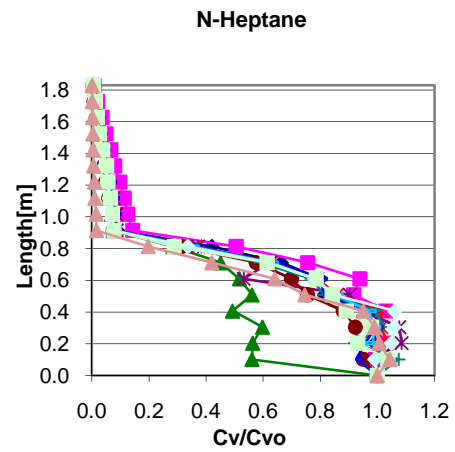
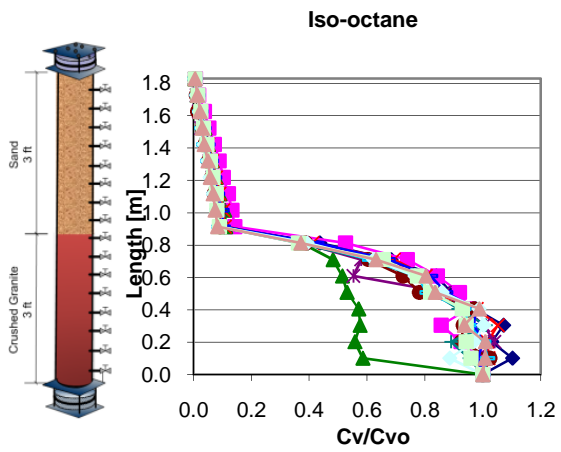
COLUMN C – ANAEROBIC PROFILES



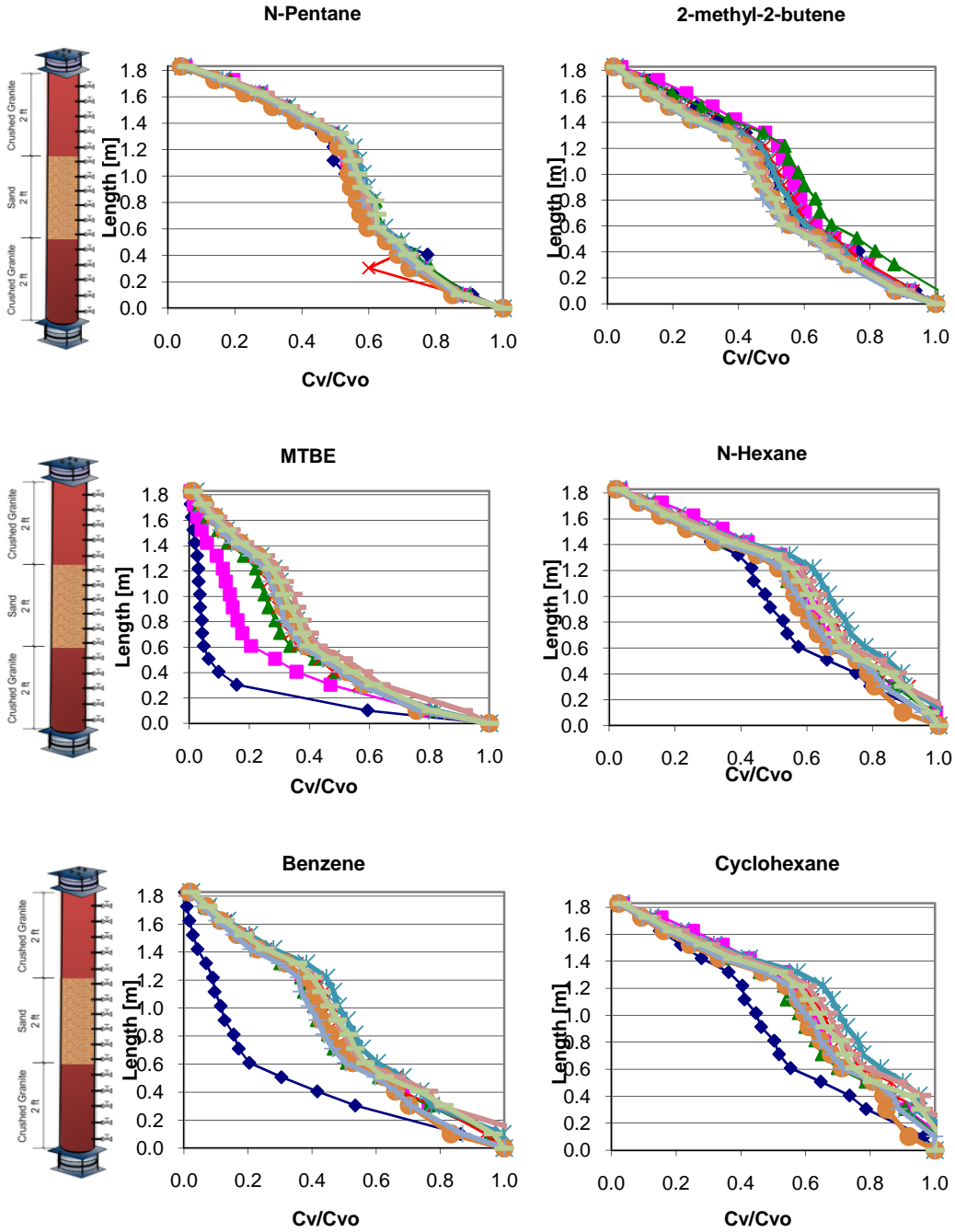
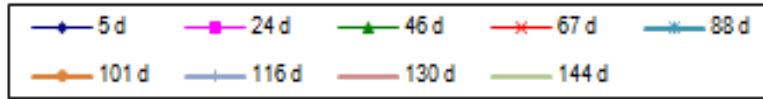


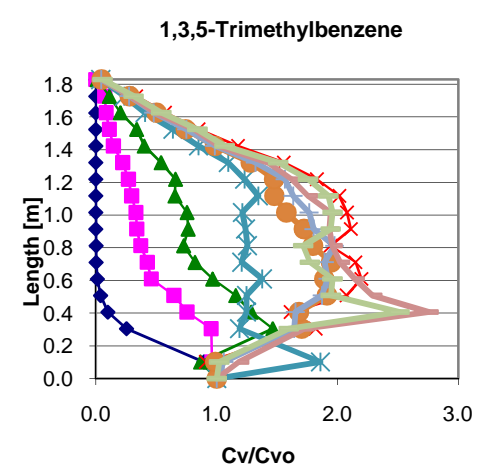
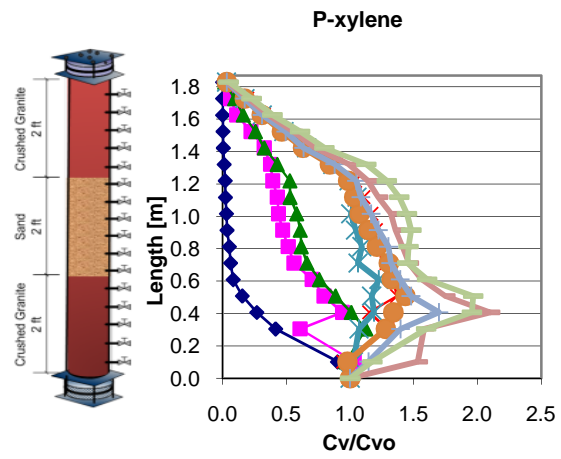
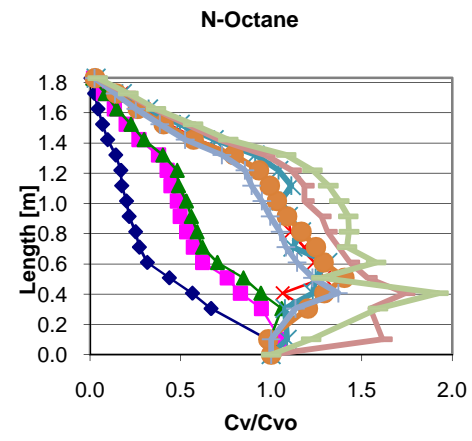
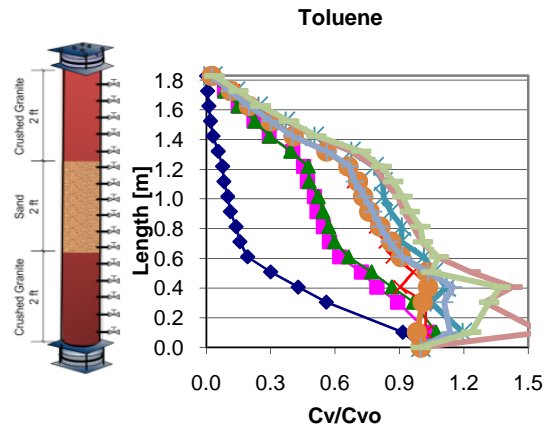
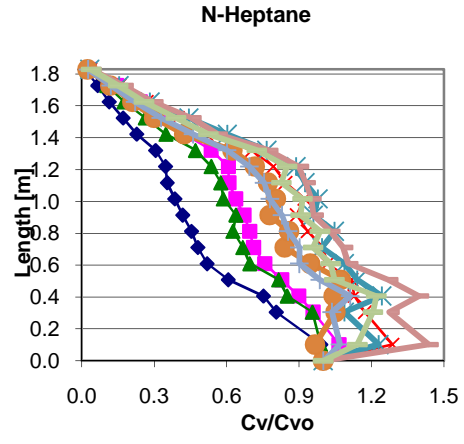
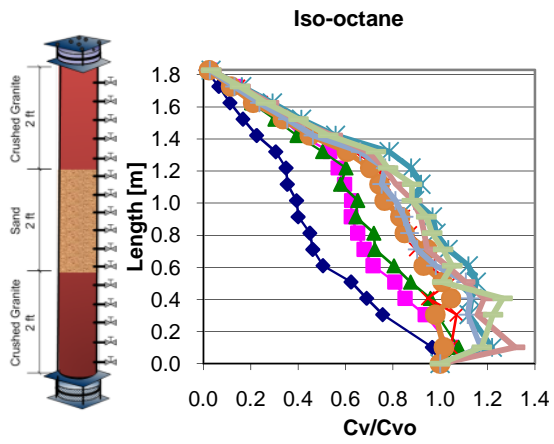
COLUMN D – ANAEROBIC PROFILES



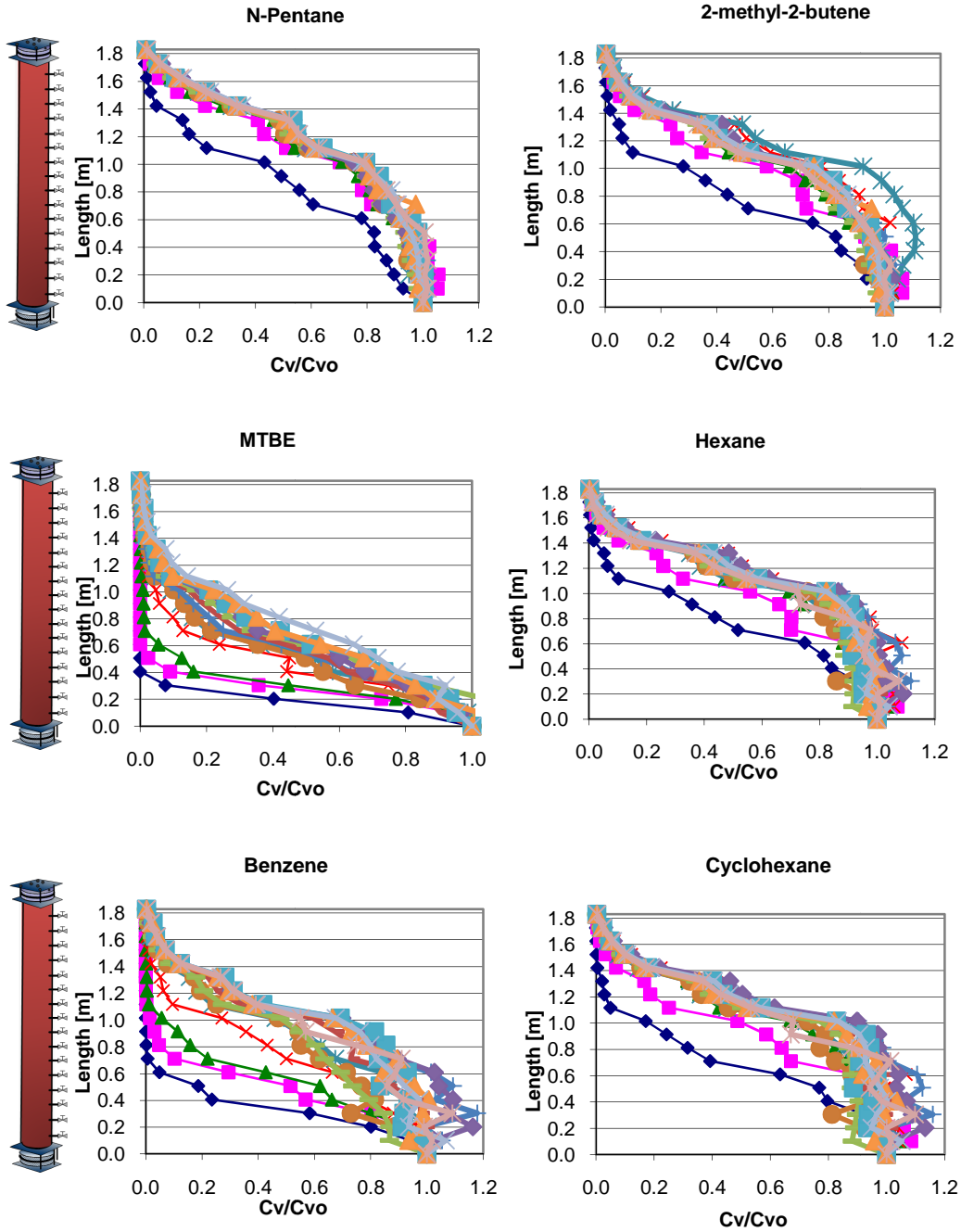


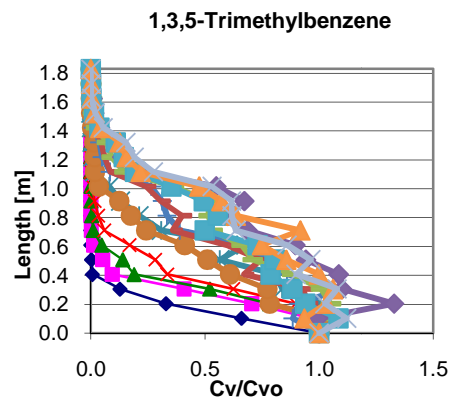
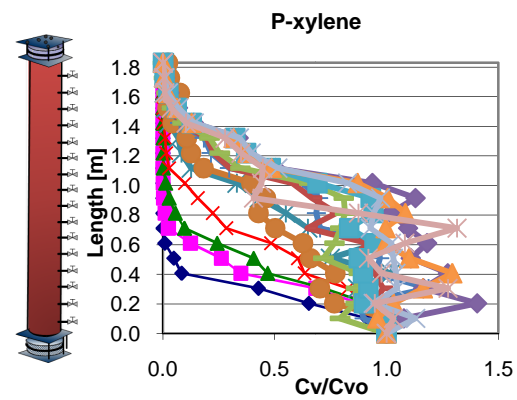
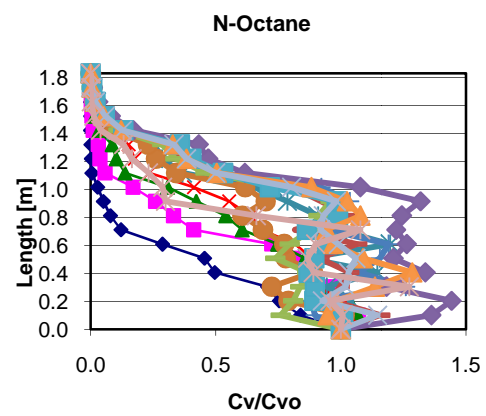
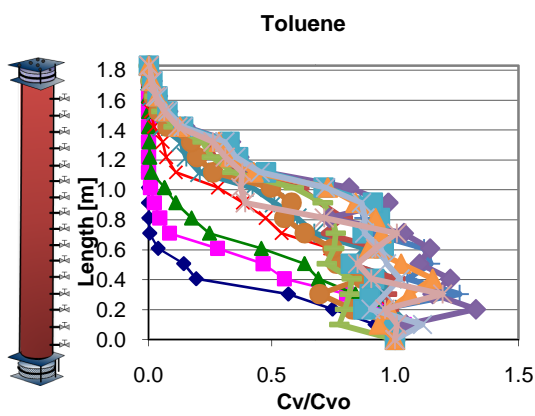
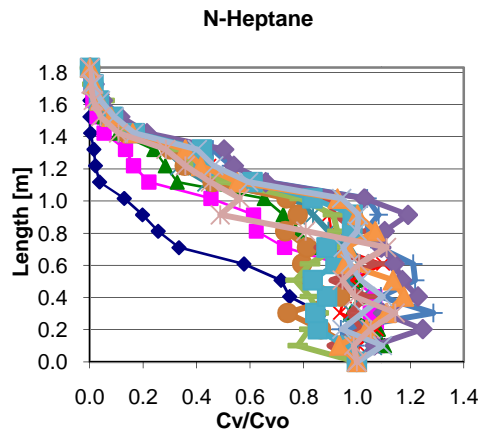
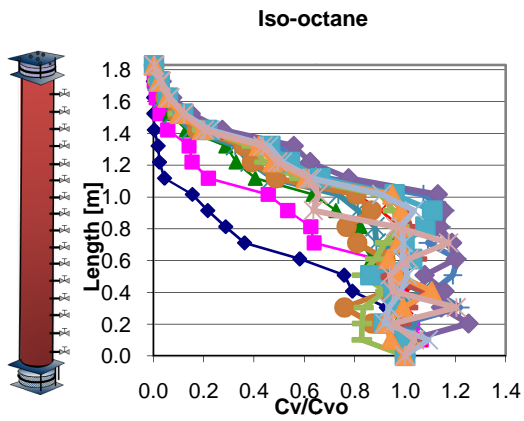
COLUMN E – ANAEROBIC VAPOR PROFILES





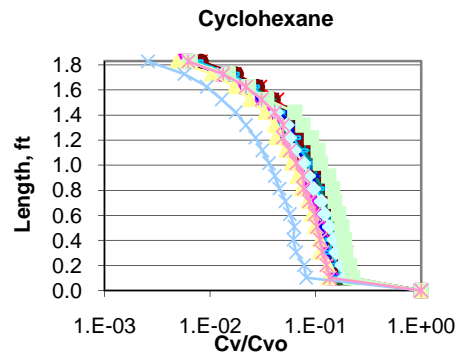
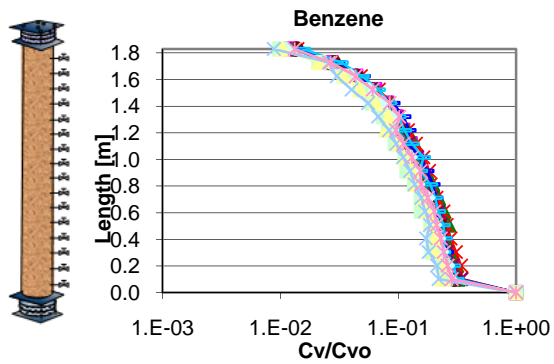
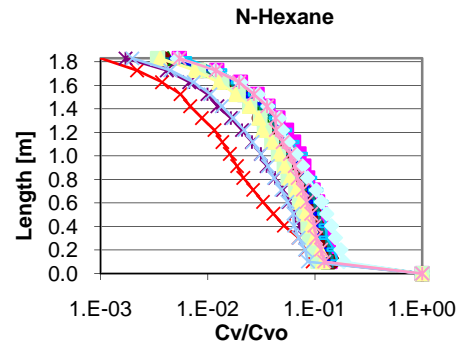
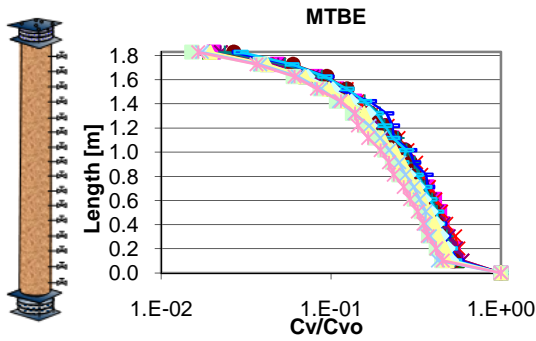
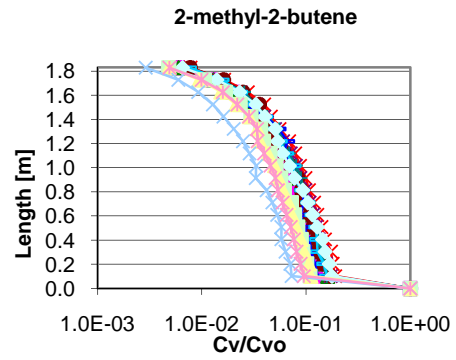
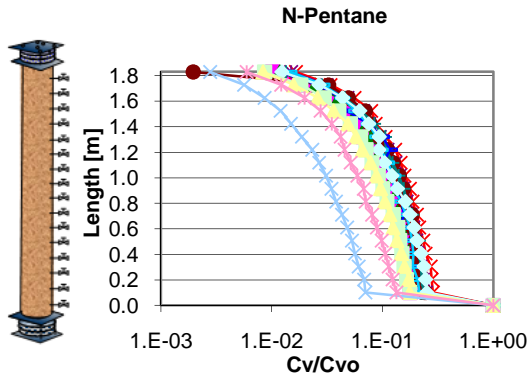
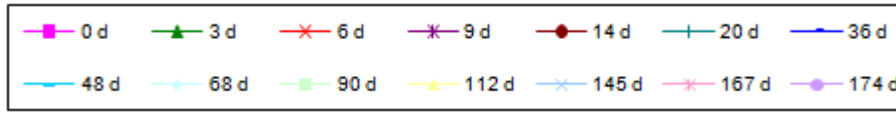
COLUMN F- ANAEROBIC VAPOR PROFILES

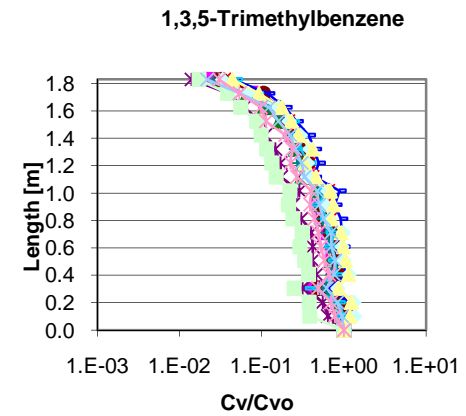
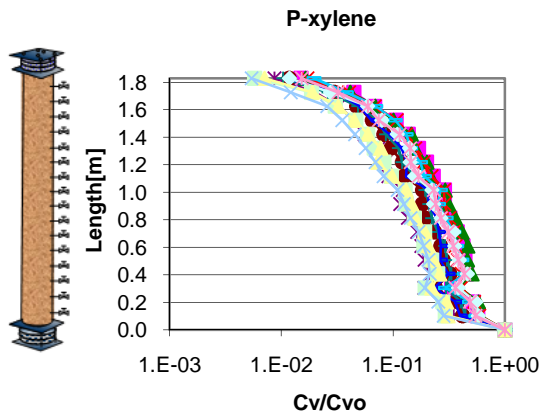
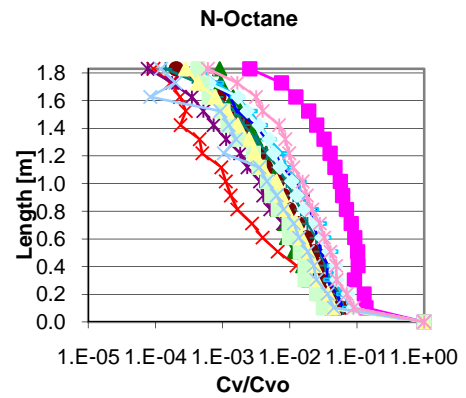
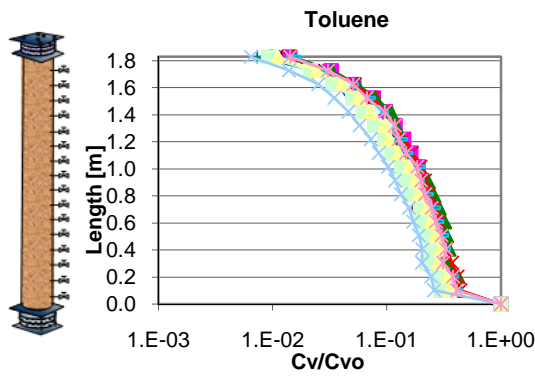
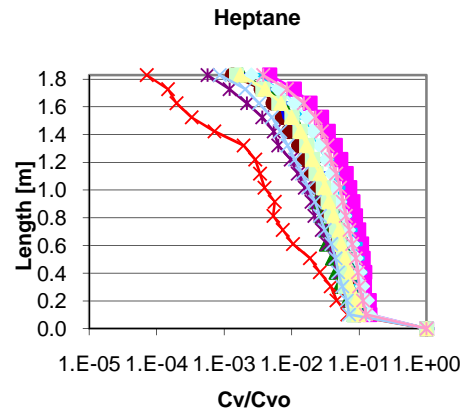
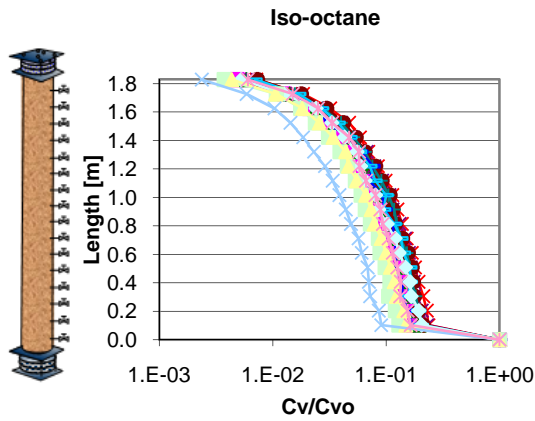




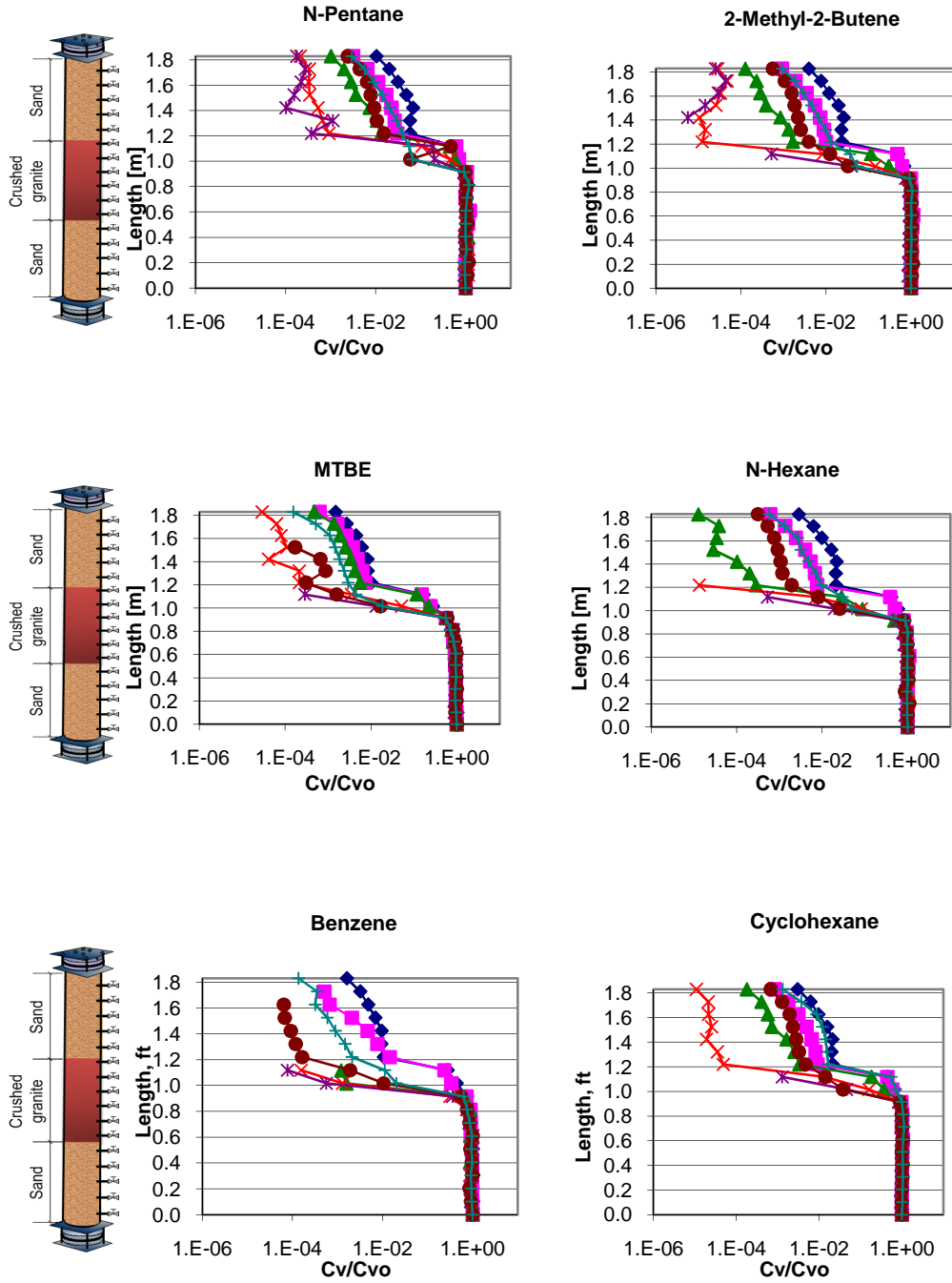
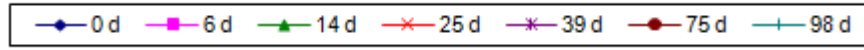
APPENDIX IV:
VAPOR CONCENTRATION PROFILES.
AEROBIC PHASE

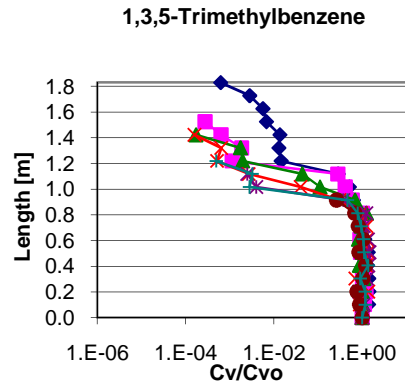
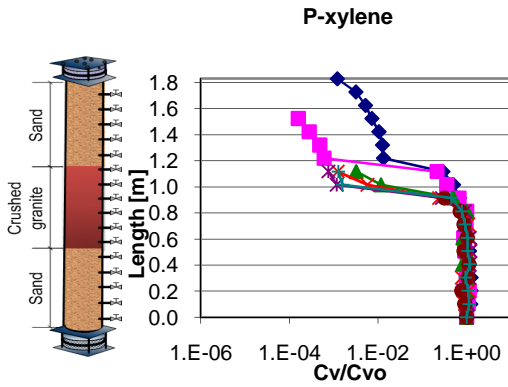
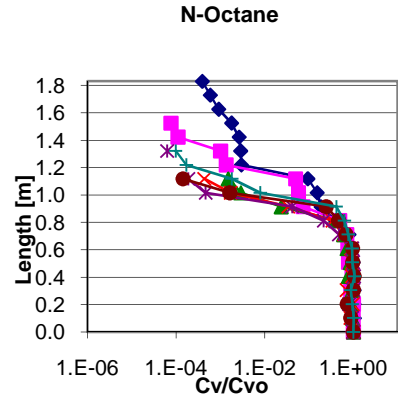
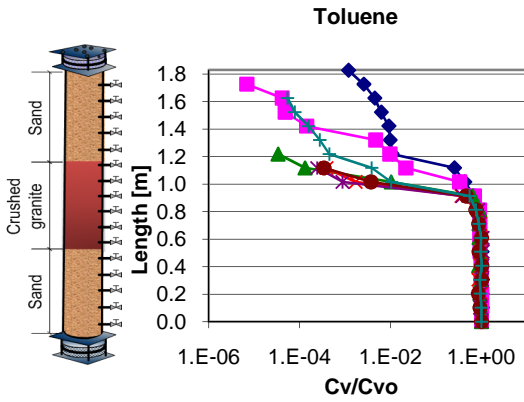
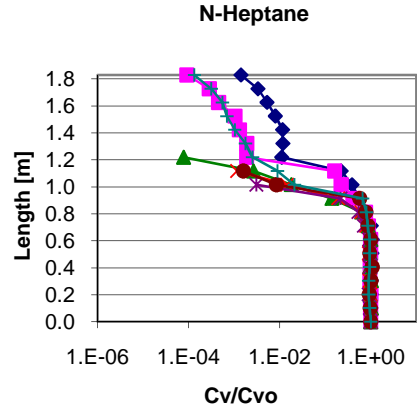
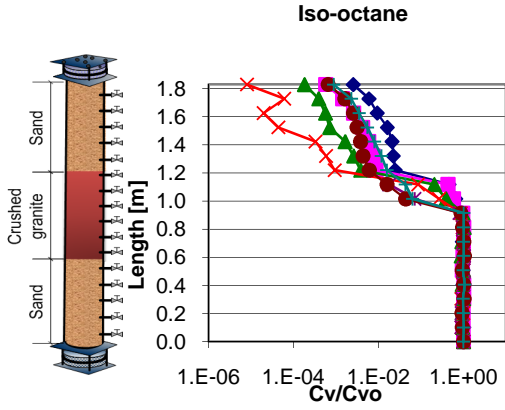
COLUMN A – AEROBIC PROFILES



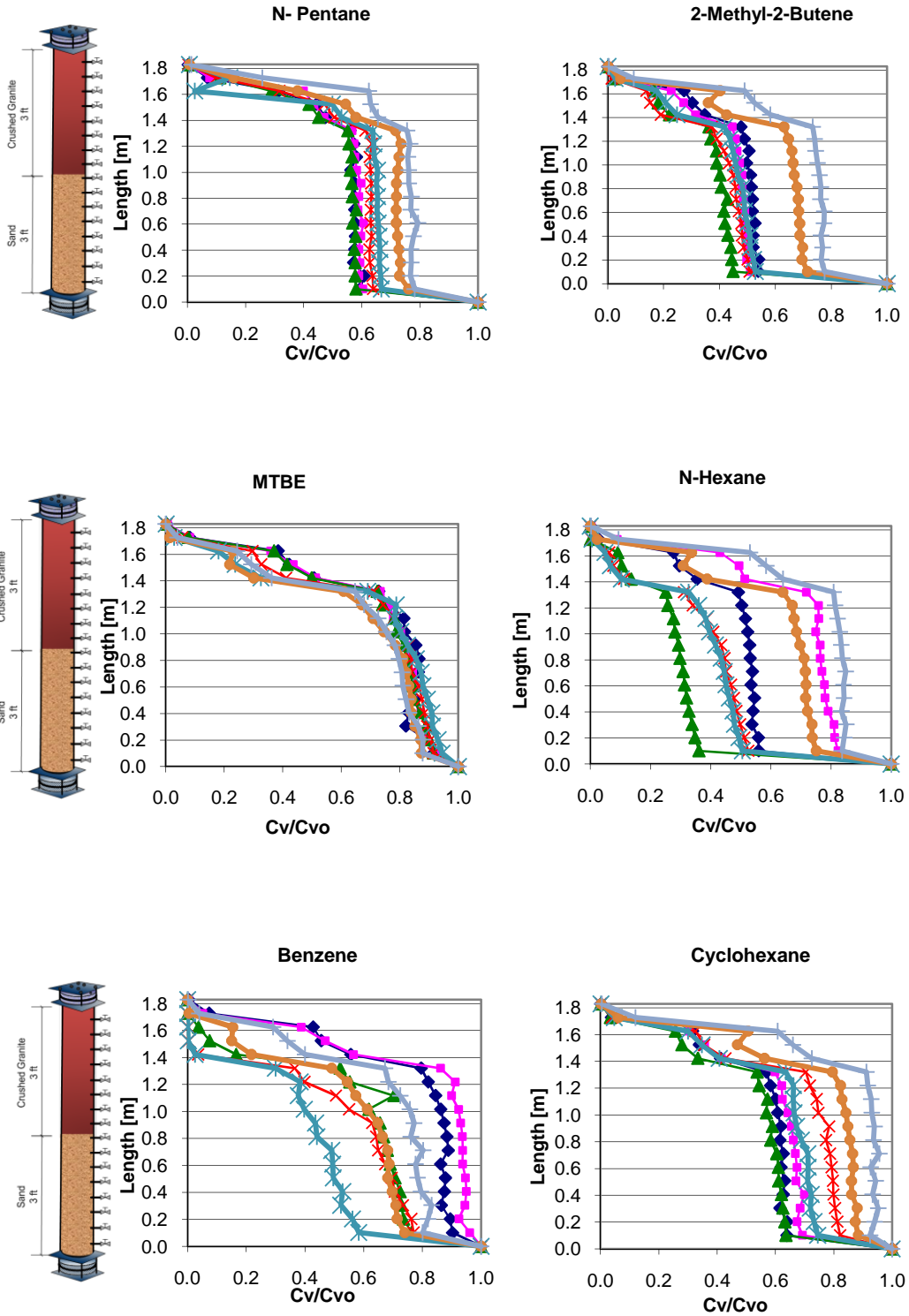
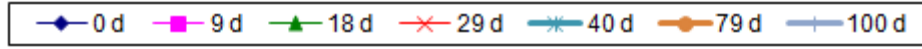


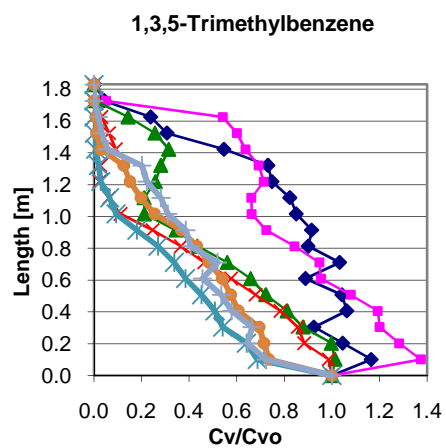
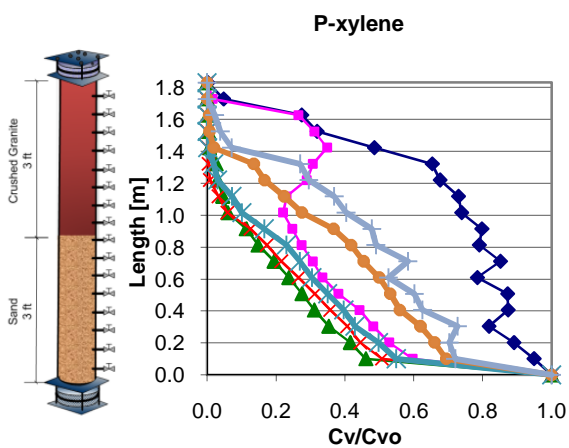
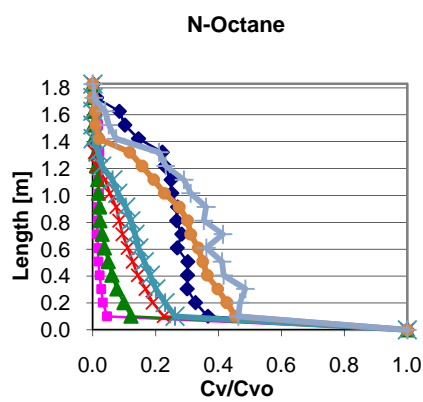
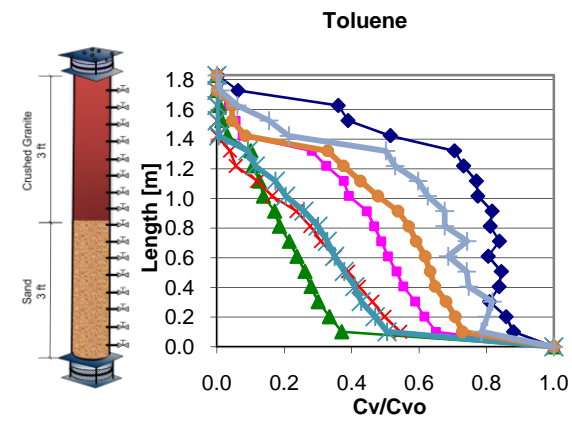
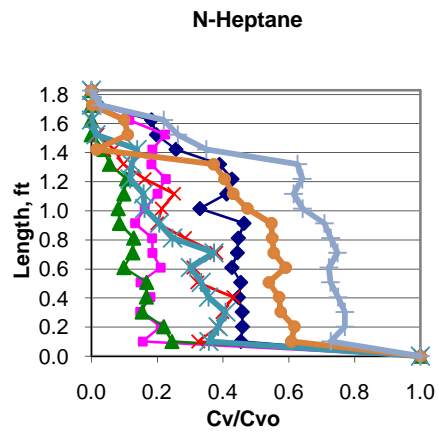
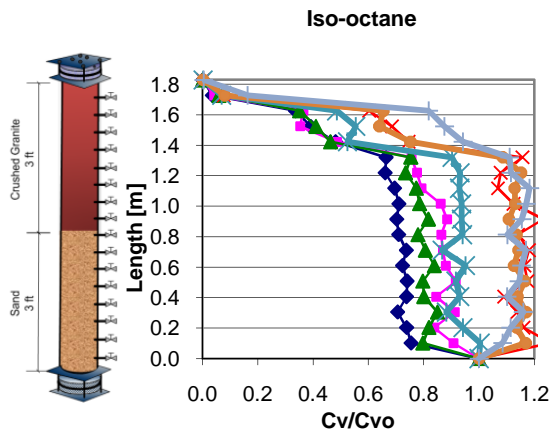
COLUMN B – AEROBIC PROFILES



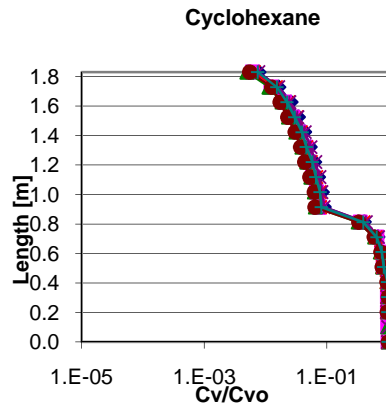
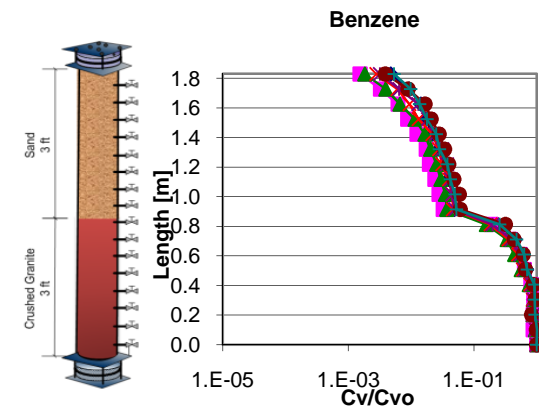
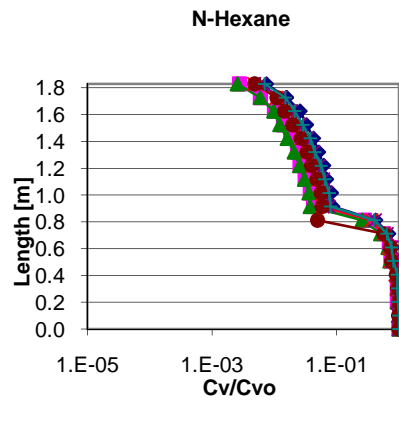
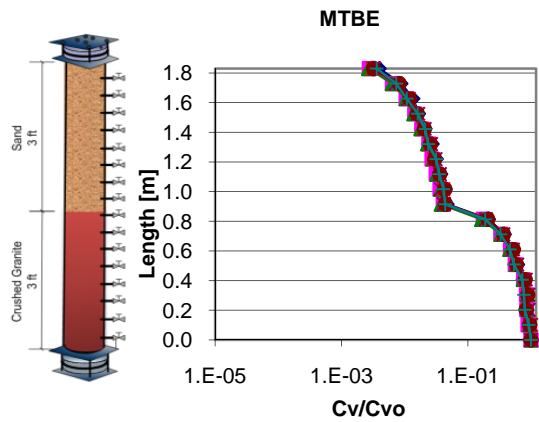
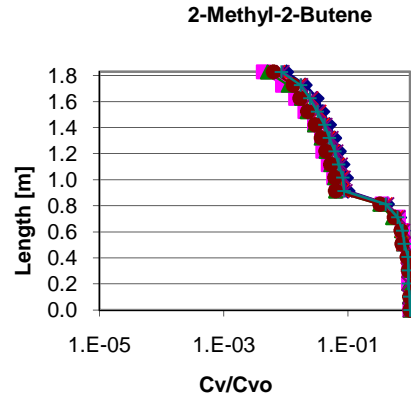
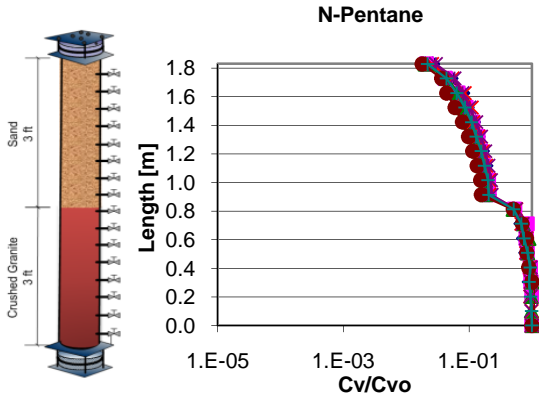
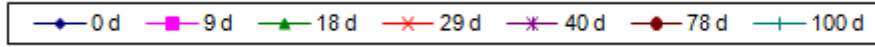


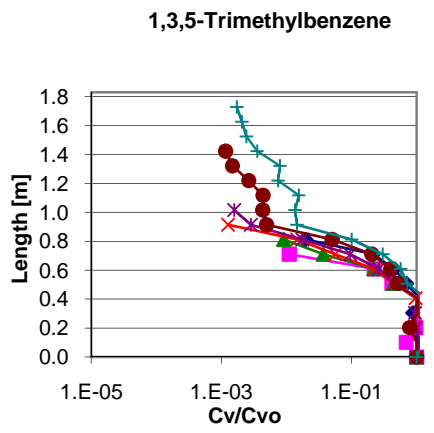
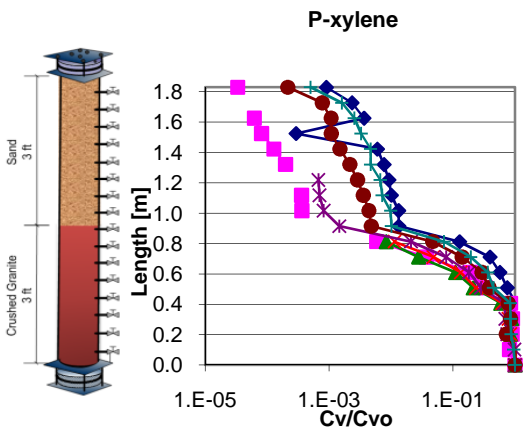
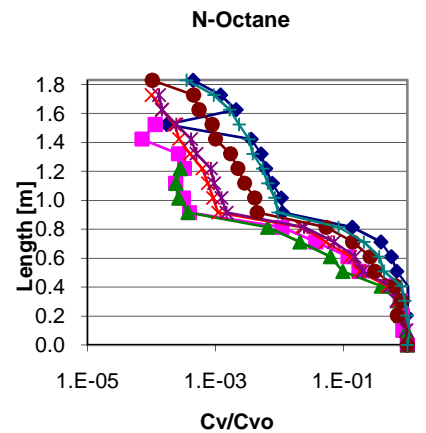
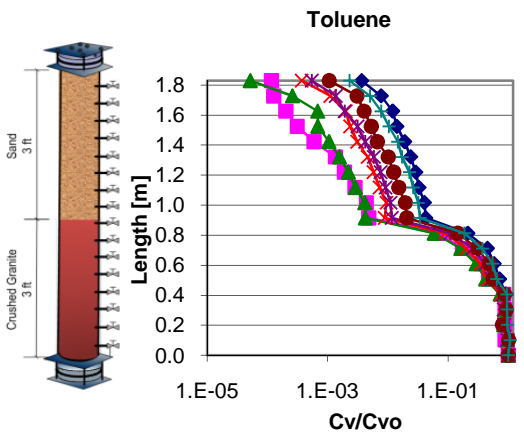
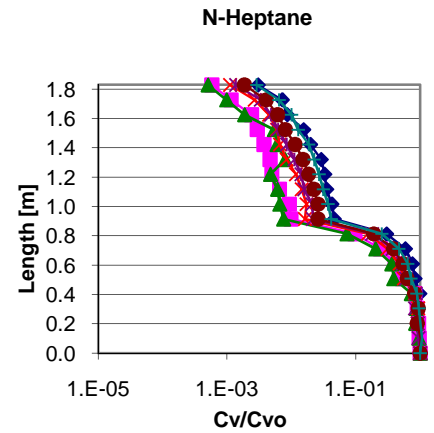
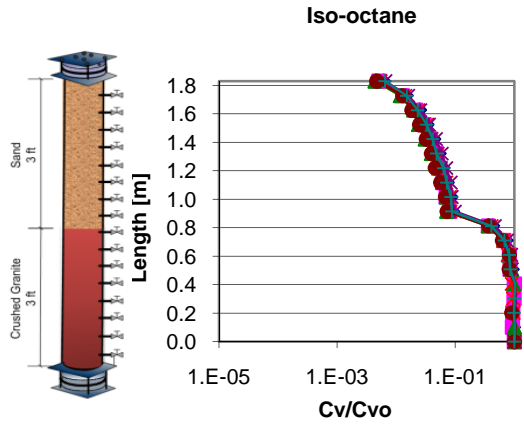
COLUMN C – AEROBIC PROFILES



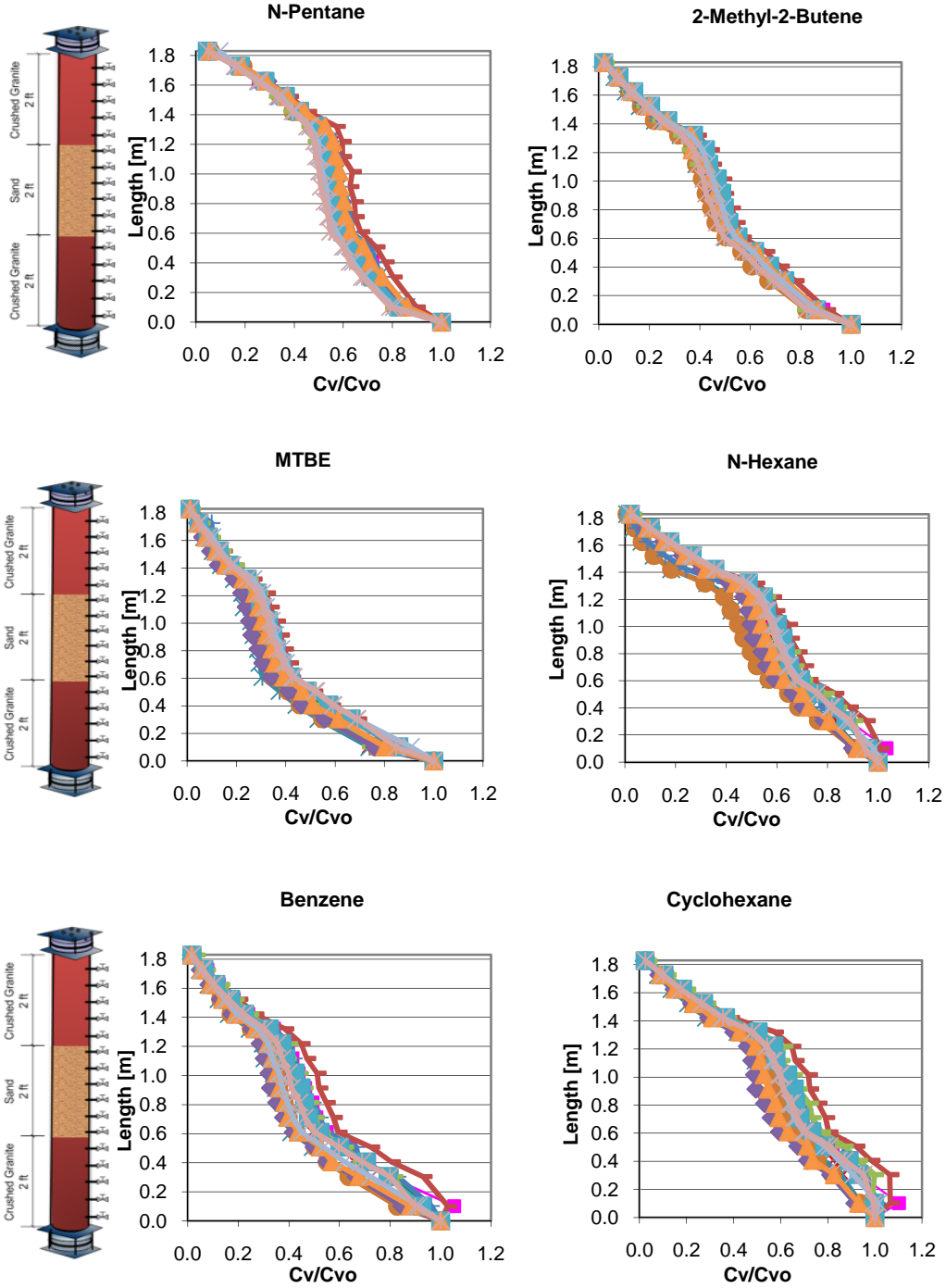
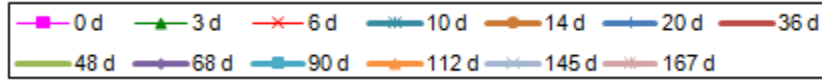


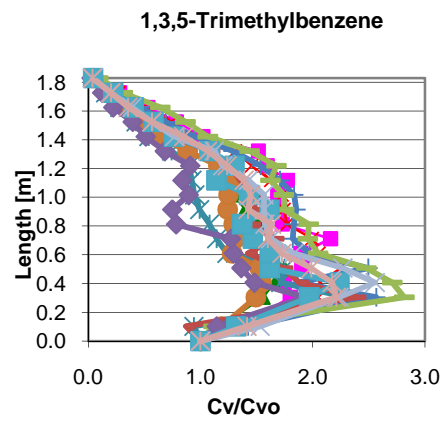
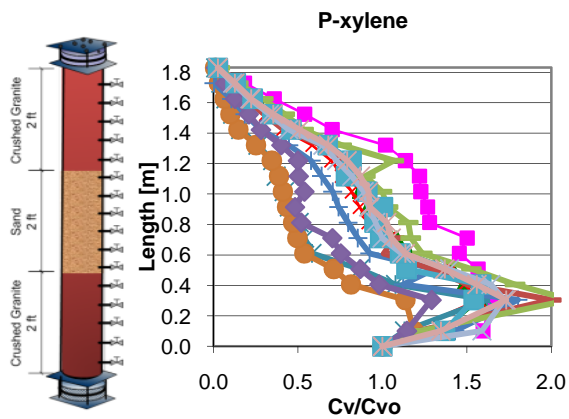
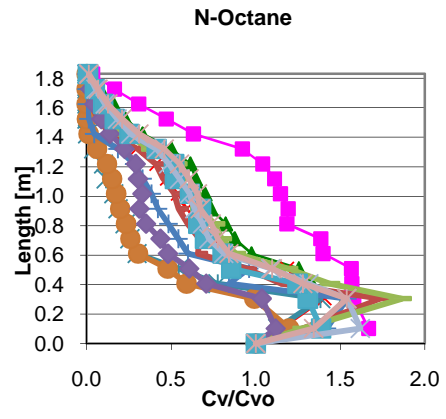
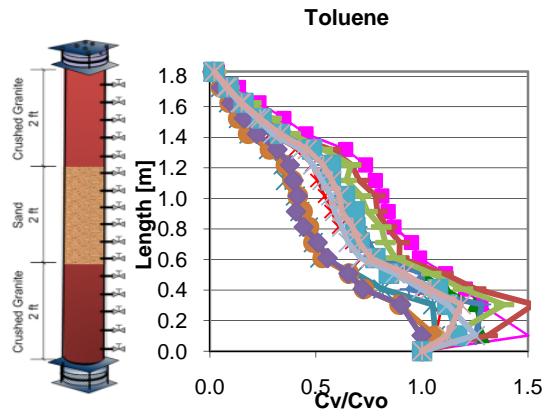
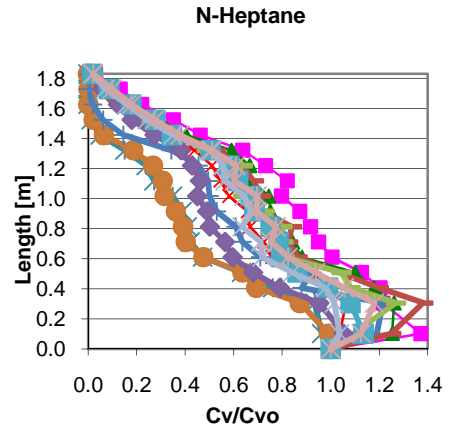
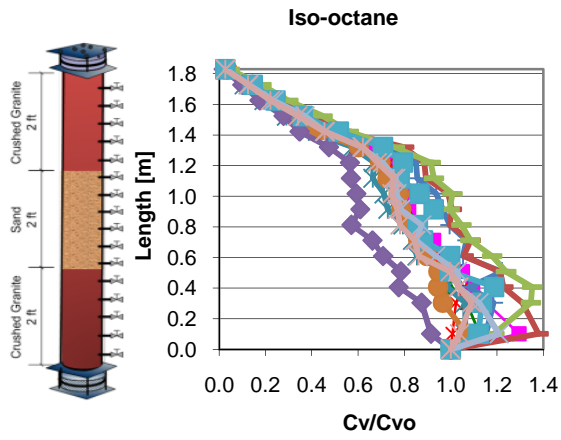
COLUMN D – AEROBIC PROFILES



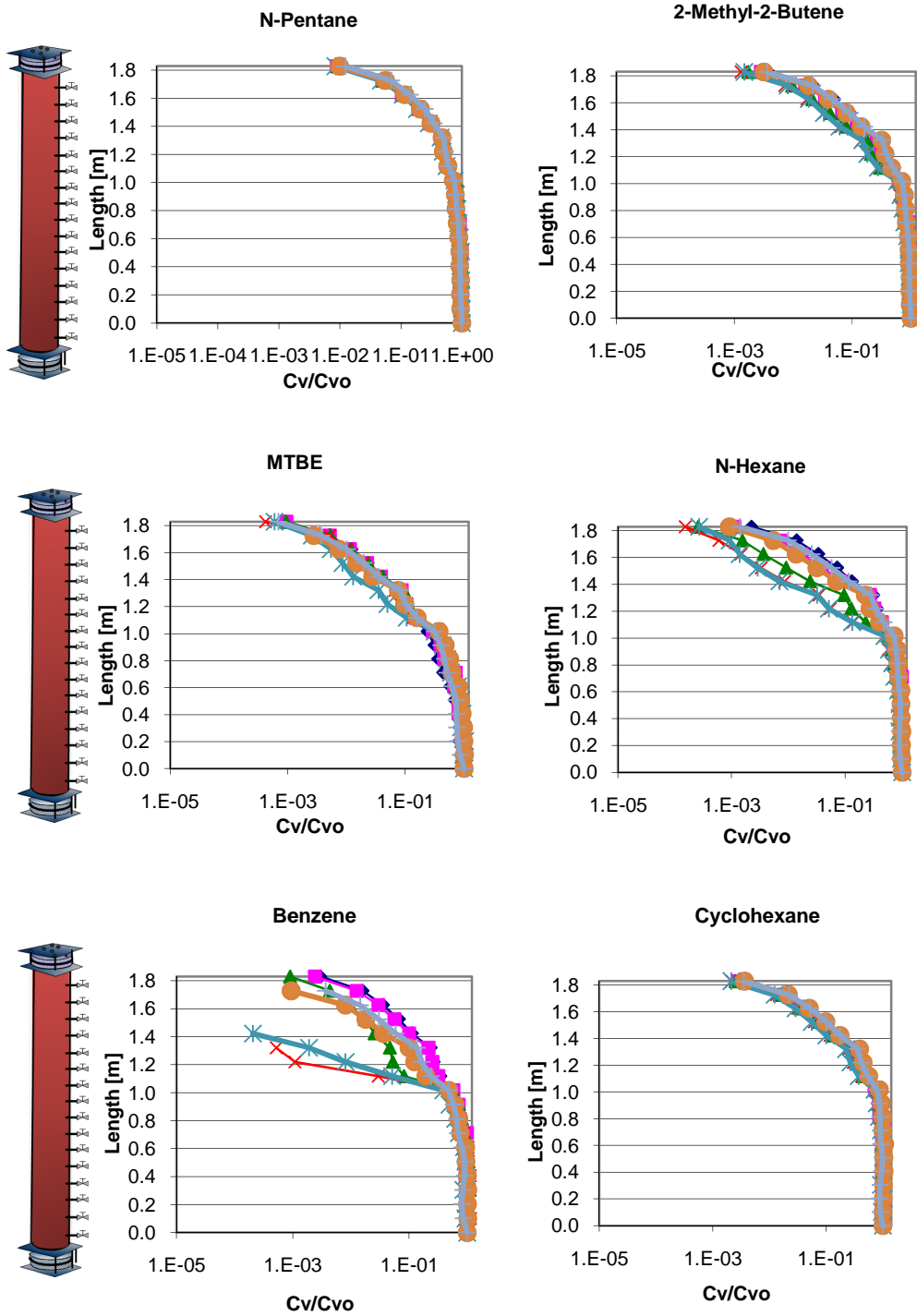
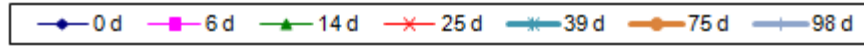


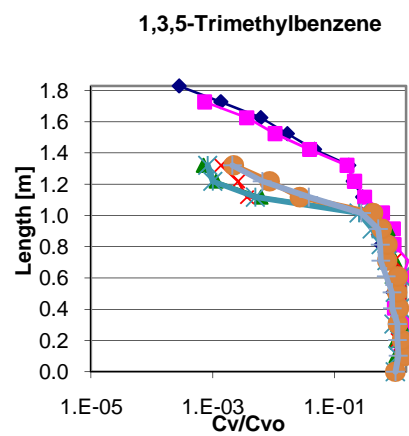
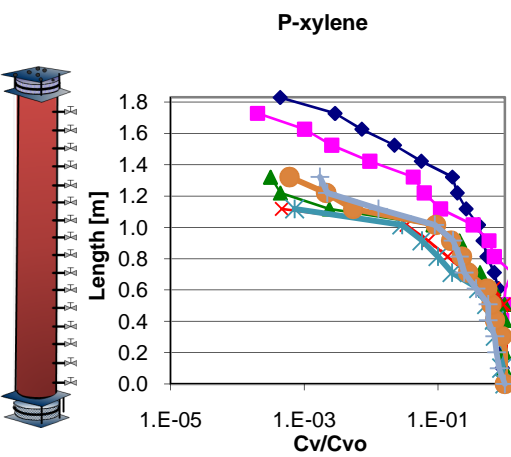
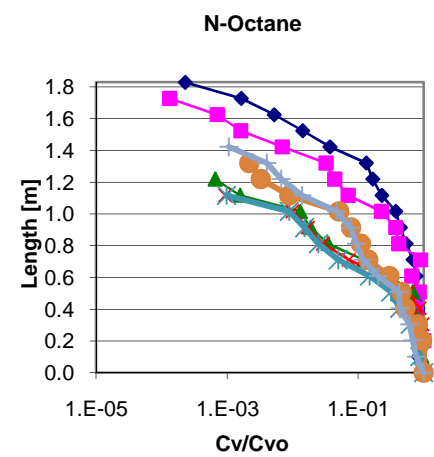
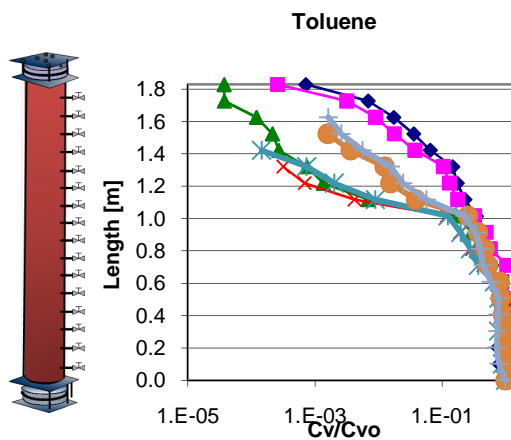
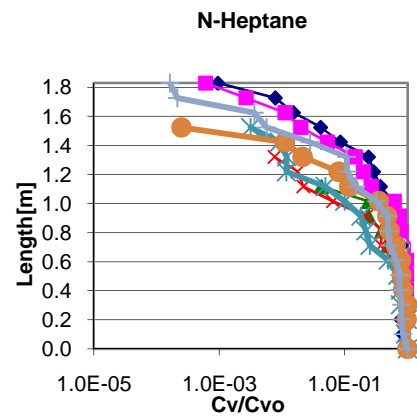
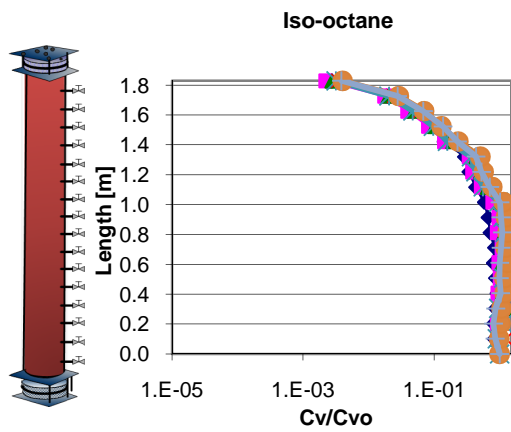
COLUMN E – AEROBIC PROFILES





COLUMN F – AEROBIC PROFILES



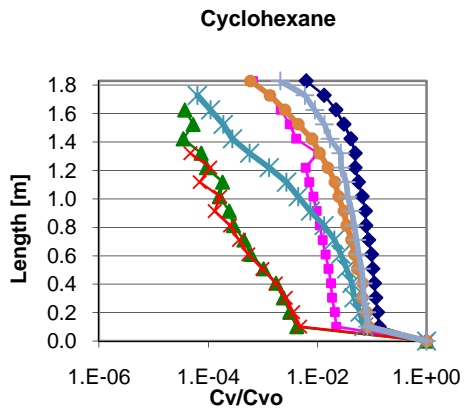
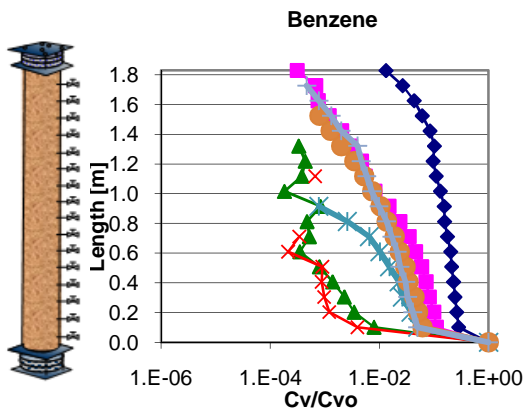
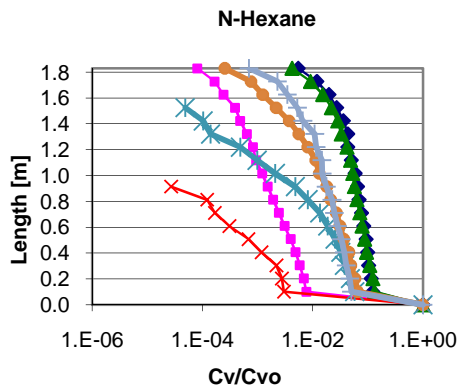
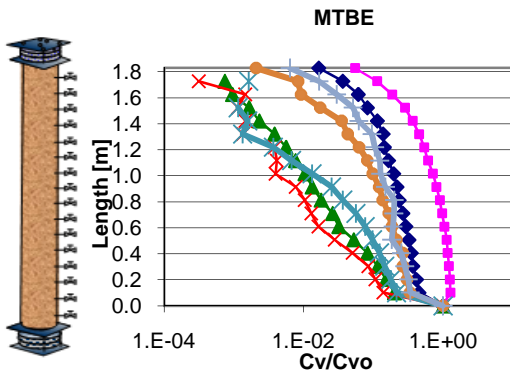
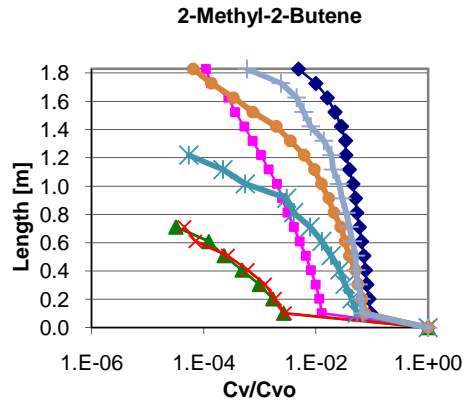
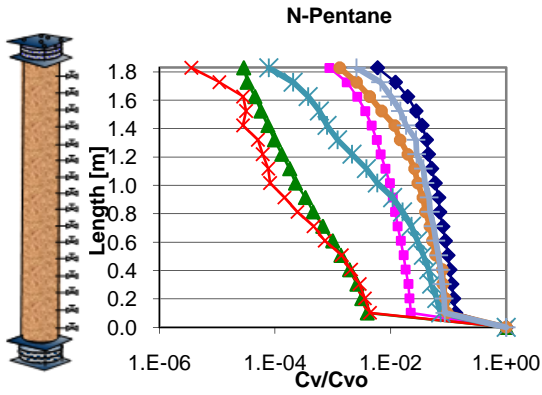
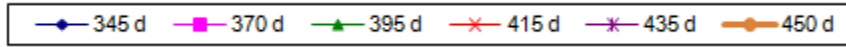


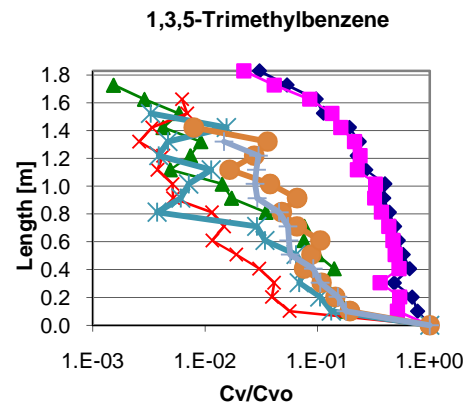
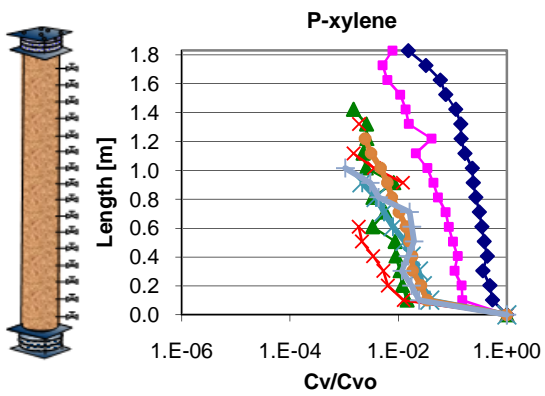
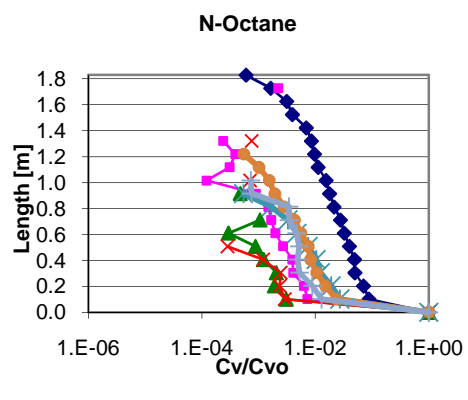
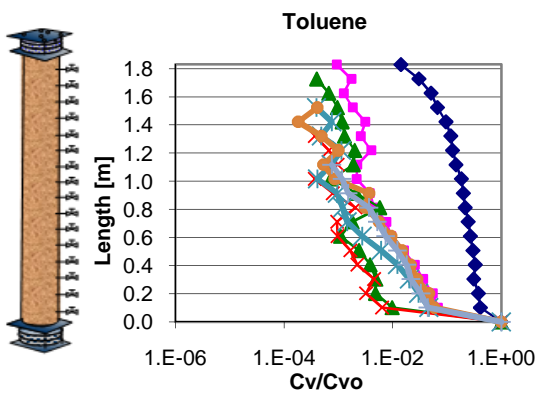
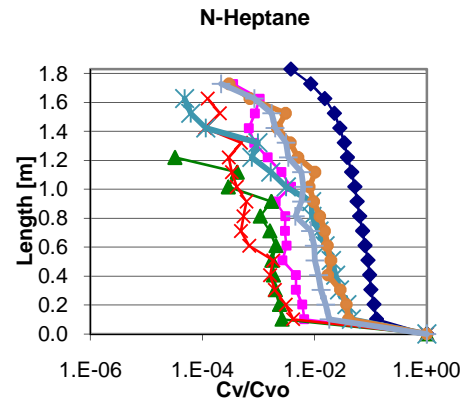
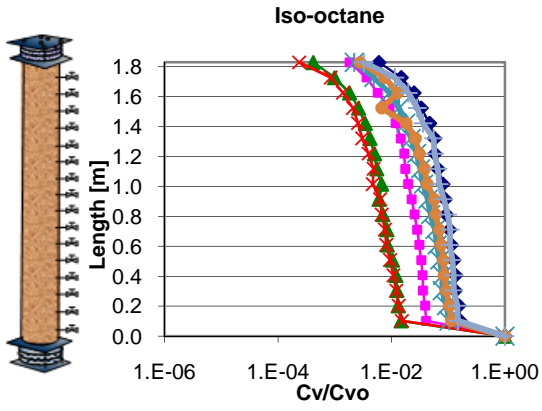
APPENDIX V:

VAPOR CONCENTRATION PROFILES.

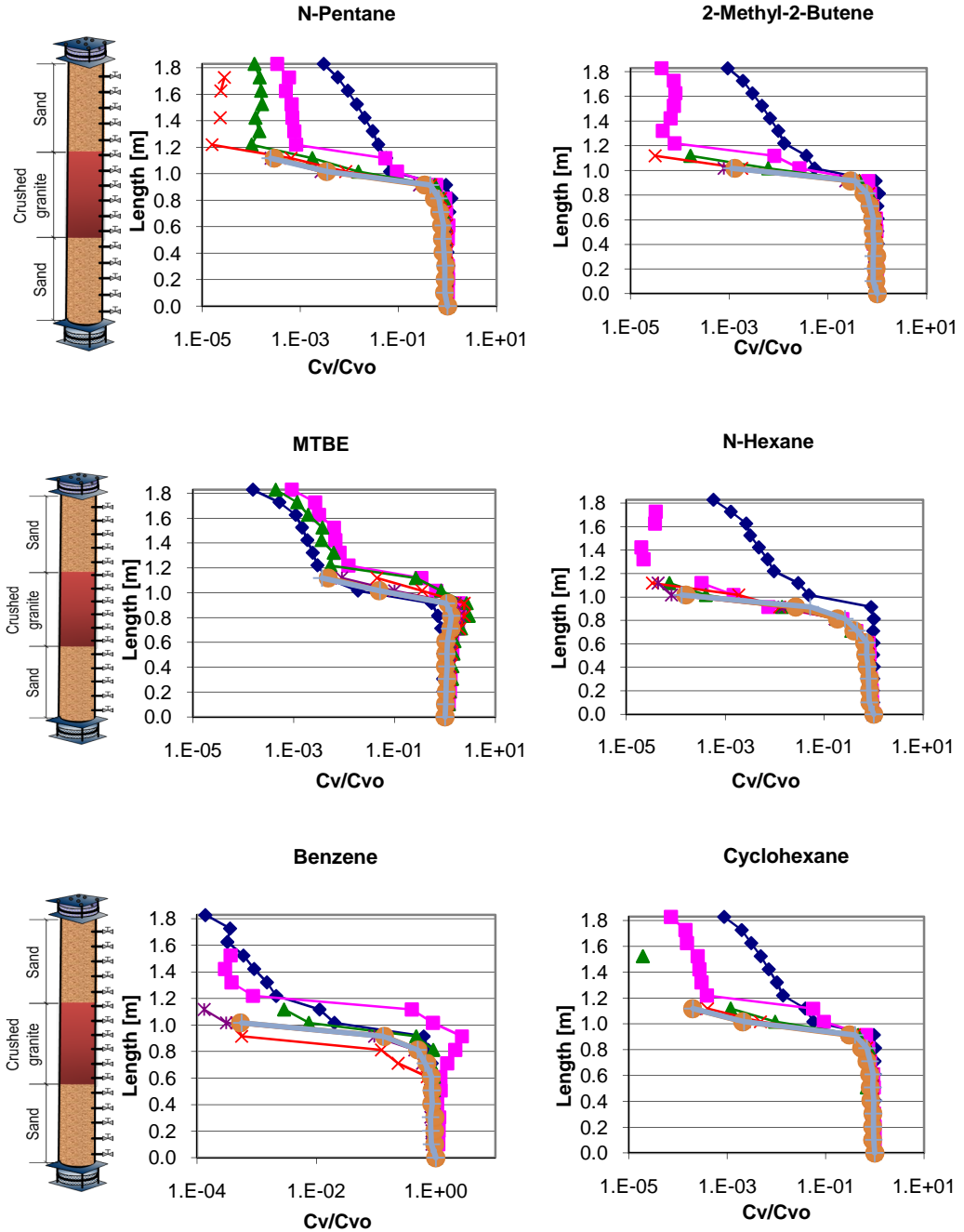
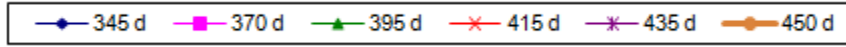
PHASE III: 10X LOWER VAPOR SOURCE CONCENTRATION - AEROBIC

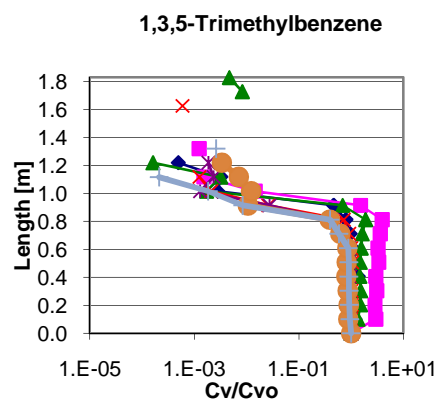
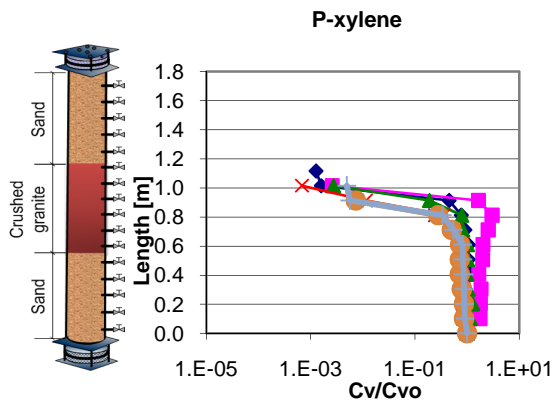
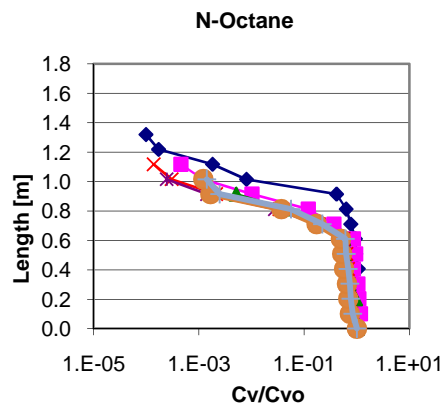
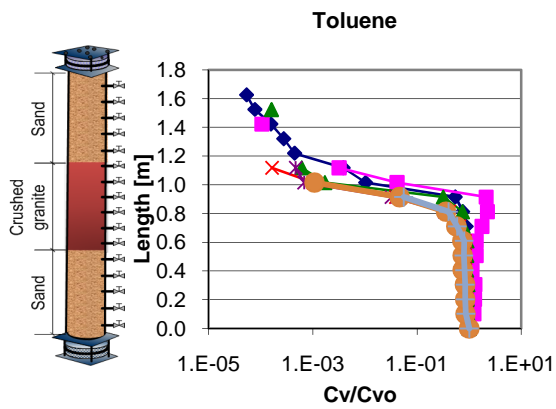
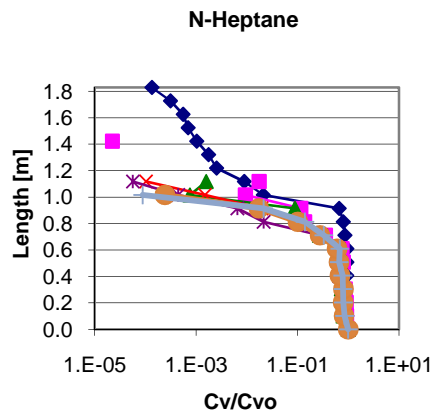
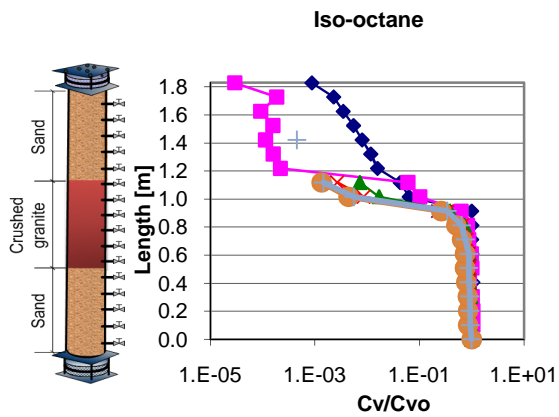
COLUMN A – 10X LOWER VAPOR SOURCE CONCENTRATION



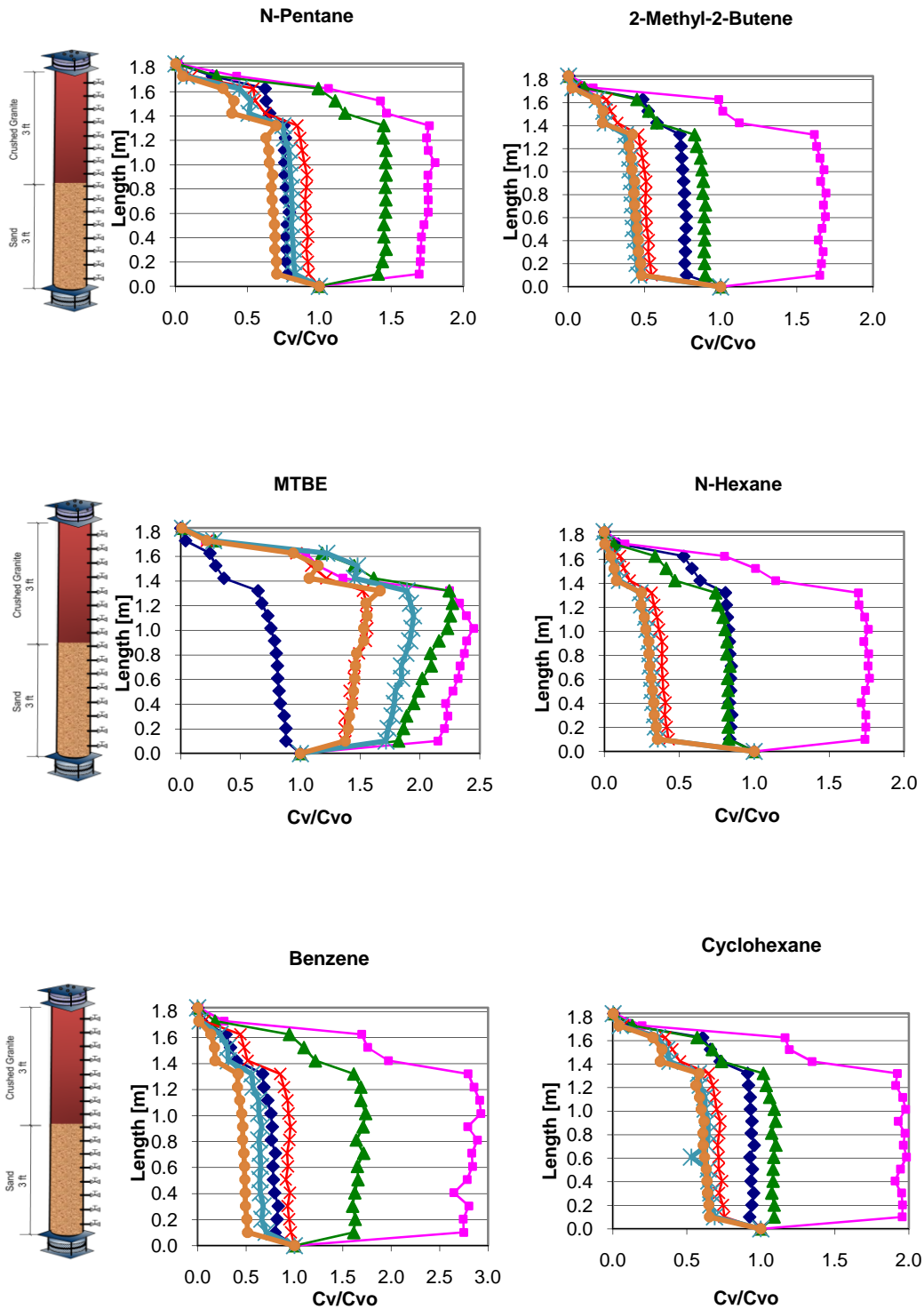
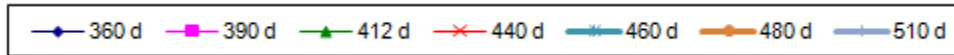


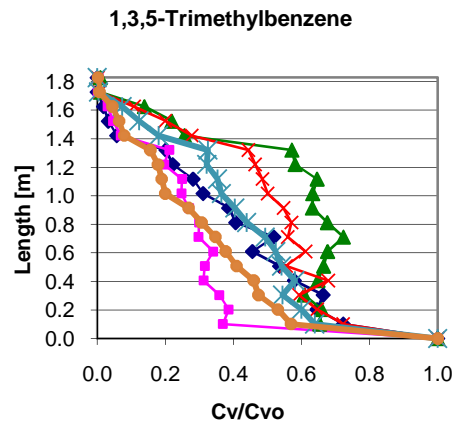
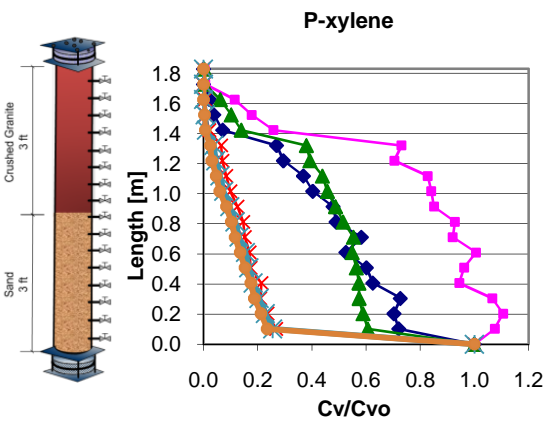
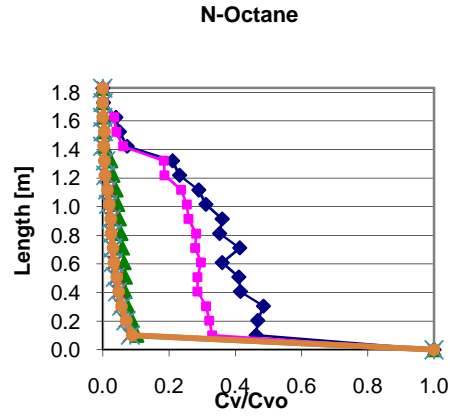
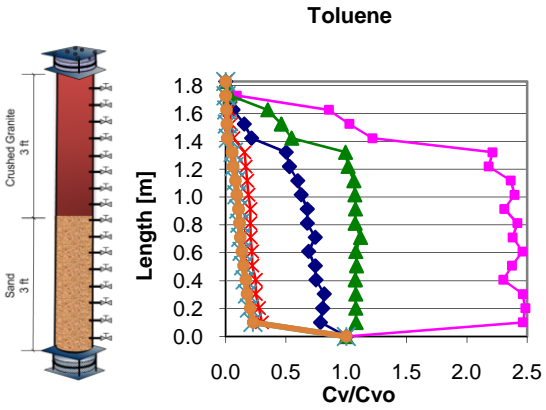
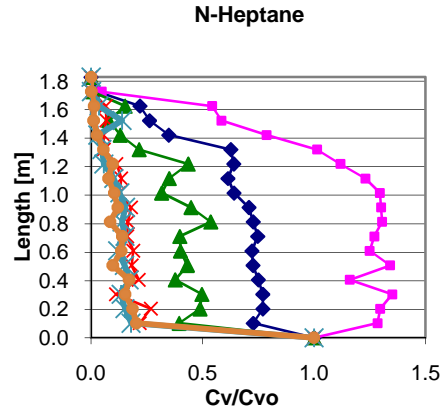
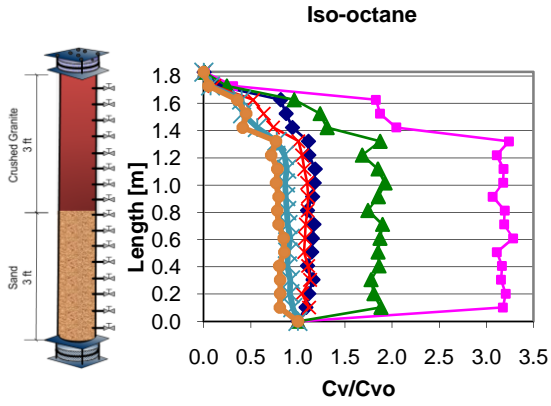
COLUMN B – 10X LOWER VAPOR SOURCE CONCENTRATION



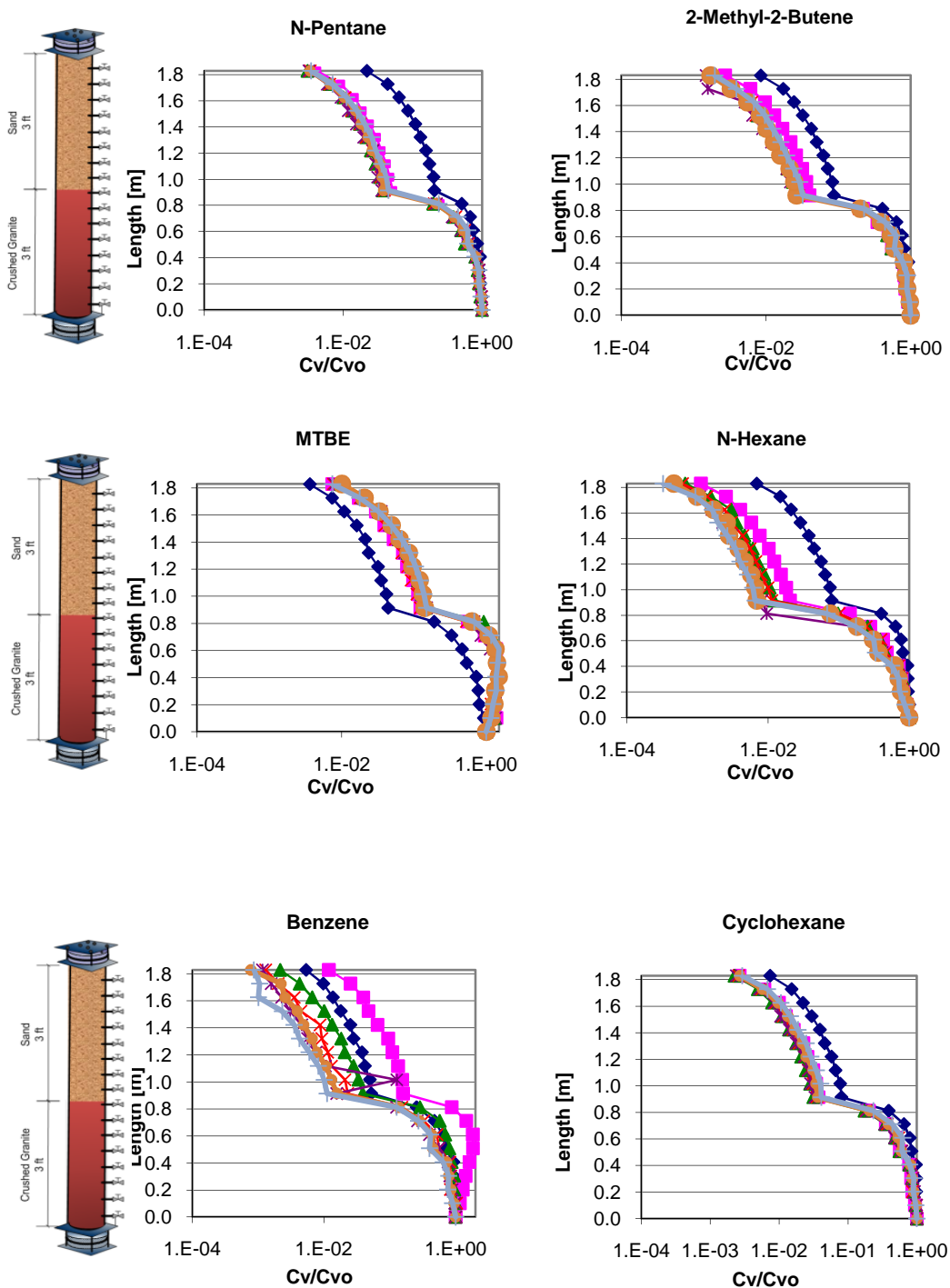
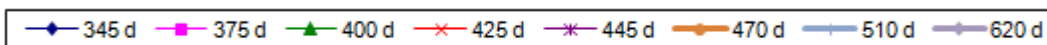


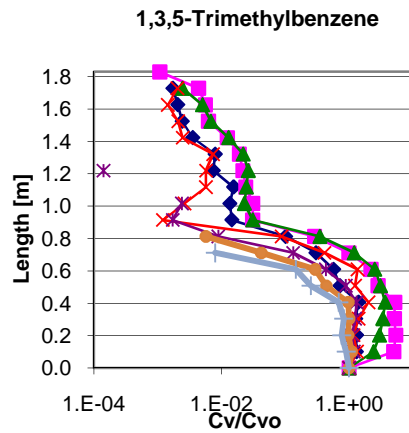
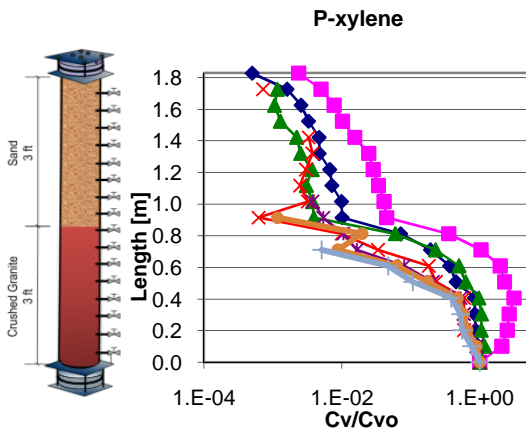
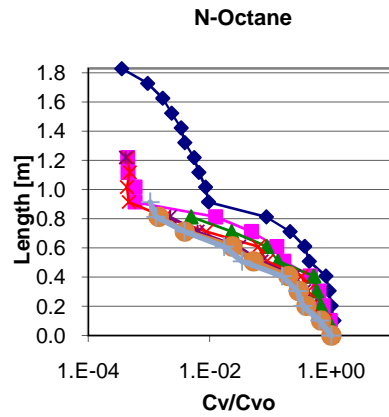
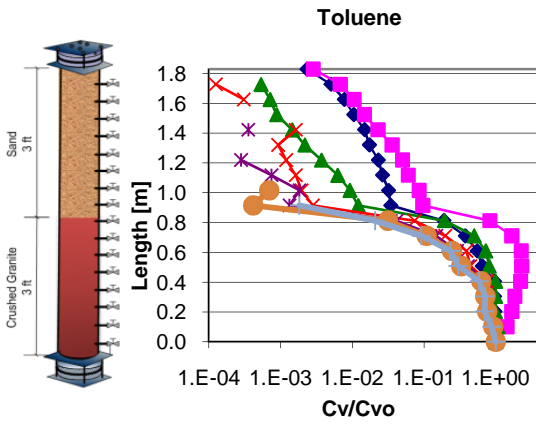
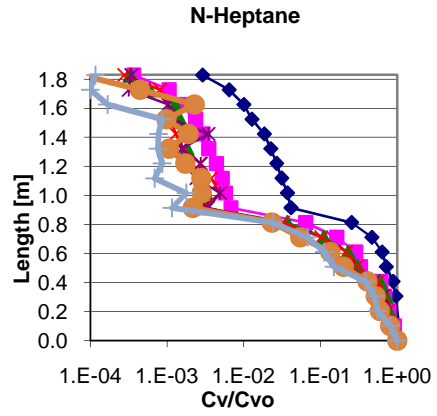
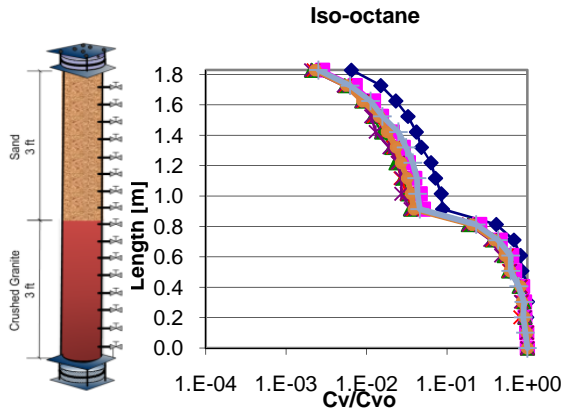
COLUMN C – 10X LOWER VAPOR SOURCE CONCENTRATION



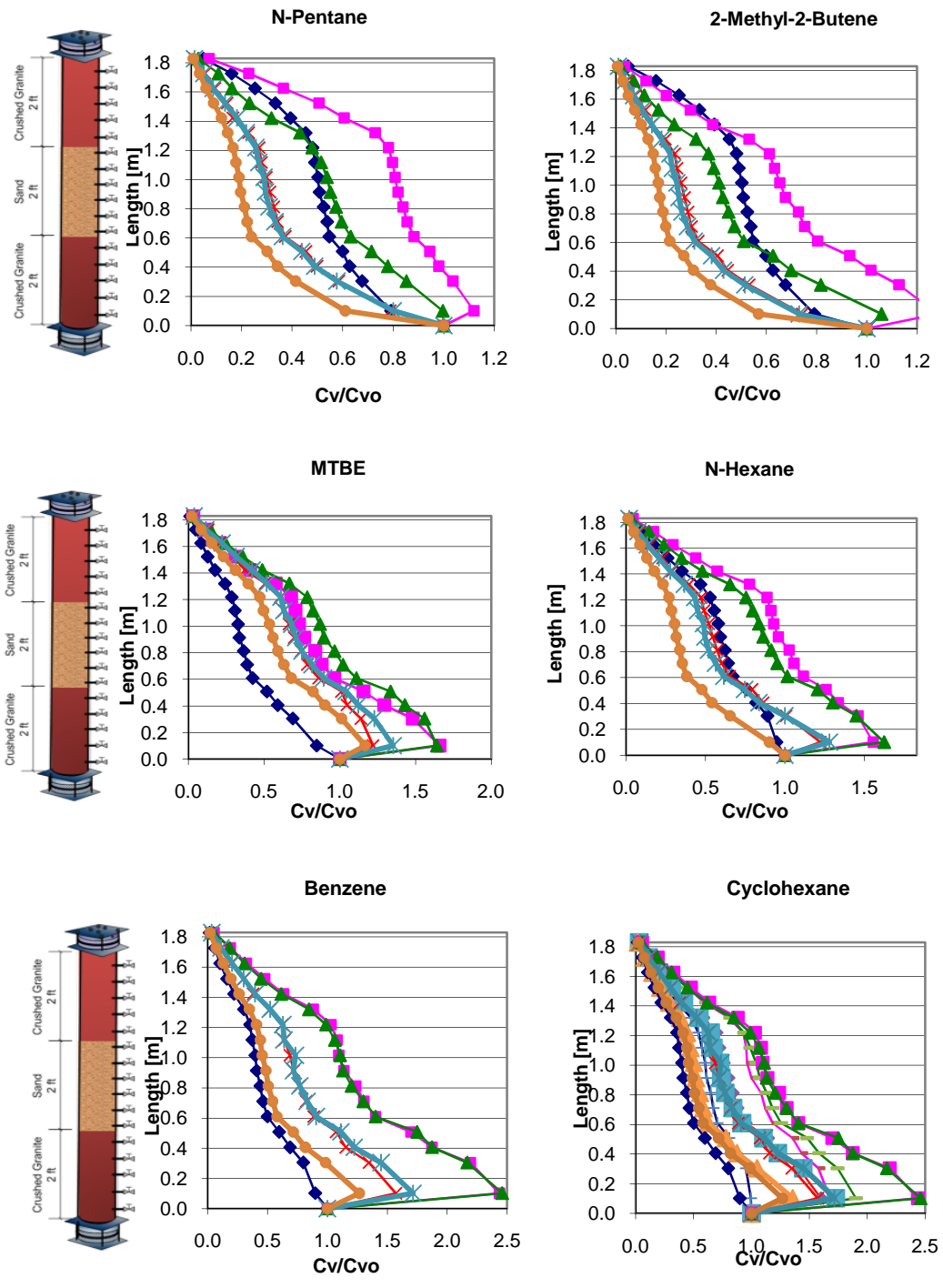
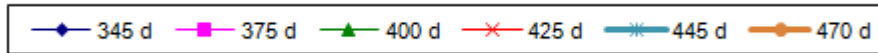


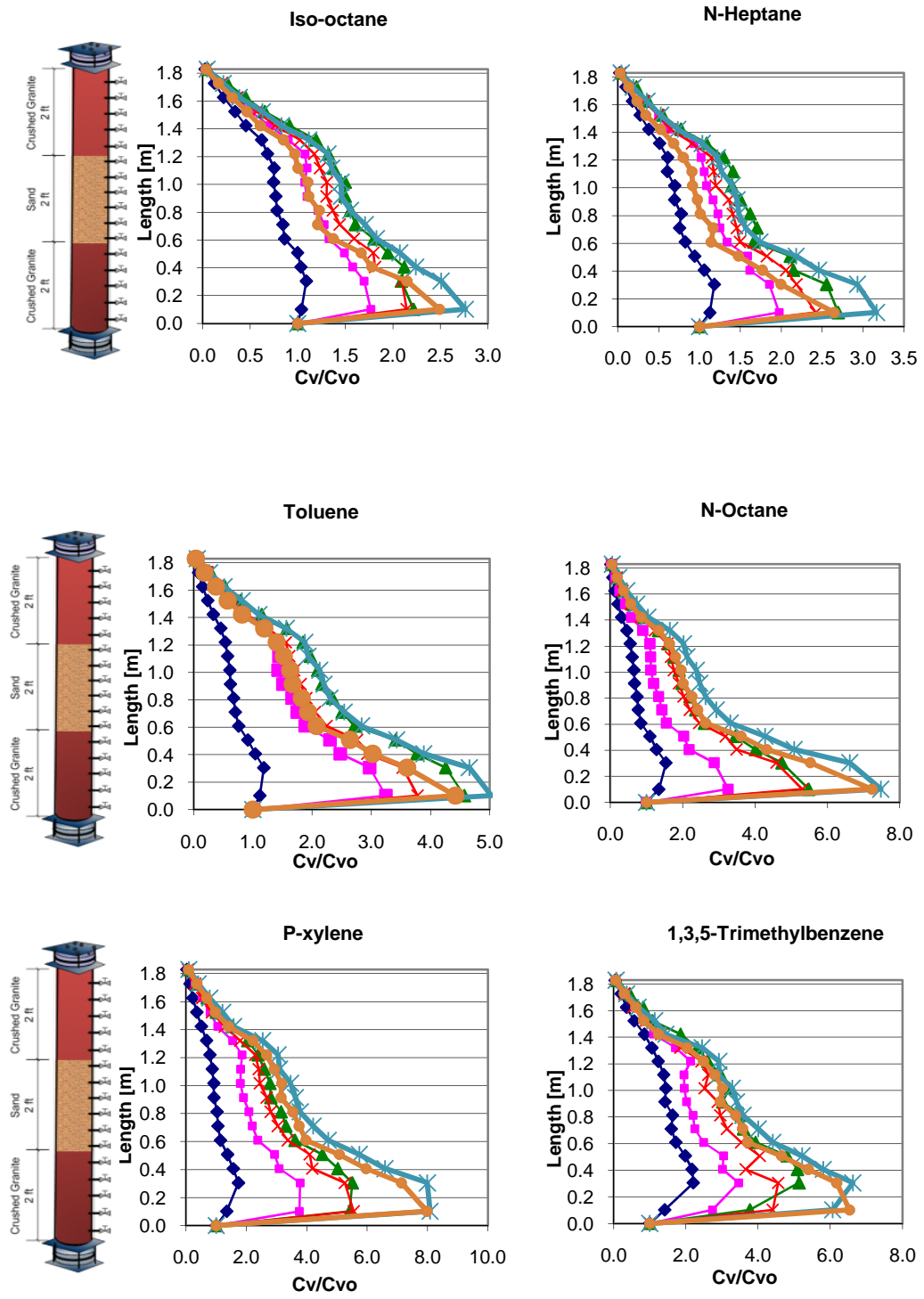
COLUMN D – 10X LOWER VAPOR SOURCE CONCENTRATION



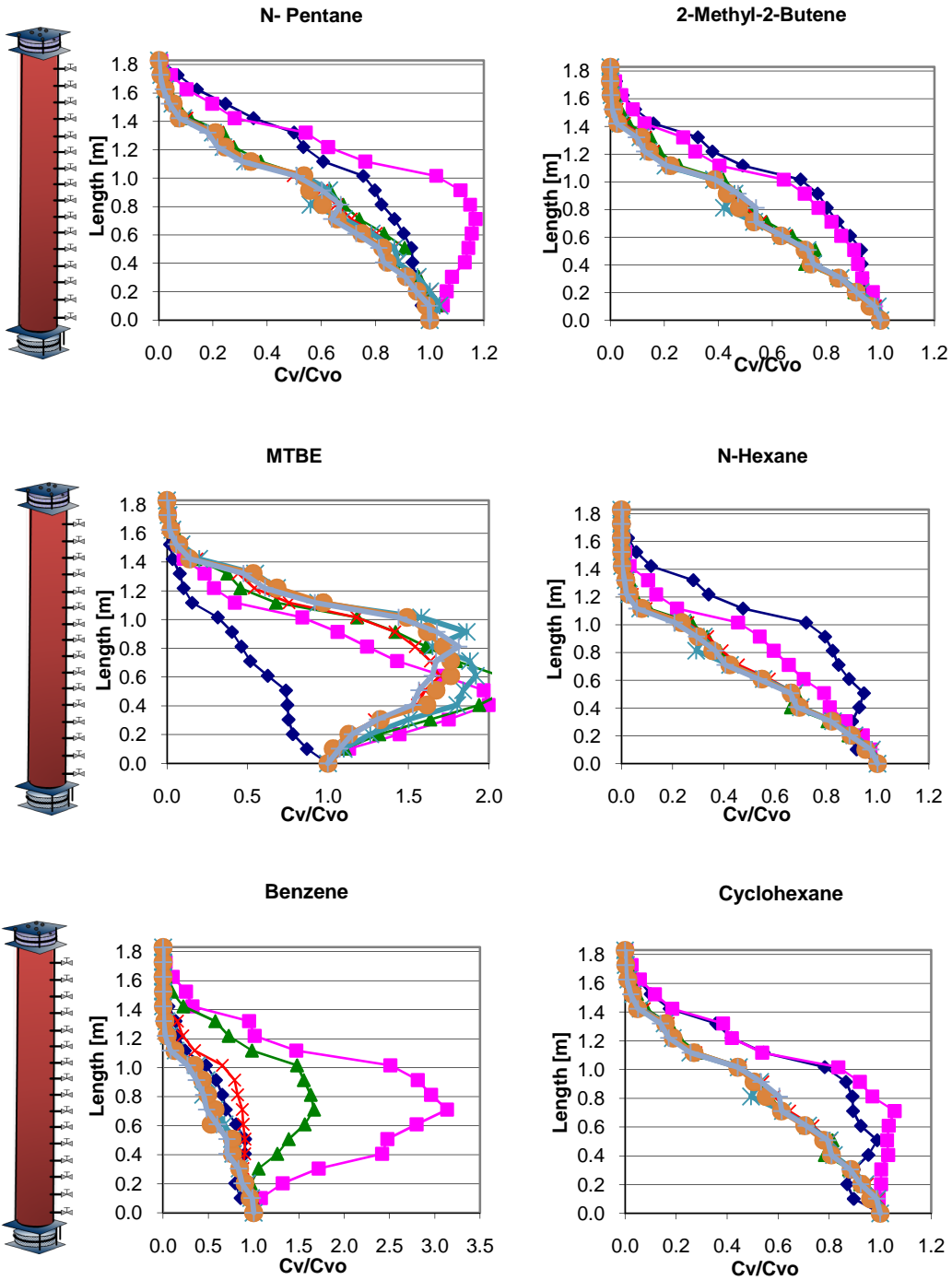
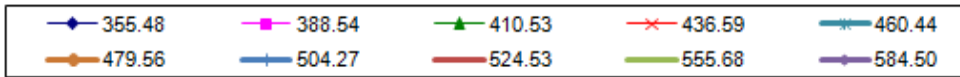


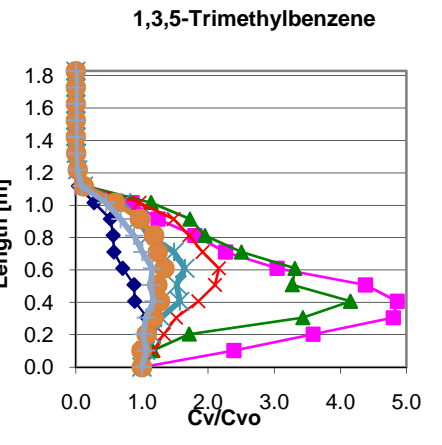
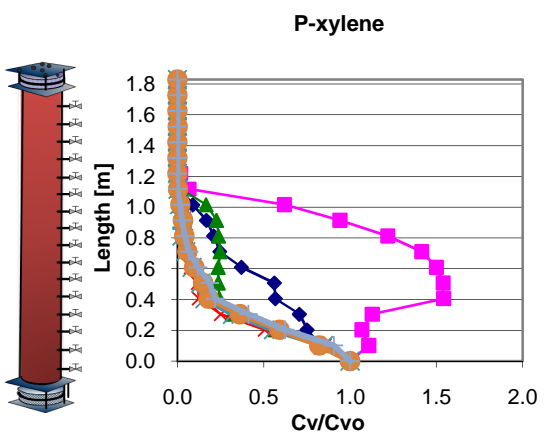
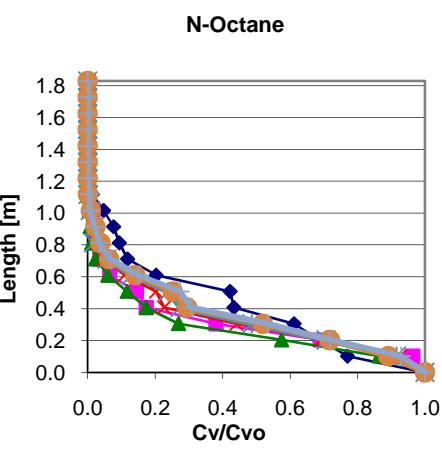
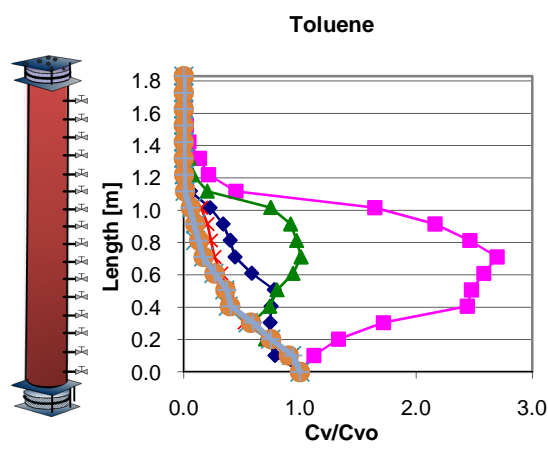
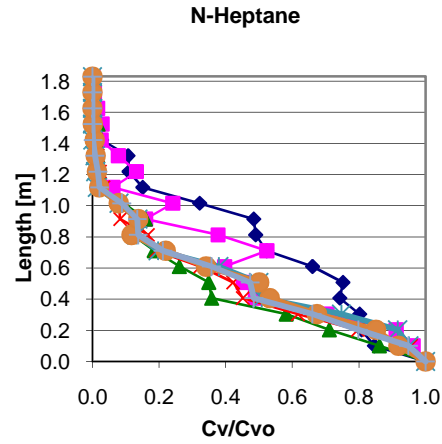
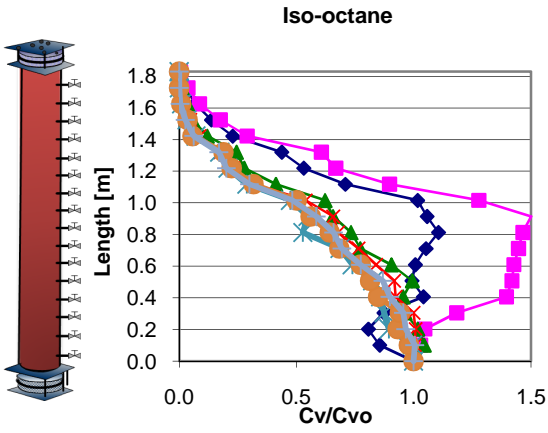
COLUMN E – 10X LOWER VAPOR SOURCE CONCENTRATION





COLUMN F – 10 X LOWER VAPOR SOURCE CONCENTRATION



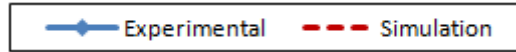


APPENDIX VI

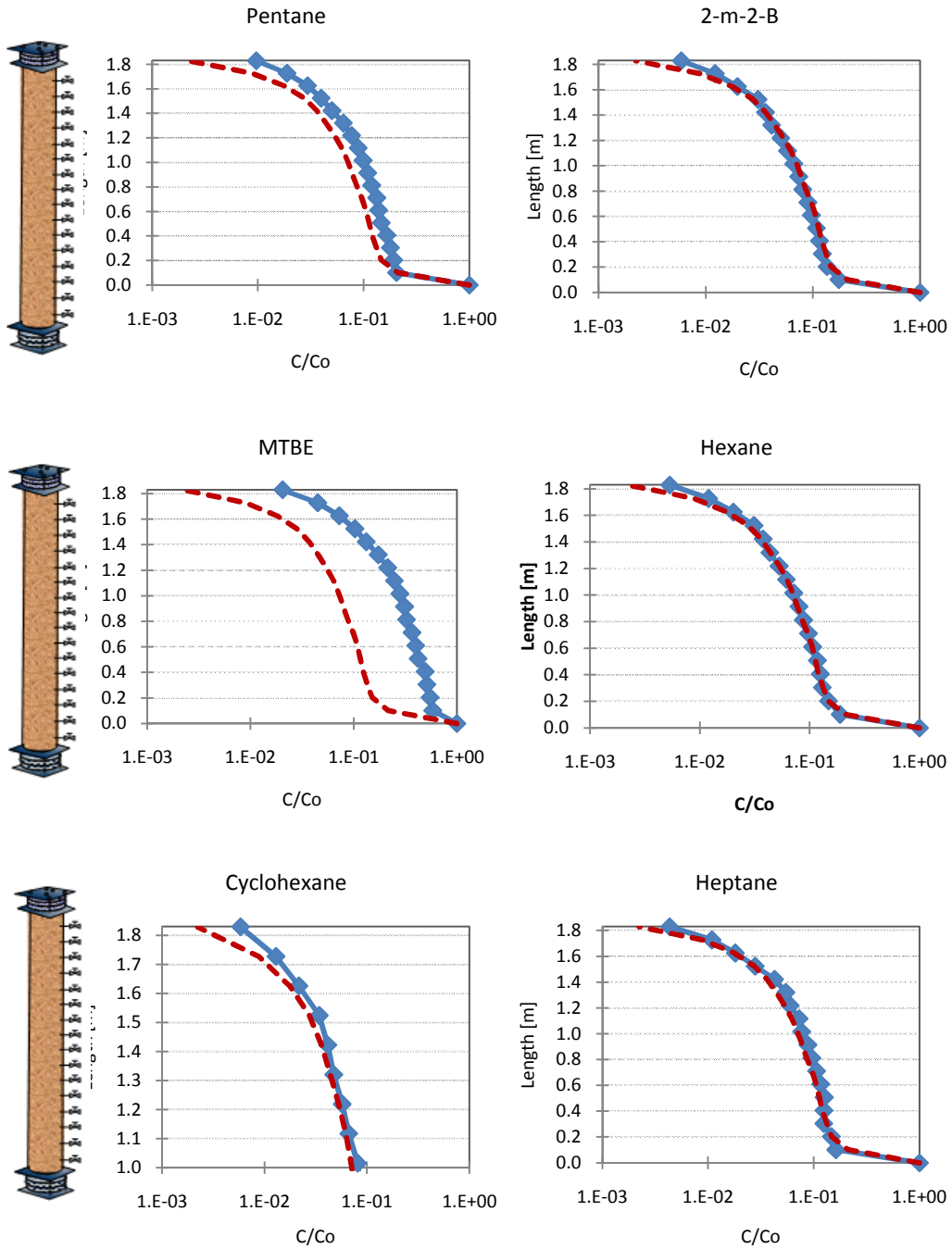
NEAR-STEADY CONDITIONS SIMULATION RESULTS:

VAPOR CONCENTRATION PROFILES

PHASE I SIMULATION (ANAEROBIC CONDITIONS)

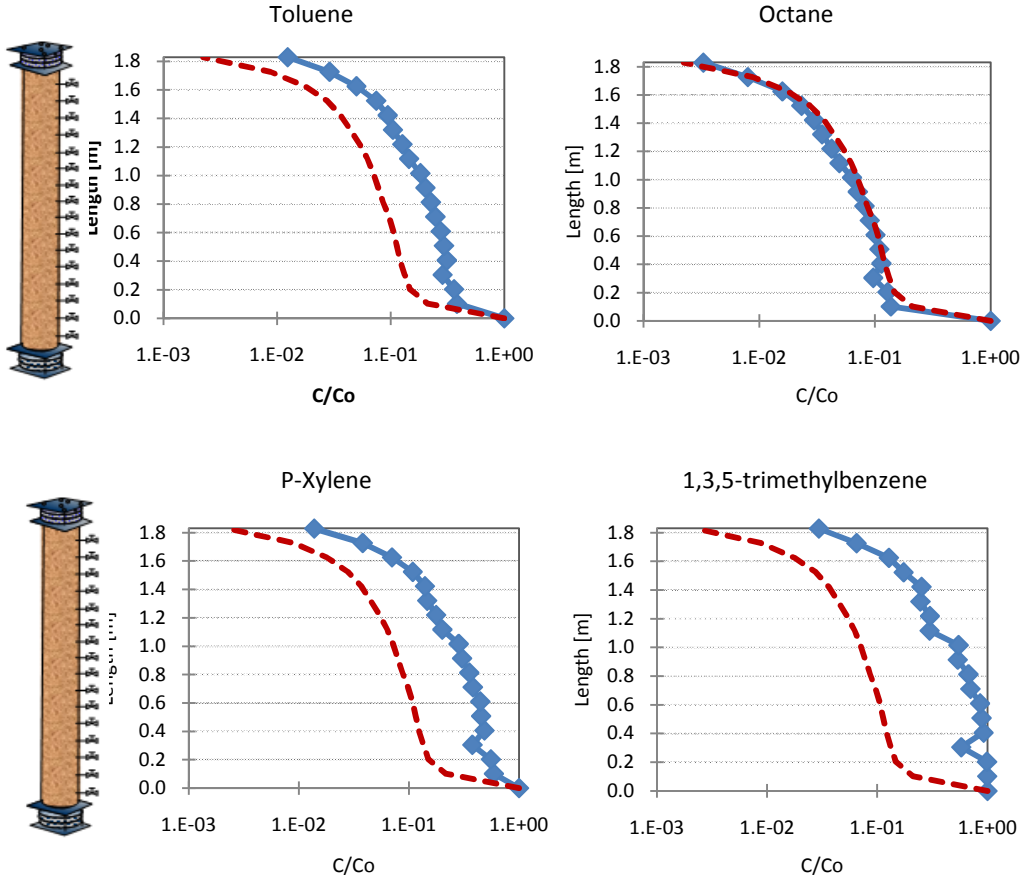


Column A

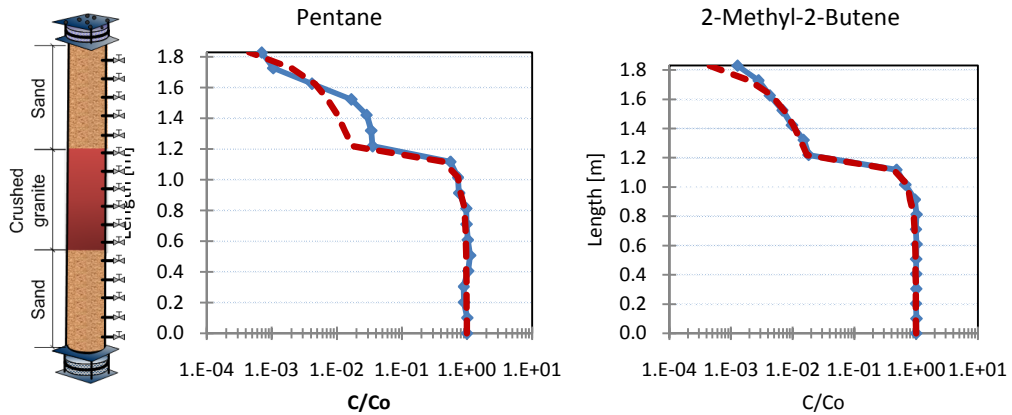




Column A (continue)

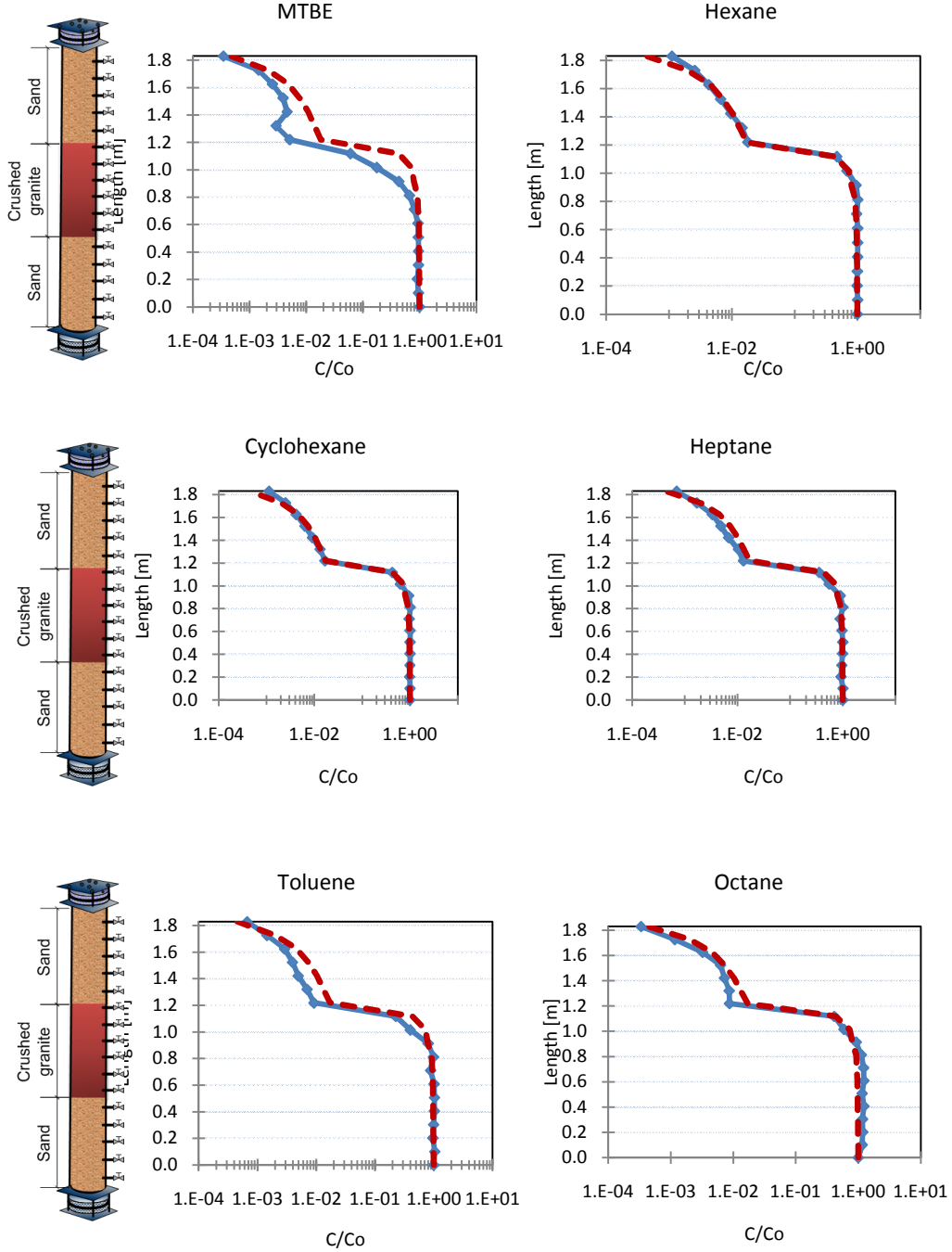


Column B



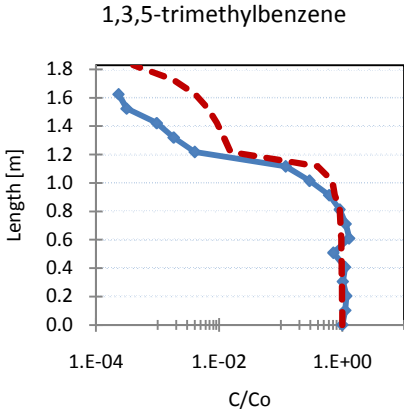
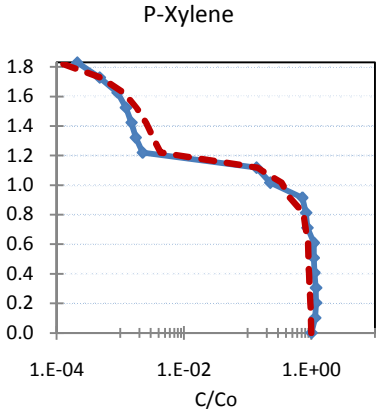
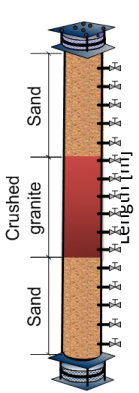


Column B(continue)

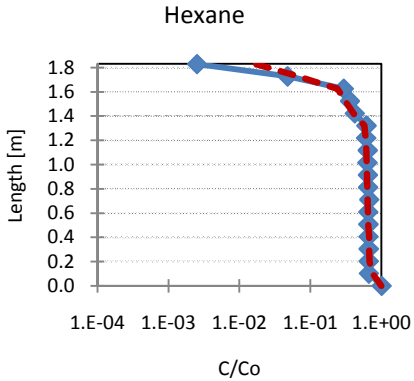
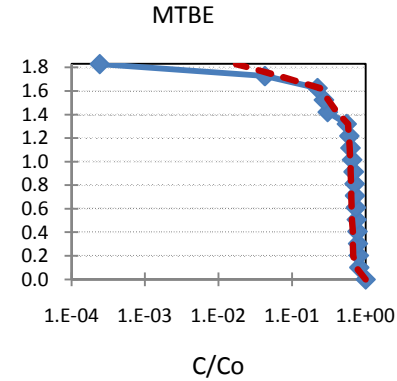
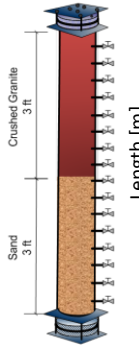
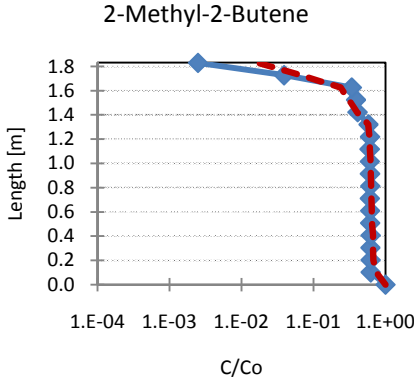
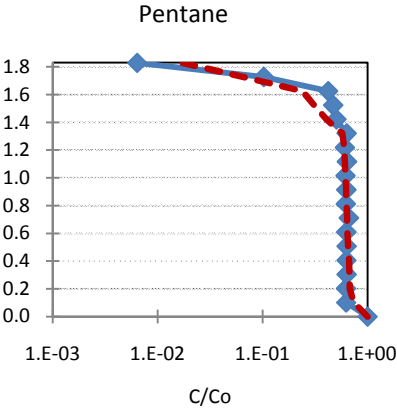
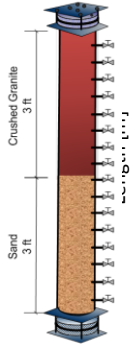




Column B (continue)

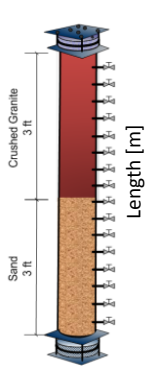


Column C

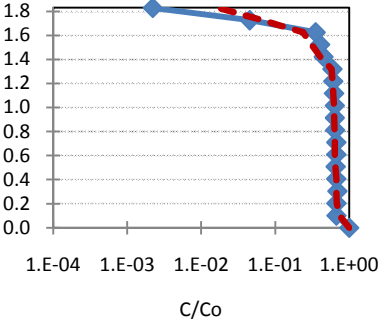




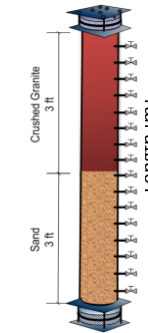
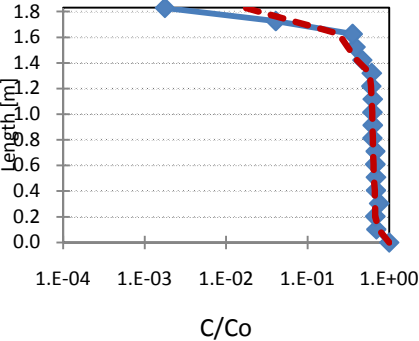
Column C (continue)



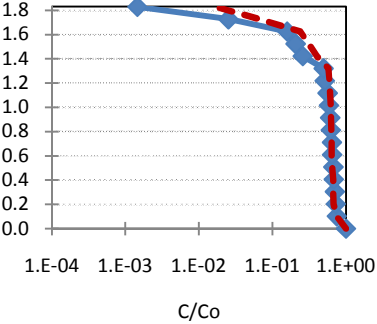
Cyclohexane



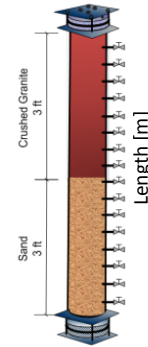
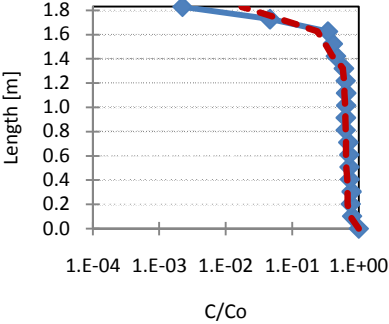
Heptane



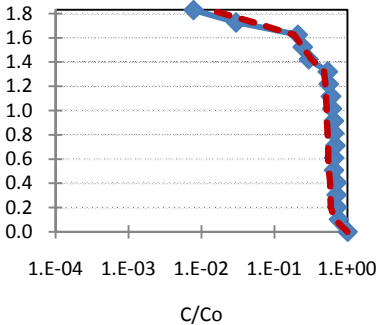
Toluene



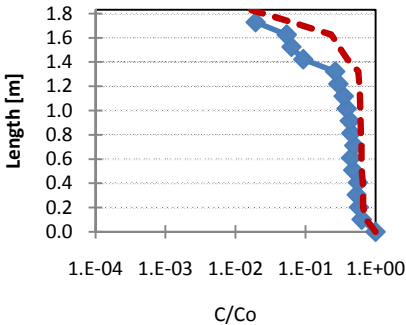
Octane



P-Xylene

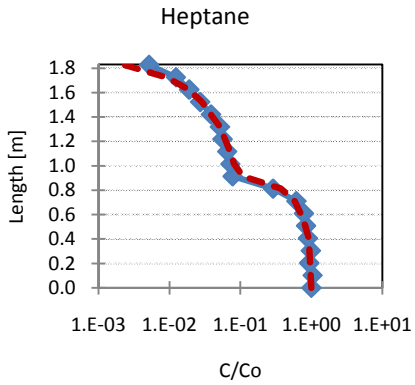
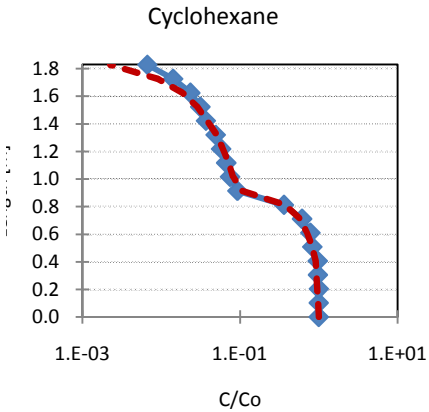
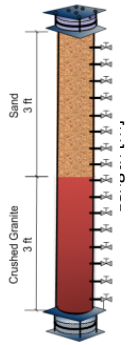
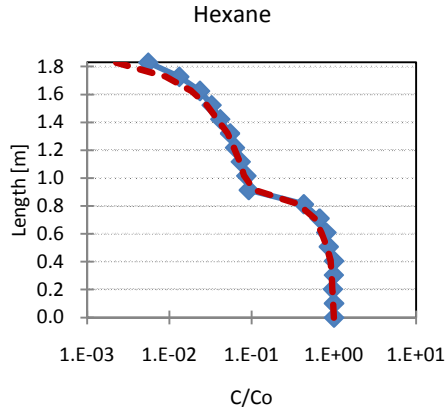
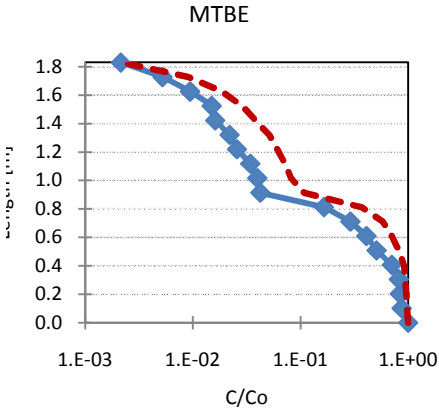
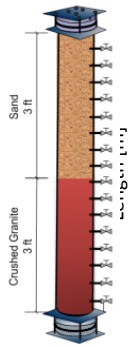
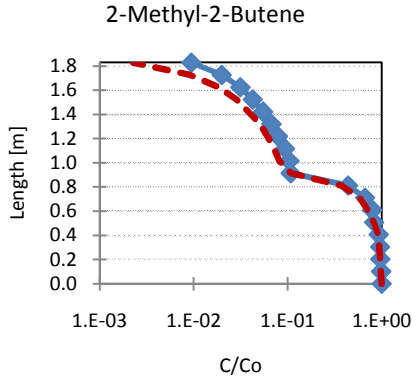
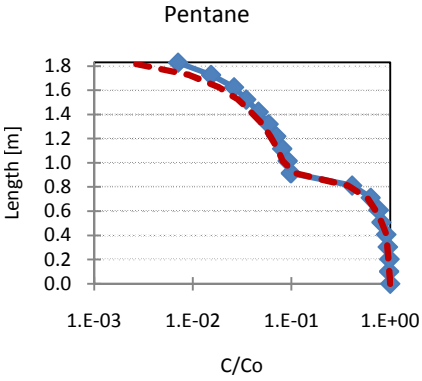
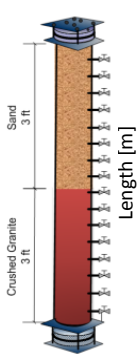


1,3,5-trimethylbenzene



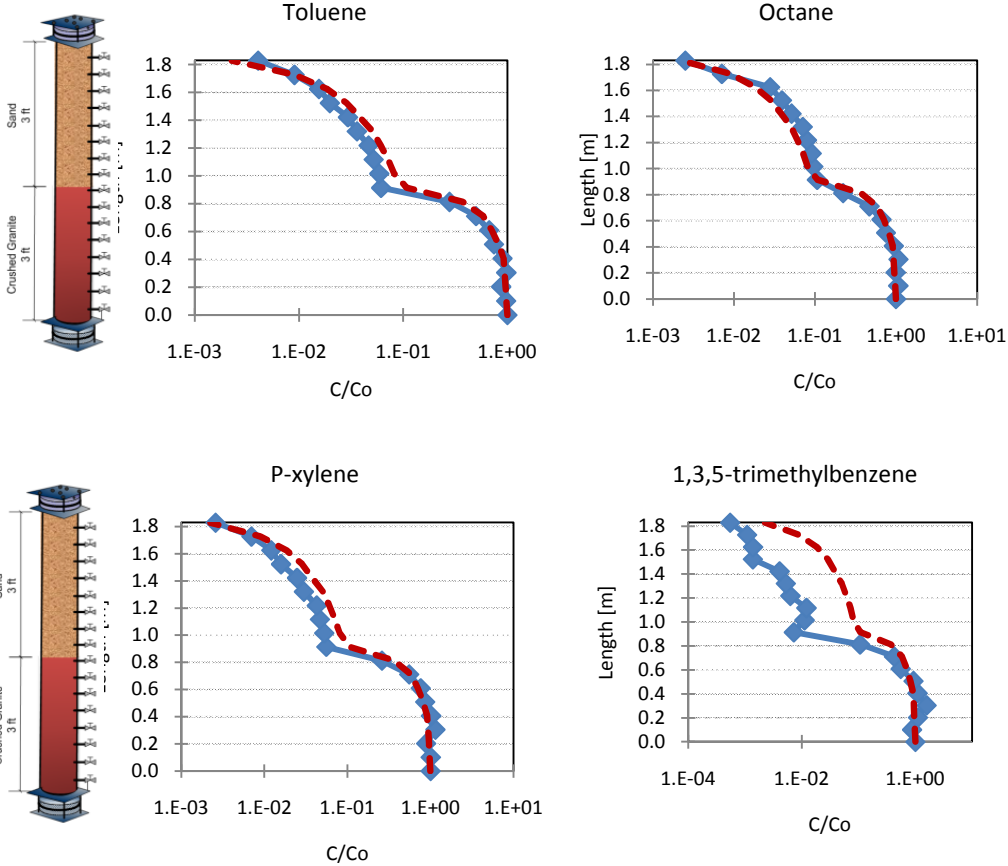


Column D

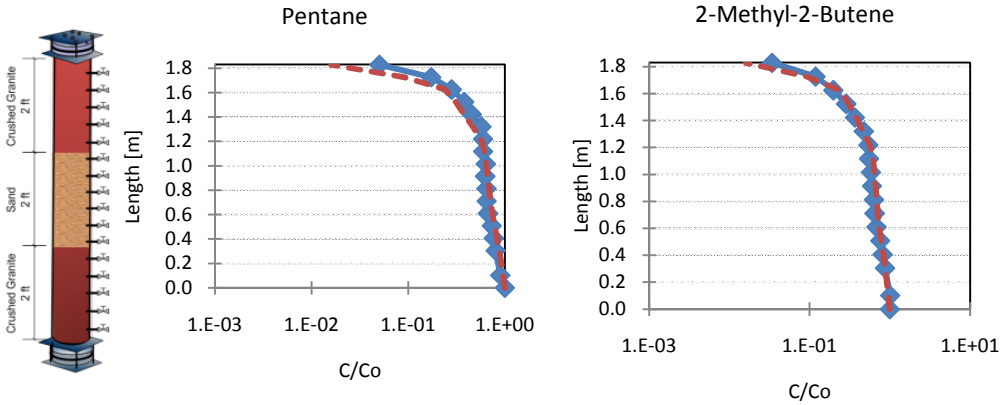




Column D (continue)

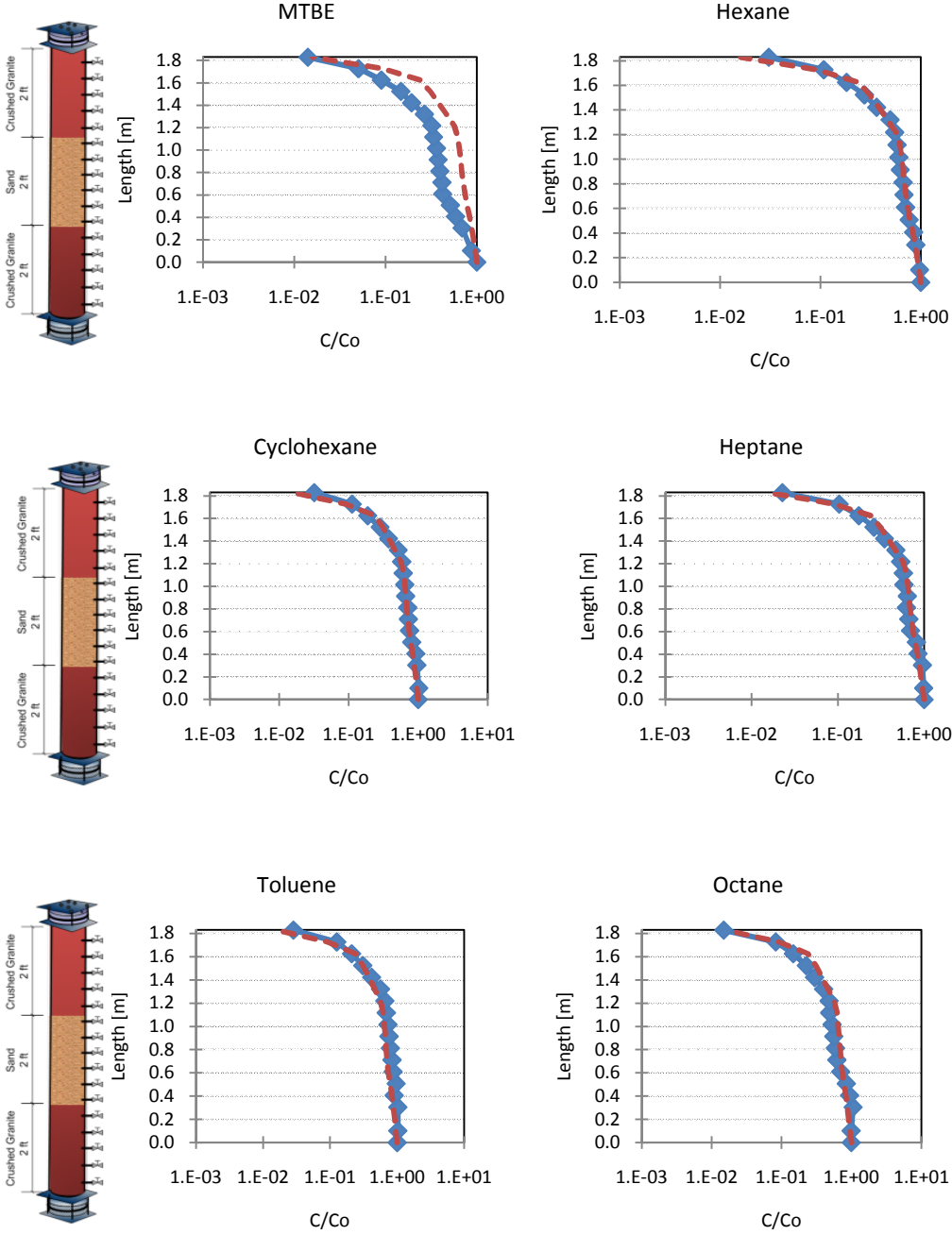


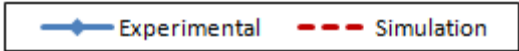
Column E



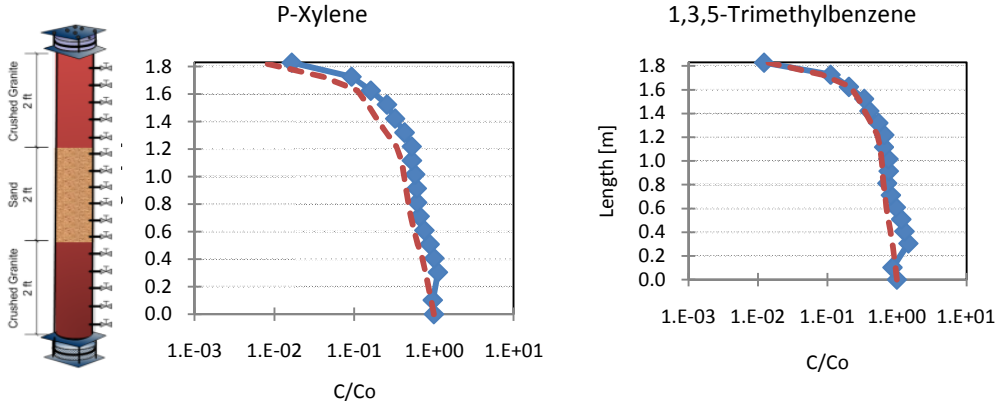


Column E (continue)

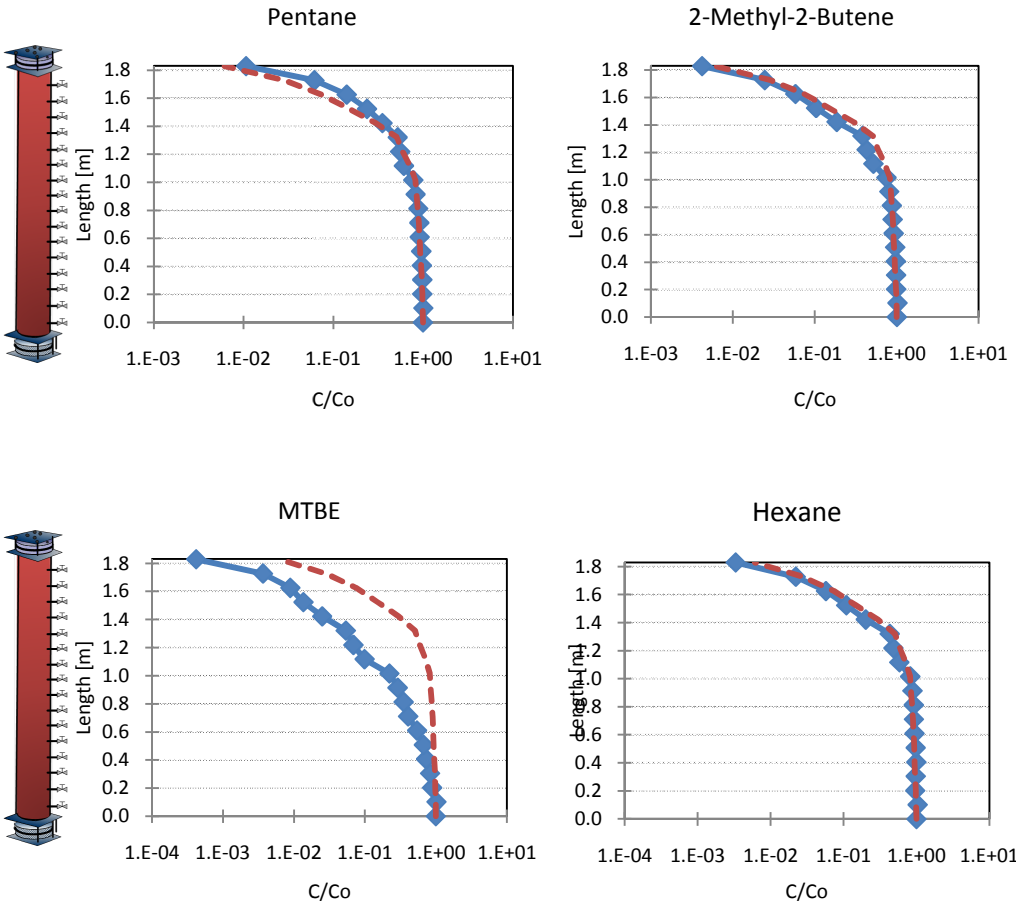




Column E (continue)

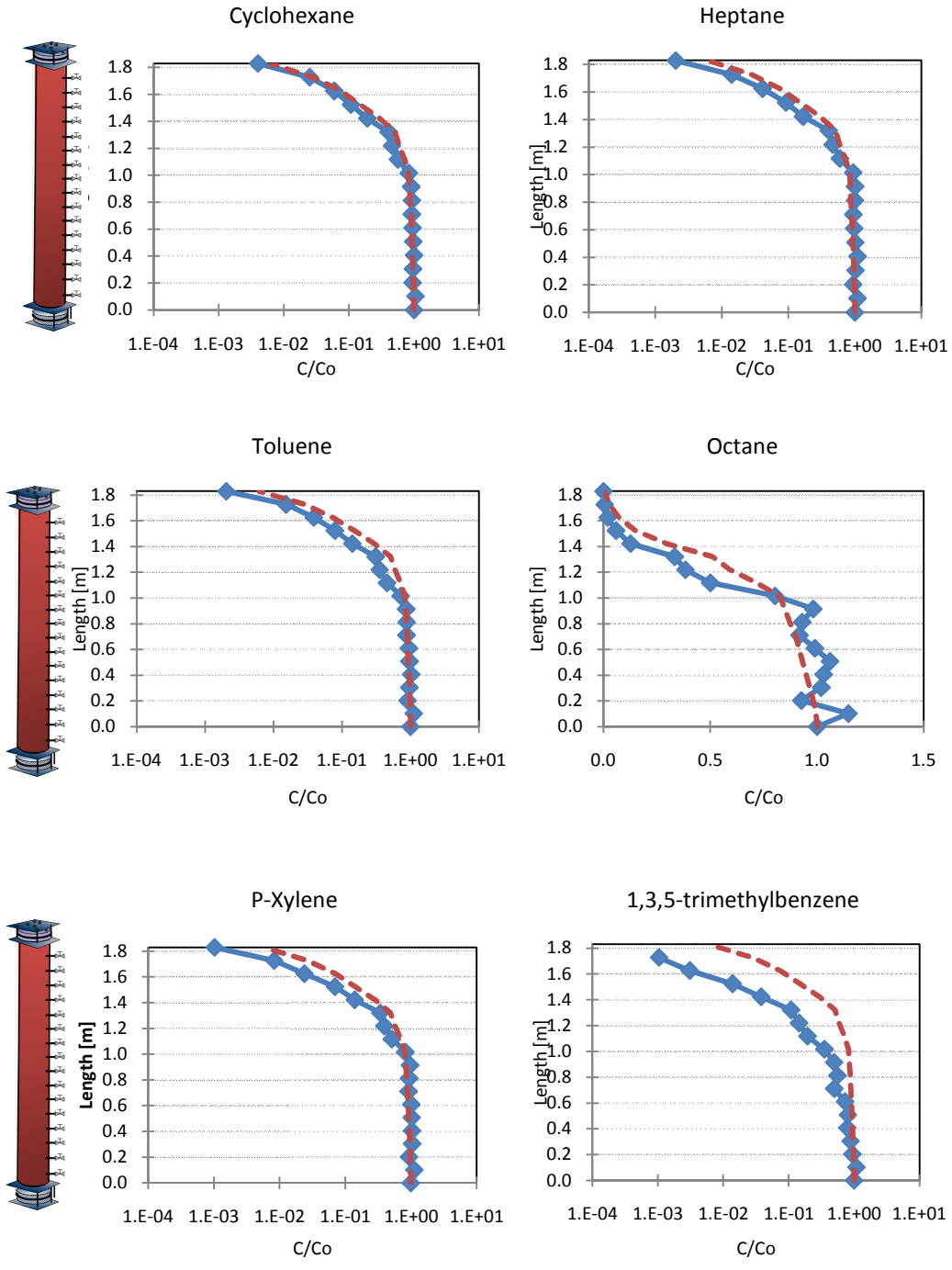


Column F





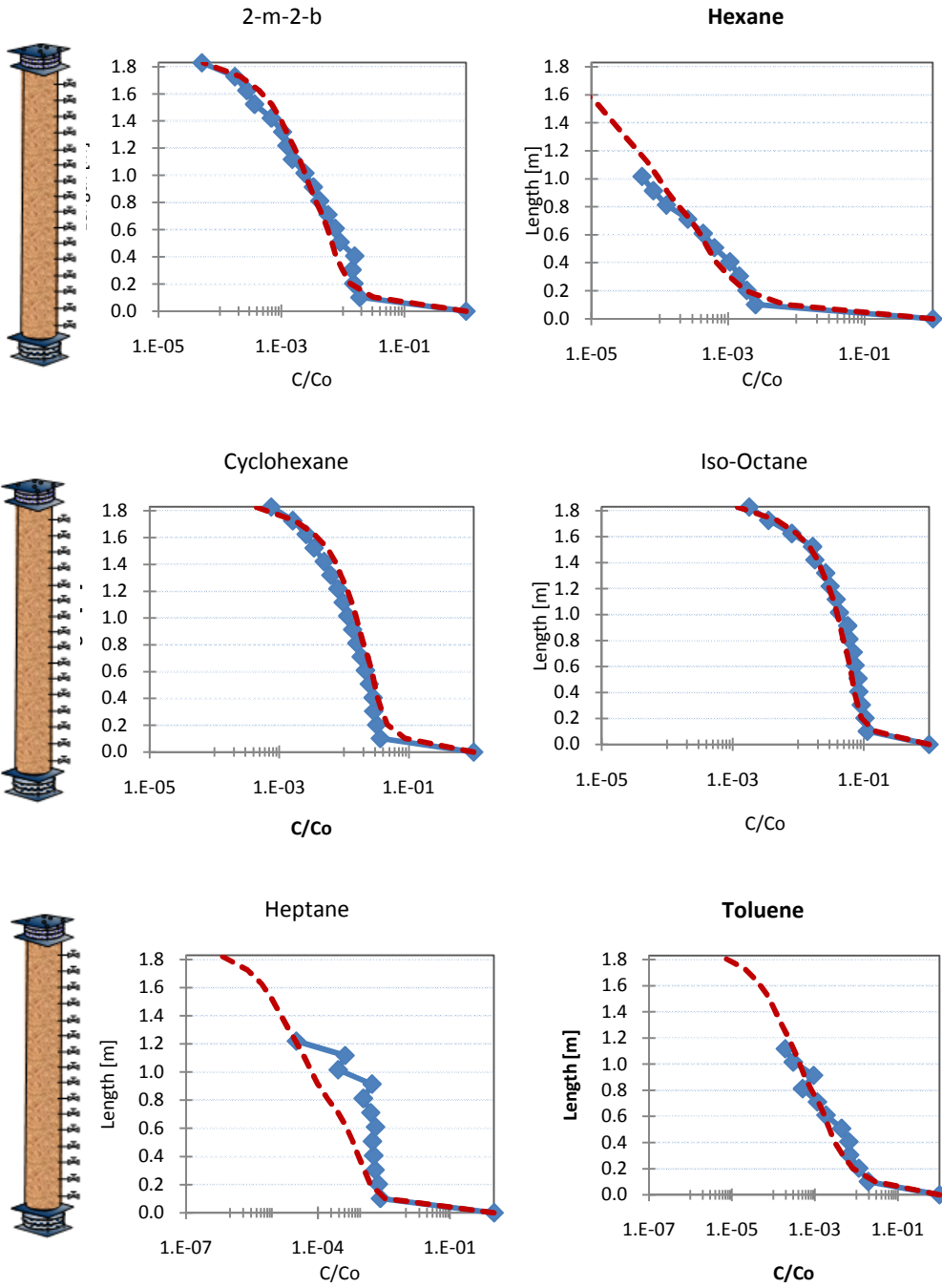
Column F (continue)



PHASE III: (10X LOWER CONCENTRATION VAPOR SOURCE, AEROBIC)

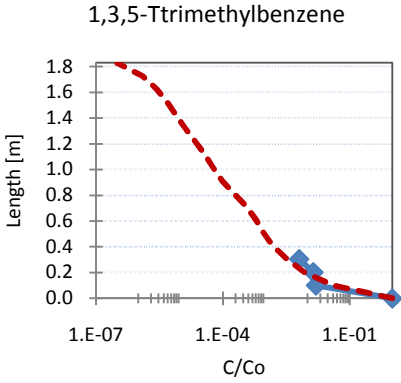
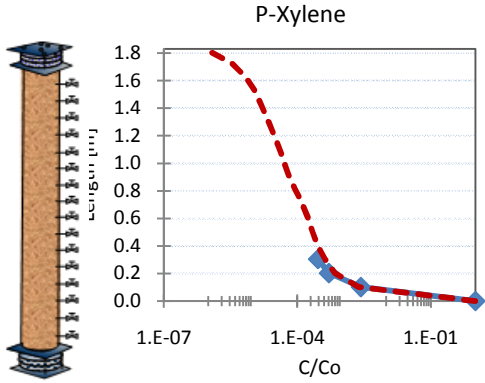


Column A

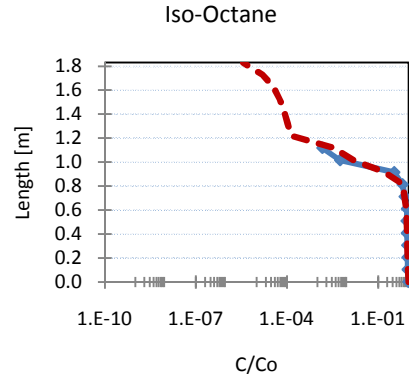
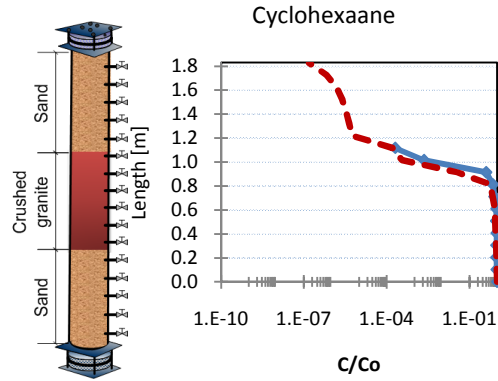
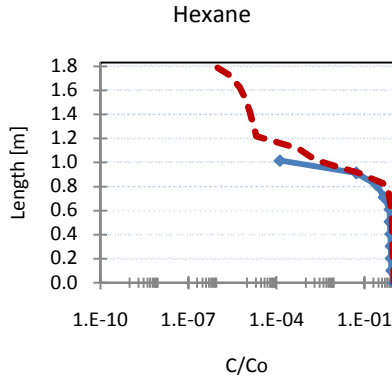
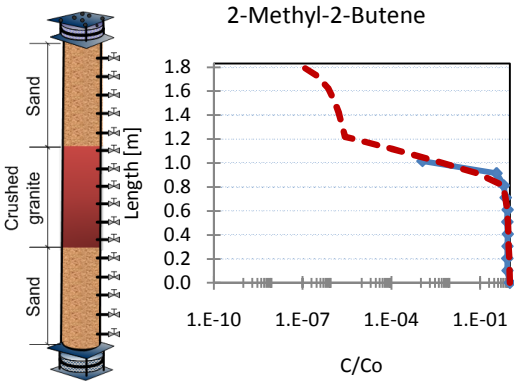




Column A (continue)

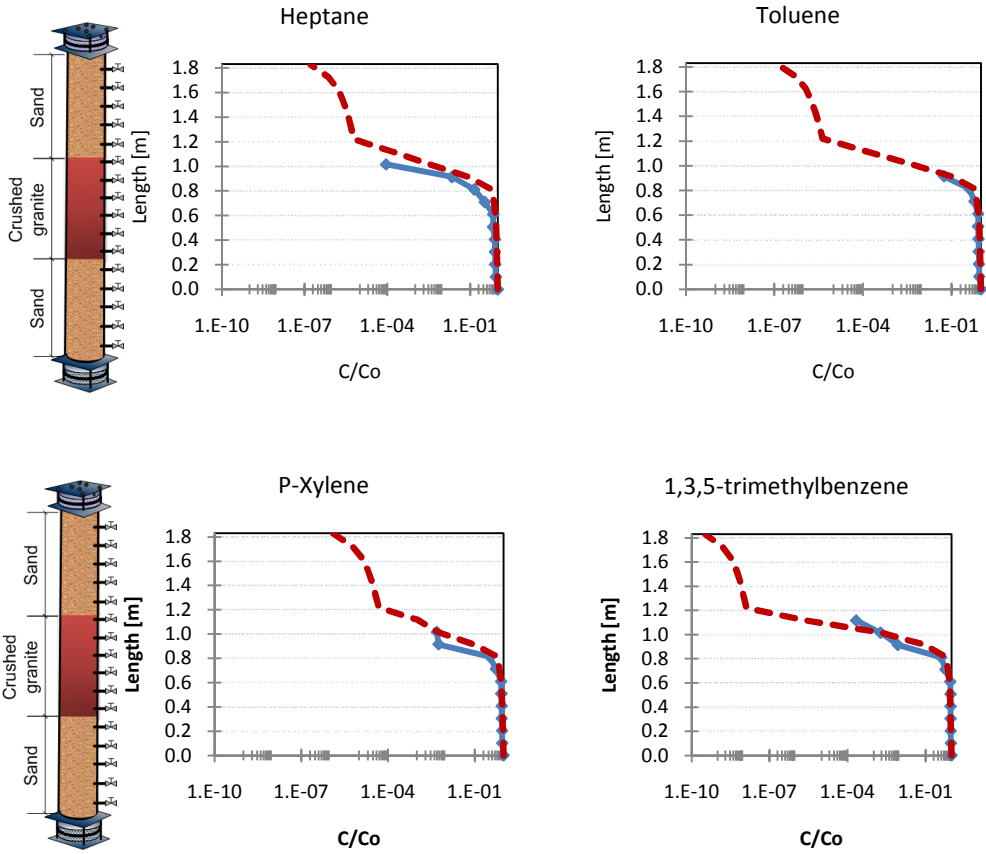


Column B

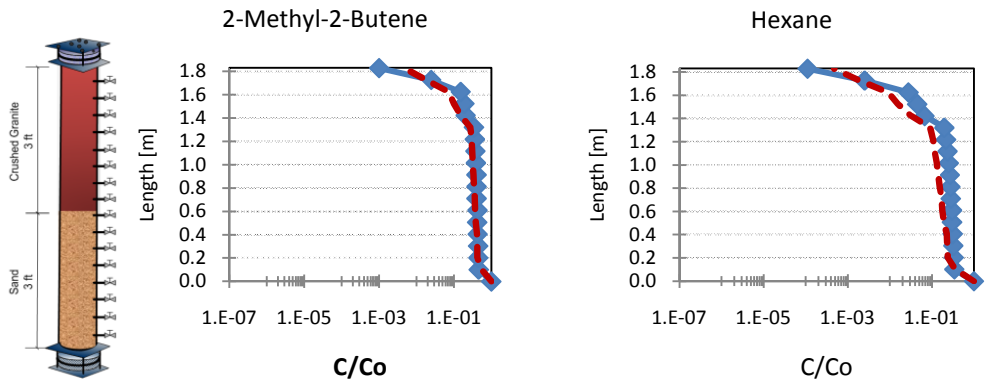




Column B(continue)

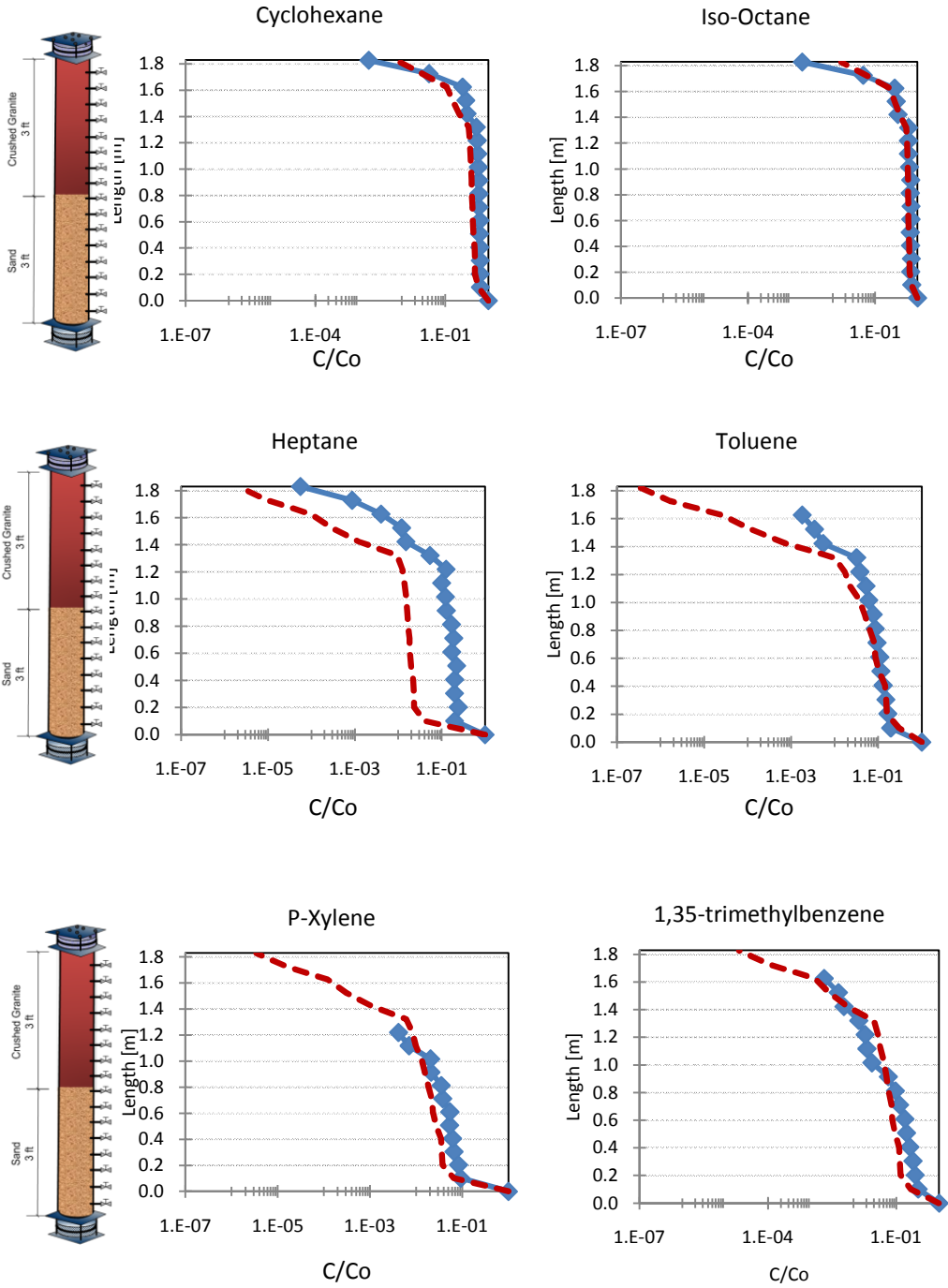


Column C



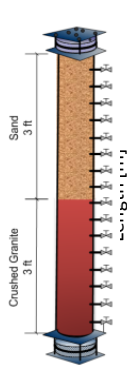


Column C (Continue)

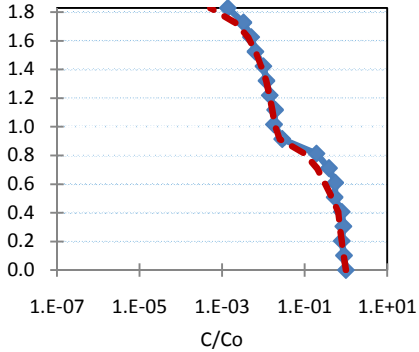




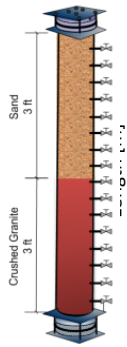
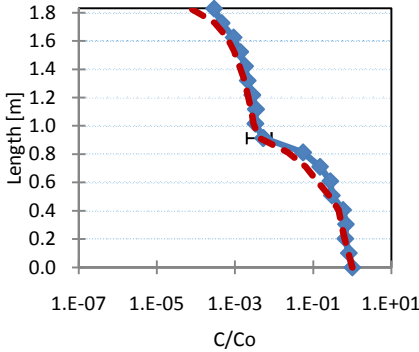
Column D



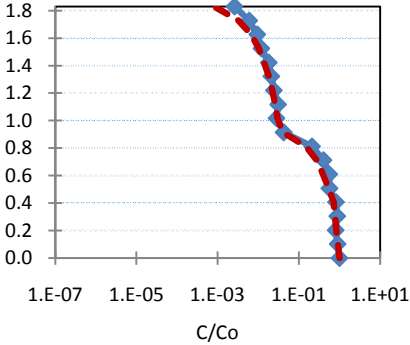
2-M-2-B



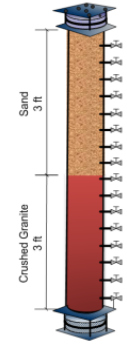
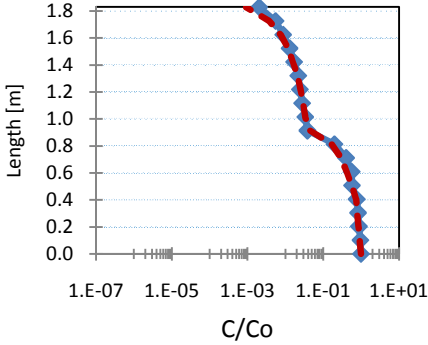
Hexane



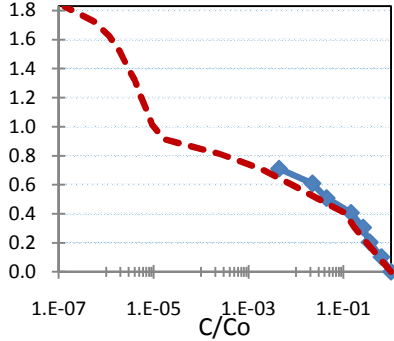
Cyclohexane



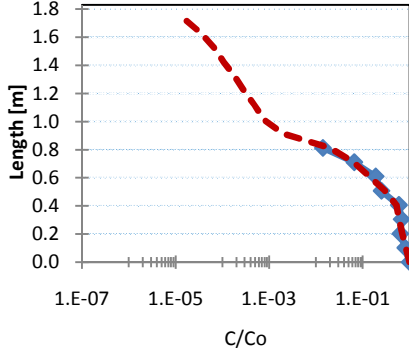
Iso-Octane



Heptane

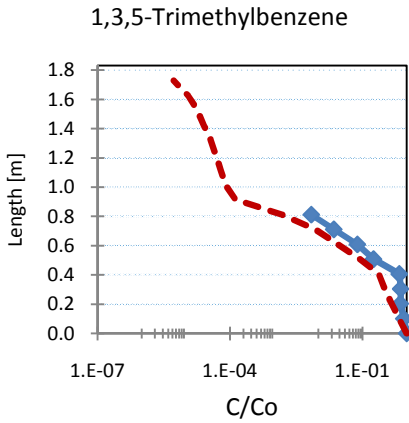
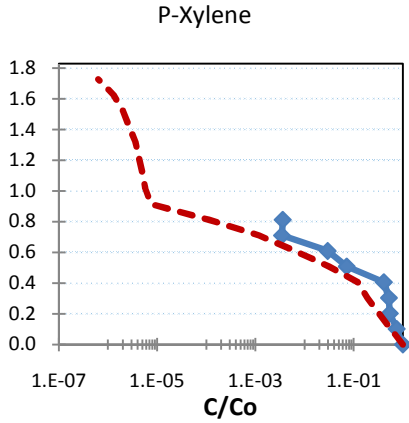
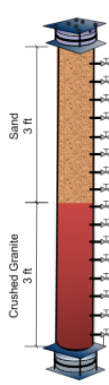


Toluene

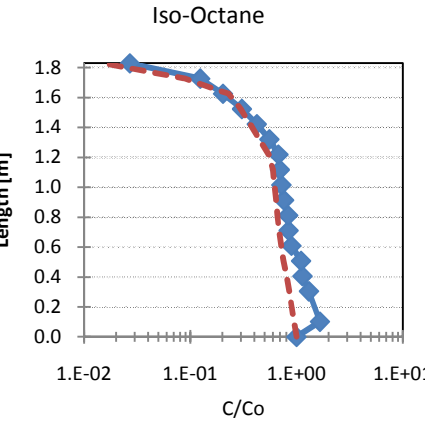
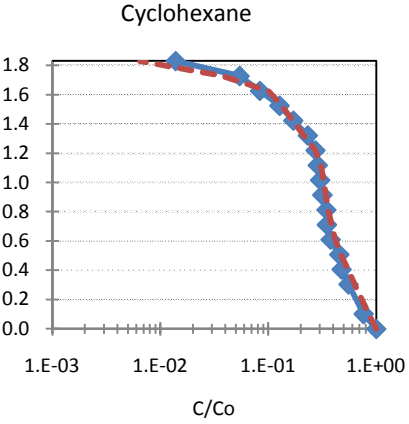
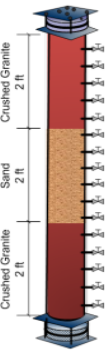
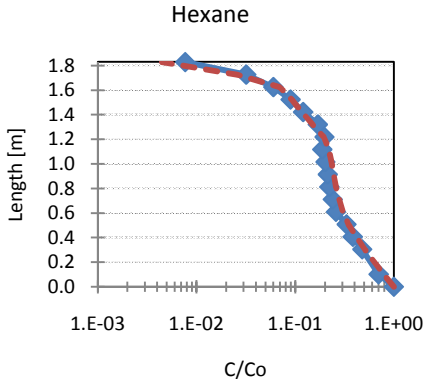
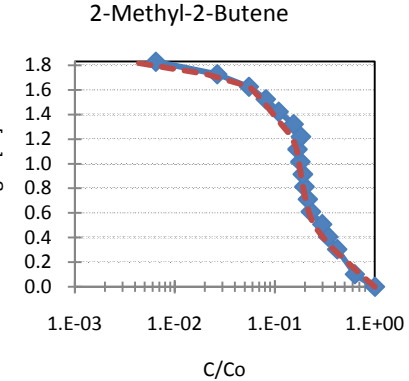
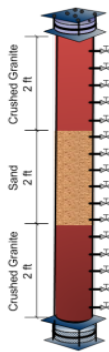


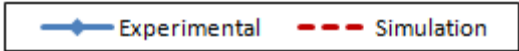


Column D (continue)

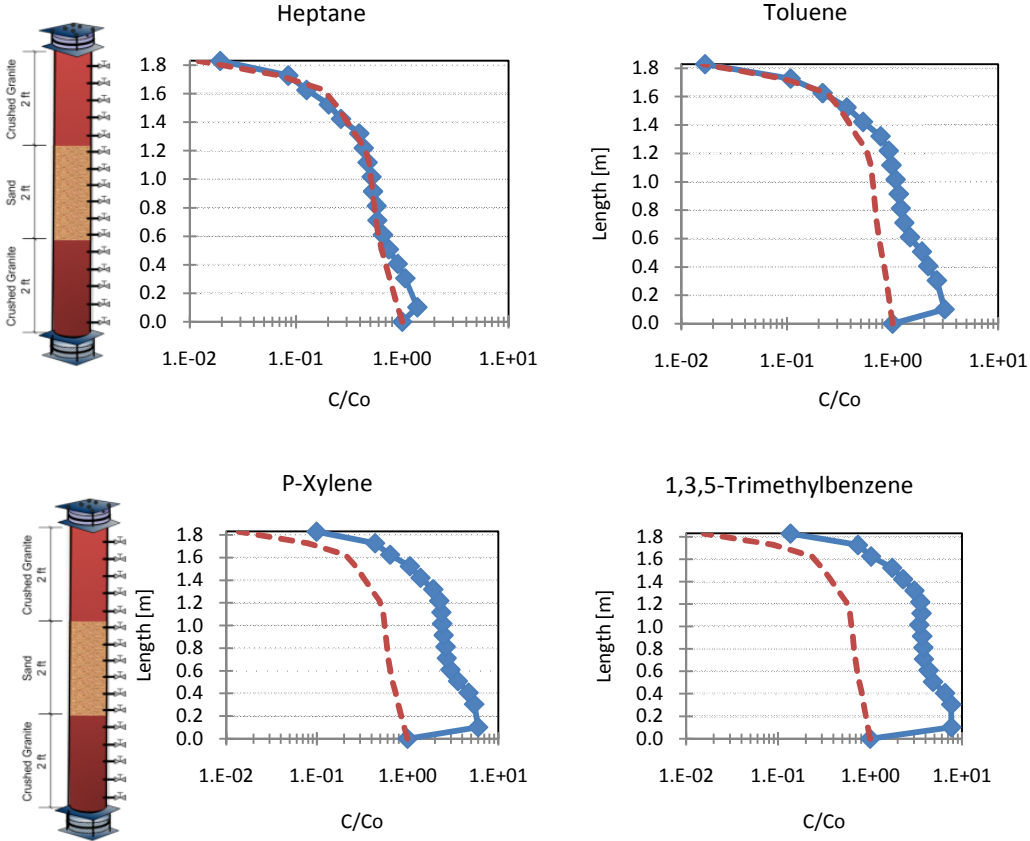


Column E

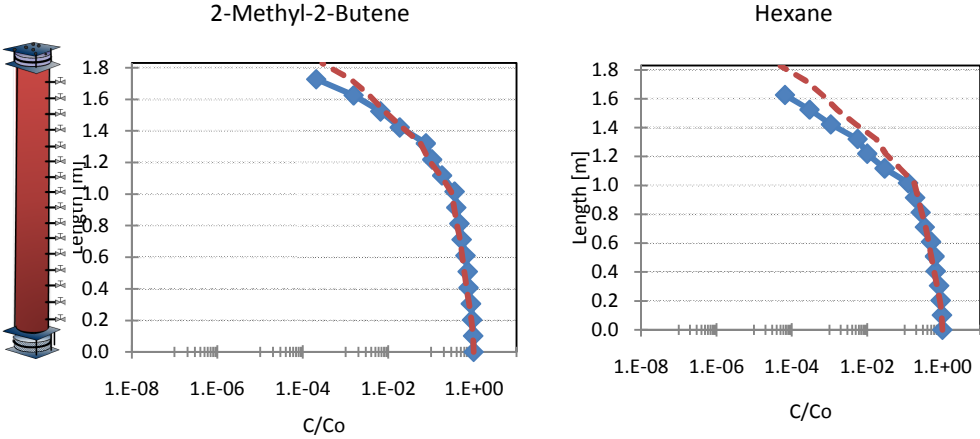




Column E (continue)



Column F





Column F (continue)

